

# **Long-Term In-Service Evaluation of Two Bridges Designed with Fiber-Reinforced Polymer Girders**

By

Bernard Leonard Kassner

Thesis submitted to the Faculty of the  
Virginia Polytechnic Institute and State University  
in partial fulfillment of the requirements for the degree of

Master of Science  
In  
Civil Engineering

Thomas E. Cousins, Chair  
John J. Lesko  
Carin L. Roberts-Wollmann

September 2, 2004  
Blacksburg, Virginia

Keywords: Fiber-reinforced polymer (FRP), pultruded composite girders, durability, wheel load distribution, dynamic load allowance, deflection

## **Long-Term In-Service Evaluation of Two Bridges Designed with Fiber-Reinforced Polymer Girders**

Bernard Leonard Kassner

### (ABSTRACT)

A group of researchers, engineers, and government transportation officials have teamed up to design two bridges with simply-supported FRP composite structural beams. The Toms Creek Bridge, located in Blacksburg, Virginia, has been in service for six years. Meanwhile, the Route 601 Bridge, located in Sugar Grove, Virginia, has been in service for two years.

Researchers have conducted load tests at both bridges to determine if their performance has changed during their respective service lives. The key design parameters under consideration are: deflection, wheel load distribution, and dynamic load allowance.

The results from the latest tests in 2003 yield little, yet statistically significant, changes in these key factors for both bridges. Most differences appear to be largely temperature related, although the reason behind this effect is unclear. For the Toms Creek Bridge, the largest average values from the 2003 tests are  $440 \mu\epsilon$  for service strain, 0.43 in. ( $L/484$ ) for service deflection, 0.08 ( $S/11.1$ ) for wheel load distribution, and 0.64 for dynamic load allowance. The values for the Route 601 Bridge are  $220 \mu\epsilon$ , 0.38 in. ( $L/1230$ ), 0.34 ( $S/10.2$ ), and 0.14 for the same corresponding parameters.

The recommended design values for the dynamic load allowance in both bridges have been revised upwards to 1.35 and 0.5 for the Toms Creek Bridge and Route 601 Bridge, respectively, to account for variability in the data. With these increased factors, the largest strain in the Toms Creek Bridge and Route 601 Bridge would be less than 13% and 12%, respectively, of ultimate strain. Therefore, the two bridges continue to provide a large factor of safety against failure.

## Acknowledgements

The author would like to thank the following people for their support and contribution to this thesis:

- **Dr. Tommy Cousins**, chiefly for being my advisor during this seemingly interminable process, but also for helping me to become a better bridge engineer. Of course, there were usually other interesting things to discuss instead of bridges, such as camping, geo-political issues, and the “first rule of electricity.” Lastly, words could never express my gratitude for him helping me obtain employment at the Virginia Transportation Research Council.
- **Dr. Jack Lesko**, for serving on my committee, but more specifically for serving as the “go-to guy” when it came to dealing with material issues and statistical analysis for this research. His expertise in composite materials proved valuable in looking at this project from a different angle.
- **Dr. Carin Roberts-Wollmann**, for serving on my committee, and for teaching me that “forces are smart,” but also for enduring me as a student for four separate concrete-related classes. Much appreciation also for supporting my idea of building an electronic fence or electronic collar for Dr. Cousins so that he could never stray too far from his office for an extended length of time.
- **Chris Link**, for his assistance in instrumenting the Toms Creek Bridge and being the photographer during testing, as well as his ability to pass the time by singing songs that he just could not get out of his head.
- **Nick Amico**, also for his assistance in instrumenting the Toms Creek Bridge, and volunteering to be the one to wear the waders with the hole in one leg.
- **Bertha and Bubba**, the two resident black snakes at the Toms Creek Bridge who kept me company when neither Chris nor Nick was there. Thanks for scaring the living daylights out of me the first time around, and for keeping me on my toes the rest of the time.
- **Jeremy Lucas**, for his assistance in instrumenting the Route 601 Bridge and for sharing that cool moment in nature when a flock of ducks came waddling underneath the bridge.

- **Kim Phillips**, for helping out during testing for the Route 601 Bridge and using Dr. Cousins' camera to shoot the short digital movies during a test.
- **Chris Waldron**, for offering to come down to for the Route 601 Bridge just so that he could have an excuse to go eat at the Sugar Grove Diner.
- **Brett Farmer and Dennis Huffman**, for their time and advice in preparing for the field instrumentation that needed to be done.

A special “thank you” goes out to **Michael Lineberry** and his wife, **Cami** – two truly great peeps! I cannot truly express how grateful I am for their friendship and laughter during the past decade. The phone conversations and kayak adventures provided much needed inspiration in getting it all done. Bona Tempora!

Lastly, my deepest love and appreciation for my parents, **Dennis and Jo Anne Kassner**, and my grandmother, **Kathryn Mudloff**, for their loving support through all of the years and for the financial investment that they have placed in my education. Certainly, the money can be repaid, but I will be in debt for a lifetime for all the love that they've shown me.

## Table of Contents

List of Tables .....	vii
List of Figures.....	ix
<b>Chapter 1: Introduction and Literature Review.....</b>	<b>1</b>
1.1 Introduction .....	1
1.1.1 Advantages and Disadvantages of FRP .....	2
1.1.2 FRP Fabrication .....	3
1.2 Literature Review .....	3
1.2.1 Durability Research .....	3
1.2.2 Large-Scale Field Experimentation .....	5
1.2.3 The Toms Creek Bridge.....	8
1.2.4 The Route 601 Bridge.....	9
1.2.5 AASHTO Bridge Design Guidelines.....	11
1.2.5.1 Deflection Control.....	12
1.2.5.2 Wheel Load Distribution Factor, $g$ .....	14
1.2.5.3 Dynamic Load Allowance, $IM$ .....	16
1.3 Scope and Objectives of This Study.....	18
1.4 Tables and Figures.....	20
<b>Chapter 2: Experimental Procedure.....</b>	<b>27</b>
2.1 Bridge Instrumentation.....	27
2.1.1 Strain Gages .....	27
2.1.2 Deflectometers .....	28
2.2 Data Acquisition.....	29
2.3 Calibrations .....	30
2.4 Field Tests .....	31
2.4.1 Toms Creek Bridge.....	31
2.4.2 Route 601 Bridge .....	33
2.5 Data Organization.....	35
2.6 Data Reporting .....	36
2.7 Tables and Figures.....	37
<b>Chapter 3: Results for Service Strains and Deflections .....</b>	<b>45</b>
3.1 Service Strain and Deflection Results for the Toms Creek Bridge.....	45
3.1.1 Results from Current Study of the Toms Creek Bridge.....	45
3.1.2 Comparison of Current Study with Previous Toms Creek Bridge Tests .....	46
3.2 Service Strain and Deflection Results for the Route 601 Bridge .....	50
3.2.1 Results from Current Study of the Route 601 Bridge.....	50
3.2.2 Comparison of Current Study with Previous Route 601 Bridge Tests .....	51
3.3 Axial Strains .....	54
3.4 Tables and Figures.....	55
<b>Chapter 4: Results for Wheel Load Distribution, <math>g</math>.....</b>	<b>69</b>
4.1 Procedure for Calculating the Wheel Load Distribution.....	69
4.2 Wheel Load Distribution Results for the Toms Creek Bridge .....	71

4.2.1 Results from Current Study of Toms Creek Bridge.....	71
4.2.2 Comparison of Current Study with Previous Toms Creek Bridge Tests .....	72
4.3 Wheel Load Distribution Results for the Route 601 Bridge .....	75
4.3.1 Results from the Current Study of Route 601 Bridge.....	75
4.3.2 Comparison of Current Study with Previous Route 601 Bridge Tests .....	77
4.4 Tables and Figures.....	83
<b>Chapter 5: Results for Dynamic Load Allowances, <i>IM</i>.....</b>	<b>111</b>
5.1 Procedure for Calculating the Dynamic Load Allowance.....	111
5.2 Dynamic Allowance Results for the Toms Creek Bridge .....	111
5.2.1 Dynamic Load Allowance from Current Study of Toms Creek Bridge .....	111
5.2.2 Comparison of <i>IM</i> Results with Previous Toms Creek Bridge Tests .....	113
5.3 Dynamic Allowance Results for the Route 601 Bridge .....	116
5.3.1 Dynamic Allowance Results from Current Study of Route 601 Bridge.....	116
5.3.2 Comparison of <i>IM</i> with Previous Route 601 Bridge Tests.....	117
5.4 Tables and Figures.....	120
<b>Chapter 6: Bridge Inspections .....</b>	<b>129</b>
6.1 Beams .....	129
6.2 Abutments .....	131
6.3 Beam Clearance.....	132
6.4 Road Surface .....	132
6.5 Toms Creek Bridge Inspection.....	133
6.6 Figures .....	134
<b>Chapter 7: Conclusions and Recommendations .....</b>	<b>139</b>
7.1 Conclusions .....	139
7.1.1 Toms Creek Bridge.....	139
7.1.2 Route 601 Bridge .....	141
7.2 Recommendations .....	144
7.3 Tables .....	147
<b>Appendix A: Sample Calculation for Effect of Moisture Content on Deflection.....</b>	<b>152</b>
<b>Appendix B: Test Data .....</b>	<b>155</b>
<b>Vita .....</b>	<b>165</b>

## List of Tables

Table 2-1. Test log for the Toms Creek Bridge. Data Set #1 was an initializer, so no data was recorded. Data Set #29 was discarded due to improper truck alignment.....	37
Table 2-2. Test log for the Route 601 Bridge tests. Data sets that do not appear were discarded due to errors in using the TCS software.....	37
Table 3-1. Maximum and average peak flexural strain (in microstrain) for the most the heavily loaded girder for the different truck orientations and speeds in the Toms Creek Bridge. ....	55
Table 3-2. Maximum and average peak deflection (in inches) for the most the heavily loaded girder for the different truck orientations and speeds in the Toms Creek Bridge.....	55
Table 3-3. Peak strain in the Toms Creek Bridge as a fraction of ultimate.....	56
Table 3-4. Maximum and average peak flexural strain in the most the heavily loaded girder for the different truck orientations and speeds in the Route 601 Bridge (measured in microstrain).....	57
Table 3-5. Maximum and average peak deflection in the most the heavily loaded girder for the different truck orientations and speeds in the Route 601 Bridge (measured in inches). ....	57
Table 3-6. Peak strain in the Route 601 Bridge as a fraction of ultimate strain; percentages are for largest average peak strain amongst all three load tests.....	58
Table 4-1. Wheel load fractions based on strain data for the Toms Creek Bridge.....	83
Table 4-2. Wheel load fractions based on deflection data for the Toms Creek Bridge.....	83
Table 4-3. Maximum and average total flexural strain in all girders for the Toms Creek Bridge for the various truck orientations and speeds at the time of peak flexural strain (in microstrain).....	84
Table 4-4. Maximum and average total deflection in the all of the girders for the Toms Creek Bridge, recorded at the time of peak deflection (measured in inches).....	84
Table 4-5. Wheel load fractions based on strain data for the Route 601 Bridge. Fractions for multiple trucks are listed on a per truck basis.....	85
Table 4-6. Wheel load fractions based on deflection data for the Route 601 Bridge. Fractions for multiple trucks are listed on a per truck basis. ....	85
Table 4-7. Maximum and average total flexural strain in all of the girders for the Route 601 Bridge for the different truck orientations and speeds, recorded at the time of peak flexural strain (measured in microstrain). ....	86
Table 4-8. Maximum and average total deflection in the all of the girders for the Route 601 Bridge for the different truck orientations and speeds, recorded at the time of peak deflection (measured in inches). ....	86
Table 5-1. Dynamic load allowances for the Toms Creek Bridge, based on strain data. ....	120
Table 5-2. Dynamic load allowances for the Toms Creek Bridge, based on deflection data. ....	120

Table 5-3. Dynamic load allowances for the Route 601 Bridge, based on (a) strain and (b) deflection.....	121
Table 7-1. Summary of results for the key design parameters in the Toms Creek Bridge.....	147
Table 7-2. Summary of results for the key design parameters in the Toms Creek Bridge.....	147

## List of Figures

Figure 1-1. View of the Toms Creek Bridge looking (a) at the upstream elevation, and (b) toward the northbound approach. ....	20
Figure 1-2. Toms Creek Bridge cross-section (Neely, 2000). ....	21
Figure 1-3. Cross-section of the 8-in. FRP composite DWB used in the Toms Creek Bridge (Neely, 2000). ....	21
Figure 1-4. Plan view of the Toms Creek Bridge (Neely, 2000). ....	22
Figure 1-5. Detail of girder-to-abutment and deck-to-girder connections (Neely, 2000). ....	22
Figure 1-6. View of the Route 601 Bridge, looking (a) at the upstream elevation, and (b) toward the eastbound approach. ....	23
Figure 1-7. Cross-sectional view of the Route 601 Bridge (Restrepo, 2002). ....	24
Figure 1-8. Plan view of the Route 601 Bridge (Restrepo, 2002). ....	24
Figure 1-9. Cross-section of the 36-in. (1.1-m) DWB used in the Route 601 Bridge (Waldron, 2002). ....	25
Figure 1-10. Deck-to-girder connection for the Route 601 Bridge (Restrepo, 2002). ....	25
Figure 1-11. Visualization of relative stiffness between slab and girder, where (a) the slab is not stiff, and (b) the slab is very stiff compared to the supporting girders (Barker and Puckett, 1997). ....	26
Figure 2-1. Instrumentation for the Toms Creek Bridge; cross-section is looking in the south direction (Neely, 2000). ....	38
Figure 2-2. Instrumentation for the Route 601 Bridge; cross-section is looking in the east direction (Restrepo, 2002). ....	38
Figure 2-3. Deflectometer for the Toms Creek Bridge. ....	39
Figure 2-4. Deflectometer for the Route 601 Bridge. ....	39
Figure 2-5. Sketch showing the dimensions and weight distribution of the VDOT dump truck used for testing the Toms Creek Bridge. ....	40
Figure 2-6. Sketch of weight distribution and dimensions of truck T4 used in for the Route 601 Bridge load tests. ....	41
Figure 2-7. Sketch of weight distribution and dimensions of truck T5 used in for the Route 601 Bridge multiple-lane load tests. ....	41
Figure 2-8. Exterior truck orientations for the Route 601 Bridge: (a) West Exterior, (b) Multiple-Lane, (c) East Exterior (Restrepo, 2002). ....	42
Figure 2-9. Interior truck orientations for the Route 601 Bridge: (a) West Interior, (b) Center, (c) East Interior (Restrepo, 2002). ....	43
Figure 2-10. Typical comparison between filtered and unfiltered data. Data shown is for Girder 16 during a single test of the northbound lane orientation of the Toms Creek Bridge; filtered data was shifted upwards 20 $\mu\epsilon$ for comparison purposes. ....	44

Figure 2-11. Typical comparison between smoothed and unsmoothed data. Data shown is for Girder 16 during a single test of the northbound lane orientation of the Toms Creek Bridge; smoothed data has been set to zero. ....	44
Figure 3-1. Average peak strain in the most heavily loaded girder for the different truck orientations and travel speeds in the Toms Creek Bridge.....	59
Figure 3-2. Average peak deflection in the most heavily loaded girder for the different truck orientations and travel speeds in the Toms Creek Bridge.....	60
Figure 3-3. Error bars for the average peak (a) strain and (b) deflection for the most heavily loaded girder in the Toms Creek Bridge. Data points marked “N/A” do not have enough tests to produce a statistically reliable set of bars; data points without error bars have errors that are too small to appear on the graph. ....	61
Figure 3-4. Average peak strain shown with the average temperature at the Toms Creek Bridge. ....	62
Figure 3-5. Average peak strain shown with rainfall at the Toms Creek Bridge. Amount of rainfall is the precipitation over a seven-day period prior to the respective test dates. ....	63
Figure 3-6. Average peak (a) strain and (b) deflection in the most heavily loaded girder for the different interior truck orientations and travel speeds in the Route 601 Bridge. ....	64
Figure 3-7. Average peak (a) strain and (b) deflection in the most heavily loaded girder for the three exterior truck orientations in the Route 601 Bridge; all exterior orientations were tested at static speed.....	65
Figure 3-8. Error bars for the average peak (a) strain and (b) deflection for the most heavily loaded girder for the interior orientations in the Route 601 Bridge.....	66
Figure 3-9. Average peak (a) strain and (b) shown with the average temperature during testing at the Route 601 Bridge. ....	67
Figure 3-10. Average peak (a) strain and (b) deflection shown with the total rainfall during the week prior to testing at the Route 601 Bridge. ....	68
Figure 4-1. Typical girder responses to a load truck for the various truck orientations on the Toms Creek Bridge, shown at the time of maximum strain at static speed.....	87
Figure 4-2. Typical girder responses to a load truck for the East Interior, Center, and West Interior orientations on the Route 601 Bridge, shown at the time of maximum deflection at static speed. ....	88
Figure 4-3. Typical girder responses to a load truck for the East Exterior, Multiple Lanes, and West Exterior orientations on the Route 601 Bridge, shown at the time of maximum deflection at static speed. ....	89
Figure 4-4. Average wheel load distributions for the Toms Creek Bridge over time, based on strain measurements at three different speeds. ....	90
Figure 4-5. Average wheel load distributions for the Toms Creek Bridge over time, based on deflection measurements at three different speeds. ....	91
Figure 4-6. Error bars for average wheel load distributions in the Toms Creek Bridge, based on (a) strain and (b) deflection measurements. Data points marked “N/A” do not have enough	

tests to produce a statistically reliable set of bars; data points without error bars have errors that are too small to appear on the graph. ....	92
Figure 4-7. Average total peak strain in all of the girders for the different truck orientations and travel speeds in the Toms Creek Bridge. ....	93
Figure 4-8. Average total peak deflection in all of the girders for the different truck orientations and travel speeds in the Toms Creek Bridge. ....	94
Figure 4-9. Percentage change of (a) peak strain versus total peak strain and (b) peak deflection versus total peak deflection from the given test date to the Summer 2003 test for the Toms Creek Bridge in the various truck orientations at static speed. ....	95
Figure 4-10. Percentage change of (a) peak strain versus total peak strain and (b) peak deflection versus total peak deflection from the given test date to the Summer 2003 test for the Toms Creek Bridge in the various truck orientations at 25 mph (40 kph). ....	96
Figure 4-11. Percentage change of (a) peak strain versus total peak strain and (b) peak deflection versus total peak deflection from the given test date to the Summer 2003 test for the Toms Creek Bridge in the various truck orientations at 40 mph (64 kph). ....	97
Figure 4-12. Comparison of AASHTO <i>Standard Specifications</i> and <i>LRFD Specifications</i> with the overall results for wheel load distributions in the Toms Creek Bridge, based on (a) strain and (b) deflection. The averages shown here combine the results for all truck orientations and are calculated “per axle.” Error bars are equivalent to $\pm 2\sigma$ . ....	98
Figure 4-13. Average wheel load distributions for the Route 601 Bridge over time for three speeds, based on strain. ....	99
Figure 4-14. Average wheel load distributions for the Route 601 Bridge over time for three speeds, based on deflection. ....	99
Figure 4-15. Average wheel load distributions calculated from strain data for the exterior orientations in the Route 601 Bridge. Note that these tests were only conducted at static speed. ....	100
Figure 4-16. Average wheel load distributions calculated from strain data for the exterior orientations in the Route 601 Bridge. Note that these tests were only conducted at static speed. ....	100
Figure 4-17. Error bars for average maximum wheel load distributions at three different speeds of the interior orientations in the Route 601 Bridge, based on strain measurements. ....	101
Figure 4-18. Error bars for average maximum wheel load distributions at three different speeds of the interior orientations in the Route 601 Bridge, based on deflection measurements. .	102
Figure 4-19. Average total peak (a) strain and (b) deflection in all of the girders for the Interior truck orientations at the various speeds in the Route 601 Bridge. ....	103
Figure 4-20. Average total peak (a) strain and (b) deflection in all of the girders for the Exterior truck orientations at static speed in the Route 601 Bridge. ....	104
Figure 4-21. Percentage change of (a) peak strain versus total peak strain and (b) peak deflection versus total peak deflection from the given test date to the Fall 2003 test for the various interior truck orientations in the Route 601 Bridge at static speed. ....	105

Figure 4-22. Percentage change of (a) peak strain versus total peak strain and (b) peak deflection versus total peak deflection from the given test date to the Fall 2003 test for the various interior truck orientations in the Route 601 Bridge at 25 mph (40 kph).....	106
Figure 4-23. Percentage change of (a) peak strain versus total peak strain and (b) peak deflection versus total peak deflection from the given test date to the Fall 2003 test for the various interior truck orientations in the Route 601 Bridge at 40 mph (64 kph).....	107
Figure 4-24. Percentage change of (a) peak strain versus total peak strain and (b) peak deflection versus total peak deflection from the given test date to the Fall 2003 test for the exterior truck orientations in the Route 601 Bridge at static speed. Note that the East and West Exterior orientations were not tested in the Fall of 2001.....	108
Figure 4-25. Comparison of AASHTO <i>Standard Specifications</i> and <i>LRFD Specifications</i> with the overall average wheel load distribution in the Route 601 Bridge for a (1) single interior lane loaded and (2) single exterior lane loaded, based on (a) strain and (b) deflection. The averages shown here are calculated “per axle.” Error bars are equivalent to $\pm 2\sigma$ . ....	109
Figure 4-26. Comparison of AASHTO specifications with the average wheel load distribution in the Route 601 Bridge for multiple exterior lanes loaded, based on (a) strain and (b) deflection. The averages shown here are calculated for a single truck axle. Error bars are equivalent to $\pm 2\sigma$ . ....	110
Figure 5-1. Typical comparison of peak dynamic loading versus static loading for the Toms Creek Bridge, with the <i>IM</i> factor based on strain measurements. ....	122
Figure 5-2. Comparison of peak dynamic loading versus static loading for the Route 601 Bridge, with the <i>IM</i> factor based on deflection measurements.....	122
Figure 5-3. Average dynamic load allowance over time for the Toms Creek Bridge for two different speeds, based on strain data. ....	123
Figure 5-4. Average dynamic load allowance over time for the Toms Creek Bridge for two different speeds, based on deflection data. ....	123
Figure 5-5. Error bars for average dynamic load allowances for the (1) 25 mph and (2) 40 mph travel speeds across the Toms Creek Bridge. Dynamic load allowances based on (a) strain and (b) deflection measurements. Data points marked “N/A” do not have enough tests to produce a statistically reliable set of bars. ....	124
Figure 5-6. Comparison of temperature over time with dynamic load allowance at 40 mph in the Toms Creek Bridge. Based on (a) strain and (b) deflection. ....	125
Figure 5-7. Overall dynamic load allowances calculated at (a) 25 mph and (b) 40 mph, averaged for all of the truck orientations on a given test date, shown with error bars, both AASHTO Specifications recommendations, and Neely’s proposed <i>IM</i> . Averages shown here are based on deflection measurements, which tend to give the worst-case results. ....	125
Figure 5-8. Average dynamic load allowances at 25 mph (40 kph) for the different interior orientations in the Route 601 Bridge, based on (a) strain and (b) deflection. ....	126
Figure 5-9. Average dynamic load allowances at 40 mph (64 kph) for the different interior orientations in the Route 601 Bridge, based on (a) strain and (b) deflection. ....	126

Figure 5-10. Average dynamic load allowances at 25 mph (40 kph) shown with error bars, based on (a) strain and (b) deflection.....	127
Figure 5-11. Average dynamic load allowances at 40 mph (64 kph) shown with error bars, based on (a) strain and (b) deflection.....	127
Figure 5-12. Average dynamic load allowance shown with temperature for the Route 601 Bridge at (a) 25 mph and (b) 40 mph, based on strain data.....	128
Figure 5-13. Comparison of AASHTO Specifications with overall dynamic load allowances at (a) 25 mph and (b) 40 mph for the Route 601 Bridge, based on strain measurements.....	128
Figure 6-1. Detail of locations for possible damage or deterioration in Beams 1, 5, and 6 in the Route 601 Bridge.....	134
Figure 6-2. Detail of locations for possible damage or deterioration in Beams 7 and 8 in the Route 601 Bridge.....	135
Figure 6-3. Matrix resin material splintering off from Girder 5 of the Route 601 Bridge (courtesy of Strongwell Corp). .....	136
Figure 6-4. Typical blister on the surface of the bottom flange in an exterior girder for the Route 601 Bridge.....	136
Figure 6-5. Crack down center of east abutment of the Route 601 Bridge. ....	137
Figure 6-6. Extent of river stone pile-up at east abutment during Fall 2003 inspection of the Route 601 Bridge.....	137
Figure 6-7. Extent of river stone pile-up at east abutment during Spring 2004 inspection of the Route 601 Bridge.....	138
Figure A-1. Cross-section used for calculating the effects of moisture content on the deflection of the Toms Creek Bridge.....	152
Figure A-2. Cross-section used for calculating the effects of moisture content on the deflection of the Route 601 Bridge.....	153

# Chapter 1: Introduction and Literature Review

## 1.1 Introduction

In its 2001 report on the assessment of this country's infrastructure, the American Society of Civil Engineers (ASCE) stated that the Federal Highway Administration (FHWA) found that 27.5% of the country's bridges were either structurally deficient or functionally obsolete, where

a structurally deficient bridge is closed or restricted to light vehicles because of its deteriorated structural components ... a functionally obsolete bridge has older design features and while it is not unsafe for all vehicles, it cannot safely accommodate current traffic volumes, and vehicle sizes and weights (ASCE, 2001).

The FHWA has set a target of having less than 25% of all bridges being classified as structurally deficient by the year 2008. The cost for eliminating these deficiencies is estimated at \$9.4 billion a year for the next twenty years, with an extra \$5.8 billion a year needed to maintain the remaining bridges. However, in its 2003 progress report to the 2001 assessment, the ASCE cited questionable progress in reaching FHWA's goal due to trends in funding by state transportation departments (ASCE, 2003).

In making policy recommendations to promote progress, the ASCE suggested using the latest technology for designing and constructing bridges. One such technology is fiber-reinforced polymer (FRP) composite material. FRP has actually been around since its debut in British Spitfire fighter planes at the end of World War II, but the concept did not develop further until glass fiber-reinforced polymers gained prominence within the boating industry during the 1950's. Carbon fiber-reinforced polymers came on board during the 1960's due to superior strength and stiffness needed in the aerospace industry (Mirmiran et al., 2003). However, this strength and stiffness came at a cost premium. Thus, the FRP industry began focusing on the sporting industry during the 1970's to encourage mass production, and consequently, lowering the material cost (Bakis et al., 2002). Nonetheless, it was not until later when the civil engineering industry began utilizing FRP composites in construction (Hollaway and Head, 2001).

### **1.1.1 Advantages and Disadvantages of FRP**

One major reason for the sluggish uptake in using FRP in the civil infrastructure is that the material continues to have high initial costs when compared to traditional building materials such as concrete, steel, or wood. Additional obstacles include the absence of a design code for FRP, the lack of educational programs about the material for civil engineers, a paucity of long-term field tests and durability data for structures constructed with FRP, difficulty in connection design, and a lower elastic modulus along with the material's sudden, brittle failure mode (Mirmiran et al., 2003; Karbhari et al., 2003).

Despite these problems that might cause a civil engineer to shy away from designing bridges with the material, FRP shows many promising qualities which deserve consideration. Foremost is the material's high strength-to-weight and stiffness-to-weight ratio, resulting in an overall lightweight structure. Just as a comparison, typical bridge decks constructed with FRP can be 75% to 80% lighter than comparable decks made out of reinforced concrete (Karbhari et al., 2000). The decrease in weight helps in several different ways. First, less weight in elements such as deck structures can allow a higher live load rating for a bridge, thus keeping the structure functionally efficient. Secondly, lighter superstructural elements lead to less expensive column and foundation elements in terms of design and construction costs (Seible, 2003). Additionally, lower weight in construction materials means lower costs in transporting those materials to the work site, and likewise, lower construction costs since smaller machinery and less labor would be required for installing the lightweight members (Wallace, 1999). Lastly, bridges made with FRP components typically take less time to construct, thus adding additional savings in labor costs, but more importantly, saving money for the local economy affected by the closure of a main thoroughfare (Foster et al., 2000). Another important quality for FRP is its resistance to corrosion; corrosion in steel beams and reinforced concrete members requires costly maintenance and places a large burden on state transportation department budgets. With its corrosion resistance, FRP has the potential to last much longer than bridges constructed with other traditional materials (Karbhari and Seible, 2000). So, despite the high initial material costs, the summation of the aforementioned advantages can lead to lower overall lifecycle costs, thus making FRP a more attractive material to build with over the long term.

### **1.1.2 FRP Fabrication**

For the short term, the demand for FRP in the high-priced defense industry has decreased, thus lowering the material's cost somewhat (Seible, 2003). Meanwhile, improvements in the manufacturing process have further improved the economy of FRP for use in civil infrastructure. In the past, hand lay-up procedures and vacuum assisted resin transfer molding have provided simple and easily-customized shapes; however, these processes are expensive in terms of labor and cycle times (Lesko et al., 2001). On the other hand, the pultrusion process has established itself as the method of choice for a mass-production scale in a cost effective fashion. In this automated, continuous process, reinforcing fibers impregnated with a resin matrix are pulled through a heated curing die at a speed of about 10 ft (3 m) per minute (Bakis et al., 2002).

The fibers are what provide the strength in the FRP, while the resin matrix holds the fibers in position as well as defends against chemical attack. Fibers are typically made of carbon, glass, or aramid. Although carbon is more expensive, glass is highly susceptible to both alkaline and chloride environments, and to a smaller degree, so is aramid (Balázs and Borosnyó, 2001). For pultrusion, these fiber reinforcements typically come in the form of fiber bundles, continuous strand mats, and non-woven surfacing veils. The reinforcements can also consist of bidirectional, multidirectional woven, braided or stitched fabrics (Bakis et al., 2002). The resin matrix used in the pultrusion process is generally either vinyl ester or polyester, although vinyl ester has proven its superiority in performance against alkaline attack, UV deterioration, and moisture absorption (Balázs and Borosnyó, 2001).

## **1.2 Literature Review**

### **1.2.1 Durability Research**

As mentioned before, one of the reasons why civil engineers have been reluctant to embrace FRP as a construction material is because of the lack of long-term data on the material. Karbhari et al. (2003) provide an analysis on the state of knowledge about FRP's durability, which the authors defined as the material's

ability to resist cracking, oxidation, chemical degradation, delamination, wear, and/or the effects of foreign object damage for a specified period of time, under the appropriate load conditions, under specified environmental conditions.

The report divided the issue into seven environmental foci: moisture/solution, alkali, thermal, creep and relaxation, fatigue, ultraviolet radiation, and fire. Researchers rated each area based on two factors: the availability of pertinent data and the importance of the data that remains unknown. All seven areas were either in moderate or critical need of additional study for determining their long-term effects on FRP. The authors recommended establishing an integrated knowledge system for all of the data that is already in existence, as well as devising a methodology for gathering data that still needs to be collected. More importantly, however, the authors cited the critical need for new durability data to come from field tests, as opposed to accelerated laboratory experiments which yield results that can differ substantially from long-term field tests.

Of the recent durability research, much of the emphasis appears to be on glass fiber-reinforced polymers (GFRP). Nishizaki and Meiarashi (2002) studied the long-term deterioration of GFRP in wet environments by submersing square and rectangular tubes in distilled water at a constant 105 F (40 C) or 140 F (60 C), as well as subjecting similar shapes to constant humidity levels of 65% and 85% under the same aforementioned range of temperatures. After 420 days of 105 degree temperatures, specimens kept in 85% humidity lost about 24% of their initial bending strength, while specimens kept in water lost nearly 45%. The authors concluded that the main cause in strength reduction was the separation of the reinforcing fibers from the resin matrix or a reduction in the resin strength.

According to the analysis by Karbhari et al., another important subject which needs further study is creep strain in FRP. While a few studies have looked at creep, most have only tested coupons or relatively short specimens. Choi and Yuan (2003) have taken research one step further by testing 4-ft (1.2-m) long GFRP columns having either box or wide-flanged cross-sectional shapes. The applied load ranged from 20% to 40% of the ultimate strength. Across the different stress levels, the results showed that the wide-flanged specimens had an average 11% increase in creep strain beyond the initial elastic strain after 2500 hours of applied constant load; 54% of that creep strain occurred within the first 24 hours of loading. The box sections had creep strains that were slightly lower than those of the wide-flanged sections. The researchers were successfully able to fit the data results to Findley's power law model in estimating the time-dependent deformation of pultruded GFRP columns. From this model, their conclusion was that

the compressive elastic modulus for GFRP subjected to constant axial load would decrease by 30% over a 50-year period.

GFRP was the focus of another study, which examined fatigue characteristics (Nagaraj and Gangarao, 1998). Here, the research tested 6-ft (1.83-m) long wide-flanged and box sections for flexural fatigue and compared the results with a typical wide-flanged section made of A36 steel. Just looking at the composite sections by themselves, the wide-flanged sections displayed no sign of deterioration in stiffness, i.e., modulus reduction, until the tests reached about 80% to 90% of their fatigue life, but showed upwards of a 20% decline in stiffness at about 95% of their fatigue life. The reasoning behind this sharp drop-off in stiffness was that fiber breakage initiated at this stage in the fatigue life. Additional tests on the wide-flanged section showed that there was no loss in stiffness when the specimen was cycled  $6 \times 10^6$  times at incremental levels of ultimate strain (27% to 50% of  $\epsilon_{ult}$ ). As was expected from earlier research, the composite material had a greater fatigue limit than steel, where the fatigue limit was defined as the strain level corresponding to a fatigue life of  $10^6$  cycles. Furthermore, the steel exhibited a more rapid decline in fatigue life for an incremental increase in strain level near the endurance limit for the respective materials.

### **1.2.2 Large-Scale Field Experimentation**

All of the studies discussed above involved small-scale studies performed in a laboratory. Again, the Karbhari et al. paper emphasizes the need to take the research out into actual environmental exposure conditions in order to establish appropriate durability-based design factors. Indeed, large-scale projects have made use of FRP in the form of pultruded structural shapes such as: highway bridge decks, girders, prestressed and non-prestressed internal reinforcements for concrete, and cables for external post-tensioning and cable-stayed bridges. Researchers have also tested FRP in externally-bonded reinforcements for seismic retrofitting of columns, strengthening masonry walls, and repairing reinforced concrete (Bakis et al., 2002; Meier, 2000).

Among some of the research looking into using FRP as the main load-carrying members in bridges, the Eastern Federal Lands Highway Division (EFLHD) of the Federal Highway Administration investigated using FRP composite structural shapes as truss members for the Falls Creek Trail Bridge in the Gifford Pinchot National Forest in Washington State (Wallace,

2000). In conjunction with the United States Forest Service (USFS), the EFLHD set the bar fairly high when specifying the design requirements: the design needed to be repeatable for future bridges, the bridge needed to be constructed with readily available parts, all construction materials were to be “packed” into the remote location, and consequently, could not require heavy machinery or tools for construction. Once constructed, the bridge should need little or no maintenance as well as have enough strength to support considerable snow loads during the winter seasons. The 45.5-ft (13.87-m) long pedestrian bridge was designed as a Pratt truss, which allowed for ease of duplication and expansion for other bridges. Strongwell Corporation provided the truss members and deck grating from its EXTREN product line, thus satisfying the “readily available” requirement. The construction was estimated to take two days, with the work performed by USFS personnel.

Moving from bridges designed for pedestrian traffic to those designed for vehicular traffic, Bridge 1-351 over Muddy Run Creek in Glasgow, Delaware is an all-FRP, simply-supported “sandwich” construction that spans 31.8 ft (9.7 m) [Gillespie et al., 2000]. The sandwich construction implies two FRP face sheets sandwiching a web core, where the web core consists of 893 vertical foam rectangular prisms wrapped with FRP sheets. The total weight of this FRP structure is about 10% of the weight of a traditional concrete slab girder bridge, yet Bridge 1-351 carries business traffic including light trucks. While a monitoring system has been set up to observe long-term behavioral changes in the bridge, to date, no data has been published regarding these observations.

A project designed to carry much heavier traffic is the “Tech 21” Bridge, which carries Smith Road over the Great Miami River in Butler County, Ohio (Foster et al., 2000). Designed for American Association of State Highway and Transportation Officials (AASHTO) HS-20 load requirements, the bridge spans the 33-ft (10-m) distance using a combination of U-shaped FRP composite box beams and a deck consisting of FRP trapezoidal tube sections sandwiched between two FRP composite face plates. Both the box beams and the deck components were fabricated from E-glass fibers and an isopolyester resin mix. The entire construction time took only six weeks, versus an estimated ten weeks that would have been needed for a traditional reinforced concrete structure. Furthermore, the 5-in. thick asphalt wearing surface weighed more than the rest of the entire bridge. Similar to Bridge 1-351, the “Tech 21” Bridge has sensors for

continuous monitoring; however, no updates on the bridge's performance have been published at the time of writing this report.

Like Ohio, Missouri has its own all-FRP composite bridge at the University of Missouri-Rolla (UMR) campus (Watkins et al., 2001). Although the 30-ft (9.1-m) long bridge was designed for AASHTO H20 loading and a maximum  $7/16$ -in. (11-mm) deflection, the bridge has primarily been used as a pedestrian bridge mixed with some light traffic. The design is a modular assembly of seven layers of pultruded FRP square tubes alternating in longitudinal and transverse orientations. In order to maximize material strengths and reduce costs, the bottom layer and the next-to-top layer were manufactured with carbon fibers and vinyl ester resin matrix. The remaining layers contain glass fibers and polyester resin matrix; all layers were constructed by coating each tube with epoxy on two sides and then screwing and clamping the adjoining tubes during a curing process. Placing the bridge at the site took less than 3 hours, and a fiber-optic data line has since been installed for continual monitoring of the bridge's performance. As with the other bridges, no long-term results have been published to date.

While the three previously described bridges solely comprise FRP composite materials, one idea that is gaining interest is using FRP in a hybrid fashion with traditional materials in order to best utilize each material's strength. One idea that Kitane et al. (2004) have tested is a hybrid fiber-reinforced polymer-concrete structural system. The cross-section initially comprises three glass-vinyl ester pultruded FRP trapezoidal box beams that are about 3.8 ft (1.16 m) in height. The three box beams are assembled together, with the middle box beam being inverted in relation to the two outside beams, and wrapped with an FRP laminate to create an integral superstructure. Then, the top 4 in. of the assembly is filled with a lightweight concrete. Thus, the concrete portion carries the compressive loads, the bottom portion of the FRP assembly carries the tension loads, and the web walls formed by the adjoining trapezoidal shapes take care of the shear forces, with each of the three sections being customized to work most efficiently. From small scale testing, the authors estimated that the inclusion of the concrete in this structure will help to increase flexural stiffness by 40% and could easily satisfy AASHTO live load deflection recommendations. Additional tests show excellent fatigue resistance and strength, which is eight times greater than that required by the design codes for a live tandem load. Failure at ultimate strength occurred in the concrete region, but did not lead to catastrophic collapse of the entire structure. Although this type of design still needs a full scale test as well as

a long-term field test, utilizing different materials in a hybrid structure certainly holds promise for greater efficiency in civil structures in the future.

### **1.2.3 The Toms Creek Bridge**

The Toms Creek Bridge carries Toms Creek Road over Toms Creek in Blacksburg, Virginia. In 1990, this bridge was identified as needing a complete rehabilitation. However, by 1996, the Town of Blacksburg was only looking for a temporary solution since town planners were expecting to widen the roadway within the next 15 years. At the same time, Strongwell Corporation was collaborating with Dr. Abdul Zureick of Georgia Tech in designing a new pultruded hybrid FRP double-web beam (DWB) as part of the Advanced Technology Program sponsored by the National Institute of Standards and Technology. As a part of the development process for this technology, Strongwell manufactured a prototype beam and was seeking a small demonstration project to showcase its product. Thus, the Town of Blacksburg and Strongwell had an answer for each other's needs (Hayes, 1998).

The Town of Blacksburg and Strongwell collaborated with a team of engineers and researchers from Virginia Tech, the Virginia Transportation Research Council (VTRC), and the Virginia Department of Transportation (VDOT) in rehabilitating the two-lane Toms Creek Bridge (see Figure 1-1). While the old bridge consisted of twelve steel stringers supporting transverse wood planking and asphalt, the new bridge has 24 FRP composite beams supporting a glulam deck and an asphalt wearing surface. See Figure 1-2 for a cross-sectional schematic of the bridge. Measuring 8 in. deep by 6 in. wide (200 mm by 150 mm), the beams' cross-section includes a double-web and sub-flanges, as seen in Figure 1-3. The double-web and sub-flanges aid in providing buckling, torsion, and shear deformation resistance. The pultruded FRP material itself contains a hybrid combination of glass fibers in the webs and carbon fibers in the flanges, where the carbon fibers provide a threefold increase in flexural stiffness compared to having glass fibers in the flanges. This additional flexural stiffness is a great benefit considering that designing with FRP is typically deflection-controlled. Having a fiber volume fraction of around 55%, all of the fibers are embedded in a vinyl ester resin matrix. Although the vinyl ester does not contain any UV inhibitors, the beams themselves have a sufficient amount of carbon black filler to protect against UV radiation (Hayes, 1998; Neely, 2000).

Prior to designing the Toms Creek Bridge, Michael Hayes (1998) determined that these beams have an average modulus of elasticity of 6670 ksi (45.9 GPa), which is about one-fifth

that of the original steel stringers. The lower material modulus combined with the shorter geometry of the FRP beams to result in a lower bending stiffness when compared to the original steel beams. Therefore, every steel stringer was replaced by two FRP composite beams in order to insure that the bridge would meet the AASHTO design requirements for a HS20-44 loading. The design with the FRP beams maintains the same 17.5-ft (5.33-m) span and 12.5° skew as the prior bridge (see Figure 1-4). The beams themselves are simply supported on the original concrete abutments, and are held in place by 2 x 4 pressure-treated timber sections clamping down on top of the bottom flanges through the force of anchor bolts. Likewise, the glulam deck panels are connected to the beams with bolt-tightened 2 x 4 timber sections against the bottom of the top flanges. Figure 1-5 shows a detail for the two different connections. The entire deck consists of seven glulam panels measuring 24.5 ft by 2.83 ft by 5<sup>1</sup>/<sub>8</sub> in. (7.47 m by 860 mm by 130 mm), with the longer dimension oriented transversely to the longitudinal direction of the beams. The wearing surface across the glulam deck is a 6-in. (150-mm) asphalt course (Neely, 2000).

Construction of the bridge only took four days; the bridge was opened to traffic in June of 1997. That time marked the beginning of a series of five load tests that researchers at Virginia Tech conducted every six months. The purpose of these interval tests was to determine if there were any changes in the bridge's maximum deflection, wheel load distribution, and dynamic load allowance. In addition, after fifteen months of service, two beams were replaced with fresh beams, while the extracted beams underwent tests for determining if there had been any losses in ultimate strength or stiffness. Neely reported that there was no apparent loss in either of these two properties. The latest average daily traffic (ADT) count, taken in 1996 prior to the new bridge design, is 1141, consisting of mostly small to medium-sized vehicles (R. Formica, personal communication, July 26, 2004).

#### **1.2.4 The Route 601 Bridge**

The FRP beams used in the Toms Creek Bridge were actually a prototype for 36-in. (915-mm) DWB designed by Strongwell and Dr. Zureick; Strongwell was also looking for an appropriate project for demonstrating the larger beams. In 1998, inspectors found that the Route 601 Bridge over Dickey Creek in Sugar Grove, Virginia was in "poor condition" and in need of a complete overhaul. This bridge provided a unique opportunity for engineers and researchers at

Virginia Tech, VTRC and VDOT to collaborate with Strongwell in utilizing this new technology (Waldron, 2001). The results of this collaboration can be seen in Figure 1-6.

As a preliminary design for the bridge, researchers at Virginia Tech used material properties of the 36-in. (915-mm) DWB measured through laboratory testing and a finite difference model developed by Hayes (1998). The beam had an average bending modulus of 6000 ksi (41.4 MPa) and a shear stiffness of 20 Msi-in<sup>2</sup> (89.0 MPa-m<sup>2</sup>). Assuming a 30% dynamic load allowance and the controlling load being two AASHTO HS20-44 trucks, the researchers used a deflection limit target of  $L/800$  to determine that the girder spacing would be 3.5 ft (1.1 m). Note that  $L$  is the span length of the bridge, measured in feet. Since there are no specifications for FRP beams, the engineers selected the same distribution factor specified for a steel girder, timber deck bridge, which was  $S/5$ , where  $S$  is the girder spacing. Thus, with a girder spacing of 3.5 ft (1.1 m), the wheel load distribution became 0.70, meaning that 70% of a single wheel line goes to a single girder. With this knowledge, the engineers applied both a theoretical HS20-44 and HS20-AML (Alternate Military Loading) load to a beam and determined that the beams would have sufficient bending strength for the controlling load, which was the HS20-44 loading (Waldron, 2001).

After all of the design work was complete, the plans called for eight 36-in. (1.1 m) DWB spanning 39 ft (11.9 m) from center-to-center of the supports, as shown in Figure 1-7 and Figure 1-8. The girders have a similar geometry and material composition as the beams used in the Toms Creek Bridge (see Figure 1-9). In between the girders are a set of three diaphragms: one at each end of the beams and a third one that is 1 ft off-center from midspan. Sitting on top of 2-in. (50-mm) thick neoprene pads, each girder is connected to concrete abutments by two steel angles on either side of the girder. One angle leg is perpendicular to the abutment while the other angle leg fits over an anchor bolt in the abutment and lays flush against the top of the bottom beam flange. A nut threaded onto each anchor bolt kept the angles in place. For the deck-to-girder connections, two pairs of steel double angles work to keep the deck in place. One double angle has its flange flush against the girder with its stem facing outward. Likewise, the other double angle has its flange flush against the bottom of the deck with its stem facing downward. The two stems meet in a perpendicular fashion and are bolted in place, as shown in Figure 1-10. The deck itself is a set of ten 5<sup>1</sup>/<sub>8</sub>-in. thick glulam panels, which support an asphalt wearing surface (Restrepo, 2002).

Bridge construction took nearly four months, but this time included widening the river channel and constructing new abutments. The Route 601 Bridge was opened to traffic in October of 2001 and has had an ADT count of 550 small to medium-sized vehicles per day (S. B. Buston, personal communication, July 26, 2004). Shortly after the bridge had opened, researchers at Virginia Tech performed a load test to compare the in-situ performance with the design calculations and finite element models. A second test took place eight months later in an effort to gauge the bridge's performance over time with regards to deflection, wheel load distribution, and dynamic load allowance. The Route 601 Bridge performed better than what was calculated in the design or the results of the finite element models. This performance was attributed to generally conservative assumptions in the design and material properties, including neglecting the benefits of stiffening from the timber curb and railing, as well as the partial flexural restraint provided by the bearing supports (Restrepo, 2002).

### **1.2.5 AASHTO Bridge Design Guidelines**

Currently, there are two different design principles that structural engineers use in the United States: Allowable Stress Design (ASD) and Load and Resistance Factor Design (LRFD). The ASD approach has been employed since the 19<sup>th</sup> century, when large structures were primarily constructed from steel. Steel generally has a well-documented yield point that is well below the failure stress; however, as an added precaution, engineers incorporated a safety factor into the equation such that the design loads multiplied by this safety factor would be less than the stress at yield. Hence, the name Allowable Stress Design.

However, this design philosophy was developed for a homogenous material being used in statically determinate structures. In more modern times, ASD has become less applicable in structures using complex types of materials and higher levels of redundancy. Additionally, the ASD safety factors were only applied to the loads, not to the resistance, i.e., the ultimate strength in the materials. Furthermore, these safety factors were based merely on past experience and judgment; there were no statistical measures of the risks or safety involved in the design. Thus, researchers developed a new approach that was based on the strength of the material, the variability in both the loads and the resistance to those loads, and a factor of safety that was related to probability. Hence, the name Load and Resistance Factor Design. The variability in the resistance side of the equation included uncertainty in the material properties, mathematical models used in the design, and quality control. On the other side of the equation, the variability

in the loads considered the uncertainty in the magnitude of those loads and the probability of the combination of two or more different types of loads (Barker and Puckett, 1997).

Many engineers still prefer the ASD approach to design due to its familiarity and ease of use. However, there is a big push, especially from academia, to move into the LRFD realm. Many large firms are making the switch, and many states, such as Virginia, will be training their engineers on this probability-based method. Since the two bridges in this study were designed under the ASD guidelines, both the AASHTO *Standard Specifications for Highway Design* (1996), which uses ASD, and the AASHTO *LRFD Bridge Design Specifications* (1998) will be discussed here with regards to deflection control, wheel load distribution, and dynamic load allowance.

Note that neither of these design codes deals with the topic of fiber-reinforced polymers. In the U.S., much of the focus has been on using FRP for internally and externally reinforcing concrete. The American Concrete Institute has come up with standards in these two fields. Canada and other countries in Europe have also come up with some specifications in using concrete reinforced with FRP. However, Japan has taken the global lead in providing guidance for its engineers regarding FRP (Bakis et al., 2002). In addition to The Japan Society of Civil Engineers (JSCE) formulating specifications for testing and designing with internal FRP reinforcements, they have also covered the use of FRP sheets for repairing or retrofitting bridge piers and columns. The JSCE has also devoted some resources to looking at FRP structural shapes (Ueda, 2002). Nevertheless, using FRP shapes in bridge design is by far the most neglected topic in terms of design standards (Bakis et al., 2002).

#### **1.2.5.1 Deflection Control**

Both the AASHTO *Standard Specifications* and AASHTO *LRFD Specifications* leave the topic of deflections as an optional design criterion, although currently the design codes recommend that deflection be considered when designing for service live loads and impact. In fact, some state transportation departments, such as VDOT, typically require designs to satisfy certain deflection limits. There are several reasons for limiting the deflection in a bridge. First, excessive deformations can cause damage to non-structural elements, such as cracks in asphalt wearing surfaces or concrete slabs, which can make it easier for water to reach the structural elements. Secondly, limiting the deflection is thought to control the vibrations in the bridge as a vehicle travels across it. These vibrations tend to give riders and or pedestrians the uneasy

feeling that the bridge is not safe to travel across, when in fact the bridge is structurally sound. A third reason is more for aesthetic purposes; a sagging bridge gives the perception that the bridge is near collapse and is not safe to travel under. Such public sentiment is critical in the public's view of the performance of state transportation departments.

However, there has been an ongoing debate regarding the validity of these reasons because there is little available data relating a bridge's deflection to its durability. Furthermore, the in-situ deflection in a bridge is typically less than the deflection calculated in the design because the actual deflection can be influenced by many different factors that are either ignored or at best estimated. For example, the overall stiffness of the bridge can depend on the stiffness of the deck-girder system or the edge stiffness provided by barriers and curbs along the sides of the bridge. Regarding the issue of rider comfort when traveling across the bridge, some researchers have shown that instead of comfort being dependent on the deflection magnitude, the issue is related to the acceleration of the deflection. In this case, acceleration is a function of the bridge's fundamental frequency (AASHTO, 1998). Resolution to this debate is quite important to FRP gaining wider acceptance in the design community, since designing with FRP is typically controlled by deflection limits.

Absent any consensus on the importance of deflection control, AASHTO continues to offer limits for design. In the *Standard Specifications*, these limits are discussed in Section 8.9 for reinforced concrete, Section 9.11 for prestressed concrete, Section 10.6 for steel, and Section 13.4 for bridges constructed out of timber. For bridges constructed with reinforced concrete, prestressed concrete, and steel, the deflection limits are as follows:

$$\delta \leq \frac{L}{800} \quad \text{for bridges with vehicular traffic} \quad (1-1)$$

$$\delta \leq \frac{L}{1000} \quad \text{for bridges with vehicular and/or pedestrian traffic} \quad (1-2)$$

For timber bridges, the deflection limit is:

$$\delta \leq \frac{L}{500} \quad \text{for bridges with vehicular and/or pedestrian traffic} \quad (1-3)$$

where  $\delta$  is the deflection due to the combination of a service live load and an impact factor, which is discussed in Section 1.2.5.3 of this report;  $L$  is the span length, measured in feet, from center-to-center of the supports.

The AASHTO *LRF D Specifications* have the same recommended deflection limits for reinforced concrete, prestressed concrete, and steel girder bridges, as discussed in Section 2.5.6.2.2 of the code. However, the limits for timber bridges are slightly different than those in the *Standard Specifications*:

$$\delta \leq \frac{L}{425} \quad \text{for bridges with vehicular and/or pedestrian traffic} \quad (1-4)$$

$$0.10 \text{ in.} \quad \text{relative deflection between adjacent planks or panels} \quad (1-5)$$

Note that deflection is a service limit state. Service limit states also include slenderness, flexibility, and fatigue; all of these factors can affect the lifetime performance of a bridge.

### **1.2.5.2 Wheel Load Distribution Factor, $g$**

Most bridges in the U.S. are of a slab-and-girder design. As a vehicle travels over this type of bridge, the portion of that load which a girder carries is primarily a function of the relative stiffness between the slab and the girders. In other words, a slab that is relatively flexible compared to the girders results in the girder directly beneath the load deflecting much more than any of the other girders. That amount of deflection is indicative of the amount of load the girder is carrying. On the other hand, if the slab is stiffer than the beams, then the slab tends to distribute the load in a more uniform fashion, as shown in Figure 1-11 (Barker and Puckett, 1997).

However, there are many other factors aside from this relative stiffness that can affect wheel load distribution, and consequently, the demand on a girder. Such factors include girder spacing, span length, flexural and torsional stiffness, deck properties, and bridge skew. The AASHTO *Standard Specifications* simplify such a large number of complex factors by employing the load distribution method in Sections 3.23 through 3.30. From Table 3.23.1, a load distribution factor for an interior stringer or beam is calculated as:

$$g = \frac{S}{D} \quad (1-6)$$

where  $g$  is the wheel load distribution factor,  $S$  is the girder spacing, measured in feet, and  $D$  is a variable dependent on the type of bridge and the number of traffic lanes. On the other hand, Section 3.23.2.3 states that the girder distribution factor for an exterior stringer or beam must be calculated by what is known as the “lever rule.” In this case, the deck is assumed to have hinges

at the girders, thus creating a determinate structure. From static analysis, the reaction at the exterior girder gives the load distribution factor for that girder (AASHTO, 1996).

The engineer can determine the design live load moment for each girder by positioning a load truck at the location along the girder which results in the maximum bending moment and then multiplying that moment by  $g$  from Eq. (1-6). When considering multiple-lane bridges, i.e., bridges with more than two lanes, the AASHTO *Standard Specifications* call for including a reduction factor for multiple presence. This reduction factor on the live load accounts for the probability of some or all of the lanes being loaded with a truck at the same time and at the same longitudinal location along the bridge (AASHTO, 1996).

Although easy to use, Eq. (1-6) does not always give an accurate indication of the true value for  $g$  in a bridge. For one, this formulation was developed by idealizing a bridge as an orthotropic plate free of edge stiffening and without any skew. Also, the researchers assumed that the maximum distance between a line of wheels and the outside edge of the bridge would be 3.5 ft (1.1 m). These two assumptions tend to lead to overly conservative values for  $g$ , especially when considering exterior girders. Further more, Eq. (1-6) does not consider the stiffness of the deck or the girders, or the span length of the bridge (Barr et al., 2001; Kim and Nowak, 1997).

To bring the girder distribution factor more in line with results from actual bridges, Zokaie et al. (1991) developed some refined empirical formulations for  $g$  based on girder spacing, span length, stiffness parameters, and skew. The AASHTO *LRFD Specifications* have adopted much of this work and addresses it in Section 4.6.2, where the equations used for calculating the distribution factor are in Table 4.6.2.2.1-1. Note that in order to compare the two design specifications, the engineer must divide  $g_{Std}$  by two in order to get an equivalent value for  $g_{LRFD}$ , where  $g_{Std}$  and  $g_{LRFD}$  are the girder distribution factors calculated using the AASHTO *Standard Specifications* and *LRFD Specifications*, respectively. This is because the equations in the *LRFD Specifications* are based on a “per axle” or “two wheel line” basis, whereas the Eq. (1-6) has been derived on a “per wheel line” basis.

Similar to the AASHTO *Standard Specifications*, the AASHTO *LRFD Specifications* require that the distribution factor for an exterior girder be determined using the “lever rule,” as discussed earlier. However, unlike the AASHTO *Standard Specifications*, calculations for  $g$  using the AASHTO *LRFD Specifications* do not need to account for multiple presence on a bridge. This is because that factor is implicitly included in the LRFD equations, which Zokaie et

al. developed for the most critical case in multiple-lane loaded scenarios. Still, the equations in the AASHTO *LRFD Specifications* have their limitations. In order to use these equations, the basic bridge design must match one of a handful of designs identified in the code. Also, the bridge must have a constant cross section and a minimum of four beams that have approximately the same stiffness. Furthermore, the curvature of the bridge in plan view must be small. Lastly, the roadway portion of the cantilever hanging over the exterior girder must not exceed 3 ft (915 mm) [AASHTO, 1998].

### **1.2.5.3 Dynamic Load Allowance, *IM***

As a vehicle travels across a bridge, the roadway surface is not always smooth. There may be an incongruity where the approach meets the abutment; the bridge deck might contain uneven deck joints, potholes, and patches; and the roadway itself might have rough condition before the vehicle even reaches the bridge. All of these circumstances can cause the suspension system in a vehicle to mitigate the effects of these conditions through extension and compression. When accelerating upward in extension, the suspension system increases the effective static weight of the vehicle axle by applying an “opposite” reaction force to the roadway. Hence, the term dynamic loading, or what is also called “impact” (Taly, 1998).

The AASHTO design codes account for this dynamic loading by increasing the static loading by a dynamic load allowance, or impact factor, *IM*. *IM* in the AASHTO *Standard Specifications* is addressed in Section 3.8.2, and has the formula:

$$IM = \frac{50}{L + 125} \leq 30\% \quad (1-7)$$

where *IM* is the fraction of the combination of the lane and truck load due the dynamic loading, and *L* is the span length of the bridge, measured in feet (AASHTO, 1996). Thus, the full loading during a dynamic event can be calculated as:

$$P_{\text{dyn}} = P_{\text{stat}}(1 + IM) \quad (1-8)$$

where  $P_{\text{dyn}}$  is the dynamic loading,  $P_{\text{stat}}$  is the static load of the vehicle, and *IM* is expressed in a decimal format (Barker and Puckett, 1998).

This dynamic effect can be affected by a number of factors such as: the aforementioned surface conditions, the dynamic characteristics of both the load truck and the bridge, simple span versus continuous span, vehicle speed, vehicle mass, the number of axles, and even the vehicle’s

tire pressure (Laman et al., 1997). However, the development of Eq. (1-7) was based on load tests performed on railroad bridges. Typically, the impact factor on highway bridges is less than 30%, but other studies found that in actuality, there is wide variability in *IM*. Some results even exceeded a dynamic load allowance of 2.0, particularly for short-span bridges (Taly, 1998).

The AASHTO *Standard Specifications* dictate that Eq. (1-8) is only applicable to straight bridges. Also, all forces due to dynamic loading must be included in the loads applied to all substructural elements. On the other hand the AASHTO *LRFD Specifications* state that *IM* need not be applied to retaining walls that are not subjected to vertical forces from the superstructure, nor to any portions of the foundation that are entirely below grade (AASHTO, 1998).

The AASHTO *LRFD Specifications* list the *IM* values in Section 3.6.2. Unlike Eq. (1-7), which determines the dynamic load allowance solely on the span length, the *IM* in the *LRFD Specifications* is based on the type of bridge component and the design limit:

Deck joints (all limit states)	75%
All other components	
Fatigue and Fracture Limit State	15%
All other limit states	33%

These impact factors already have the lane loading factored in; therefore, only the truck loads are factored by the *IM* values listed above. Additionally, when designing for timber structures, the dynamic load allowances listed above may be reduced by 50% due to the high damping nature of wood (AASHTO, 1998).

When testing in the field for dynamic load allowance, this value is typically based on either strain or deflection measurements and is computed as:

$$IM = \frac{R_{dyn}}{R_{stat}} - 1 \quad (1-9)$$

where  $R_{dyn}$  is the measured quantity during dynamic loading and  $R_{stat}$  is the measured quantity during static loading. Using Eq. (1-9) generally results in the *IM* for a bridge decreasing with the weight of the truck because the truck's dynamic effect remains fairly constant while the deflection during static loading increases. While the normal instinct might be to find the largest possible dynamic load allowance, using a heavily-loaded truck is satisfactory because the goal is to determine the highest possible moment or shear demand on the bridge. Having a much larger

static load with a slightly smaller impact factor, vis-à-vis a load truck, will help obtain that design load (Barker and Puckett, 1997).

### 1.3 Scope and Objectives of This Study

The Toms Creek Bridge and the Route 601 Bridge are pioneer designs that use double-web beams as the main load-carrying structural components in a bridge. At the completion of construction, Neely and Restrepo performed live load tests to assess the respective bridges' performance. This study serves as a continuation of their work and to monitor the two bridges after an extensive period of actual in-situ loading conditions.

In doing so, this research has conducted an additional load test on each bridge. The test for Toms Creek Bridge is the sixth experiment conducted, and took place six years after the bridge opened to traffic. The test for the Route 601 Bridge is the third in a series of tests, and took place two years after construction was completed. Each load test considers both the peak strain and deflection in the girders as a load truck crossed the bridge. Lastly, an in-depth inspection for each bridge will give an added assessment on the health of these two bridges.

The foremost objectives for this research are to determine the following performance characteristics in each bridge:

- service strains
- service deflections
- wheel load distributions,  $g$
- dynamic load allowances,  $IM$

Secondly, this study will compare the results of the latest tests for the Toms Creek Bridge and the Route 601 Bridge with the results that Neely and Restrepo achieved in their research. These comparisons will help to learn whether or not there has been any significant change in the behavior of either of these two bridges over time. Any changes can give some indication about the long-term durability of FRP.

Additionally, this project will compare the results from the entire series of load tests for each bridge with those requirements established for more traditional bridge designs in the *AASHTO Standard Specifications* and *LFRD Specifications*. As noted in Section 1.2.5, there are no guidelines for using FRP as the main load carrying element in a bridge. This research hopes to take a step toward filling that void.

Lastly, this thesis will detail three field inspections at the two bridges. The purpose of these inspections is to serve as an additional system for monitoring the conditions of the Toms Creek Bridge and Route 601 Bridge.

## 1.4 Figures



(a)



(b)

**Figure 1-1.** View of the Toms Creek Bridge looking (a) at the upstream elevation, and (b) toward the northbound approach.

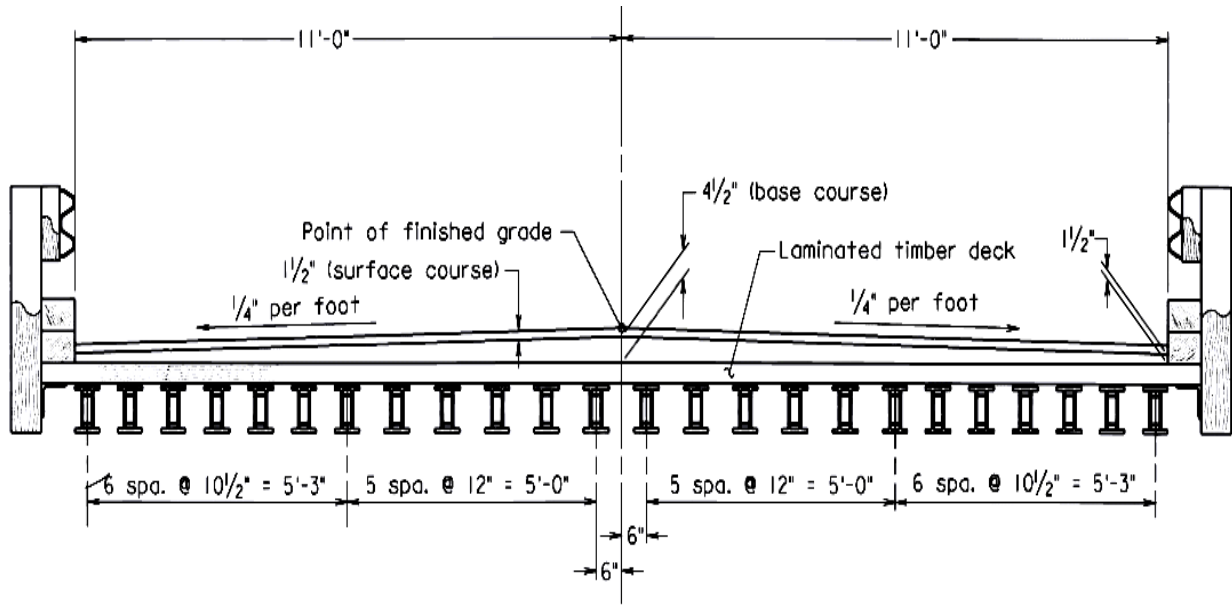


**Figure 1-2.** Toms Creek Bridge cross-section (Neely, 2000).

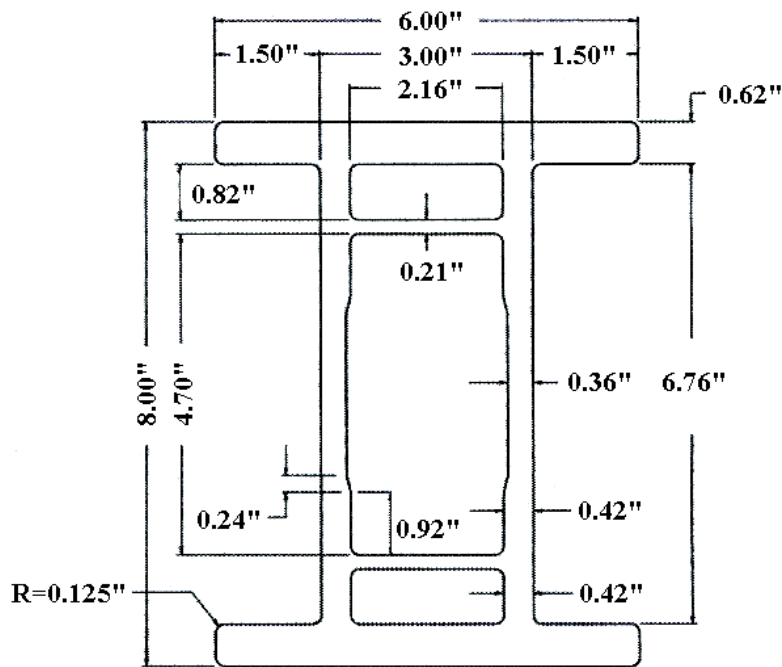


**Figure 1-3.** Cross-section of the 8-in. FRP composite DWB used in the Toms Creek Bridge (Neely, 2000).

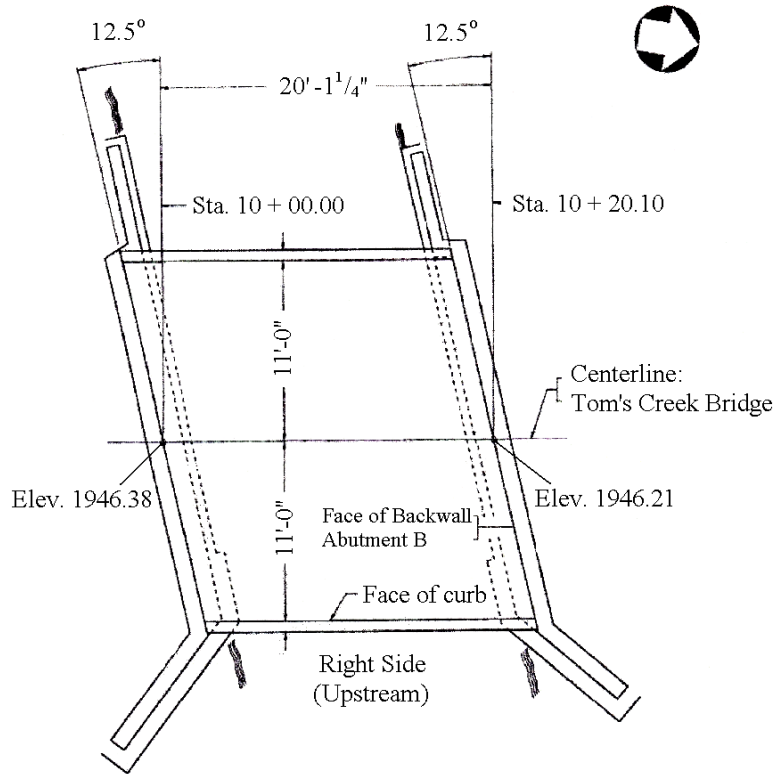


**Figure 1-4.** Plan view of the Toms Creek Bridge (Neely, 2000).

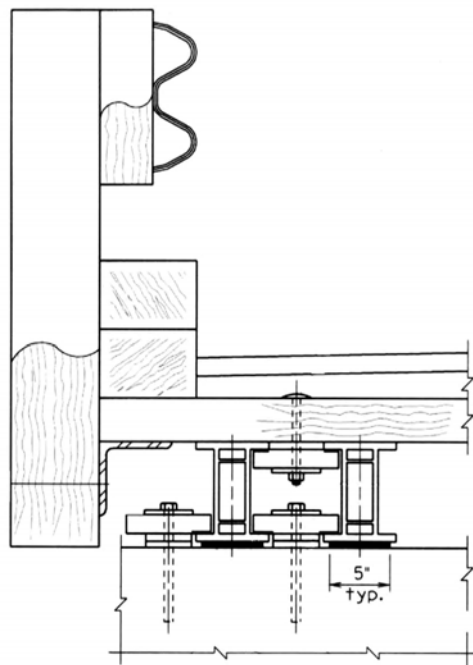


**Figure 1-5.** Detail of girder-to-abutment and deck-to-girder connections (Neely, 2000).



(a)



(b)

**Figure 1-6.** View of the Route 601 Bridge, looking (a) at the upstream elevation, and (b) toward the eastbound approach.

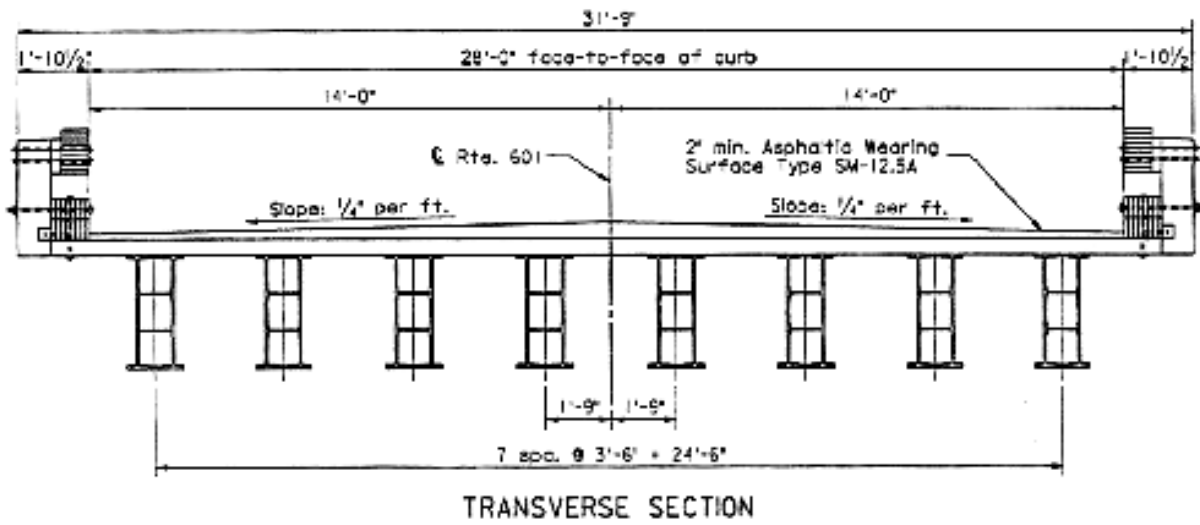


Figure 1-7. Cross-sectional view of the Route 601 Bridge (Restrepo, 2002).

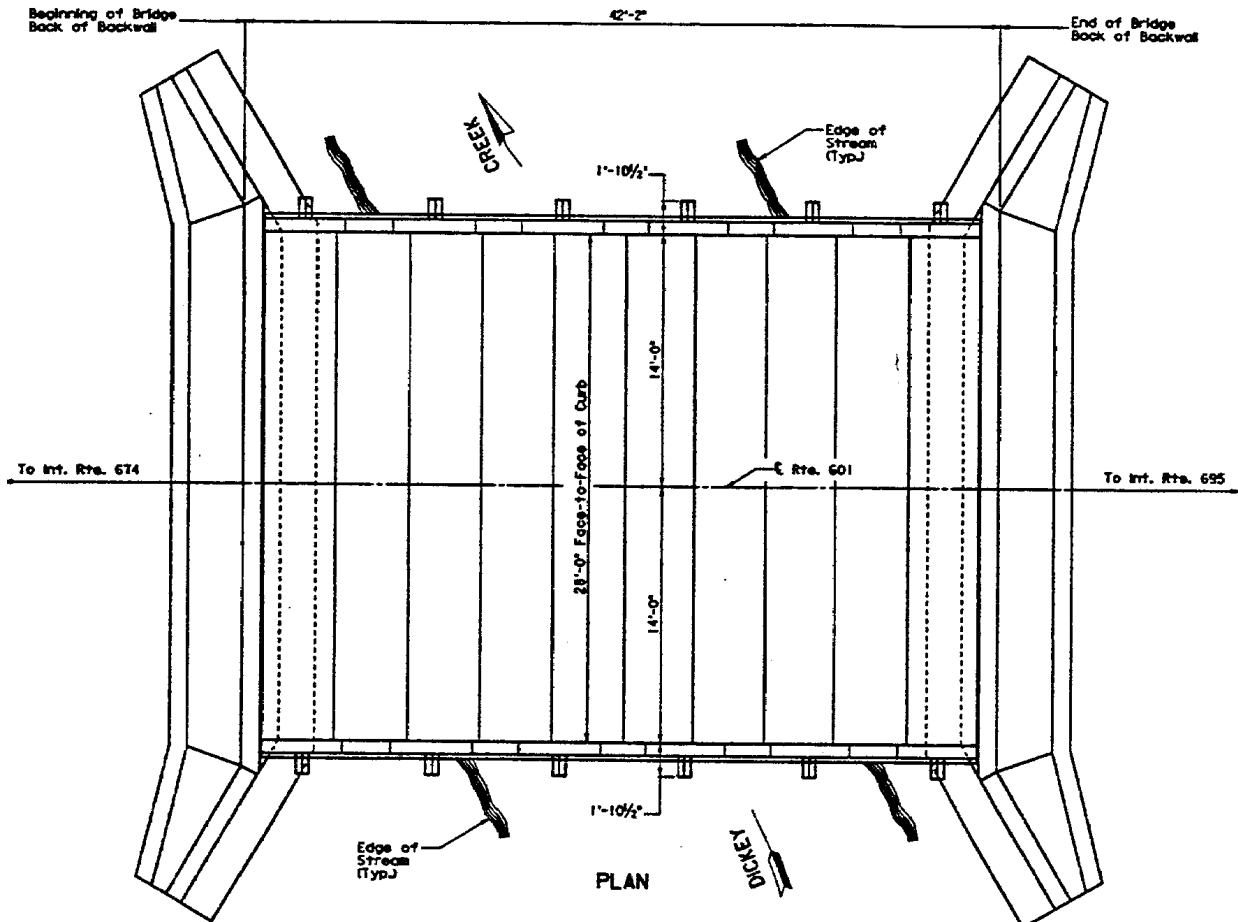
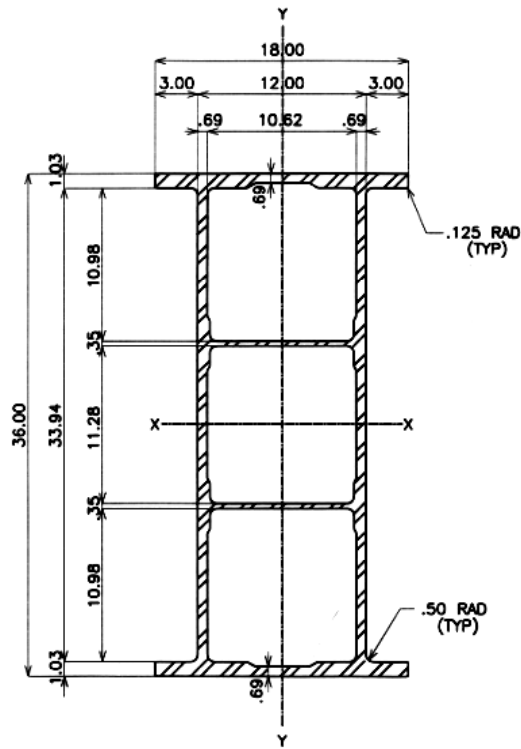
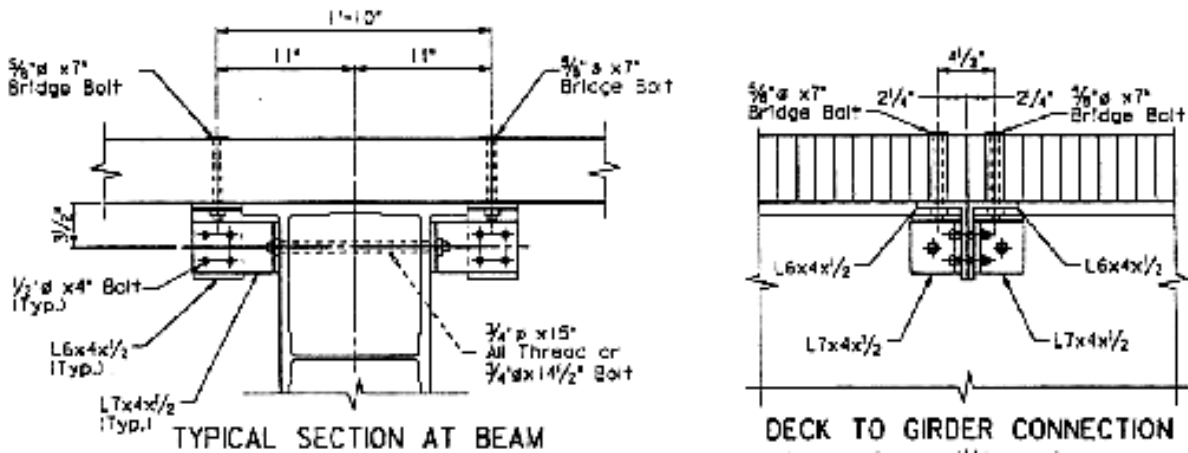


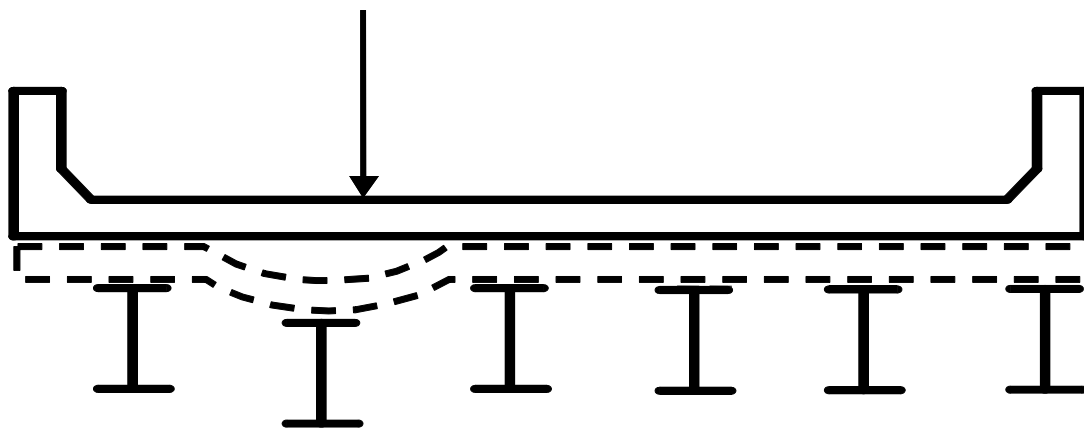
Figure 1-8. Plan view of the Route 601 Bridge (Restrepo, 2002).



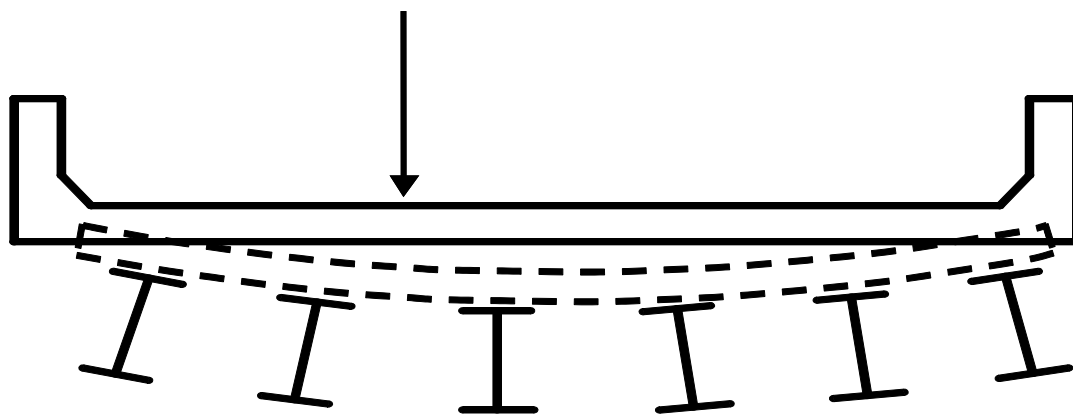
**Figure 1-9.** Cross-section of the 36-in. (1.1-m) DWB used in the Route 601 Bridge (Waldron, 2002).



**Figure 1-10.** Deck-to-girder connection for the Route 601 Bridge (Restrepo, 2002).



(a)



(b)

**Figure 1-11.** Visualization of relative stiffness between slab and girder, where (a) the slab is not stiff, and (b) the slab is very stiff compared to the supporting girders (Barker and Puckett, 1997).

## Chapter 2: Experimental Procedure

### 2.1 Bridge Instrumentation

In order to determine the girder distribution factors, dynamic load allowances, and deflections, both the Toms Creek Bridge and Route 601 Bridge were instrumented with quarter-bridge strain gages and deflectometers at midspan. For the Toms Creek Bridge, only a select number of the beams were instrumented because of the large number of beams versus the relative few number of available deflectometers and the extensive time that would be involved in placing strain gages on all 24 beams. Unlike the Toms Creek Bridge, all of the girders in the Route 601 Bridge had gages and deflectometers at midspan. For both bridges, gages measuring axial strain were on only two of the girders, because all previous testing showed axial strain to be negligible. See Figure 2-1 and Figure 2-2 for a sketch of the instrumentation layout for the two bridges.

#### 2.1.1 Strain Gages

Micro-Measurements Group, located in Raleigh, North Carolina, manufactured the strain gages used in all of the tests. These quarter-inch gages had a nominal resistance of 350 ohms and a gage factor of 2.11. Prior to adhering a strain gage to a beam, the beam's surface was sanded smooth with a 200-grit silicon-carbide paper. After all the sanding residue was removed with Micro-Measurements' M-Prep Conditioner, the beam surface was prepared for bonding with the gage using Micro-Measurements' M-Prep Neutralizer. A combination of M-Bond 200 catalyst and M-Bond 200 adhesive worked to bond the gage to the beam.

Once the strain gage had properly adhered to the beam, lead wires from a cable were soldered to the gage. The cable wire used in all of these tests was a "special purpose audio communication and instrumentation cable," manufactured by Belden Inc. This cable had two pairs of plastic-coated wires wrapped in foil, with a fifth exposed ground wire.

After soldering the lead wires, the strain gage instrumentation was weatherproofed using Micro-Measurements' M-Coat F protection kit. This protection consisted of coating the exposed portions of the lead wire and the strain gage with M-Coat D, followed by a layer of neoprene rubber, butyl rubber, and aluminum tape. Finally, a double coating of nitrile rubber sealed the edges of the aluminum tape. The neoprene rubber provided some impact protection should

anything hit the gage connection; the butyl rubber, aluminum tape, and nitrile rubber helped to provide protection against moisture.

As mentioned before, the strain gages measured both flexural and axial strain. The flexural strain gages were located at midspan of each beam, and were placed on the bottom of the bottom flanges, centered across the flange width. The axial strain gages were only located at one abutment (the south abutment for the Toms Creek Bridge and the west abutment for the Route 601 Bridge). These axial gages were placed at the mid-height of the web, 12 in. and 3 ft (305 mm and 910 mm) away from the center of the support, for the Toms Creek Bridge and Route 601 Bridge, respectively. Except for Girder 12 in the Toms Creek Bridge, which had axial gages on both sides of the beam, all axial gages were placed on the upstream side of the beam.

### **2.1.2 Deflectometers**

Since the FRP behavior is highly influenced by shear effects, flexural strain gages may not give an accurate indication of the load distribution during testing. On the other hand, deflectometers can directly measure both flexural and shear deflections in the beams, as well as help calculate the wheel load distributions and dynamic load allowances. The disadvantage to deflectometers is that their accuracy was somewhat limited when testing in the field. With all things considered, the deflectometers serve as a comparison to the measurements recorded from the flexural strain readings.

The deflectometers used for testing the Toms Creek Bridge and the Route 601 Bridge were a home-grown variety, produced at Virginia Tech. Essentially, a deflectometer consisted of a full-bridge set of gages on a lever arm that was held in place by two plates. The lever arm was a  $\frac{1}{8}$ -in. (3 mm) thick aluminum plate that extended  $12\frac{1}{2}$  in. (320 mm) beyond the edge of the other two plates holding it in place. This lever arm was 4 in. (100 mm) wide at the edge of the plates and tapered down to 1 in. (25 mm) at its tip. Located at the tip was an eye hook which served to deflect the lever arm, as explained later.

The two base plates that sandwiched the lever arm were also made of aluminum, and generally measured  $6\frac{1}{8}$  in. by 4 in. by  $\frac{3}{8}$  in. (155 mm by 100 mm by 10 mm). For the Route 601 Bridge, the bottom plate was 18 in. (460 mm) long, for the purposes of being able to clamp the deflectometers to the bottom of the beams. Three bolts kept the two base plates in place with the lever arm; two were located at the edge from which the lever arm extended, and the third bolt was on the opposite edge of the plates.

For measuring the deflection, a full-bridge set of strain gages was placed near the base of the lever arm, with two gages positioned perpendicularly to each other on both sides of the lever arm. The gages were protected in the same manner as described in Section 2.1.1. The wires leading from the strain gages were grouped into a connector, which was used to hook up a cable that extended to a data acquisition system.

In the field tests, each deflectometer was placed against the bottom of the bottom flange of a beam. The deflectometer was situated with the base of the lever arm as close as possible to the beam's midspan without causing interference with the flexural strain gage and all of its weather protection. Four C-clamps at the flange edges tightened the base plates to the beam. Before testing commenced, each deflectometer was pre-deflected approximately 1-in. (25 mm) away from the beam. This deflection was held in place by 20-gauge wire extending vertically downward from the eyehook at the lever arm's tip to a concrete-filled cinder block that sat in the creek bed. The cinder block was designed to be heavy enough so that the lever arm's position would be fixed relative to the creek bed. As a load caused a beam to deflect, the relative distance between the lever arm and beam would change, thus allowing for a direct measurement in the beam's deflection. See Figure 2-3 and Figure 2-4 for a photo of the deflectometers used for the Toms Creek Bridge and Route 601 Bridge.

## **2.2 Data Acquisition**

All of the cable wires coming from the strain gages and deflectometers were connected to the Megadac Series 3108 Data Acquisition System, which was a portable system developed by Optim Electronics. Optim Electronics also developed its own Test Control Software (TCS) to serve as an interface between the Megadac and a personal computer run by an Intel Pentium processor. Using TCS, the acquisition system was programmed to collect measurements at a rate of four hundred times per second. After each test, TCS transferred the strain and deflection measurements gathered by the Megadac onto a personal computer's hard drive. After all testing was complete, this same software converted the information into ASCII format, which enabled Microsoft's Excel software to import the data for analysis. All of the equipment used for gathering the data was stored in a van that was parked approximately 50 ft to 100 ft (15 m to 30 m) away from either bridge. A portable generator supplied all of the necessary power, but was positioned away from the van so as to minimize electronic noise that might interfere with the

measurements taken during testing. Prior to the start of field testing at each bridge, the cable wires from all of the strain gages and deflectometers were connected to the Megadac and confirmed to be working properly.

### 2.3 Calibrations

Prior to being used in the field, the deflection in each deflectometers needed to be calibrated. Each deflectometer was hooked up to the Megadac with a cable wire. Large-scale calipers measured pre-determined deflections of 1 in., 1<sup>1</sup>/<sub>2</sub> in., and 1/2 in., in that order. The sensitivity (in mV/in.) for each deflectometer was adjusted for the Megadac using TCS until the read-out displayed a deflection that was accurate to the nearest 0.001 in. at each of the three pre-determined levels of deflection.

Because the gages used to measure the deflections, as well as those gages used for flexural and axial strains, were covered with weather protection, shunt calibrations on these instruments just prior to the field tests were not practical. Therefore, after all of the field testing was complete, a calibration test was done in the laboratory.

Although the resistance for the strain gage in the calibrator could be set to 350 Ω, which is the same resistance in the gages used for testing, the gage factor for the strain gage in the calibrator was 2.0, whereas the gage factor for the gages used on the bridges was 2.11. Therefore, the data calibration was more than a simple matter of comparing the known strain input from the calibrator with the strain recorded by the Megadac. From the literature provided by Micro-Measurements Group, the gage factor can be calculated by the equation:

$$GF = \frac{\Delta R / R}{\varepsilon} \quad (2-1)$$

where  $GF$  is the gage factor,  $\Delta R$  is the change in resistance,  $R$  is the resistance, and  $\varepsilon$  is the strain applied to the gage.  $\Delta R$  should be the same for lab calibration tests and the field tests. Thus, any adjustments that needed to be made to the field data could be based on the error in the change in resistance measured in the lab calibration tests.

Since the gage factor, strain, and resistance coming from the strain calibrator were known, the theoretical  $\Delta R$  could be calculated. Once  $\Delta R$  was determined, one end of a 75-ft long cable wire was connected to the strain calibrator, while the other end was connected to a given

channel in the Megadac data collector. The cable length was a typical length of cable used in both of the field tests. With a known amount of strain coming from the strain calibrator, the strain measured by the Megadac was recorded. This recorded strain was then used in Eq. (2-1) along with the gage factor and resistance of the field strain gages, to calculate the experimental  $\Delta R$ . The percentage error between the experimental  $\Delta R$  and the theoretical  $\Delta R$  is the amount by which the field data was increased or decreased, depending on the direction of the error.

Using the same 75-ft cable, this procedure was repeated for all of the channels that were used on the Megadac. Out of the 34 channels used, eight had a value for  $\Delta R$  that was about 3% below the theoretical value. Therefore, the recorded data coming through these eight channels was multiplied by a factor of 1.03. The remaining channels had an error that was less than 1% below the theoretical value, which was not considered significant enough to warrant any change in that portion of the data.

## **2.4 Field Tests**

### **2.4.1 Toms Creek Bridge**

Testing for the Toms Creek Bridge took place on the morning of July 30, 2003; the temperature that morning was constant at 66 F (19 C), and the skies were overcast. Around 7:30 a.m., a three-axle VDOT dump truck arrived filled with gravel provided by a local rock quarry. The staff from the quarry weighed the dump truck after loading the gravel. The dump truck had a gross weight of 50.1 kips (223 kN), which was just over the 50.0-kip weight limit for a three-axle truck whose outer axles are not more than 19 ft apart (*Motor Carrier Service Operations*, 2000). By weighing the dump truck with all three axles on the scale, and then with only the rear tandem axles on the scale, the quarry operators were able to determine that about 35% of gross vehicle weight went to the front axle and 65% went to the rear tandem axles. The truck's axle dimensions were measured upon arrival at the bridge site. See Figure 2-5 for a sketch showing the basic axle dimensions and weight distribution of the VDOT dump truck. VDOT also provided a traffic safety control crew to allow for safe operation on the bridge and to prevent any additional load from being on the bridge while an individual load test was occurring.

Load testing involved three basic truck orientations: the northbound lane, southbound lane, and center of the bridge. The northbound lane is on the upstream side of the bridge. For

purposes of this test, the exterior girder on the upstream side of the bridge was designated as Girder 1, while Girder 24 was the designation for the exterior girder on the downstream side. In orienting the north and southbound lanes, the truck was positioned so that the center of the wheel line adjacent to the outside edge of the respective lane was 32 in. (610 mm) away from the outside edge of the timber deck. For the center orientation, the truck was positioned such that the center of the axle was directly over the center of the bridge's width. These orientations were in accordance with those used by Neely in order to make comparisons of the bridge's behavior over time.

All three truck orientations were driven at 2 mph and 40 mph (3 kph and 64 kph). The 2 mph speed was essentially the slowest the truck could go without exhibiting any jerking motion. This speed served the purposes of applying a static load to the bridge. Although the posted speed limit for the road was 35 mph (56 kph), the maximum test speed was set at 40 mph (64 kph) for the purposes of simulating extreme conditions. In addition to these two speeds, the southbound lane orientation was also tested at 25 mph (40 kph). This intermediate speed was used in examining the effects of speed on the three characteristics under study: wheel load distribution, dynamic load allowance, and deflection.

In his research, Neely considered the effects of composite action on the Toms Creek Bridge's performance. To do so, Neely tightened the deck-to-girder connections as well as the connections at the abutments prior to testing. However, Neely concluded that there was "no increase in stiffness due to tightening of the composite connections." Aside from that conclusion, one goal in using FRP composites in bridges is to reduce life-cycle costs by reducing maintenance costs. Following the assumption of maintenance cost-reduction, this research did not assume that maintenance will be regularly scheduled for tightening the connections in future FRP structures. Hence, this study simply considered the bridge's "as-is" performance.

Each combination of orientation and speed was tested five times. For all tests in the north and southbound lane orientations, the dump truck traveled in the direction of travel for the given lane. When in the center orientation, the dump truck traveled in the north direction. See Table 2-1 for a test log showing the numbered data sets with the accompanying orientations and speeds.

## 2.4.2 Route 601 Bridge

Testing for the Route 601 Bridge took place on the morning of October 14, 2003; the temperature that morning remained fairly constant at about 60 F (16 C), and the skies were mostly cloudy. A local hauling company provided two three-axle dump trucks filled with gravel that arrived around 7:30 a.m. Similar to what was done for the Toms Creek Bridge tests, the staff from a local rock quarry that provided the gravel weighed the dump trucks after loading the gravel. The first dump truck, designated as T4, had a gross weight of 55.1 kips (245 kN), with about 30% of gross vehicle weight going to the front axle and 70% going to the rear tandem axles. The second dump truck, designated as T5, had a gross weight of 55.2 kips (246 kN), with about 28% of that weight going to the front axle and 72% going to the rear tandem axles. These gross vehicle weights were 9% and 10% (for truck T4 and T5, respectively) above the allowable weight according to the *Motor Carrier Service Operations* guidelines (2000). Axle dimensions were measured upon arrival at the bridge site. See Figure 2-6 and Figure 2-7 for sketches showing the basic axle dimensions and weight distributions of the two trucks. VDOT provided a traffic safety control crew to allow for safe operation on the bridge and to prevent any additional load from being on the bridge while an individual load test was occurring.

Load tests for the Route 601 Bridge involved six basic truck orientations: the east exterior girder, east interior girder, center of the bridge, west interior girder, west exterior girder, and multiple-lane loading (see Figure 2-8 and Figure 2-9 for a pictorial description of the respective exterior and interior orientations). Girders designated as “east” support the travel lane going in the eastbound direction; likewise, girders designated as “west” support the travel lane going in the westbound direction. The west half of the bridge is on the downstream side of the bridge. For purposes of this test, the west exterior girder was designated as Girder 1, while the east exterior girder was designated as Girder 8. For the exterior orientations, a single truck was positioned so that the center of the wheel line adjacent to the outside edge of the respective travel lane was bearing directly along the centerline of the exterior girder (i.e., 32.5 in. [825 mm] from the edge of the timber deck). For the interior orientations, a single truck was positioned so that the center of the wheel line adjacent to the outside edge of the respective travel lane was bearing directly along the centerline of the first interior girder next to the exterior girder. The center orientation had the truck positioned such that the center of the axle was directly over bridge’s longitudinal centerline. Lastly, the multiple-lane loadings used two dump trucks, one in each

travel lane. Both trucks had their exterior wheel lines aligned with the centerline of the respective exterior girders. These orientations were in accordance with those used in Restrepo's research in order to make comparisons of the bridge's behavior over time. Note that Truck T5 was only used in the multiple-lane and east interior orientations at static speed.

All six truck orientations were driven at 2 mph (3 kph), otherwise known as "static" speed. However, only the interior and center lane orientations could be conducted at the elevated speeds of 25 mph and 40 mph (40 kph and 65 kph). As with the Toms Creek Bridge, the posted speed limit for the road was 35 mph (56 kph), but the maximum test speed was set at 40 mph (64 kph) for the purposes of simulating extreme conditions. Exterior and multiple-lane orientations could not be tested at the higher speeds because the bridge was slightly wider than the roadway, making it unsafe for the truck driver to transition from the road to the bridge and back while driving directly over the exterior girders. The rationale behind using the aforementioned speeds is the same as that described in the Toms Creek Bridge tests.

In his June 2002 tests, Restrepo also tested several orientations at 15 mph (25 kph). His reasoning for doing so was because of the apparent "uplift" effect he observed while analyzing the dynamic loading data from his October 2001 tests. Restrepo's hypothesis was that this uplift was due to settlement at both abutments, which would cause a fast-traveling truck to "ramp up" as it crossed the bridge joint. According to Restrepo, this ramping action would result in preventing the full load of the dump truck from bearing down on the surface as the vehicle traversed the bridge. Thus, Restrepo added the additional 15 mph speed to his June 2002 tests in order to quantify this ramping effect. However, just prior to the October 2003 tests, VDOT attempted to level the approaches with the bridge by patching the settled areas with asphalt. Therefore, tests at the additional speed were not necessary for the current study.

Each combination of orientation and speed was tested five times, except for the west interior – 25 mph combination, which was tested six times. Unlike the Toms Creek Bridge tests, the direction that the dump truck traveled did not necessarily correspond to the direction of the travel lane. See Table 2-2 for a test log showing the numbered data sets with the accompanying orientations and speeds.

For both the Toms Creek Bridge and Route 601 Bridge tests, chalk lines were drawn on the roadway to mark where the truck needed to be positioned for each test. During the static speed tests, a researcher was able to stand in front of the dump truck and guide the driver so that

the appropriate wheel line was going directly over the proper chalk line. For obvious reasons, researchers were not able to stand in front of the dump truck during the 25 mph and 40 mph load tests. However, the driver had sufficient experience with positioning the dump truck in the roadway and achieved a relatively good degree of consistency while driving across the bridge at the higher speeds.

Restrepo's research considered the diaphragm effects on bridge behavior. In his analysis, Restrepo observed increased local strain at the diaphragm locations when the diaphragms were removed versus when they were in place. However, he also concluded that removing the diaphragms had minimal effect on the on the girder distribution factors for the overall bridge system. Thus, diaphragm effects were not considered in the current study.

## **2.5 Data Organization**

After the field tests were complete, TCS converted the data files into ASCII format for ease of data analysis in Microsoft Excel. Individual tests were grouped according to truck orientation and speed. Because the Megadac sampled the measurements four hundred times per second and typical static tests (i.e., approximately 2 mph [3 kph]) lasted up to 20 s and 40 s for a Toms Creek Bridge test and a Route 601 Bridge test, respectively, files from the static tests had a lot of data that made Excel quite unwieldy for analysis. Therefore, the data files for all of the static tests were "filtered" using a MATLAB program. This program retained every seventh data point from the Toms Creek Bridge files, which resulted in a time step of 0.015 s. For the Route 601 Bridge files, the MATLAB program took every ninth data point, which resulted in a time step of 0.0225 s. The decision on how many data points to filter out was arbitrarily made for the purposes of making the files a manageable size in Excel. These filtered files for the static tests were then imported into Excel for analysis along with the data for the other speeds. For a comparison of the filtered versus unfiltered static data, see Figure 2-10. Note that the filtered data in Figure 2-10 has been offset by +20  $\mu\epsilon$  for the purposes of comparison with the unfiltered data. None of the 25 mph or 40 mph (40 kph or 64 kph) tests needed to have the data filtered because the files were small enough for use in Excel.

Data from both bridges exhibited a fair amount of fluctuation when going from time step to time step. This fluctuation was probably due to electronic noise from the generator used to power the electronic equipment, as well as an electric transformer located at the Toms Creek

Bridge. The noise in the Toms Creek Bridge was about  $\pm 10 \mu\epsilon$ , and was about  $\pm 5 \mu\epsilon$  during the Route 601 Bridge test. To smooth out the fluctuations due to noise, a ten-point floating average was calculated for each time step and the corresponding strain and deflection measurements.

In addition to the noise that was present, the readings from the strain gages and deflectometers were not necessarily balanced to zero on the Megadac prior to the start of any individual test. Therefore, the data was zeroed out in the analysis by calculating the average measurement for each strain gage or deflectometer during the first one-half second of recording, and subtracting that average measurement from each data point for the corresponding gage or deflectometer. This half-second time frame is a period when there was no load present on the bridge. See Figure 2-11 for a typical comparison of smoothed data versus unsmoothed data, along with the effect of zeroing the data.

## **2.6 Data Reporting**

The numbers reported in the tables in the following chapters are listed to the nearest microstrain for strain measurements and to the thousandth of an inch for deflection. While the strain gages can measure with such accuracy and deflectometers have been calibrated accordingly, there is no illusion that the results from the field tests hold this level of accuracy. Uncertainties regarding the actual placement of the strain gages and deflectometers, electronic noise due to the electric generator, weight and positioning of the load trucks, approach conditions, temperature effects, and a myriad of other factors can undermine the accuracy of these measurements.

However, the true uncertainty in these values is unknown. While using three significant figures (in the case of reporting deflection measurements) may be overzealous, sticking with only two significant figures is probably too conservative. For instance, the deflection measurements could be reported to the nearest five-thousandths of an inch with a relative degree of confidence. However, for the ease of analysis in Microsoft Excel, the data has been kept in the format described above. Likewise, the results given in the main body of this thesis also have the same number of significant figures, for the ease of matching these results with their corresponding table references.

## 2.7 Tables and Figures

**Table 2-1.** Test log for the Toms Creek Bridge. Data Set #1 was an initializer, so no data was recorded. Data Set #29 was discarded due to improper truck alignment.

Data Set Number	Orientation	Nominal Speed (mph)	Travel Direction
2 - 6	Northbound	Static	North
7 - 11	Center	Static	North
12 - 16	Southbound	Static	South
17, 19, 21, 23, 25	Northbound	40	North
18, 20, 22, 24, 26	Southbound	40	South
27, 31, 33, 35, 37	Center	40	North
28, 30, 32, 34, 36	Southbound	25	South

**Table 2-2.** Test log for the Route 601 Bridge tests. Data sets that do not appear were discarded due to errors in using the TCS software.

Data Set Number	Orientation	Nominal Speed (mph)	Truck	Travel Direction
3 - 7	West exterior	Static	T4	West
8 - 12	Multiple lane	Static	T4 (West) & T5 (East)	West
13 - 17	East exterior	Static	T5	West
18, 20, 22	West interior	Static	T4	West
19, 21	West interior	Static	T4	East
24, 26, 28	East interior	Static	T4	East
25, 27	East interior	Static	T4	West
29, 31, 33, 45, 47, 49	West interior	25	T4	West
30, 32, 46, 48, 50	East interior	25	T4	East
34, 36, 39, 41, 43	West interior	40	T4	West
35, 37, 40, 42, 44	East interior	40	T4	East
51, 53, 55	Center	Static	T4	West
52, 54	Center	Static	T4	East
56, 58, 60	Center	40	T4	East
57, 59	Center	40	T4	West
61, 63	Center	25	T4	West
62, 64, 66	Center	25	T4	East

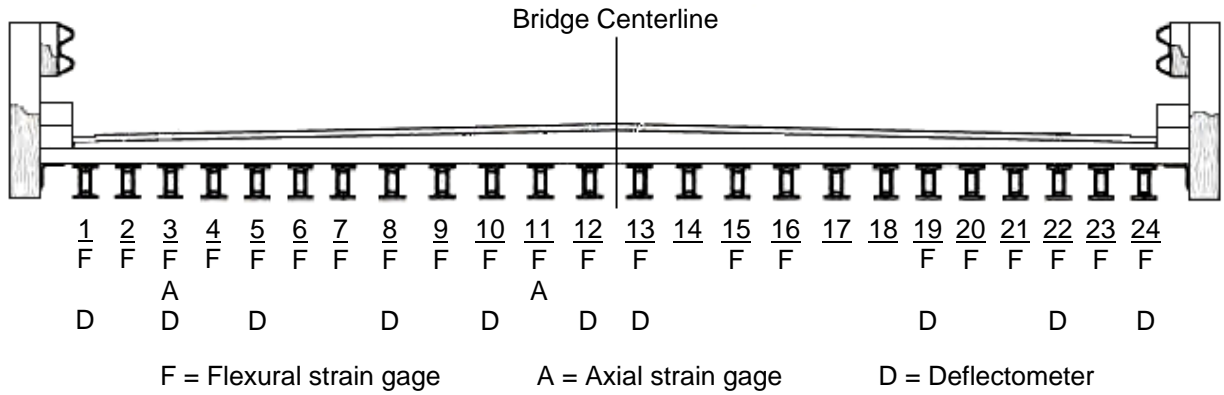


**Figure 2-1.** Instrumentation for the Toms Creek Bridge; cross-section is looking in the south direction (Neely, 2000).

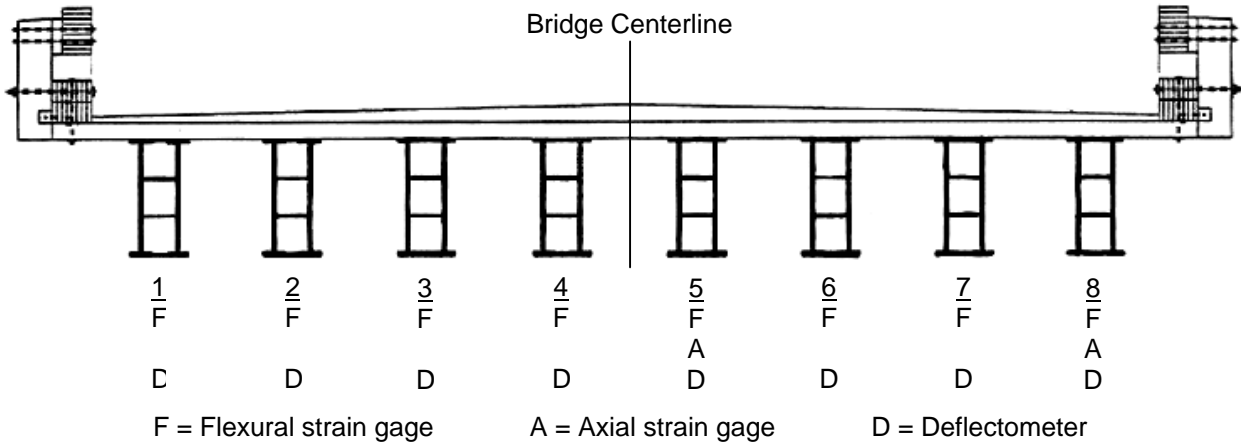


**Figure 2-2.** Instrumentation for the Route 601 Bridge; cross-section is looking in the east direction (Restrepo, 2002).

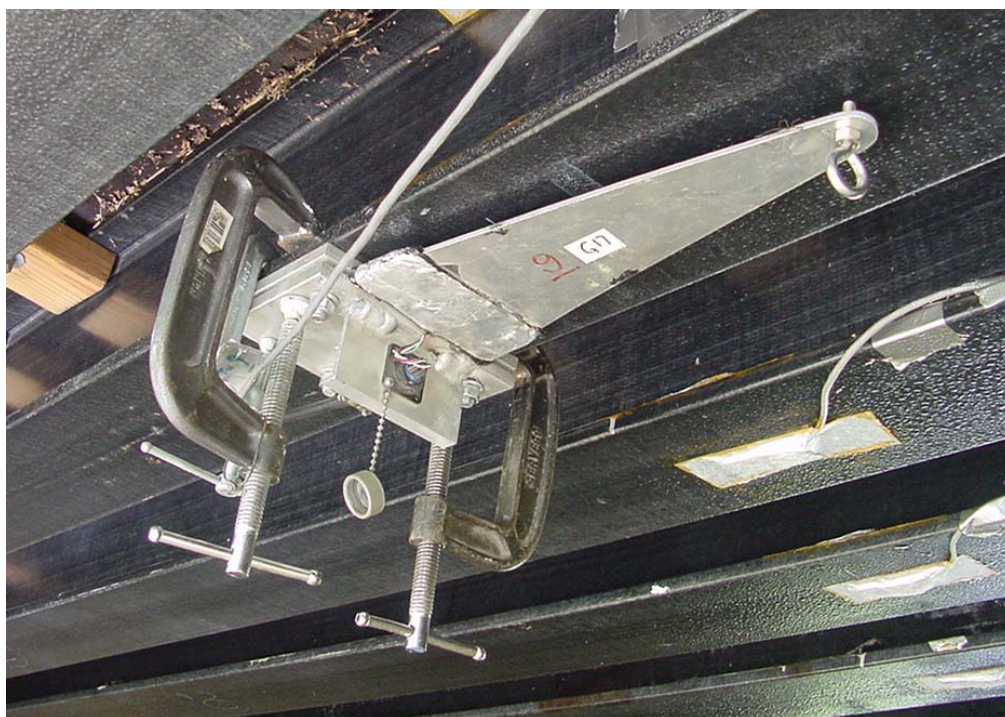


**Figure 2-3.** Deflectometer for the Toms Creek Bridge.

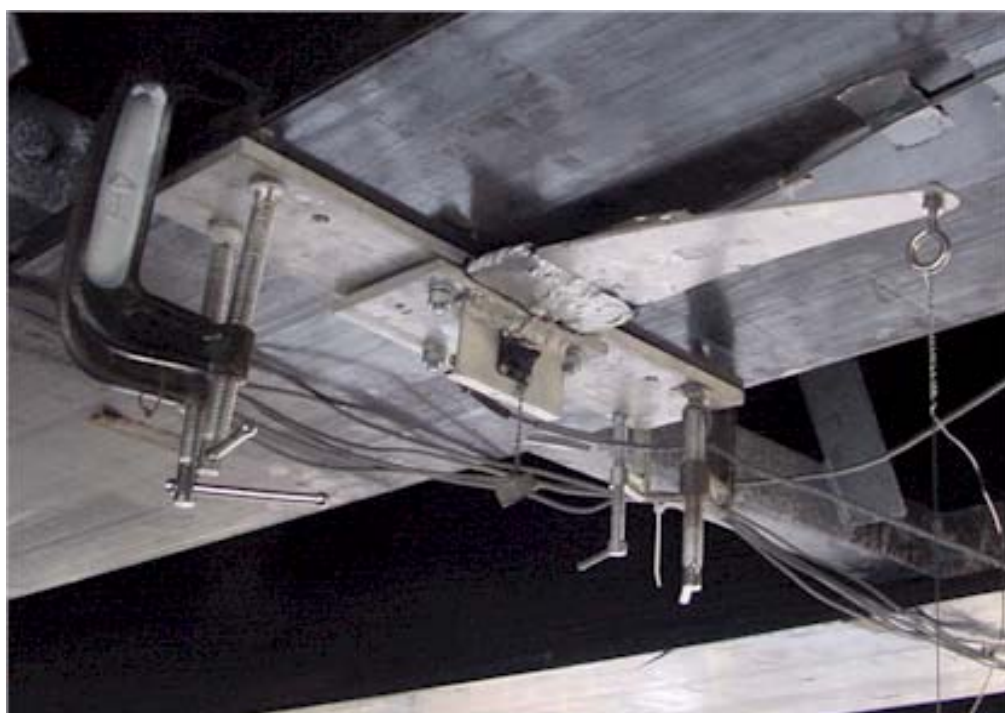


**Figure 2-4.** Deflectometer for the Route 601 Bridge.

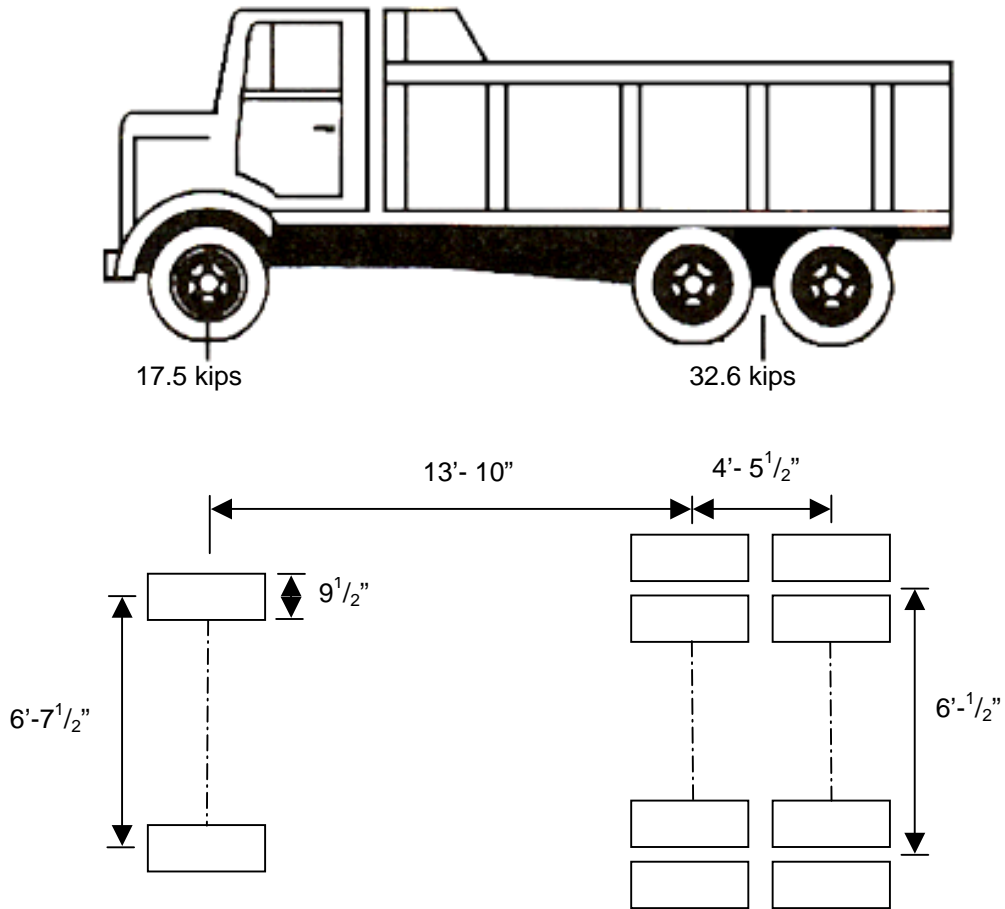


**Figure 2-5.** Sketch showing the dimensions and weight distribution of the VDOT dump truck used for testing the Toms Creek Bridge.

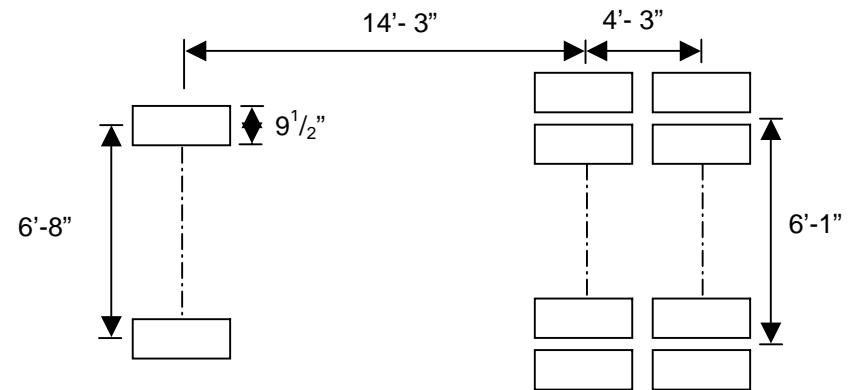
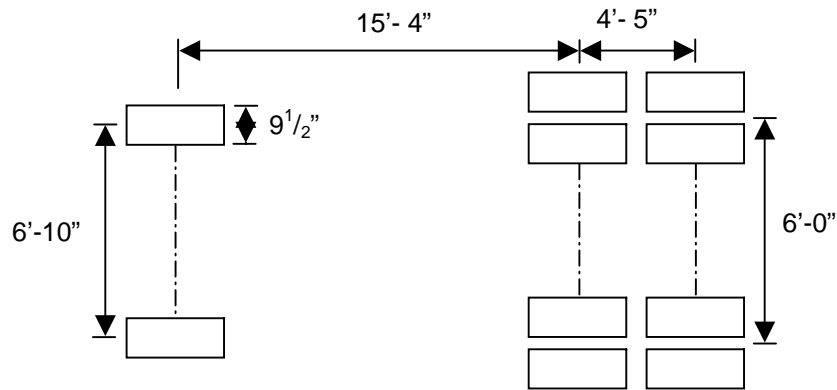
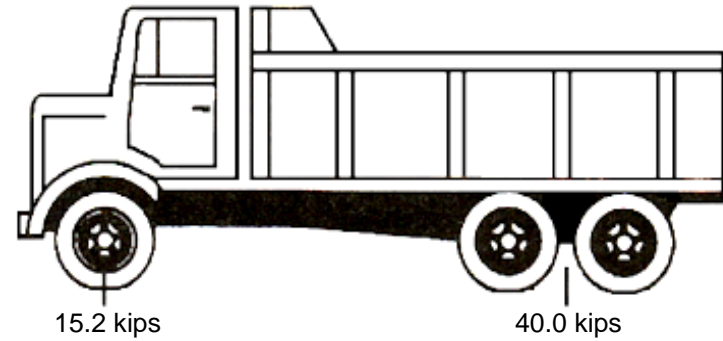
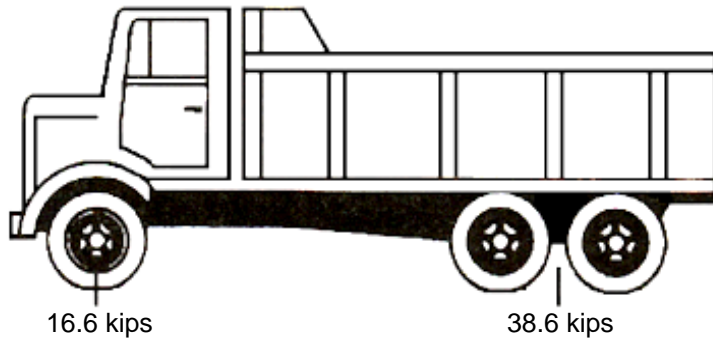


**Figure 2-6.** Sketch of weight distribution and dimensions of truck T4 used in for the Route 601 Bridge load tests.

**Figure 2-7.** Sketch of weight distribution and dimensions of truck T5 used in for the Route 601 Bridge multiple-lane load tests.

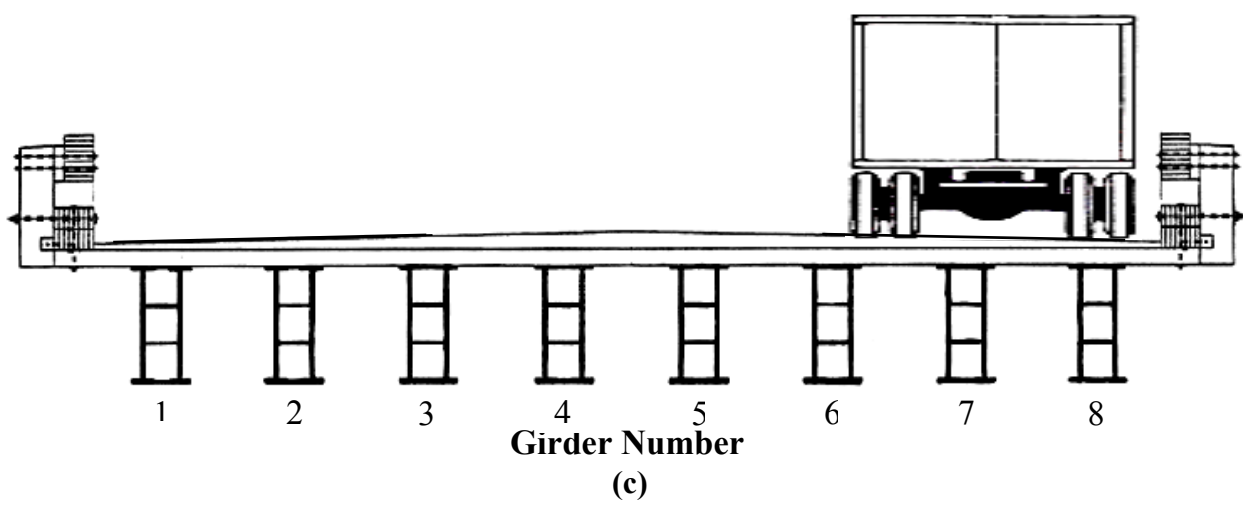
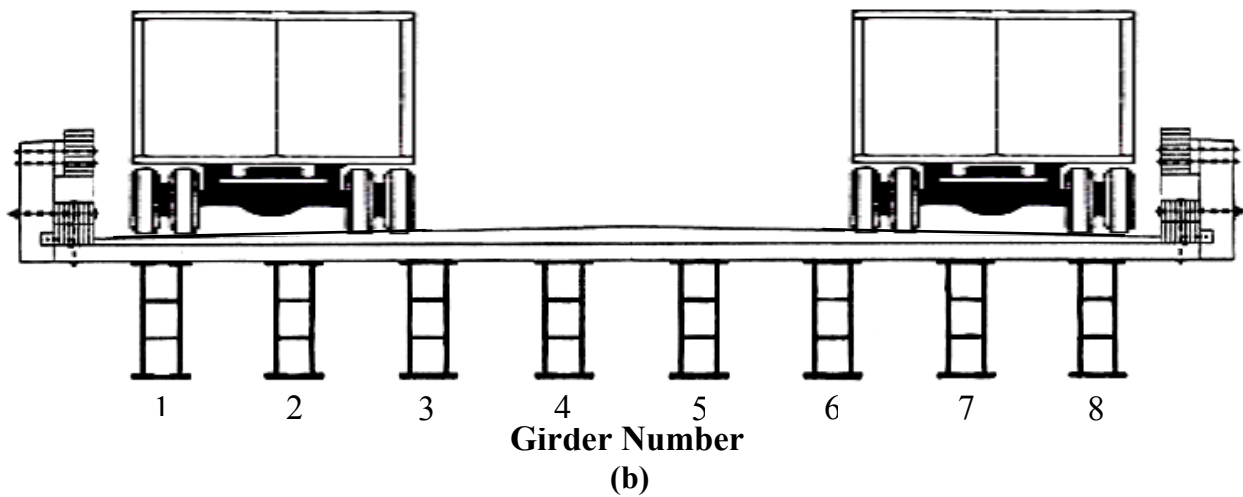
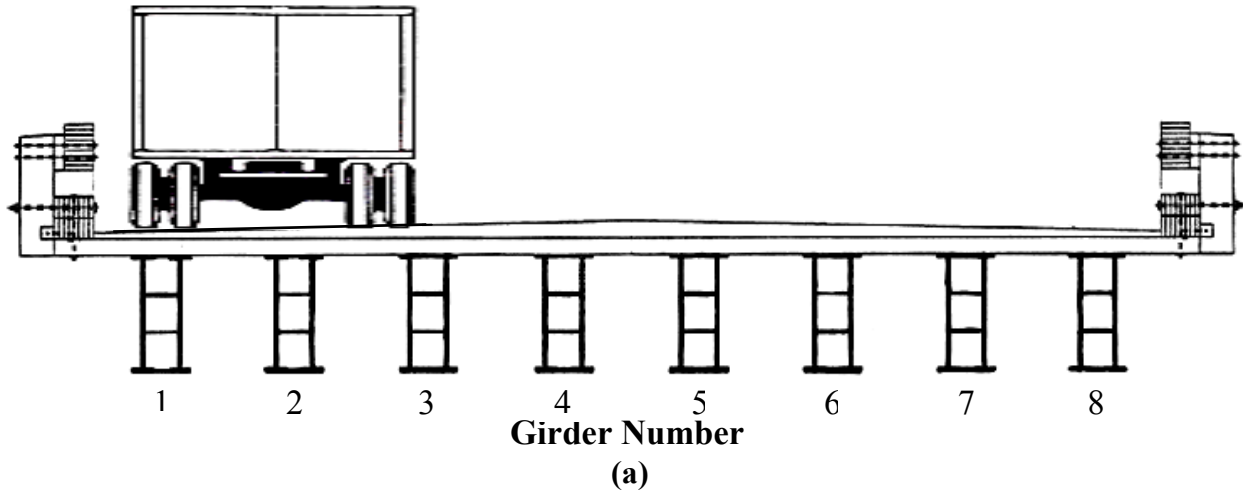


**Figure 2-8.** Exterior truck orientations for the Route 601 Bridge: (a) West Exterior, (b) Multiple-Lane, (c) East Exterior (Restrepo, 2002).

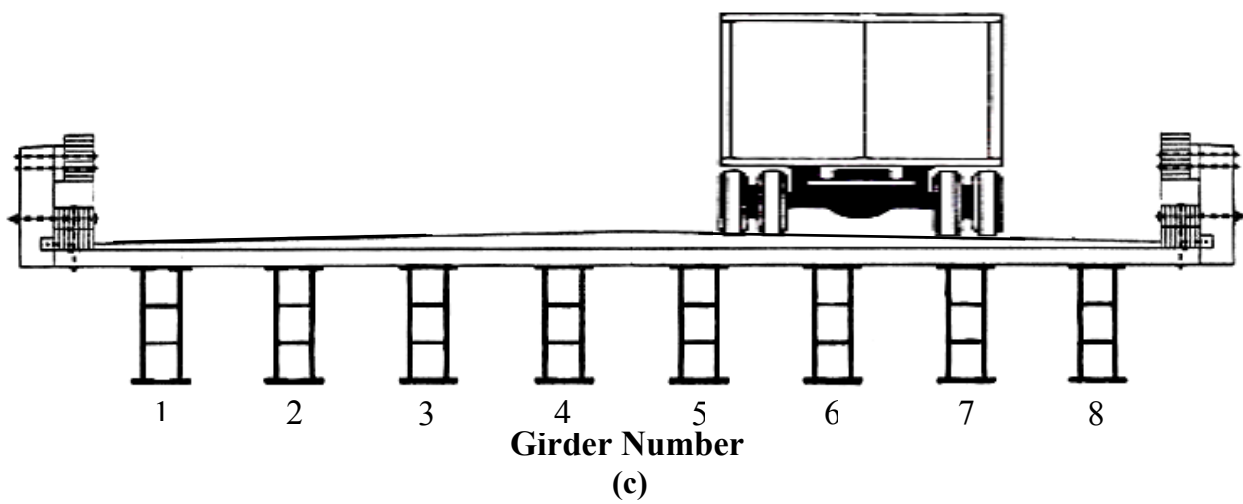
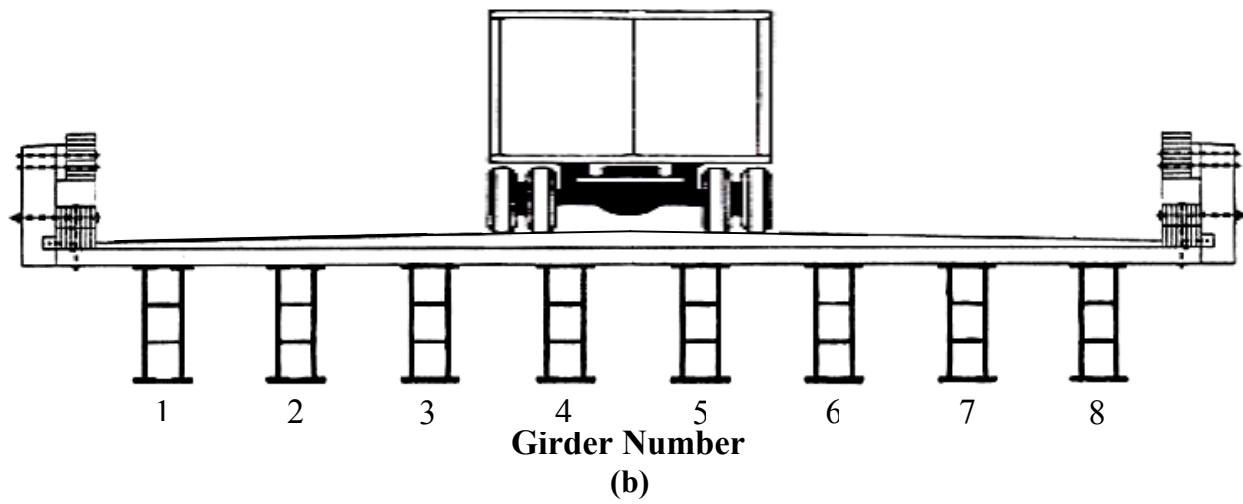
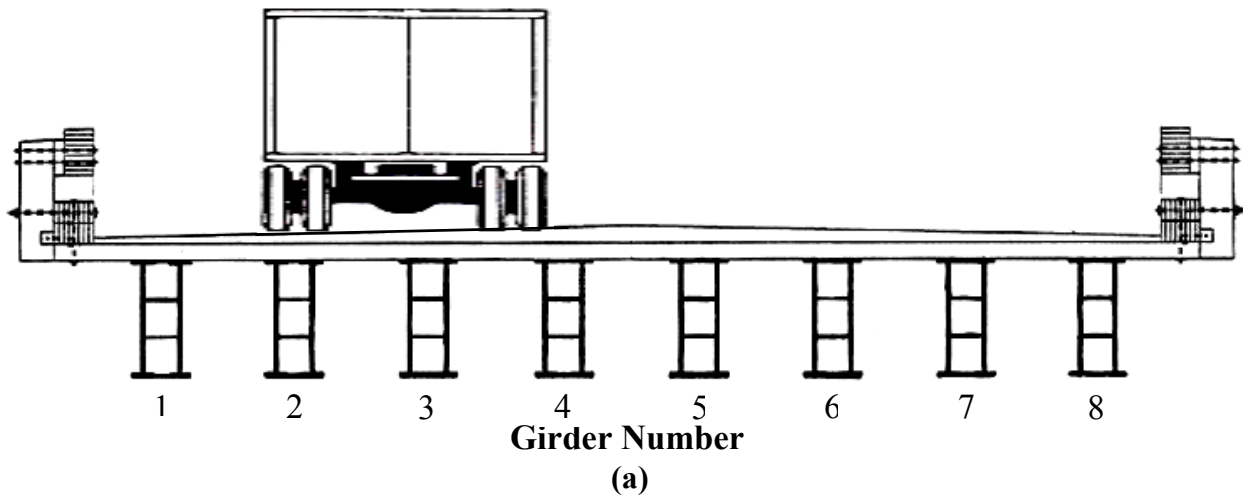


**Figure 2-9.** Interior truck orientations for the Route 601 Bridge:  
 (a) West Interior, (b) Center, (c) East Interior (Restrepo, 2002).

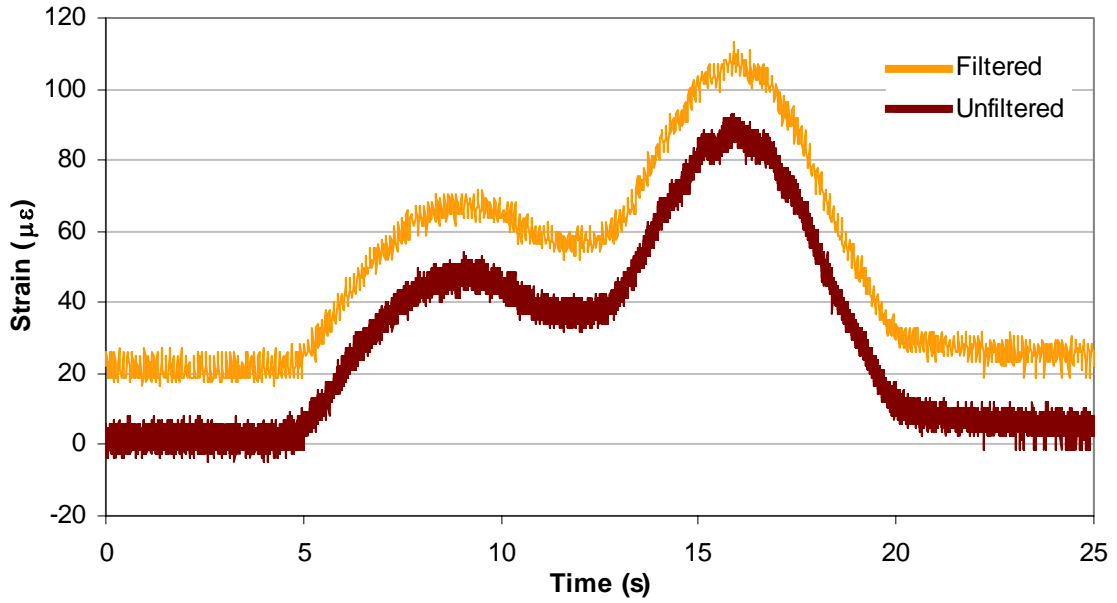


**Figure 2-10.** Typical comparison between filtered and unfiltered data. Data shown is for Girder 16 during a single test of the northbound lane orientation of the Toms Creek Bridge; filtered data was shifted upwards 20  $\mu\epsilon$  for comparison purposes.

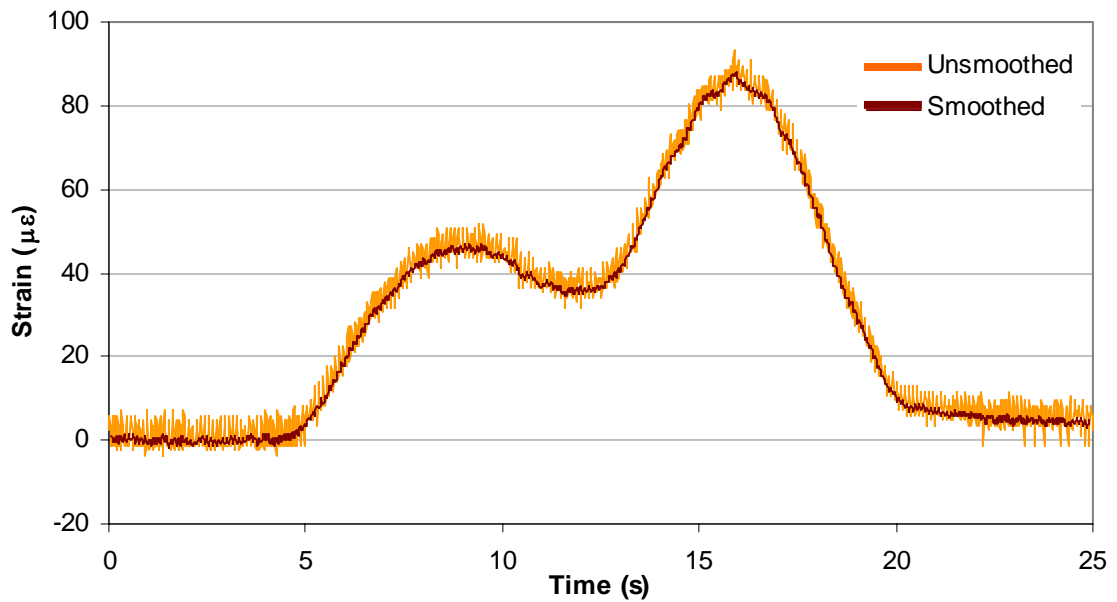


**Figure 2-11.** Typical comparison between smoothed and unsmoothed data. Data shown is for Girder 16 during a single test of the northbound lane orientation of the Toms Creek Bridge; smoothed data has been set to zero.

## Chapter 3: Results for Service Strains and Deflections

As mentioned in Section 1.2.5.1, service deflection, not strength, typically controls a design using FRP material. Therefore, an important aspect of this study is to see whether or not the Toms Creek Bridge and the Route 601 Bridge have lost stiffness over time by measuring the midspan deflection in the bridges as a load truck drives across them. Since the midspan strain serves as an indirect measure of the deflection, this study also considers the strain in these two bridges to serve as a comparison to the deflection results. In addition to the recorded strain values, this report gives the service strain in terms of the ultimate strain ( $\epsilon_{ult}$ ), which was determined in previous studies by Hayes (1998) and Waldron (2001) for the respective Toms Creek Bridge and Route 601 Bridge. The failure strain for the Toms Creek Bridge is  $6210 \mu\epsilon$ , while  $\epsilon_{ult}$  for the Route 601 Bridge is  $3150 \mu\epsilon$ .

### 3.1 Service Strain and Deflection Results for the Toms Creek Bridge

#### 3.1.1 Results from Current Study of the Toms Creek Bridge

Table 3-1 and Table 3-2 give the maximum and average *peak* midspan strain and deflection, respectively, for each combination of truck orientation and speed for the Summer 2003 tests on the Toms Creek Bridge. For this study, *peak* strain or deflection is the largest measured value recorded during a given load test. The *maximum* peak strain or deflection is the largest peak value collected from the group of five repetitions for a given combination of truck orientation and speed. Likewise, the *average* peak strain or deflection is the average of the five peak strains recorded from the five repetitions for a given combination of truck orientation and speed.

From Table 3-2, the largest average deflection during the Summer 2003 test of the Toms Creek Bridge is 0.434 in. (11 mm), which occurs in the southbound orientation when the load truck travels at 40 mph (64 kph). The high speed-large deflection relationship is indicative of the dynamic effects on the bridge, which are discussed later in Chapter 5. The 0.434 in. (11 mm) deflection equates to a ratio of  $L/484$ , which is less than the  $L/425$  deflection limit recommended for a timber bridge in the AASHTO *LRFD Specifications*, but is slightly greater than the  $L/500$  limit listed in the AASHTO *Standard Specifications* for the same type of bridge. For the same

40 mph (60 kph) speed, the deflections in the center and northbound orientations are about 30% and 12% less than the deflection in the southbound orientation. While the higher speed exhibits a wider range in deflection, the three orientations at static speed are more in line with each other, where there is only a 2% difference between the largest and smallest deflection. As a matter of reference, the largest average peak strain is 434  $\mu\epsilon$  in the southbound orientation at 40 mph (60 kph). The strain data give similar comparisons as the deflection data, with the exception that the average peak strain at static speed in the northbound orientation is about 11% less than the southbound orientation, as opposed to the aforementioned 2% difference in the deflection data.

### **3.1.2 Comparison of Current Study with Previous Toms Creek Bridge Tests**

In addition to the Summer 2003 test, Table 3-1 and Table 3-2 also show the maximum and average strain and deflection results that Neely gathered in his research from 1997 to 1999. Figure 3-1 and Figure 3-2 assist in visualizing the results for all of the field tests. Generally speaking, the Summer 2003 average peak deflections in the southbound and center lanes are either greater or are about the same as the previous tests, regardless of speed. On the other hand, the Summer 2003 average peak deflections for the northbound orientation are generally either lower than or are about the same as the previous tests.

Some of the differences in deflection between the different field tests can be attributed to the differences in the load truck's gross vehicle weight. However, a simple check shows that the variation in weight should not have caused much more than a 5% change in deflection amongst all of the field tests. Furthermore, the differences between the Summer 2003 test and the previous tests tend to be most apparent when comparing the Summer 2003 test with those that took place in the Fall season, as opposed to those taking place in the Spring season. For example, the largest difference in strain between the Summer 2003 and the Fall 1998 test is 40% when looking at the center orientation at static speed. However, the largest difference for that same combination of truck orientation and speed is only 8% when comparing the Summer 2003 and the Spring 1999 tests. A somewhat similar pattern of results arises from the deflection data, with the exception that the northbound lane shows a less variation over time.

In looking at the variations in strain and deflection over time, the one question that comes to mind is whether or not there is any statistical significance in the differences in the data. Figure 3-3 shows the average peak strain and deflection for all truck orientations and travel

speeds. Superimposed on top of these data points are error bars, calculated as  $2\sigma$ , where  $\sigma$  is the standard deviation of the corresponding strain or deflection data.  $2\sigma$  gives a 95.4% probability that a data point will fall within the range indicated by the error bars, assuming that the data follows a normal distribution. Unfortunately, much of the results in Figure 3-3 are inconclusive because many of the tests did not have a sufficient number of repetitions to validate the error bars.

Therefore, a more rigorous investigation considered the Anderson-Darling test as well as examined the type of data distribution. Using the MIL-HDBK-17 statistical analysis program written by Material Sciences Corporation, the Anderson-Darling test showed that, when comparing all six data sets together, these sets did not come from the same population. This result would mean that there is a statistically significant difference in the peak strain and deflection values over time. Note that the data from the six different tests tend to follow a Weibull distribution (as confirmed by a chi-squared test). However, by grouping the data into two different sets, a “Fall” and “Spring” set, the Anderson-Darling test was not so conclusive. A number of truck orientation-speed combinations in the “Fall” group did come from the same population, statistically speaking. On the other hand, the “Spring” group generally came from different statistical populations. Note that the Summer 2003 test was placed in the “Spring” group since the temperature during that date was comparable to the Spring tests. Keeping all of the above in mind, the general conclusion is that the change in the results from test date to test date is statistically significant. Therefore, there must be a reason behind the variation in the average strains and deflections over time beyond the scatter amongst the entire set of data.

In trying to explain the reason behind the change in strain or deflection, Neely proposed that the ambient air temperature has a significant impact on the Toms Creek Bridge’s performance. Current analysis agrees with Neely’s conclusion. Consider Figure 3-4, which shows the average temperature at the time of testing superimposed above the average peak strains recorded in the Toms Creek Bridge. As Neely suggested, Figure 3-4 shows a fairly clear relationship between the change in temperature and the change in peak strain, particularly for the northbound and southbound orientations. A higher temperature tends to correlate with a higher peak strain. Similar results occur when considering the deflection measurements.

Unfortunately, there is no clear explanation as to which component in the bridge that temperature has such an influence on. In modeling beam lamination theory based on FRP

coupon tests, researchers at Virginia Tech concluded that a 100 F (38 C) change in temperature would yield less than a 1% change in deflection in the Toms Creek Bridge (J. Lesko, personal communication, August 9, 2004). For timber, other research tends to support that there is little, if any, change in the elastic modulus of wood for temperatures above 42 F to 70 F (6 C to 21 C) [Green et al., 1999]. One other component that temperature would affect is the asphalt wearing surface on top of the deck. However, the glass transition temperature,  $T_g$ , of asphalt is so low that this material adds very little stiffness to the bridge in the first place. Perhaps the combination of all of these causal relationships of temperature is responsible for the relatively large changes in strain and deflection.

What is interesting to note is that in some cases, the temperature on one day may be greater than another day, yet the peak strain is lower. For example, Figure 3-4 shows that the average temperature during the Spring 1998 test was 61 F, while the average temperature during the Summer 2003 was 66 F. However, the northbound orientation at static speed had an average peak strain of  $300 \mu\epsilon$  ( $0.05\epsilon_{ult}$ ) in the Spring 1998 test versus  $265 \mu\epsilon$  ( $0.04\epsilon_{ult}$ ) during Summer 2003. Similar results occurred for the center orientation at static speed ( $316 \mu\epsilon$  vs.  $299 \mu\epsilon$  [ $0.05\epsilon_{ult}$  vs.  $0.05\epsilon_{ult}$ ]) and for the center orientation at 40 mph [64 kph] ( $353 \mu\epsilon$  vs.  $331 \mu\epsilon$  [ $0.06\epsilon_{ult}$  vs.  $0.05\epsilon_{ult}$ ]). These discrepancies may be due to the differences in gross vehicle weight and truck dimensions, as well as errors in precisely aligning the truck for each repetition in a given orientation. Regardless of the discrepancies, the peak strain is minimal compared to the failure strain determined by laboratory testing (Hayes, 1998), as shown in Table 3-3. Therefore, the Toms Creek Bridge is safe from failure.

Certainly, the peak strains and deflections have increased since the Toms Creek Bridge was first constructed. However, when considering comparable temperatures, the beams appear to have maintained much of their stiffness over the span of nearly six years of service. With this knowledge, the main point to the above comparisons is that if deflection control is the driving concern when designing with FRP beams, then extreme warm weather temperatures should be taken into account. This conclusion warrants the need for future studies in determining the relationship between ambient air temperature and deflection of bridges constructed with FRP beams.

Aside from temperature, another factor that might affect the bridge's behavior is the amount of moisture present at the time of testing. In his work, Neely said that the timber curb

and guide rails offer a significant amount of edge stiffening in the Toms Creek Bridge by tying the individual glulam deck panels together. The effect of moisture content on the modulus of elasticity in wood is well documented, and is much more significant than the effect of temperature (Siimes, 1967; Green and Kretschmann, 1994). As the moisture content in wood increases up to the saturation point, the flexural modulus of elasticity decreases, thus reducing the additional stiffness that the curb and guide rails provide.

Typical laboratory experiments tend to test lumber samples having 12% moisture content. On the other hand, field tests on several timber bridges constructed in Florida, where the humidity is generally higher than in Virginia, found that the moisture content varied up to 16% (Yazdani, et al., 1999). According to the equation established by Kretschmann and Green (2000):

$$MOE_{bending} = -1.5(MC)^2 + 0.13(MC) + 2061 \quad (3-1)$$

where  $MOE_{bending}$  is the modulus of elasticity for bending, expressed in kips per square inch and  $MC$  is the moisture content, expressed in percent. When going from 12% to 16% moisture content in Southern Pine lumber, the modulus of elasticity decreases by 10%. Calculations detailed in Appendix A show that a 10% reduction in the modulus would result in a 3% increase in the deflection for the Toms Creek Bridge.

While none of the field tests for this bridge recorded moisture content information, a look at the amount of rainfall occurring prior to the individual test dates can give a somewhat qualitative analysis of the effects on moisture on the Toms Creek Bridge. Consider Figure 3-5, which shows the average peak beam strains recorded in the Toms Creek Bridge superimposed with the local precipitation for a seven-day period prior to the respective test dates. The rainfall data was obtained from the National Weather Service via the Internet (Weather Underground, 2004). The seven-day time frame for precipitation was chosen arbitrarily, but was also partially based on work by Yazdani, et al. (1999), who observed that the moisture content in a wooden bridge stabilized two weeks after being flooded. In looking at the three different test speeds over the different test dates, the change in precipitation appears to correlate most closely with the change in strain for the 40 mph (64 kph) tests at all three truck orientations. The other two speeds, static speed and 25 mph (40 kph), show a similar correlation, except when going from the Fall 1997 to the Spring 1998 tests. In this case, the amount of precipitation decreases

slightly, but the strain increases in all three truck orientations, which is the opposite of the anticipated result. Although there is no data for examining the change in deflection from the Fall 1997 tests to the Spring 1998 tests, results for the remaining test dates are similar to the strain data.

Relative humidity was another factor considered for the moisture content in the timber components for this bridge. However, there is even less of a relationship in daily relative humidity with the variation in the peak strains and deflections than there is for the weekly rainfall.

Taking the above results into account with the fact that the rainfall pattern appears to match the temperature pattern amongst the six tests, as well as the realization that there is no direct data regarding the moisture content in the timber elements of the Toms Creek Bridge, no definitive conclusion can be made with regards to the effect of moisture on the bridge's performance. Regardless, concerns over moisture content in the structural elements may make it necessary to disregard the stiffness benefits that timber guide rails provide when designing this type of bridge. Additionally, the effects that moisture might have in an FRP bridge's performance may warrant future study.

## **3.2 Service Strain and Deflection Results for the Route 601 Bridge**

### **3.2.1 Results from Current Study of the Route 601 Bridge**

Table 3-4 and Table 3-5 show the maximum and average peak midspan strain and deflection, respectively, for the Fall 2003 tests on the Route 601 Bridge. From Table 3-5, the largest average deflection in the Route 601 Bridge is 0.254 in. (6 mm), which occurs when the truck is in the west exterior orientation. The multiple-truck orientation gives a marginally smaller deflection than the west exterior orientation. Since the exterior orientations were only tested at static speed, an estimated deflection at 40 mph (64 kph) would be the deflection at static speed multiplied by the sum of unity plus the dynamic load allowance. As will be explained in Section 5.3.2, the conservative recommendation for the dynamic load allowance for the Route 601 Bridge is 0.50. Therefore, the estimated deflection in the bridge with a heavily loaded truck traveling across the bridge at 40 mph (64 kph) is 0.38 in. (10 mm). Even with the conservative dynamic load allowance, this deflection is approximately equivalent to  $L/1230$ , which is well

below the AASHTO-recommended limit for a steel, prestressed concrete, or reinforced concrete bridge without pedestrian traffic, i.e.,  $L/800$ .

Just as a matter of reference, the west exterior orientation did not have the largest average strain result. Instead, the east exterior orientation averaged the largest strain at  $220 \mu\epsilon$  ( $0.07\epsilon_{ult}$ ). The difference in strain between these two orientations is about 5%. The difference between the deflection and strain results may be due to the problems with the strain gage in Girder 1 failing during testing or the fact that the strain gages do not capture the shear strain that the beams undergo during testing, as explained in Section 2.1.2.

### **3.2.2 Comparison of Current Study with Previous Route 601 Bridge Tests**

In addition to the Fall 2003 test, Table 3-4 and Table 3-5 also show the maximum and average strain and deflection results that Restrepo gathered in his research from the Fall 2001 and Summer 2002 field tests. Figure 3-6 and Figure 3-7 assist in visualizing the results for all of the field tests.

A complete comparison between the two Fall field tests is not possible, since the Fall 2001 test did not include the west and east exterior orientations. Therefore, determining if the west exterior orientation yielded the largest deflection in the Fall 2001 test as it did in the Fall 2003 test is not possible. However, comparisons for other combinations of truck orientation and speed show that there is a small amount of difference between the two Fall tests, where the Fall 2003 results generally seem to have smaller deflections than the Fall 2001 tests. Based on both the static and dynamic tests for the west interior and center orientations, the Fall 2003 tests have deflections that are 10 to 15% lower than in Fall 2001. These differences in deflection are not necessarily due to the different trucks used in the two series of tests because the deflections should be essentially the same based on the dimensions and the accuracy of the gross weight of the trucks crossing a theoretical simply-supported bridge. One notable exception in comparing the two Fall tests is the deflection in the east interior orientation with the truck traveling at 40 mph (60 kph). In this case, the Fall 2003 test shows an average deflection that is about 18% *greater* than the average deflection for the Fall 2001 test. The reason for this sizable increase when the other orientations show a decrease in deflection is not clear.

As a point of reference, the peak strains in the Route 601 Bridge are generally slightly larger in the Fall 2003 field tests than those in the Fall 2001 tests. Except for the multiple lane

orientation, which shows a decrease in measured strain that is comparable to the strain from the Fall 2001 tests, the Fall 2003 tests show increases that are 1 to 16% greater than two years before. As with the deflection data, the east interior exhibits the greatest amount of increase in strain.

The differences in deflection between the two Fall field tests are relatively small compared to the large differences between the Summer 2002 and Fall 2003 tests, where the latter deflections are 4 to 37% lower than the those measured in Summer 2002. The change in the deflection from one field test to the next is not necessarily dependent on any one truck orientation or speed. For example, the east exterior orientation at static speed and the west interior orientation at 40 mph (60 kph) exhibit some of the highest percentage change in deflection (32% and 37%, respectively).

Note that the maximum average deflection amongst all three field tests is 0.309 in. (8 mm), for the east exterior orientation at static speed during the Summer 2002 test. Using the same recommended dynamic load allowance as mentioned in Section 3.2.1, the deflection for this same orientation at 40 mph (60 kph) would be approximately 0.46 in. (12 mm). This deflection is equivalent to  $L/1017$ , which is still below the optional  $L/800$  limit suggested by AASHTO for steel, prestressed concrete, or reinforced concrete bridges with vehicular loads.

As with the Toms Creek Bridge, the question that lies herein is whether or not the relatively large changes in strain and deflection are statistically significant. Consider Figure 3-8, which shows the standard  $2\sigma$  error bars superimposed onto the average peak strains and deflections for the interior orientations in the Route 601 Bridge. In the case of the static speed, there is little doubt that the different field tests give statistically significant differences in measurements. However, the charts for the other two speeds give somewhat of a mixed signal. Therefore, additional analysis used the aforementioned MIL-HDBK-17 statistical analysis program concluded that the average measurements shown in Figure 3-6 and Figure 3-7 do not belong to the same population and thus are significantly different, meaning that changes in these measurements over time are not simply due to scatter in the data.

Therefore, there must be a reason as to why the strains and deflections in the Route 601 Bridge tend to change over time. Certainly, the minor differences in the load trucks' gross vehicle weight and dimensions do not warrant the large decreases in girder deflections between the last two field tests for the Route 601 Bridge. Therefore, like the Toms Creek Bridge,

temperature and moisture effects need to be considered in explaining the reason for these changes. Similar to the Toms Creek Bridge, the ambient air temperature appears to have a major effect on the Route 601 Bridge's performance, as shown with the interior truck orientations in Figure 3-9. With the exception of the average peak strain in the east interior orientation at 40 mph (60 kph) during the Fall 2003 test, an increase or decrease in temperature corresponds to a increase or decrease in the peak measured value.

However, there does appear to be a slight discrepancy between the strain and deflection data. In looking at the two tests performed in the Fall season, the temperature during the 2003 test was slightly lower than the 2001 test. The deflection results tend to reflect this fact in that the deflections in the 2003 tests are generally lower than those in the 2001 tests, particularly the west interior and center truck orientations. On the other hand, the strain results show that the strains in the 2003 tests are generally *higher* than those in the 2001 tests.

Like the Toms Creek Bridge, there is no clear explanation as to why the variation in temperature plays a major role in the Route 601 Bridge's behavior. One factor that might exacerbate the temperature effects on this bridge's performance is the effect on the neoprene bearing pads that support the girders sitting on top of the concrete abutments. These bearing pads offer less resistance to rotation at higher temperatures. This decrease in rotational stiffness may result in the beams deflecting more.

Moisture probably has less of an effect on the bearing pads, and according to Figure 3-10, has no apparent effect on the behavior of the bridge as a whole. The amount of rainfall one week prior to the date of testing remains essentially unchanged when comparing the Fall 2001 test with the Summer 2002 test, however, both the strain and deflection measurements for the interior truck orientations on the Route 601 Bridge show dramatic increases in the Summer 2002 results over the Fall 2001 tests. On the other hand, the amount of rainfall *increased* in the Fall 2003 tests, yet the strains and deflections decrease dramatically in those Fall 2003 tests. Therefore, the conclusion is that there is no relationship between the amount of moisture present at the bridge and the amount of strain or deflection that occurs in the bridge as a load travels across it. This conclusion is more definitive than the conclusion made for the Toms Creek Bridge. The reason may be that relative stiffness of the timber curb and guide rails compared to the stiffness of the girders in the Route 601 Bridge is much lower than the Toms Creek Bridge. Thus the moisture effects should be less dominant in the Route 601 Bridge. Calculations detailed in Appendix A

show that a 10% change in the elastic modulus of timber yields virtually no change in the deflection in the Route 601 Bridge.

Despite the small discrepancies between the strain and deflection data, and the fluctuations in stiffness behavior over time, the most important observation is that the Route 601 Bridge is sufficiently designed against catastrophic failure. The safety against failure is indicated in Table 3-6, which gives the peak strain in the beams as a fraction of the failure strain.

### **3.3 Axial Strains**

Axial strain gages were placed on Girders 3 and 12 in the Toms Creek Bridge, and were placed on Girders 5 and 8 in the Route 601 Bridge. Both field tests showed that there was little axial strain occurring at the ends of the beams. Furthermore, the electronic noise level was 20% to 25% of the peak measurements for both bridges. Thus, there is little certainty as to the accuracy of the data. These results concur with the observations that both Neely and Restrepo made in their research.

### 3.4 Tables and Figures

**Table 3-1.** Maximum and average peak flexural strain (in microstrain) for the most the heavily loaded girder for the different truck orientations and speeds in the Toms Creek Bridge.

Researcher	Test Date	Speed (mph)	Truck Orientation								
			Southbound Lane			Center Lane			Northbound Lane		
			No. of Tests	Max. Peak Strain	Avg. Peak Strain	No. of Tests	Max. Peak Strain	Avg. Peak Strain	No. of Tests	Max. Peak Strain	Avg. Peak Strain
Neely	Fall 1997	Static	2	235	232	2	230	229	2	271	268
		25	2	227	214	3	219	214	2	266	255
		40	2	419	383	2	374	343	2	358	356
	Spring 1998	Static	4	290	275	4	321	<b>316</b>	4	323	<b>300</b>
		25	3	310	300	4	317	299	3	318	299
		40	3	470	383	4	407	<b>353</b>	4	369	314
	Fall 1998	Static	6	218	213	6	222	213	5	259	255
		25	5	248	239	7	223	206	4	284	268
		40	4	373	367	5	311	272	5	428	393
	Spring 1999	Static	6	280	262	6	331	324	6	303	297
		25	3	274	268	6	310	290	3	299	285
		40	4	447	433	6	432	376	4	449	419
	Fall 1999	Static	6	246	235	5	253	219	6	285	265
		25	3	230	224	3	202	197	3	245	231
		40	5	396	385	5	317	272	6	409	381
Kassner	Summer 2003	Static	5	296	295	5	302	<b>299</b>	5	267	<b>265</b>
		25	5	319	295	5	—	—	5	—	—
		40	5	505	<b>438</b>	5	364	<b>331</b>	5	406	376

**Table 3-2.** Maximum and average peak deflection (in inches) for the most the heavily loaded girder for the different truck orientations and speeds in the Toms Creek Bridge.

Researcher	Test Date	Speed (mph)	Truck Orientation									
			Southbound Lane			Center Lane			Northbound Lane			
			No. of Tests	Max. Peak Deflect.	Avg. Peak Deflect.	No. of Tests	Max. Peak Deflect.	Avg. Peak Deflect.	No. of Tests	Max. Peak Deflect.	Avg. Peak Deflect.	
Neely	Fall 1998	Static	6	0.188	0.179	6	0.213	0.208	5	0.261	0.252	
		25	5	0.203	0.196	7	0.206	0.195	4	0.304	0.271	
		40	4	0.381	0.372	5	0.288	0.257	5	0.465	0.430	
	Spring 1999	Static	6	0.241	0.226	6	0.327	0.323	6	0.280	0.272	
		25	3	0.227	0.223	6	0.276	0.259	3	0.277	0.264	
		40	4	0.413	0.394	6	0.415	0.357	4	0.410	0.384	
	Fall 1999	Static	6	0.200	0.181	5	0.229	0.184	6	0.322	0.262	
		25	3	0.191	0.183	3	0.173	0.169	3	0.262	0.233	
		40	5	0.378	0.360	5	0.300	0.247	6	0.446	0.415	
	Kassner	Summer 2003	Static	5	0.267	0.264	5	0.269	0.266	5	0.260	0.258
			25	5	0.286	0.274	5	—	—	5	—	—
			40	5	0.475	<b>0.434</b>	5	0.331	0.304	5	0.404	0.383

**Table 3-3.** Peak strain in the Toms Creek Bridge as a fraction of ultimate strain; percentages are for largest average peak strain amongst all six load tests.

<b>Truck Orientation</b>	<b>Speed</b>	<b>% of <math>\epsilon_{ult}</math></b>
Northbound	Static	0.05
	40	0.07
Center	Static	0.05
	40	0.06
Southbound	Static	0.05
	25	0.05
	40	0.07

**Table 3-4.** Maximum and average peak flexural strain in the most the heavily loaded girder for the different truck orientations and speeds in the Route 601 Bridge (measured in microstrain).

Researcher	Test Date	Test Speed (mph)	Truck Orientation											
			West Exterior		West Interior		Center		Two Trucks		East Interior		East Exterior	
			<i>Max. Peak Strain</i>	<i>Avg. Peak Strain</i>										
Restrepo	October 2001	Static	—	—	181	180	185	182	221	218	173	171	—	—
		25	—	—	203	192	204	181	—	—	194	188	—	—
		40	—	—	183	175	176	166	—	—	182	178	—	—
	June 2002	Static	236	229	211	210	206	206	245	238	201	200	247	240
		25	—	—	241	228	231	222	—	—	219	208	—	—
		40	—	—	276	271	279	253	—	—	214	199	—	—
Kassner	October 2003	Static	213	210	191	190	190	189	216	213	187	185	222	<b>220</b>
		25	—	—	209	194	201	194	—	—	198	189	—	—
		40	—	—	197	190	192	186	—	—	215	206	—	—

**Table 3-5.** Maximum and average peak deflection in the most the heavily loaded girder for the different truck orientations and speeds in the Route 601 Bridge (measured in inches).

Researcher	Test Date	Test Speed (mph)	Truck Orientation											
			West Exterior		West Interior		Center		Two Trucks		East Interior		East Exterior	
			<i>Max. Peak Defl.</i>	<i>Avg. Peak Defl.</i>										
Restrepo	October 2001	Static	—	—	0.217	0.214	0.213	0.211	0.266	0.261	0.195	0.193	—	—
		25	—	—	0.236	0.228	0.212	0.203	—	—	0.211	0.205	—	—
		40	—	—	0.224	0.219	0.203	0.197	—	—	0.204	0.194	—	—
	June 2002	Static	0.293	0.276	0.242	0.240	0.249	0.243	0.315	0.305	0.225	0.222	0.316	<b>0.309</b>
		25	—	—	0.271	0.258	0.269	0.254	—	—	0.236	0.228	—	—
		40	—	—	0.314	0.309	0.309	0.296	—	—	0.252	0.237	—	—
Kassner	October 2003	Static	0.256	<b>0.254</b>	0.195	0.193	0.187	0.187	0.256	0.252	0.200	0.200	0.216	0.211
		25	—	—	0.205	0.193	0.185	0.181	—	—	0.206	0.201	—	—
		40	—	—	0.200	0.194	0.204	0.194	—	—	0.238	0.228	—	—

**Table 3-6.** Peak strain in the Route 601 Bridge as a fraction of ultimate strain; percentages are for largest average peak strain amongst all three load tests.

<b>Truck Orientation</b>	<b>Speed</b>	<b>% of <math>\epsilon_{ult}</math></b>
West Exterior	Static	0.07
	Static	0.07
West Interior	25	0.07
	40	0.09
Center	Static	0.07
	25	0.07
	40	0.08
Multiple Lanes	Static	0.08
East Interior	Static	0.06
	25	0.07
	40	0.07
East Exterior	Static	0.08

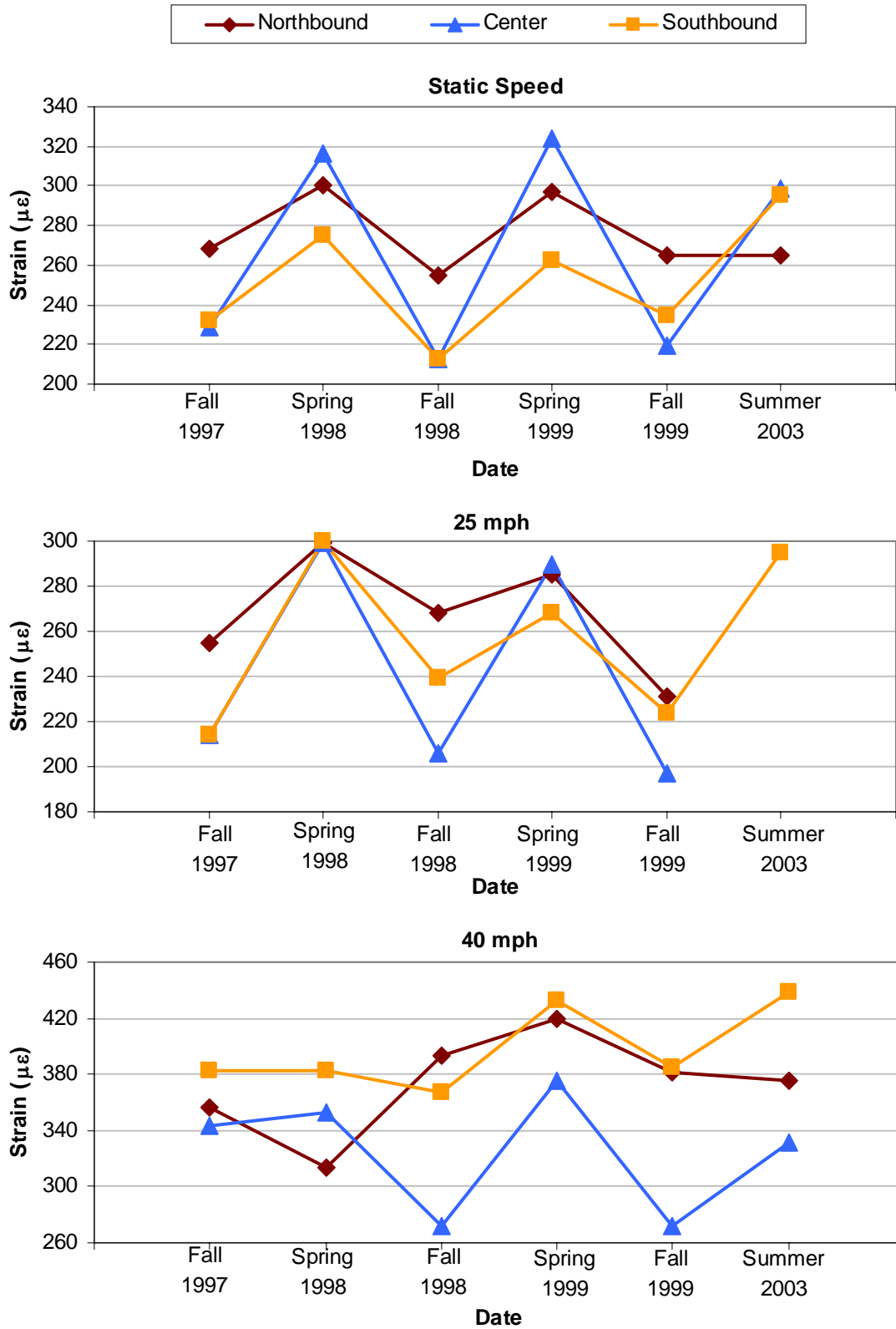


**Figure 3-1.** Average peak strain in the most heavily loaded girder for the different truck orientations and travel speeds in the Toms Creek Bridge.

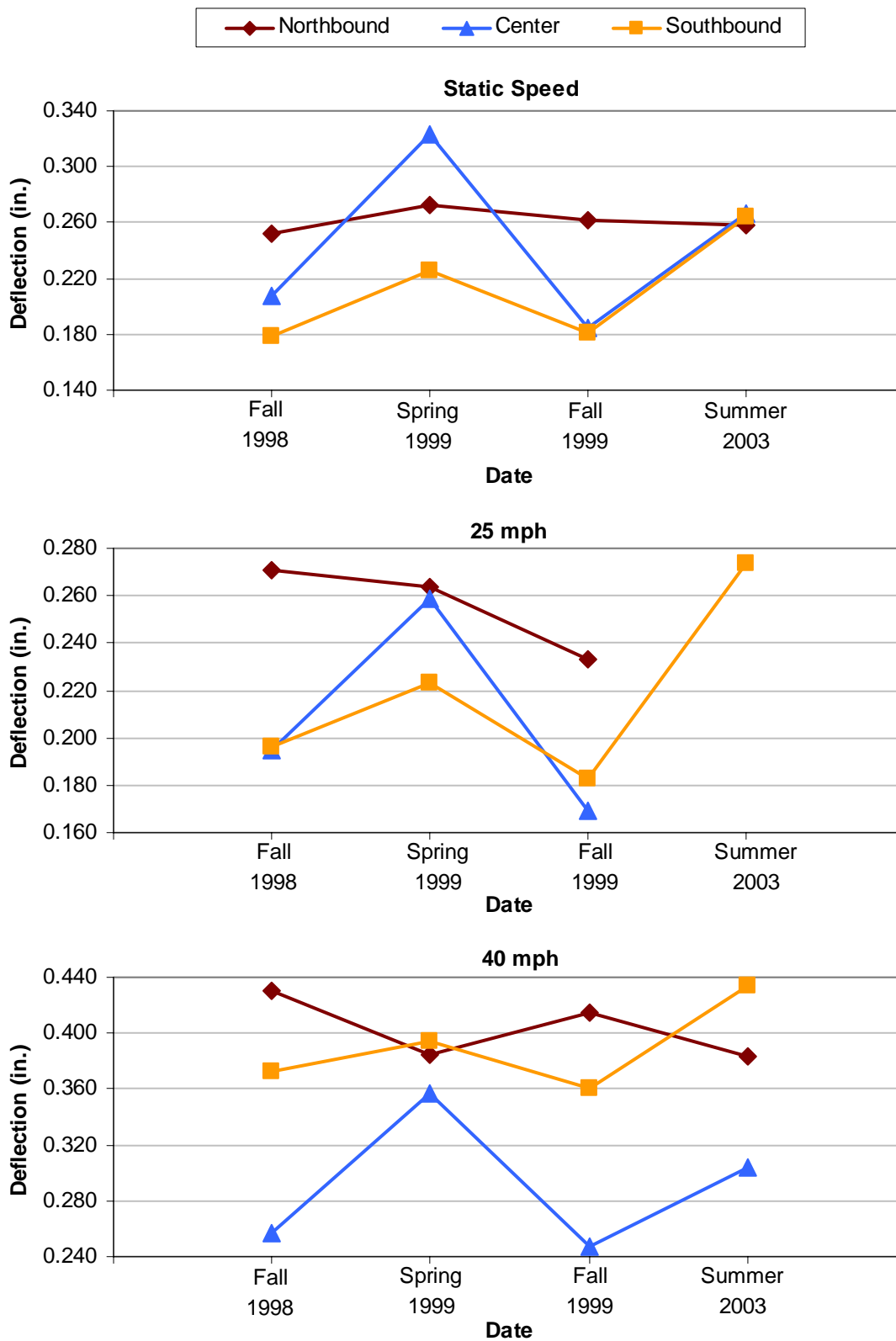
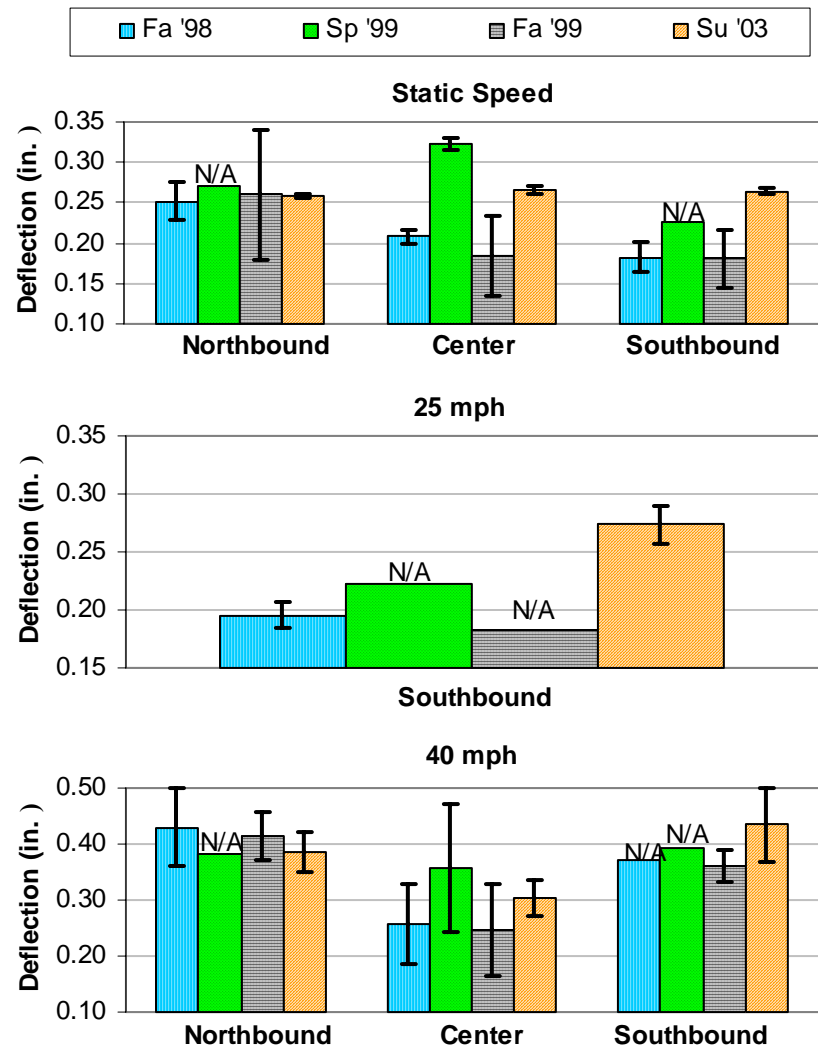
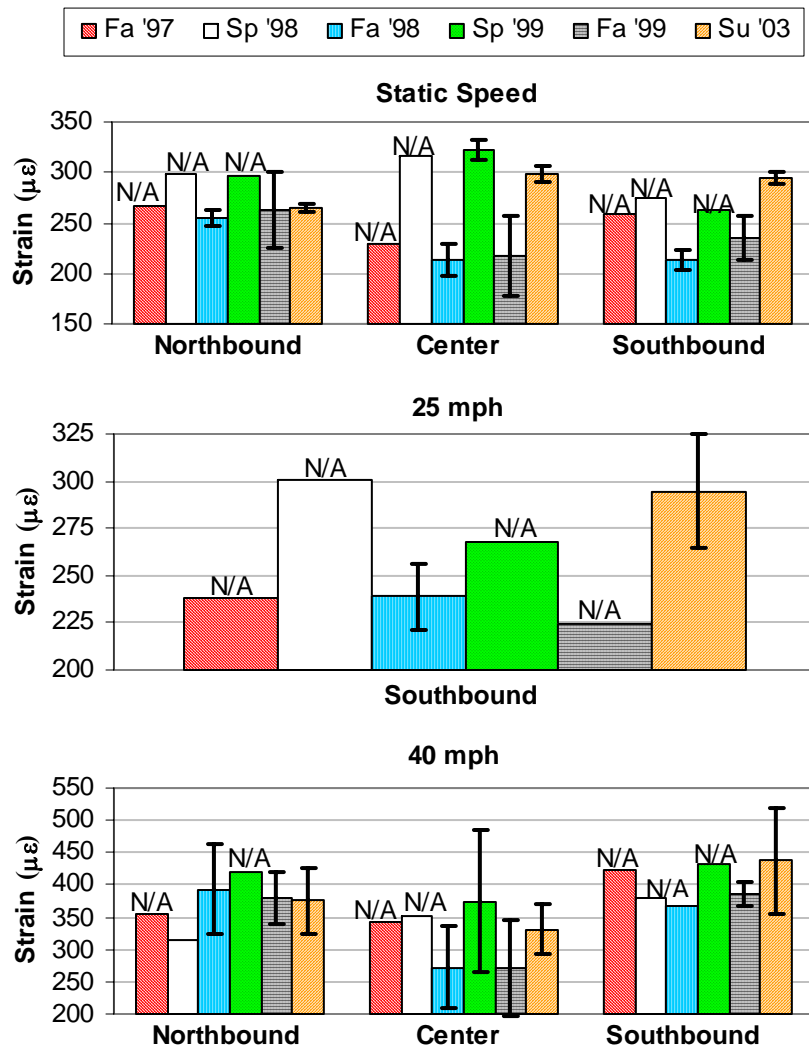


**Figure 3-2.** Average peak deflection in the most heavily loaded girder for the different truck orientations and travel speeds in the Toms Creek Bridge.



(a)

(b)

**Figure 3-3.** Error bars for the average peak (a) strain and (b) deflection for the most heavily loaded girder in the Toms Creek Bridge. Data points marked “N/A” do not have enough tests to produce a statistically reliable set of bars; data points without error bars have errors that are too small to appear on the graph.

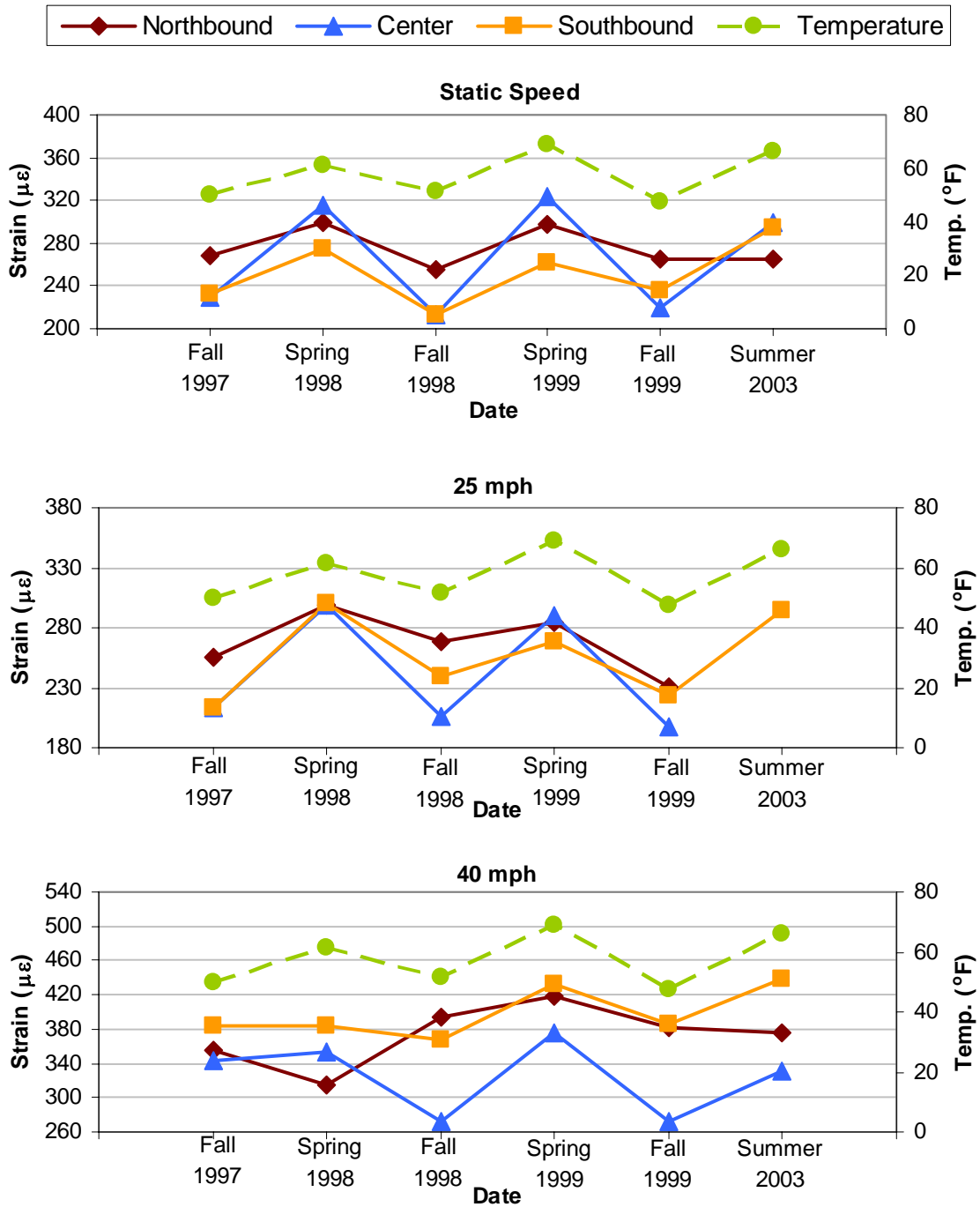
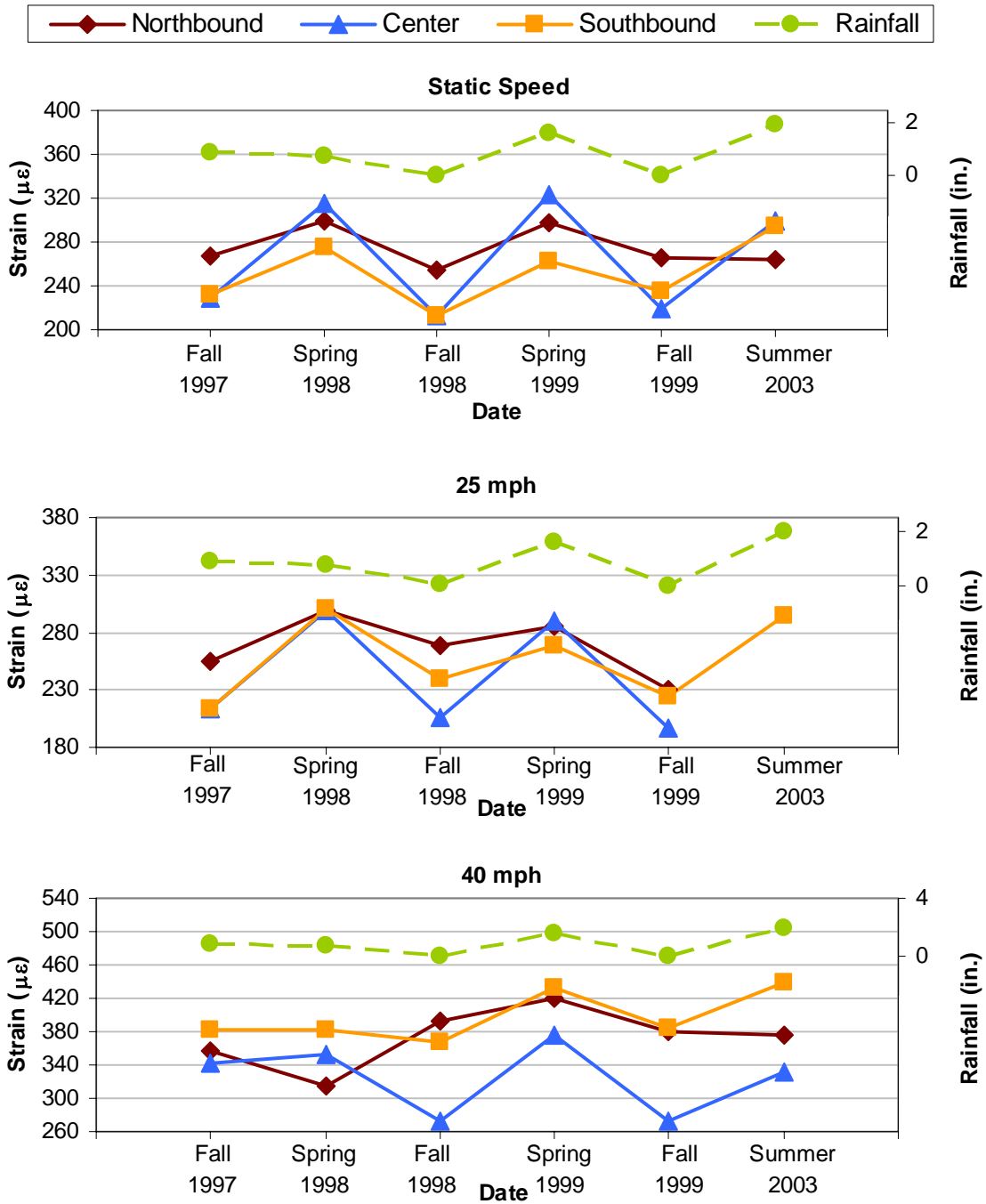
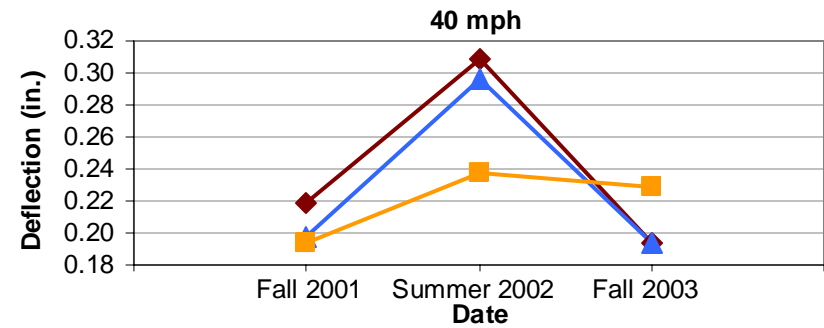
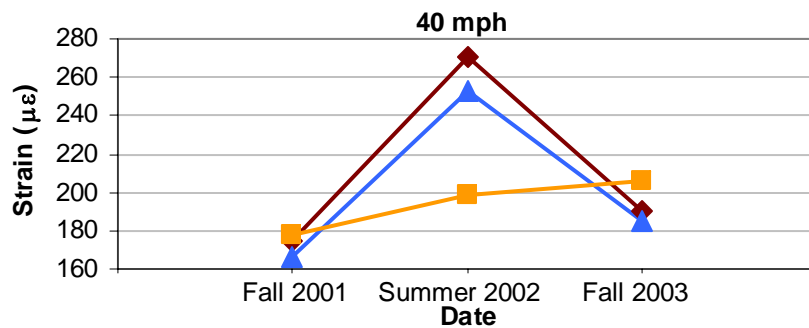
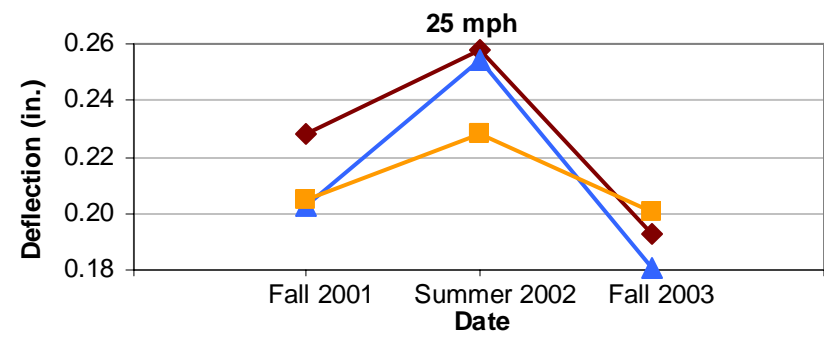
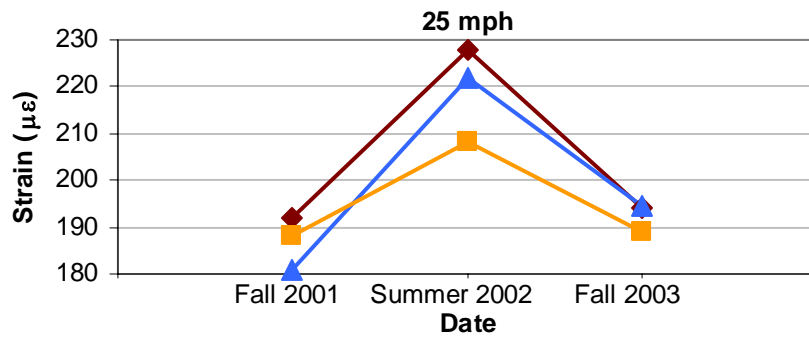
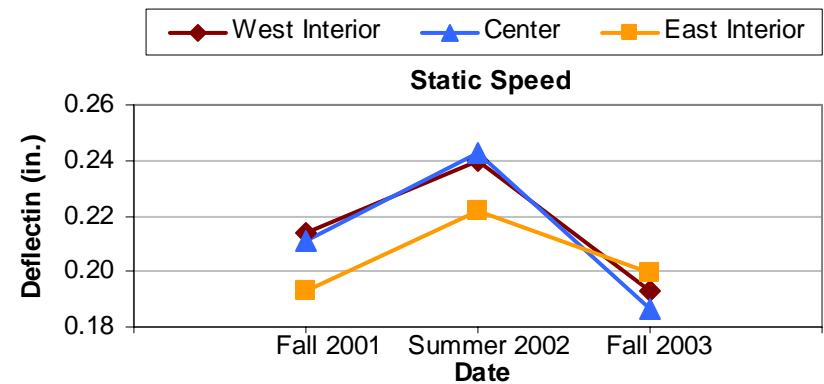
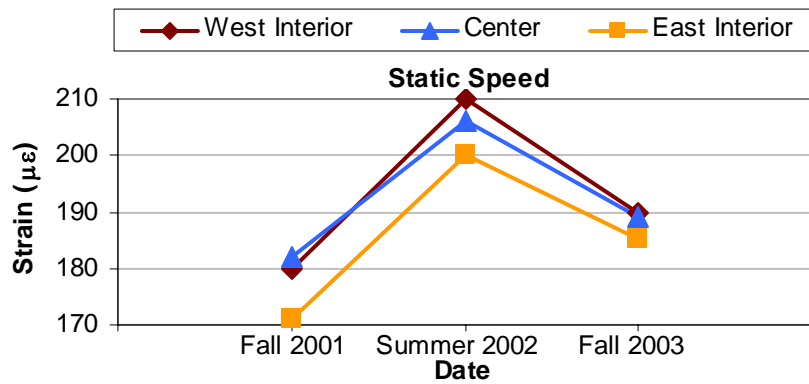


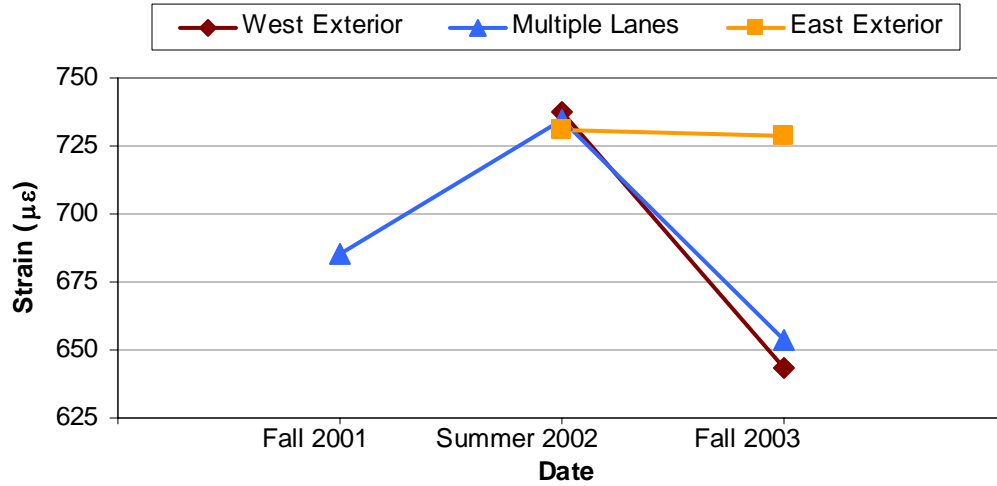
Figure 3-4. Average peak strain shown with the average temperature at the Toms Creek Bridge.



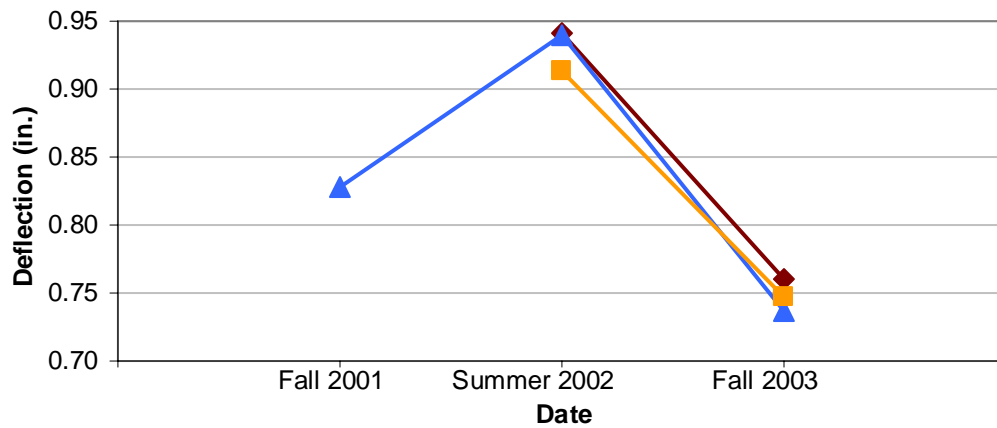
**Figure 3-5.** Average peak strain shown with rainfall at the Toms Creek Bridge. Amount of rainfall is the precipitation over a seven-day period prior to the respective test dates.



(a) (b)  
**Figure 3-6.** Average peak (a) strain and (b) deflection in the most heavily loaded girder for the different interior truck orientations and travel speeds in the Route 601 Bridge.

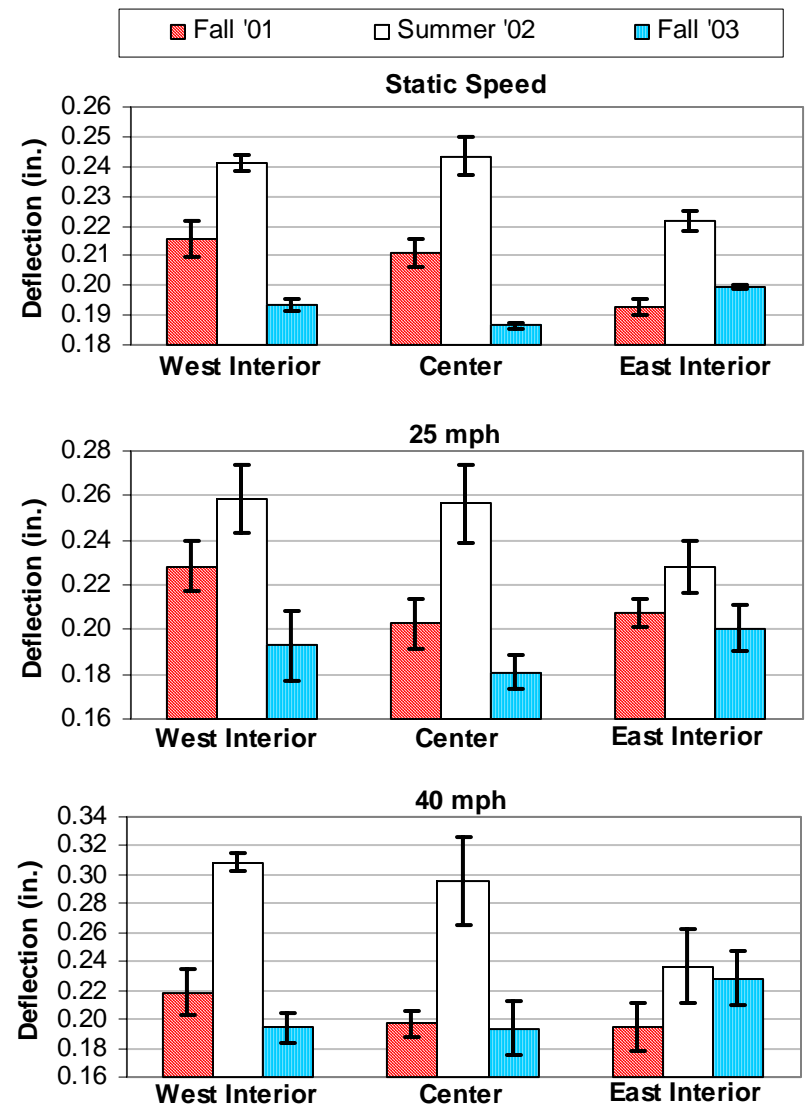
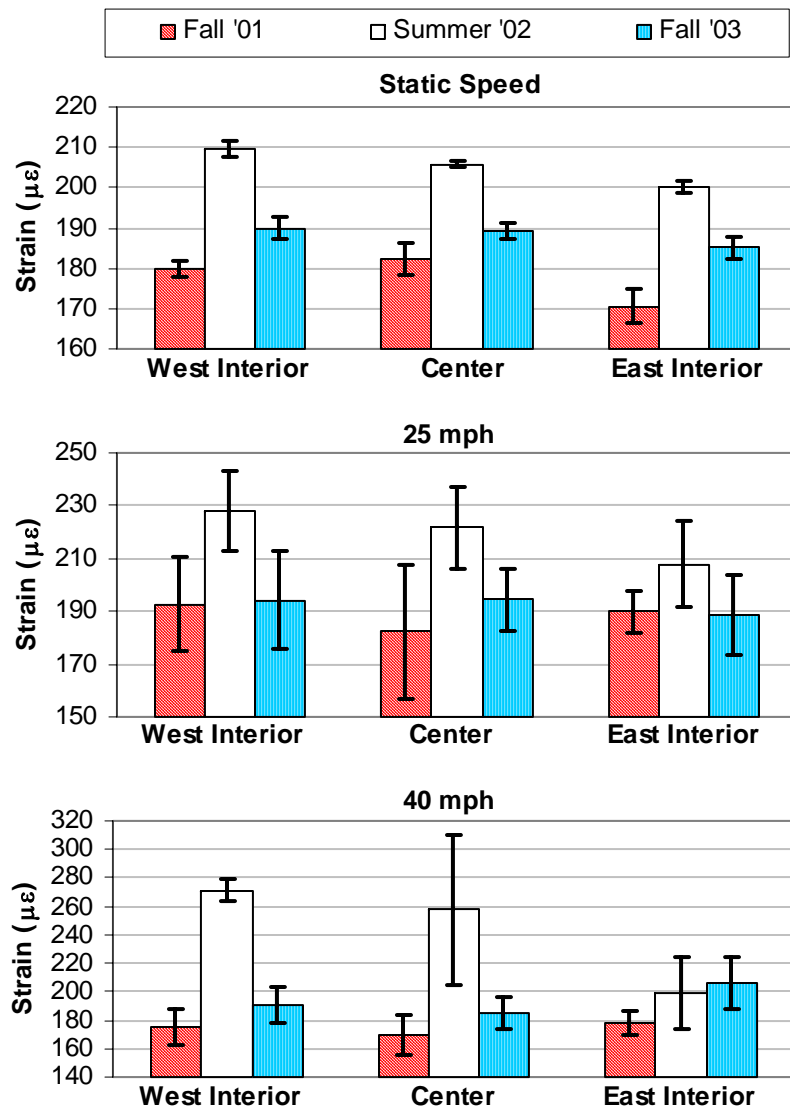


(a)

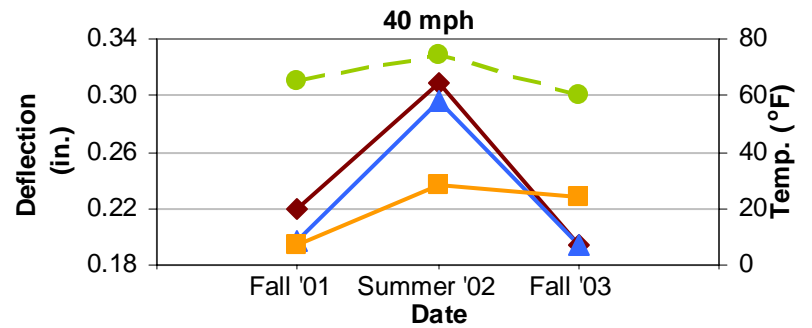
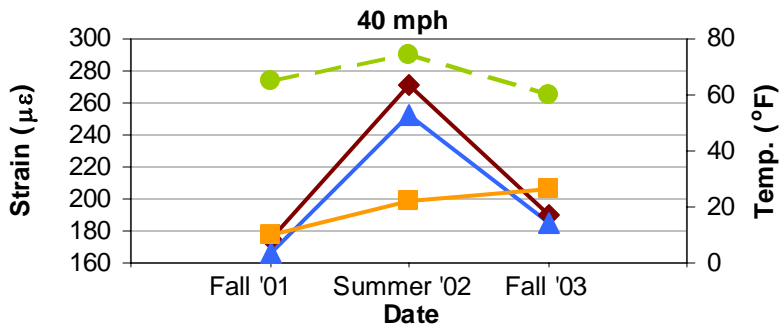
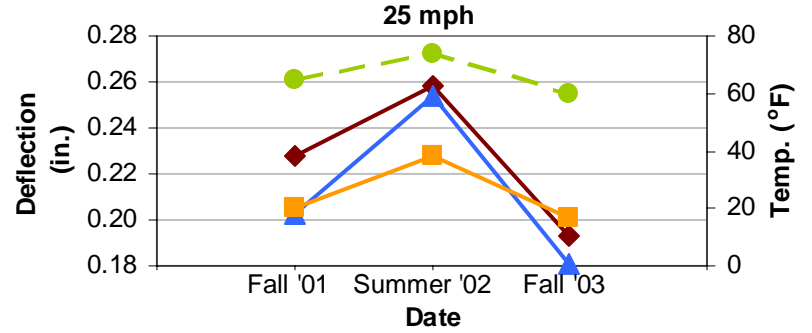
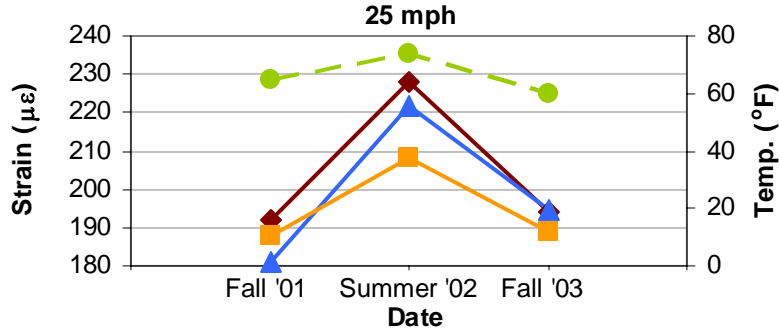
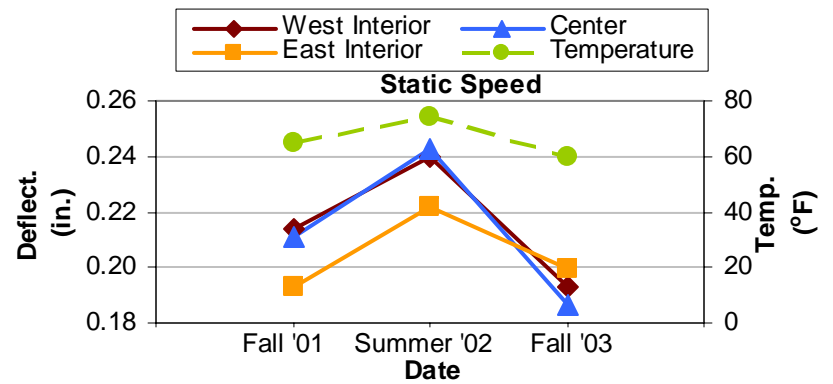
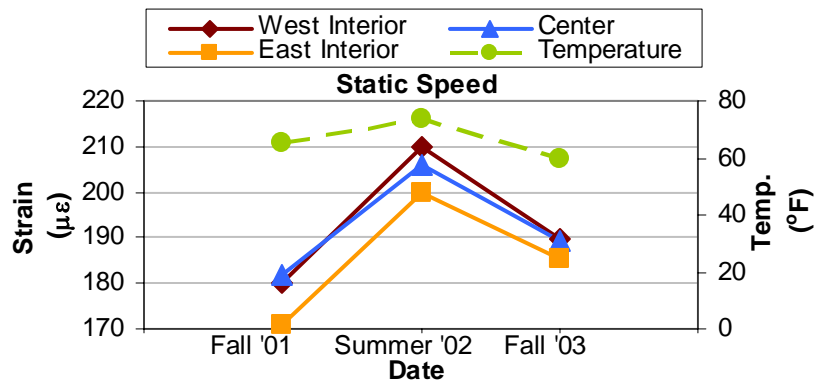


(b)

**Figure 3-7.** Average peak (a) strain and (b) deflection in the most heavily loaded girder for the three exterior truck orientations in the Route 601 Bridge; all exterior orientations were tested at static speed.



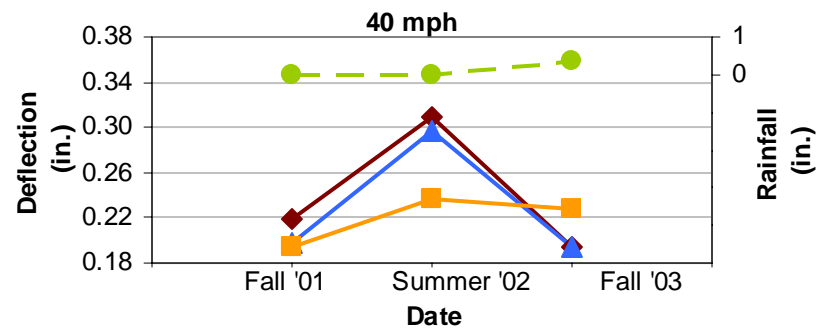
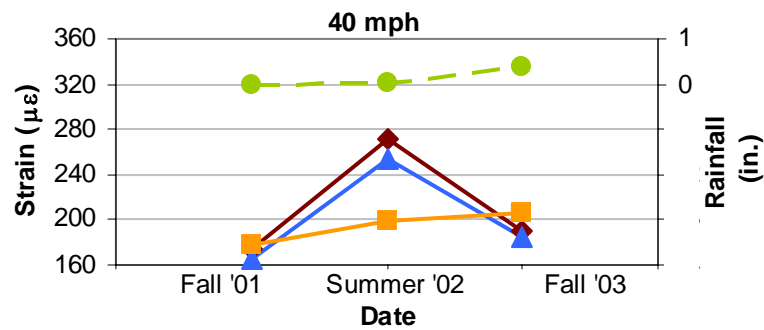
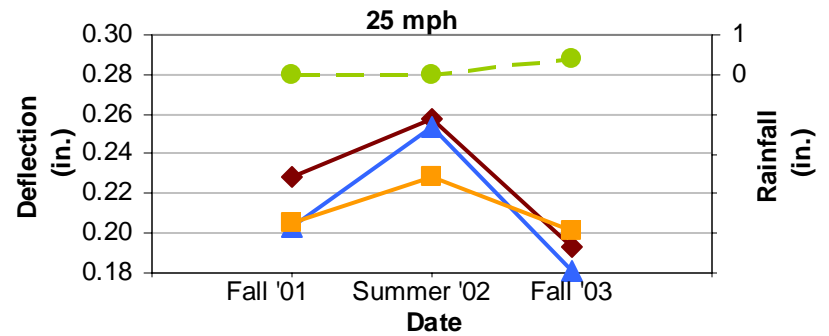
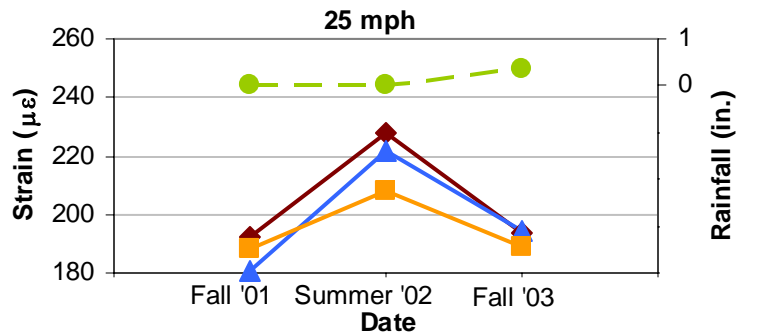
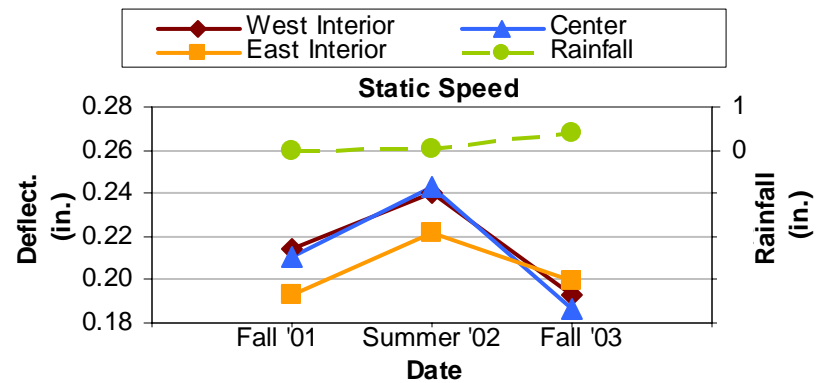
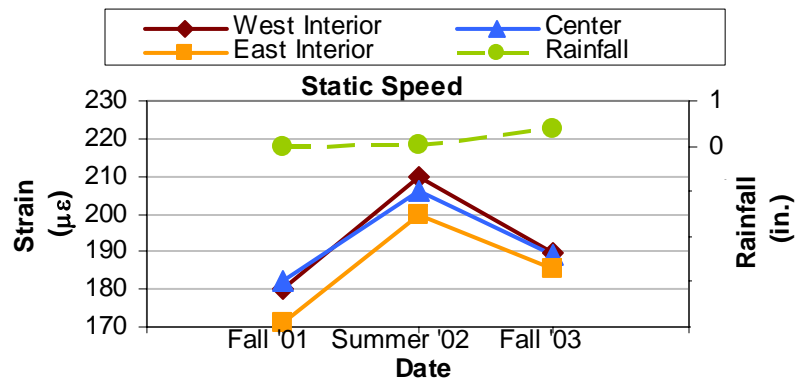
**(a)** **(b)**  
**Figure 3-8.** Error bars for the average peak (a) strain and (b) deflection for the most heavily loaded girder for the interior orientations in the Route 601 Bridge.



(a)

(b)

Figure 3-9. Average peak (a) strain and (b) shown with the average temperature during testing at the Route 601 Bridge.



(a) (b)  
**Figure 3-10.** Average peak (a) strain and (b) deflection shown with the total rainfall during the week prior to testing at the Route 601 Bridge.

## **Chapter 4: Results for Wheel Load Distribution, *g***

The transverse wheel load distribution was determined using both the midspan flexural strain and deflection measurements. Figure 4-1 through Figure 4-3 show the typical load distribution to the supporting beams in the Toms Creek Bridge and Route 601 Bridge. Although all of these graphs show data from static speed tests, the distribution behavior is similar regardless of the truck speed.

Figure 4-1 has been developed using the strain data for the Toms Creek Bridge because a larger number of beams had strain gages on them versus the number of beams instrumented with deflectometers. Note that for the purposes of data analysis of the Toms Creek Bridge, both strains and deflections in those beams that did not have the respective instrumentation have been linearly interpolated using measurements in adjacent beams.

Unfortunately for the Route 601 Bridge tests, the midspan flexural strain gage for Girder 1 (i.e., the west exterior girder) failed after testing began. Therefore, Figure 4-2 and Figure 4-3 have been generated using deflection measurements. For the purposes of data analysis in the Route 601 Bridge, the strain measurements for Girder 1 have been extrapolated using either a two-point linear fit or a three-point or four-point parabolic fit of the strain recordings in the respective number of beams adjacent to Girder 1. The decision on which type of fit to use in the extrapolation for each truck orientation has been based on how close a given model reflects the recorded behavior of the east side of the bridge, where all of the gages were functioning properly. An additional adjustment has been applied to Girder 1 in accordance with the percent error in the extrapolation model when compared to the actual recorded value for Girder 8 (i.e., the east exterior girder that had a functioning strain gage).

### **4.1 Procedure for Calculating the Wheel Load Distribution**

For the purposes of consistency in comparing results, the procedure listed below for calculating the wheel load distribution is the same procedure that both Neely and Restrepo used in their research. The procedure follows the same steps regardless of whether the calculations used midspan strain or deflection data in the analysis. The first step was to determine the maximum recorded value amongst all of the beams for each individual load test. The corresponding girder number and the time at which the maximum measurement occurred were

also noted. Next, the strains or deflections in all of the other beams at the time of the maximum recorded value were collected within each load test. From this information, the wheel load distribution was calculated using the equation:

$$g = \frac{R_{\max}}{\sum R_i} \quad (4-1)$$

where  $g$  is the wheel load distribution, expressed in a decimal format,  $R_{\max}$  is the maximum response recorded during an individual load test, and  $R_i$  is the strain or deflection in the  $i$ -th girder at the time of the maximum response. Note that Eq. (4-1) assumes that all of the beams have the same section modulus. This assumption is not completely accurate because of the edge stiffening effect of the timber curbs and guide rails (Kim and Nowak, 1997). However, for the purposes of this study, this discrepancy has been deemed negligible.

Note that Eq. (4-1) only calculates the maximum  $g$  in any given load test. This calculation is sufficient because the AASHTO guidelines for bridge design allow for a beam-line analysis of the most heavily loaded girder to estimate the load effect across the entire bridge system (Barker and Puckett, 1997). From the values calculated in Eq. (4-1), an average wheel load distribution was calculated using all of the repetitions for a given combination of truck orientation and speed mentioned in Sections 2.4.1 and 2.4.2.

As noted above,  $g$  is in a decimal format. However, as discussed in Section 1.2.5.2 of this report, wheel load distribution has traditionally been represented as a distribution factor in the form of Eq. (1-6). Therefore, the wheel load distributions calculated using Eq. (4-1) will also be referenced to Eq. (1-6) for the Toms Creek Bridge and the Route 601 Bridge, where  $S$  is 0.94 ft and 3.5 ft, respectively. Note that  $S$  for the Toms Creek Bridge is merely the average beam spacing across the width of the bridge, since the beams are not evenly spaced, as shown in Figure 1-2. For the purposes of this study, girder distribution factors will be expressed on a “per axle” basis, which is the practice specified in the AASHTO LRFD design guidelines. This practice is different from the AASHTO *Standard Specifications*, where the distribution factor is calculated “per wheel line,” or half of the axle weight. In order to convert the “LRFD” distribution factor into “Standard” terms, the distribution factor must be multiplied by two.

## 4.2 Wheel Load Distribution Results for the Toms Creek Bridge

### 4.2.1 Results from Current Study of Toms Creek Bridge

The maximum and average results for the wheel load distribution determined from the Summer 2003 field tests appear in Table 4-1 for the strain measurements and Table 4-2 for the deflection measurements. Looking at the Summer 2003 combinations of truck orientation and truck speed, the individual values for  $g$  calculated from the strain measurements are essentially equal (i.e., within 0.01 of each other). The maximum average load distribution based on strain is 0.084 ( $S/11.1$ ) in the southbound orientation at static speed, while the lowest average value for  $g$  is 0.073 ( $S/12.8$ ) in the center orientation at 40 mph (64 kph). Likewise, the wheel load distributions calculated using the recorded deflections are also similar amongst all of the orientation-speed combinations. The largest average deflection-based value of  $g$  is 0.078 ( $S/12.0$ ), which occurred in the southbound orientation at 40 mph (60 kph). The smallest average load distribution was 0.069 ( $S/13.6$ ), at 40 mph (60 kph) in the center orientation.

Except for the  $g$  calculated for the southbound lane using deflection measurements, the wheel load distributions for the static load tests were equal to or greater than those distributions from the dynamic tests. However, any differences are small. Hence, one can conclude that the effect of a vehicle's speed on  $g$  is not significant in the Toms Creek Bridge. Based on the largest average distribution value from the strain data collected during the July 2003 tests, the wheel load distribution for the Toms Creek Bridge is 0.084 ( $S/11.1$ ).

Generally speaking, the wheel load distributions determined from the deflection measurements are about the same as the distributions calculated from the strain measurements, matching the predicted behavior prior to the field tests. Although the  $g$  calculated from the flexural strain measurements does not include the shear strains in the beams,  $g$  calculated from the deflection does include the shear deflection as well as the flexural deflection. In many applications with FRP, shear strain is important because the ratio of in-plane longitudinal elastic modulus versus the in-plane shear modulus for composite materials is ten to thirty times greater than the same ratio for isotropic materials. Hence, the Bernoulli-Euler beam theory is not applicable for FRP beams, regardless of whether the loading is static or dynamic (Bank, 1987). Therefore, shear deformation must be considered in the deflections of thin-walled composite structures. However, even though shear strain is not included when calculating the girder

distribution factor using flexural strain measurements, the shear contribution is virtually cancelled out since the shear strain is in each term in the summation in the numerator and denominator. Thus, the results for  $g$  calculated using either the flexural strain or the deflection data should give approximately the same values, as stated above.

#### **4.2.2 Comparison of Current Study with Previous Toms Creek Bridge Tests**

In addition to the Summer 2003 tests, Table 4-1 and Table 4-2 also summarize the results from the previous tests that Neely performed from 1997 to 1999. The average  $g$  data in these two tables are also graphically represented in Figure 4-4 and Figure 4-5. There are no results for load distribution factors based on deflection data for the Fall 1997 and Spring 1998 tests because there were not enough deflectometers available to warrant this calculation. As noted for the Summer 2003 data in the previous section, the wheel load distributions calculated from the deflection measurements in the previous test dates tend to be about the same as those values that were determined from the strain data.

In general terms, the average wheel load distributions from the Summer 2003 tests are equal to or less than those values calculated in 1997-1999 load tests. Looking at the strain data, the largest difference occurred between the Fall 1998 and the Summer 2003 tests for the northbound orientation at 40 mph (64 kph); this difference is 0.02 (0.098 vs. 0.078 for the respective dates). For the southbound orientation, the largest difference is a 0.015 decrease (0.091 vs. 0.076) from Fall 1999 to Summer 2003, again at the 40 mph (60 kph) speed. Comparisons for the center orientation show very little change in  $g$  over time (within  $\pm 0.005$ ). The static tests exhibit similar changes. On the other hand, the results for the 25 mph (40 kph) tests show virtually no change in wheel load distribution. However, recall that the Summer 2003 field test only conducted the 25 mph (40 kph) test in the southbound orientation.

While the strain data show that the largest decrease in average wheel load distribution over time was 0.02, the deflection data show decreases that are slightly larger, with the greatest decrease being about 0.03 between the Fall 1998 and Summer 2003 dates at 40 mph (60 kph) in the northbound orientation (0.103 vs. 0.075, respectively). In fact, the Fall 1998 deflection data has the largest difference with the Summer 2003 data in the other two orientations as well. In the southbound orientation, the change in  $g$  is 0.02 (0.098 vs. 0.078, respectively, at 40 mph [60 kph]). Similar to the strain data, the center orientation at static speed shows a negligible change in  $g$  over time (0.081 vs. 0.079).

The results in Table 4-1 and Table 4-2 raise the question of whether or not there is a relationship explaining the changes in the measured distribution factors over time. Figure 4-6 shows the average wheel load distributions calculated from both the strain and deflection data for the three different orientations at static speed, along with the superimposed  $2\sigma$  error bars, as described in Section 3.1.2. Looking at the static speed graphs for strain measurements in the center orientation and the deflection measurements in the southbound orientation, the conclusion is that there is very little difference amongst the six test dates, given the confidence limits expressed by the error bars. However, the graphs for the strain measurements made in the northbound orientation and the deflection measurements in the center orientation show that the data on these dates are from different populations. Additionally, the error bars for the dynamic load tests tend to be larger, indicating a greater scatter in the data within each orientation. These larger error bars indicate greater uncertainty, and therefore not much of a statistically significant difference in the data.

However, a more rigorous investigation using the Anderson-Darling test, from the MIL-HDBK-17 statistical analysis program mentioned in Section 3.1.2, showed that the set of distribution factors for each respective orientation-speed combination from the six test dates did not come from the same population. Even when grouping the tests into “Fall” and “Spring” sets, as described in Section 3.1.2, there are mixed results as to whether the data in the respective groups come from the same population. Therefore, the resulting conclusion is that there is a statistically significant difference in the data presented in Table 4-1 and Table 4-2, meaning that there must be an external cause leading to the changes in  $g$ .

The question is, then, what is the reason for the Summer 2003 results being generally less than the results from the 1997 to 1999 tests. One point to note is that prior to testing in the Fall of 1997 and Spring of 1998, Neely tightened all of the deck-to-girder connections, as well as those connections at the abutments. The pre-tightening could potentially stiffen the structural members, thus decreasing the strain and deflection in the beams. However, Neely concluded in his work that the connections in the Toms Creek Bridge added little benefit in terms of composite action in the bridge. Hence, the differences in experimental procedure should be negligible in comparing the different tests in this study.

In looking at Eq. (4-1), there are three possible scenarios that would lead to a lower wheel load distribution over time. First, the numerator in the equation, i.e., the maximum peak strain or

deflection in any one girder could be smaller. This scenario would mean that the most heavily loaded girder is gaining stiffness over time. The second possibility is that the denominator is increasing, which would mean that all of the beams exhibit larger strains or deflections as the beams are losing stiffness over time. The third conclusion could be that both the data for the numerator and denominator are changing over time, but that one is changing at a greater rate than the other.

As a way of examining these three possibilities, refer back to Table 3-1, which presents the peak strain data for the maximum loaded beam. Then consider Table 4-3, which lists the sum of the strains in all of the beams together in the Toms Creek Bridge at the time of the maximum peak strain. Both the strain in the maximum loaded beam and the total strain in all of the beams appear to increase over time (compare Figure 3-1 and Figure 4-7). However, when comparing the Summer 2003 data with the previous tests, the percentage change in the total strain is generally greater than the percentage change in the strain for the maximum loaded beam, as evidenced by Figure 4-9 through Figure 4-11. This observation is particularly true for the northbound and southbound orientations, which explains why the wheel load distributions in those orientations have decreased slightly over time. The data for the center orientation shows that the comparative change in the two components for calculating  $g$  is small, thus resulting in the minor changes in the wheel load distribution for the center orientation over time. Similar results occur when considering the deflection data for the Toms Creek Bridge (compare Table 3-2 with Table 4-4, and compare Figure 3-2 with Figure 4-8). Therefore, the conclusion is that the wheel load distribution decreases slightly over time, and this decrease is due to the sum of all of the beams losing some stiffness.

While the information just presented provides a mathematical explanation for the change in wheel load distribution over time, this analysis does not explain why the overall beam behavior exhibits varying strains and deflections over time. Refer to Section 3.1.2 for a discussion on how the ambient air temperature and moisture might have an impact on the bridge's performance in terms of peak strain and deflection. The same argument applies to the variation of wheel load distributions over time.

In terms of relating the long-term results in the Toms Creek Bridge with AASHTO's guidelines for wheel load distributions, consider Figure 4-12. This chart shows AASHTO's recommended limits for both the *Standard Specifications* and *LRFD Specifications*, along with

the theoretical lower limit for  $g$  if the deck were infinitely stiff (i.e., a load going across the bridge would be evenly distributed amongst all of the beams). In his research, Neely recommended using the same girder distribution factors in the Toms Creek Bridge as a bridge with a 4-in. to 6-in. thick glulam deck supported by steel stringers. For this type of bridge, the *AASHTO Standard Specifications* call for  $D$  in Eq. (1-6) to be 8.0 for a single lane load case, while the *LRFD Specifications* prescribe  $D$  to be 8.8. Using the average beam spacing of 0.94 ft (285 mm),  $g$  in Eq. (1-6) works out to be 0.12 and 0.11 for the *AASHTO Standard Specifications* and *LRFD Specifications*, respectively. Note that no distinction is made between an exterior and interior girder in Figure 4-12 since none of the truck orientations had a wheel line bearing directly over either of the exterior beams.

The average experimental values in Figure 4-12 include all of the truck orientations and travel speeds tested on a given date, with the accompanying error bars indicating the amount of variation within the corresponding data set. Clearly, the average wheel load distributions are well below AASHTO's suggested limits. Even taking the data variability into account, the possible extreme values for  $g$  are within AASHTO's LRFD guidelines ( $S/8.5$ ), which are even lower than the *AASHTO Standard Specifications*. Therefore, based on the results in Figure 4-12, the suggested design wheel load distribution for bridges with 8-in. FRP DWB supporting a  $5\frac{1}{8}$ -in deck is 0.11 ( $S/8.5$ , per axle).

### **4.3 Wheel Load Distribution Results for the Route 601 Bridge**

#### **4.3.1 Results from the Current Study of Route 601 Bridge**

The results for the wheel load distribution determined from the Fall 2003 field tests appear in Table 4-5 for the strain measurements and Table 4-6 for the deflection measurements. Looking at both strain and deflection data, the exterior girders have the largest value of  $g$ , regardless of whether both lanes are loaded or only one lane is loaded. Based on the strain recordings, the largest average value for wheel load distribution is 0.326 ( $S/10.7$ ) in both the west exterior and multiple-lane orientations. This value is about 0.02 greater than  $g$  for the east exterior orientation, which is 0.302 ( $S/11.6$ ). As noted in Section 2.4.2, the distributions for these three orientations were only determined at static speed.

On the other hand, the wheel load distributions for the interior and center orientations were calculated for all three speeds (static speed, 25 mph [40 kph], and 40 mph [64 kph]). The

results for  $g$  based on strain data in these three orientations are similar within each speed category. At static speed, the largest average distribution is 0.257 ( $S/13.6$ ) in the west interior orientation, while the center orientation had the smallest value at 0.245 ( $S/14.3$ ). The other two speeds have similar results when comparing the largest and smallest values for  $g$  within the interior orientations. However, the data tends to show a consistent decline in  $g$  with an increase in speed. For example, Table 4-5 shows that the wheel load distribution for the center orientation is 0.245 ( $S/14.3$ ) at static speed, but is 0.239 and 0.222 ( $S/14.6$  and  $S/15.8$ ) for 25 mph and 40 mph (40 kph and 64 kph), respectively.

Results from the same Anderson-Darling test used in Section 3.1.2 show that these values are not from the same population; similar results occur for the west interior and east interior orientations. Hence, based on the strain measurements in the Route 601 Bridge, the conclusion is that speed does have some effect on the wheel load distribution, i.e., an increase in speed results in a lower  $g$ . However, there is no other known literature that supports this conclusion. In fact, neither the AASHTO Standard nor the AASHTO *LRFD Specifications* connect the girder distribution factor to speed. The  $g$  from the *Standard Specifications* is merely based on the type of bridge and the girder spacing, while the  $g$  from the *LRFD Specifications* is a function of girder spacing, span length, deck thickness, stiffness parameters, and skew (AASHTO, 1996; AASHTO, 1998). Although the repairs at the approaches appeared to mitigate the problems noted in Section 2.4.2, perhaps the conditions continued to have an effect on the wheel load distribution during dynamic testing.

Similar results occur when considering the deflection measurements, where there appears to be a big difference between loading the exterior girders versus the interior girders. For the exterior orientations, the average wheel load distributions range from 0.343 ( $S/10.2$ ) in the multiple-lane loading to 0.283 ( $S/12.4$ ) for the east exterior orientation. For the interior orientations,  $g$  is 0.252 ( $S/13.9$ ) for the east interior orientation, while  $g$  is 0.221 ( $S/15.8$ ) in the center loading case. Like the results from the strain data, there is a decrease in the wheel load distribution as the speed increases, although that difference is somewhat smaller.

Although the wheel load distributions calculated from deflections measurements generally parallel the calculations using the recorded strain, the differences between the two measurement methods appear to be greater than the differences in the Toms Creek Bridge results. For the different orientation-speed combinations, the wheel load distributions calculated

using the strain information is at most 0.02 greater than the distributions calculated from the deflection data. As explained in Section 4.2.1, these results are surprising in that the  $g$  calculated using the deflection measurements are generally expected to be about the same as the  $g$  calculated using the strain data.

One possible explanation for the larger difference between the strain and deflection data could be because the strain in Girder 1, i.e., the west exterior girder, needed to be extrapolated from the data for the adjacent girders since the flexural strain gage at Girder 1 failed after the onset of testing. However, one of the larger differences between the two measurement methods occurs when a single load truck is oriented in the east exterior position (i.e., a truck wheel line is positioned over Girder 8). In this orientation, the response in Girder 1 is near zero for both the measured deflection and the extrapolated strain. Therefore, any errors in calculating the wheel load distribution for the east exterior orientation using the extrapolated strain should be negligible. Since the two measurement methods do give different results, however, there must be another reason for the difference in the calculated GDF for the east exterior orientation, as well as the other orientations. A second reason could be the location of the deflectometers in relation to the beams' longitudinal midpoint, as explained in Section 4.2.1. Regardless of the reasons for the discrepancy, the suggested value for wheel load distributions in the Route 601 Bridge should be based on the strain measurements since the strain measurements yield slightly higher distributions, thus giving a slightly more conservative design.

#### **4.3.2 Comparison of Current Study with Previous Route 601 Bridge Tests**

Besides the Fall 2003 tests, Table 4-5 and Table 4-6 also present the data for the tests that Restrepo conducted in the Fall of 2001 and Summer of 2002. All of this data is graphically represented in Figure 4-13 through Figure 4-16. Like the Fall 2003 tests, the previous two tests have wheel load distributions calculated from strain data that are generally marginally greater than the distributions calculated from the deflection data. However, the Summer 2002 results for static speed in the west exterior orientation show that the strain-based wheel load distribution is actually 0.045 *less than* the deflection-based distribution.

Simply looking at the  $g$ -values calculated from the strain data, there appears to be a fairly consistent pattern amongst the interior orientations. Although the wheel load distribution values increase and decrease depending on which interior orientation, over time the results are generally within  $\pm 0.01$  of each other. On the other hand, the exterior orientations exhibit a slightly more

erratic behavior. For example,  $g$  for the east exterior orientation increases by 0.03 while  $g$  for the west exterior *decreases* by 0.03. Recall that the exterior orientations were only tested at static speed, with the east and west exterior orientations only being tested twice, in Summer 2002 and Fall 2003. Nevertheless, the strain results appear to yield similar wheel load distributions.

As mentioned earlier, the wheel load distributions calculated from the deflection data are slightly different from those calculated using the strain measurements. The largest differences in the deflection results appear in the center and east interior orientations. When going from Fall 2001 to Summer 2002, the wheel load distribution for the center orientation increases for all three test speeds, while the load distribution for the east interior orientation *decreases*. On the other hand, when comparing the Fall 2003 results with the Summer 2002 tests, the opposite results occur. Regardless, the changes over time tend to be relatively small. For example, the value for  $g$  in the center orientation decreases anywhere from 0.015 to 0.020 for the three speeds, while the wheel load distribution in the east interior orientation increases by about 0.020 to 0.030. For the west interior orientation, there is little change in  $g$ , regardless of speed or when the test occurred. Similarly, the west exterior and the multiple-lane orientations exhibit little change. However, the east exterior orientation exhibits a somewhat larger decrease in  $g$  (0.339 versus 0.283).

Like the Toms Creek Bridge data, statistical analysis provides a basis for comparing whether or not the results in the Route 601 Bridge are a part of the same population when considering the three different test dates. Figure 4-17 and Figure 4-18 show the average maximum wheel load distributions with the superimposed error bars for all test speeds the interior truck orientations, based on strain and deflection, respectively. Generally speaking, the error bars show that, given the level of confidence from the number of load tests that took place, there isn't much of a statistical difference in the results when considering the different test dates within a given orientation-speed combination. However, with the exception of the multiple-lane orientation and the west interior orientation at 25 mph (40 kph), the more rigorous statistical analysis using the Anderson-Darling test shows that, in fact, the results are not part of the same population, even when considering just the data collected during the Fall seasons. The fact that the data are not definitively from the same population in the Anderson-Darling test leads to the conclusion that the changes in the wheel load distributions over time in the Route 601 Bridge are

statistically significant and must be due to a reason other than scatter in the data collected over the span of three load tests.

In finding that reason, a comparison should be made between the average peak strain or deflection and the average sum of the respective quantity in all of the girders at the time of the peak measured value, just as was done for the Toms Creek Bridge. Table 4-7 and Table 4-8 show the average total measured strain and deflection, respectively, in the Route 601 Bridge at the time of the peak measured value. These two tables serve as a comparison to Table 3-4 and Table 3-5, which as mentioned in Section 3.2.1, give the respective peak strain and deflection in the most heavily loaded girders. Note that the data in Table 4-7 and Table 4-8 is graphically detailed in Figure 4-19 and Figure 4-20, which serve as a comparison to Figure 3-6 and Figure 3-7.

In comparing the strain data for the Fall 2001 and Fall 2003 tests, consider Figure 4-21 through Figure 4-24, which compare the percentage change from a given test date to the Fall 2003 test in peak measured data with the total measured data at the time of the peak strain or deflection for the various truck orientations and travel speeds. Generally, the peak strain in the most heavily loaded girder has a larger percentage increase than the total strain in all of the girders at the time of peak strain. Consequently, the wheel load distributions generally increase from Fall 2001 to Fall 2003. However, looking at the Summer 2002 and Fall 2003 results, the numerator and denominator for calculating  $g$  either change by the same percentage amount, or the peak strain decreases at a greater rate than the total strain at the time of peak strain. Hence, the wheel load distributions are stable or slightly lower in the Fall 2003 tests compared to the Summer 2002 tests.

Similarly, the deflection data show that both the peak deflection and the total deflection in all of the girders at the time of peak deflection decrease over time. This decrease occurs when comparing the Fall 2003 tests with either the Fall 2001 tests or the Summer 2002 tests. However, despite the fact that both the numerator and denominator in Eq. (4-1) decrease, the relative amount of change between these two factors differs amongst the various truck orientations. In the center orientation, for instance, the peak girder deflection decreases at a faster rate than the total girder deflection. Consequently,  $g$  for the center orientation is lower at all three test speeds in Fall 2003 than the other two dates. On the other hand, the east interior orientation shows that the rate of decrease in the peak deflection is less than the decline in total

deflection. Thus, the wheel load distributions tend to increase in the tests for the east orientation in Fall 2003. Meanwhile, the relative change between the peak girder deflection and total deflection is about the same for the west interior orientation, resulting in stable wheel load distributions amongst the three test dates for that orientation.

Unfortunately, there is no clear answer as to the reason behind the variation in the wheel load distributions amongst the three test dates. Unlike the Toms Creek Bridge, where the ambient air temperature appears to have a dominant effect on wheel load distribution, temperature's effect does not seem to be a significant factor on the change in  $g$  in the Route 601 Bridge. Since all of the girders experience the same change in temperature, then the resulting wheel load distributions in the respective truck orientations should follow roughly the same pattern. However, as described previously in Figure 4-14 through Figure 4-16, there is little consistency in the changes in  $g$  amongst the different orientations. The same can be said for any effects that rainfall or other moisture would have on the bridge's performance.

Loss of composite action between the glulam deck and FRP beams is another possible explanation behind the changes in wheel load distribution. Interaction between the deck and the girders can increase the effective moment of inertia, thus making the overall bridge structure stiffer and shifting the neutral axis upwards in the individual girders. The result should be a more even distribution of load to all of the girders acting compositely with the deck, hence a lower value for the maximum  $g$ . However, Waldron concluded in his work that there is very little composite action taking place in the Route 601 Bridge (2001). Although the deck-to-girder connections in the Route 601 Bridge are quite different from the design in the Toms Creek Bridge, Waldron discovered that a large amount of deformation occurs in the area where the bolts connect the glulam deck to the girders. The deformation is attributed to the poor bearing capacity in the timber deck as horizontal shear forces transfer from the girders to the deck. Consequently, the Route 601 Bridge design did not include the benefits of composite action, and any composite action that existed when the bridge was first constructed should have dissipated, certainly by the time of the Summer 2002 load tests. Therefore, loss of composite action in some of the beams cannot be counted as a major reason why the wheel load distributions have changed during the bridge's time in service.

Despite not knowing the reason behind the change in the wheel load distribution over time for the Route 601 Bridge, the general conclusion is that there is potential for  $g$  to increase

slightly over time, which contradicts the long-term results stated for the Toms Creek Bridge. Even though many of the truck orientations have values for  $g$  that remain stable or decrease slightly, the average wheel load distribution for the multiple-lane orientation increases nearly 0.04 (0.343 in Fall 2003 versus 0.306 in Summer 2002). This orientation is also the orientation with the largest wheel load distribution.

All of the above results need to be compared with the specifications set forth by AASHTO, as done in Figure 4-25 and Figure 4-26. These figures divide the wheel load distributions into three categories: a single interior lane loaded, a single exterior lane loaded, and multiple exterior lanes loaded. All of the graphs show the theoretical lower limit for  $g$ , which would be for the case of an infinitely stiff deck. Also, all of the graphs in these figures show the “proposed” wheel load distribution of 0.35, which is equivalent to  $S/10$  on a “per axle” basis, or  $S/5$  on a “per wheel line” basis. This value for  $g$  is what Waldron used in designing the Route 601 Bridge and is also what Restrepo recommended subsequent to his research. Additionally, Sub-figure (1) in Figure 4-25 shows the values for  $g$  for a single, interior lane load case. As dictated in the AASHTO *Standard Specifications* and *LRFD Specifications*, the wheel load distribution for this case is 0.389 and 0.398, respectively. Although the Route 601 Bridge has a  $5\frac{1}{8}$ -in. deck supported by FRP girders, the comparison with the *Standard Specifications* is based on a 4-in. thick glulam deck supported by steel stringers. Note that the *LRFD Specifications* make no distinction in the deck thickness when listing distribution factors for the glulam deck and steel stringer system. Sub-figure (2) in Figure 4-25, as well as Figure 4-26, shows the AASHTO requirement for  $g$  in an exterior lane. This value is determined using the Lever Rule and is equal to 0.50, regardless of which specification the engineer follows and regardless if one or multiple lanes are in consideration. Again, all of the wheel load distribution factors listed here are on a “per axle” basis.

Looking at the graphs in Figure 4-25 and Figure 4-26, the experimental girder distribution factors for all three lane categories (single interior, single exterior, and multiple exterior) fall below the limits set forth by AASHTO, regardless of when a given test took place and regardless of which design specification is considered. Likewise, the experimental averages are lower than Waldron and Restrepo’s proposed distribution factor. However, if one considers the variability in the data, there does appear to be a statistically significant chance that the girder distribution factor could be higher than the proposed value, as indicated by the error bars on the

graphs. The girder factors for the exterior lanes (both single and multiple) are the cases that are most likely to exceed the proposed value. However, the amount by which a probable experimental result would exceed the proposed limit is small, i.e., about 6% (0.37 for a probable  $g$  versus 0.35 for the proposed  $g$ ). A larger number of individual tests may help to reduce the variability in the data, thus making the proposed limit for the wheel load distribution more acceptable.

Therefore, the general conclusion for the Route 601 Bridge is that a truck positioned along an exterior girder yields larger load distribution factor. From the test results contained in this report, the recommended value for  $g$  is 0.35 ( $S/10$ , per axle) for design purposes. This conclusion is based on the deflection data for the sake of being conservative in designing with FRP beams. However, note that this recommended  $g$  is 30% below the more conservative AASHTO value of 0.50 ( $S/7$ , per axle), for both the *Standard Specifications* and *LRFD Specifications*. More testing is recommended in the future to see if in fact the load distribution continues to increase over time, particularly the east interior and exterior orientations. Additionally, further study may help to quantify the effects of temperature and moisture on the bridge's performance.

## 4.4 Tables and Figures

**Table 4-1.** Wheel load fractions based on strain data for the Toms Creek Bridge.

Researcher	Test Date	Speed (mph)	Truck Orientation								
			Southbound			Center			Northbound		
			No. of Tests	Max. g	Avg. g	No. of Tests	Max. g	Avg. g	No. of Tests	Max. g	Avg. g
Neely	Fall 1997	Static	2	0.096	0.095	2	0.077	0.076	2	0.089	0.088
		25	2	0.088	0.087	3	0.080	0.077	2	0.083	0.080
		40	2	0.101	0.089	2	0.079	0.078	2	0.084	0.081
	Spring 1998	Static	4	0.087	0.085	4	0.078	0.075	4	0.089	0.084
		25	3	0.086	0.082	4	0.078	0.074	3	0.081	0.079
		40	3	0.081	0.080	4	0.076	0.072	4	0.093	0.077
	Fall 1998	Static	6	0.097	0.088	6	0.081	0.078	5	0.099	0.096
		25	5	0.087	0.084	7	0.079	0.076	4	0.099	0.091
		40	4	0.093	0.089	5	0.078	0.073	5	0.104	<b>0.098</b>
	Spring 1999	Static	6	0.089	0.089	6	0.082	0.081	6	0.089	0.089
		25	3	0.089	0.088	6	0.081	0.080	3	0.083	0.083
		40	4	0.091	0.089	6	0.080	0.078	4	0.095	0.091
	Fall 1999	Static	6	0.098	0.095	5	0.082	0.078	6	0.098	0.095
		25	3	0.083	0.081	3	0.074	0.073	3	0.093	0.084
		40	5	0.098	<b>0.091</b>	5	0.071	0.069	6	0.097	0.093
Kasner	Summer 2003	Static	5	0.084	<b>0.084</b>	5	0.080	0.079	5	0.079	0.078
		25	5	0.081	0.079	—	—	—	—	—	
		40	5	0.077	<b>0.076</b>	5	0.074	<b>0.073</b>	5	0.085	<b>0.078</b>

**Table 4-2.** Wheel load fractions based on deflection data for the Toms Creek Bridge.

Researcher	Test Date	Speed (mph)	Truck Orientation								
			Southbound			Center			Northbound		
			No. of Tests	Max. g	Avg. g	No. of Tests	Max. g	Avg. g	No. of Tests	Max. g	Avg. g
Neely	Fall 1998	Static	6	0.087	0.081	6	0.082	<b>0.081</b>	5	0.095	0.092
		25	5	0.081	0.079	7	0.080	0.081	4	0.092	0.091
		40	4	0.101	<b>0.098</b>	5	0.081	0.079	5	0.107	<b>0.103</b>
	Spring 1999	Static	6	0.079	0.078	6	0.078	0.078	6	0.083	0.083
		25	3	0.078	0.073	6	0.077	0.077	3	0.080	0.079
		40	4	0.088	0.084	6	0.078	0.078	4	0.087	0.086
	Fall 1999	Static	6	0.081	0.079	5	0.075	0.074	6	0.099	0.091
		25	3	0.079	0.078	3	0.073	0.073	3	0.091	0.087
		40	5	0.097	0.090	5	0.072	0.072	6	0.106	0.102
Kasner	Summer 2003	Static	5	0.077	0.077	5	0.070	<b>0.070</b>	5	0.075	0.075
		25	5	0.078	0.075	—	—	—	—	—	
		40	5	0.079	<b>0.078</b>	5	0.070	<b>0.069</b>	5	0.078	<b>0.075</b>

**Table 4-3.** Maximum and average total flexural strain in all girders for the Toms Creek Bridge for the various truck orientations and speeds at the time of peak flexural strain (in microstrain).

Researcher	Test Date	Speed (mph)	Truck Orientation					
			Southbound Lane		Center Lane		Northbound Lane	
			<i>Max. Tot. Strain</i>	<i>Avg. Tot. Strain</i>	<i>Max. Tot. Strain</i>	<i>Avg. Tot. Strain</i>	<i>Max. Tot. Strain</i>	<i>Avg. Tot. Strain</i>
Neely	Fall 1997	Static	2748	2729	3048	3006	3076	3053
		25	2948	2735	—	—	—	—
		40	4763	4744	4844	4395	4465	4371
	Spring 1998	Static	3330	3235	4233	4162	3639	3526
		25	3735	3650	—	—	—	—
		40	5784	4679	5392	4797	4658	3881
	Fall 1998	Static	2508	2341	2795	2737	2766	2662
		25	2870	2795	—	—	—	—
		40	4092	4066	3998	3697	4131	4004
	Spring 1999	Static	3162	2657	4037	3959	3394	3186
		25	3110	3049	—	—	—	—
		40	4951	4833	5479	4766	4756	4502
	Fall 1999	Static	2675	2466	3101	2777	2940	2761
		25	2836	2771	—	—	—	—
		40	4439	4186	4699	3924	4344	4109
Kassner	Summer 2003	Static	3541	3521	3804	3769	3395	3383
		25	3935	3736	—	—	—	—
		40	6534	5787	5108	4564	4874	4810

**Table 4-4.** Maximum and average total deflection in the all of the girders for the Toms Creek Bridge, recorded at the time of peak deflection (measured in inches).

Researcher	Test Date	Speed (mph)	Truck Orientation					
			Southbound Lane		Center Lane		Northbound Lane	
			<i>Tot. Max. Peak Deflect.</i>	<i>Tot. Avg. Peak Deflect.</i>	<i>Tot. Max. Peak Deflect.</i>	<i>Tot. Avg. Peak Deflect.</i>	<i>Tot. Max. Peak Deflect.</i>	<i>Tot. Avg. Peak Deflect.</i>
Neely	Fall 1998	Static	2.299	2.225	2.629	2.579	2.790	2.732
		25	2.550	2.480	—	—	—	—
		40	3.885	3.791	3.574	3.255	4.363	4.181
	Spring 1999	Static	3.107	2.790	4.208	4.140	3.384	3.205
		25	2.949	2.925	—	—	—	—
		40	4.749	4.669	5.248	4.588	4.703	4.466
	Fall 1999	Static	2.545	2.296	3.051	2.495	3.244	2.852
		25	2.451	2.354	—	—	—	—
		40	4.236	3.978	4.247	3.458	4.261	4.080
Kassner	Summer 2003	Static	3.453	3.422	3.826	3.789	3.466	3.453
		25	3.773	3.635	—	—	—	—
		40	6.040	5.567	4.825	4.371	5.284	5.153

**Table 4-5.** Wheel load fractions based on strain data for the Route 601 Bridge. Fractions for multiple trucks are listed on a per truck basis.

Researcher	Test Date	Test Speed (mph)	Truck Orientation											
			West Exterior		West Interior		Center		Multiple Lanes		East Interior		East Exterior	
			Max. g	Avg. g	Max. g	Avg. g	Max. g	Avg. g	Max. g	Avg. g	Max. g	Avg. g	Max. g	Avg. g
Restrepo	Fall 2001	Static	—	—	0.248	0.247	0.240	0.236	0.330	0.322	0.242	0.240	—	—
		25	—	—	0.245	0.244	0.237	0.227	—	—	0.258	0.243	—	—
		40	—	—	0.233	0.228	0.232	0.227	—	—	0.247	0.242	—	—
	Summer 2002	Static	0.309	0.294	0.256	0.256	0.245	0.244	0.324	0.316	0.245	0.244	0.343	0.329
		25	—	—	0.253	0.251	0.243	0.239	—	—	0.245	0.242	—	—
		40	—	—	0.253	0.253	0.245	0.236	—	—	0.243	0.241	—	—
Kassner	Fall 2003	Static	0.334	<b>0.326</b>	0.260	<b>0.257</b>	0.251	<b>0.245</b>	0.343	<b>0.326</b>	0.250	0.248	0.306	<b>0.302</b>
		25	—	—	0.254	0.250	0.241	0.239	—	—	0.254	0.246	—	—
		40	—	—	0.249	0.241	0.242	0.222	—	—	0.237	0.235	—	—

**Table 4-6.** Wheel load fractions based on deflection data for the Route 601 Bridge. Fractions for multiple trucks are listed on a per truck basis.

Researcher	Test Date	Test Speed (mph)	Truck Orientation											
			West Exterior		West Interior		Center		Multiple Lanes		East Interior		East Exterior	
			Max. g	Avg. g	Max. g	Avg. g	Max. g	Avg. g	Max. g	Avg. g	Max. g	Avg. g	Max. g	Avg. g
Restrepo	Fall 2001	Static	—	—	0.242	0.241	0.233	0.232	0.310	0.306	0.234	0.233	—	—
		25	—	—	0.240	0.238	0.231	0.225	—	—	0.244	0.233	—	—
		40	—	—	0.233	0.231	0.225	0.222	—	—	0.229	0.225	—	—
	Summer 2002	Static	0.349	0.339	0.239	0.235	0.241	0.236	0.334	0.324	0.227	0.224	0.349	<b>0.339</b>
		25	—	—	0.236	0.234	0.242	0.237	—	—	0.224	0.223	—	—
		40	—	—	0.236	0.235	0.241	0.235	—	—	0.226	0.224	—	—
Kassner	Fall 2003	Static	0.339	0.334	0.239	0.238	0.223	<b>0.221</b>	0.354	<b>0.343</b>	0.253	<b>0.252</b>	0.284	<b>0.283</b>
		25	—	—	0.244	0.234	0.221	0.218	—	—	0.252	0.249	—	—
		40	—	—	0.236	0.234	0.223	0.217	—	—	0.248	0.245	—	—

**Table 4-7.** Maximum and average total flexural strain in all of the girders for the Route 601 Bridge for the different truck orientations and speeds, recorded at the time of peak flexural strain (measured in microstrain).

Researcher	Test Date	Test Speed (mph)	Truck Orientation											
			West Exterior		West Interior		Center		Two Trucks		East Interior		East Exterior	
			Max.Tot.	Avg.Tot.	Max.Tot.	Avg.Tot.	Max.Tot.	Avg.Tot.	Max.Tot.	Avg.Tot.	Max.Tot.	Avg.Tot.	Max.Tot.	Avg.Tot.
			Peak Strain	Peak Strain	Peak Strain	Peak Strain	Peak Strain	Peak Strain	Peak Strain	Peak Strain	Peak Strain	Peak Strain	Peak Strain	Peak Strain
Restrepo	October 2001	Static	—	—	744	740	790	785	1389	1370	747	737	—	—
		25	—	—	850	808	870	808	—	—	804	789	—	—
		40	—	—	831	789	788	770	—	—	790	772	—	—
	June 2002	Static	743	738	824	820	847	844	1471	1468	826	821	745	731
		25	—	—	953	907	960	926	—	—	896	859	—	—
		40	—	—	1098	1075	1146	1071	—	—	882	827	—	—
Kassner	October 2003	Static	648	643	748	740	776	771	1375	1307	752	746	732	728
		25	—	—	828	776	847	815	—	—	806	766	—	—
		40	—	—	818	789	905	839	—	—	907	876	—	—

**Table 4-8.** Maximum and average total deflection in the all of the girders for the Route 601 Bridge for the different truck orientations and speeds, recorded at the time of peak deflection (measured in inches).

Researcher	Test Date	Test Speed (mph)	Truck Orientation											
			West Exterior		West Interior		Center		Two Trucks		East Interior		East Exterior	
			Max.Tot.	Avg.Tot.	Max.Tot.	Avg.Tot.	Max.Tot.	Avg.Tot.	Max.Tot.	Avg.Tot.	Max.Tot.	Avg.Tot.	Max.Tot.	Avg.Tot.
			Peak Defl.	Peak Defl.	Peak Defl.	Peak Defl.	Peak Defl.	Peak Defl.	Peak Defl.	Peak Defl.	Peak Defl.	Peak Defl.	Peak Defl.	Peak Defl.
Restrepo	October 2001	Static	—	—	0.912	0.902	0.937	0.922	1.726	1.655	0.849	0.841	—	—
		25	—	—	0.994	0.964	0.972	0.909	—	—	0.910	0.898	—	—
		40	—	—	0.977	0.956	0.921	0.895	—	—	0.914	0.878	—	—
	June 2002	Static	0.948	0.940	1.027	1.022	1.034	1.031	1.881	1.879	0.992	0.988	0.929	0.913
		25	—	—	1.149	1.101	1.116	1.082	—	—	1.053	1.021	—	—
		40	—	—	1.329	1.313	1.331	1.263	—	—	1.126	1.057	—	—
Kassner	October 2003	Static	0.767	0.760	0.820	0.812	0.848	0.845	1.531	1.472	0.793	0.791	0.766	0.747
		25	—	—	0.874	0.821	0.853	0.830	—	—	0.825	0.806	—	—
		40	—	—	0.849	0.830	0.958	0.894	—	—	0.962	0.931	—	—

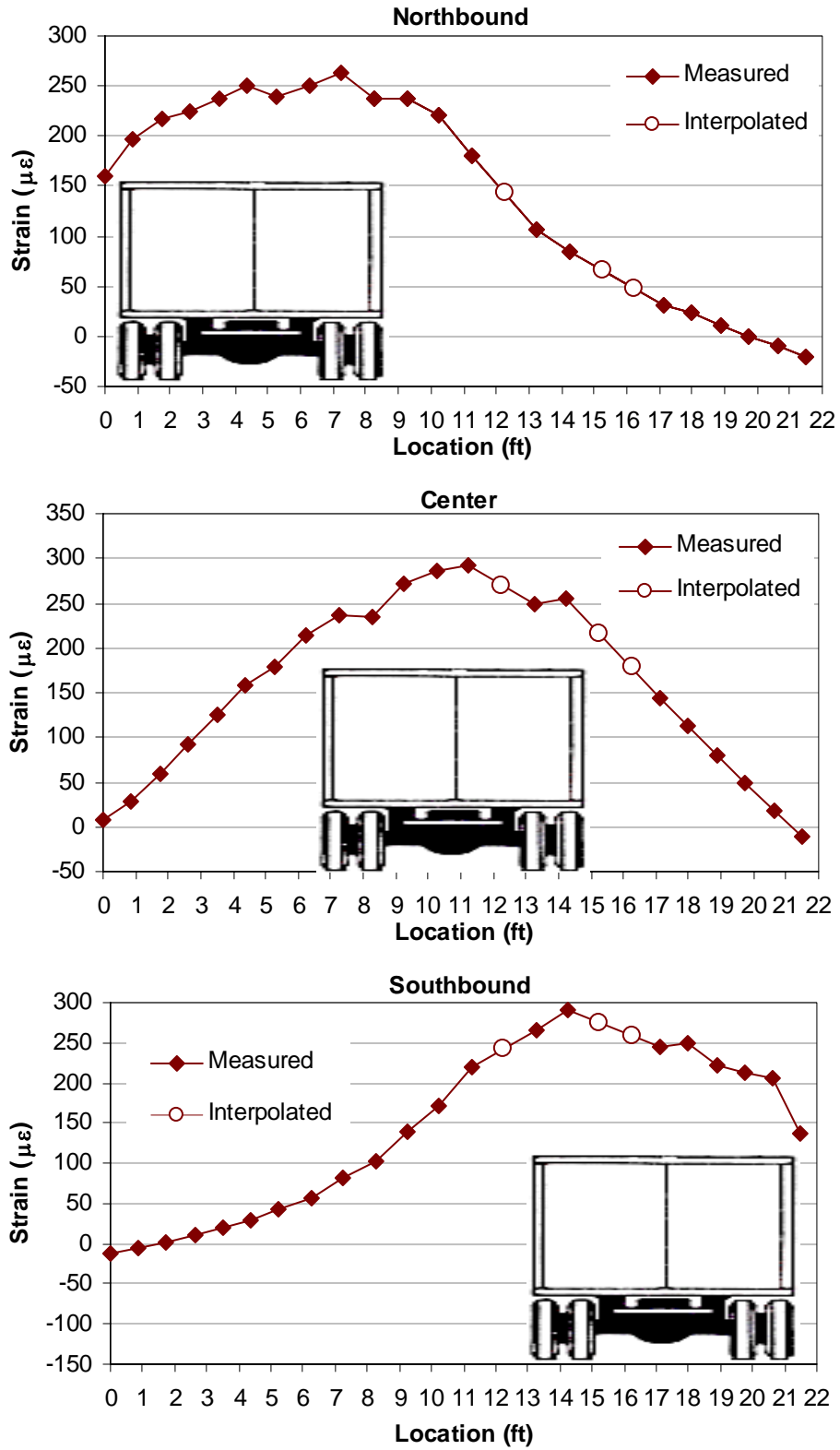


**Figure 4-1.** Typical girder responses to a load truck for the various truck orientations on the Toms Creek Bridge, shown at the time of maximum strain at static speed.

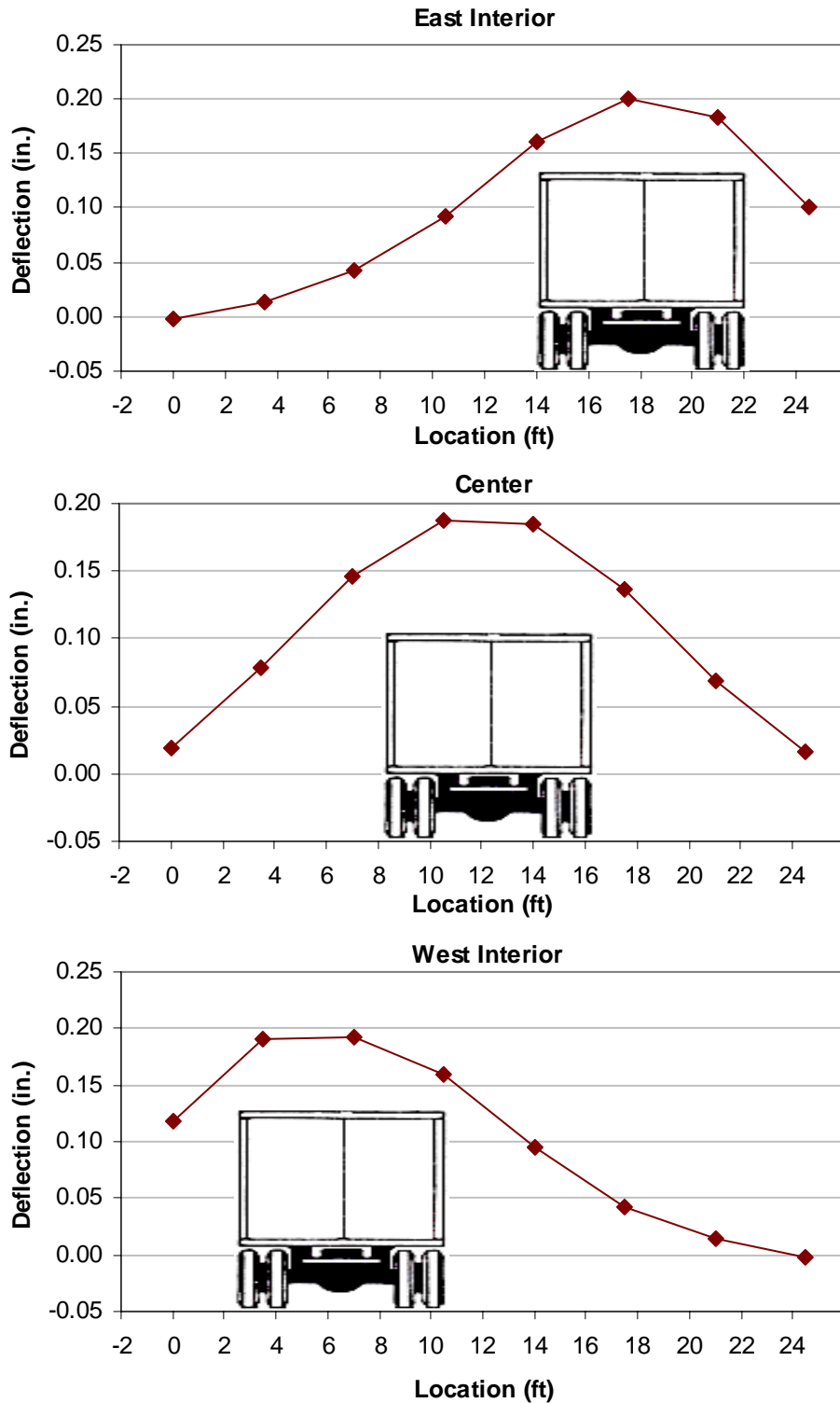


**Figure 4-2.** Typical girder responses to a load truck for the East Interior, Center, and West Interior orientations on the Route 601 Bridge, shown at the time of maximum deflection at static speed.

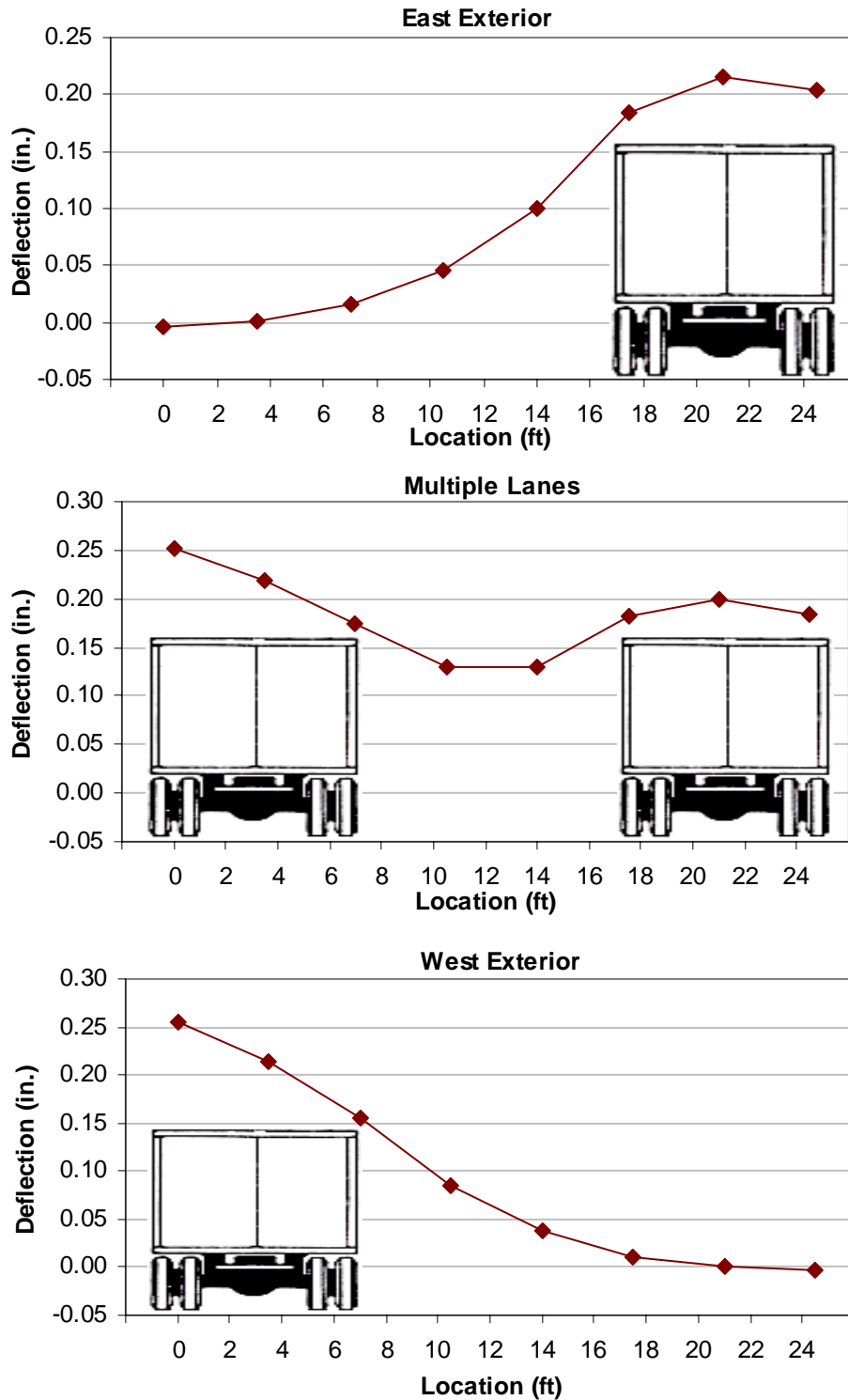


**Figure 4-3.** Typical girder responses to a load truck for the East Exterior, Multiple Lanes, and West Exterior orientations on the Route 601 Bridge, shown at the time of maximum deflection at static speed.

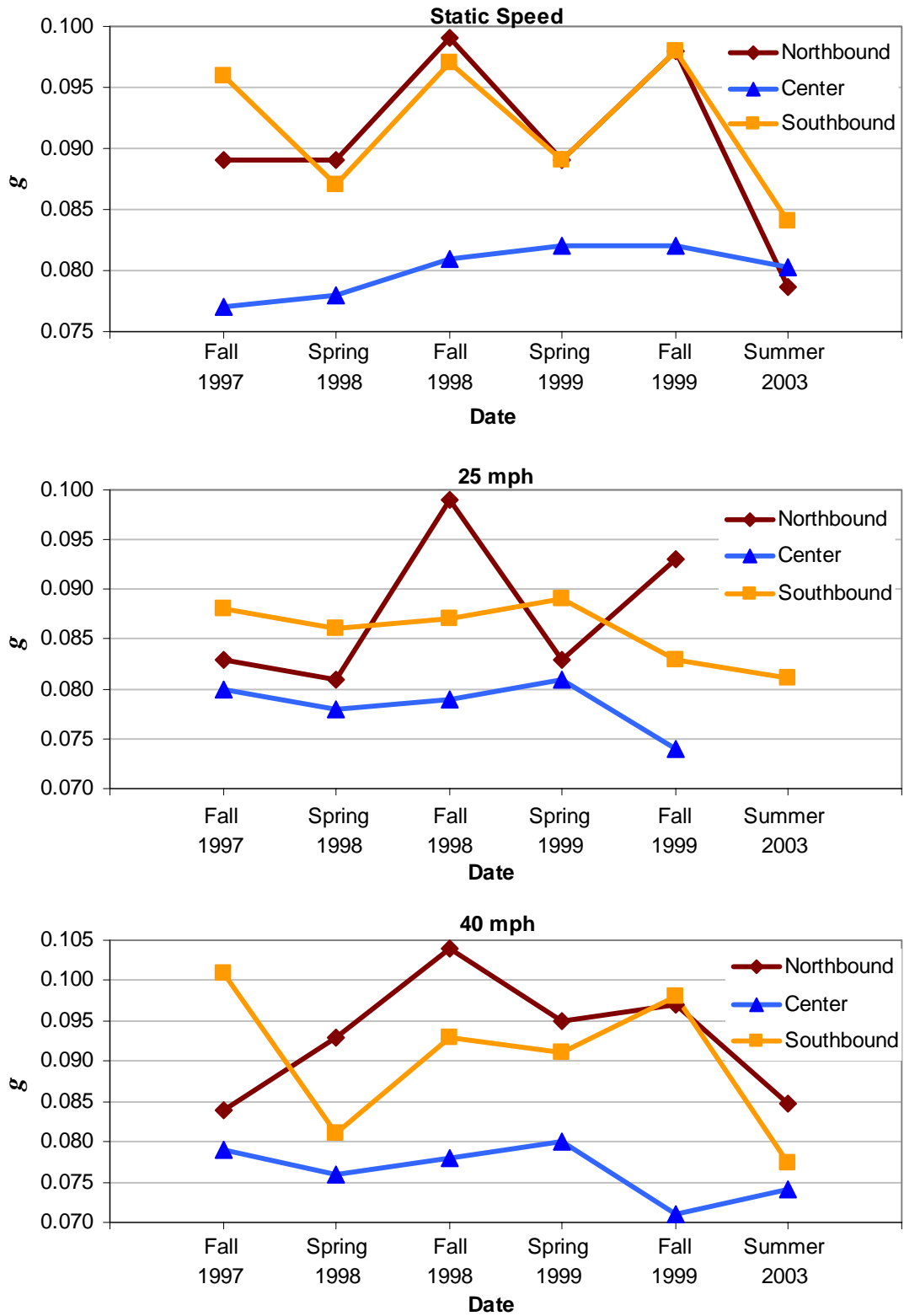


**Figure 4-4.** Average wheel load distributions for the Toms Creek Bridge over time, based on strain measurements at three different speeds.

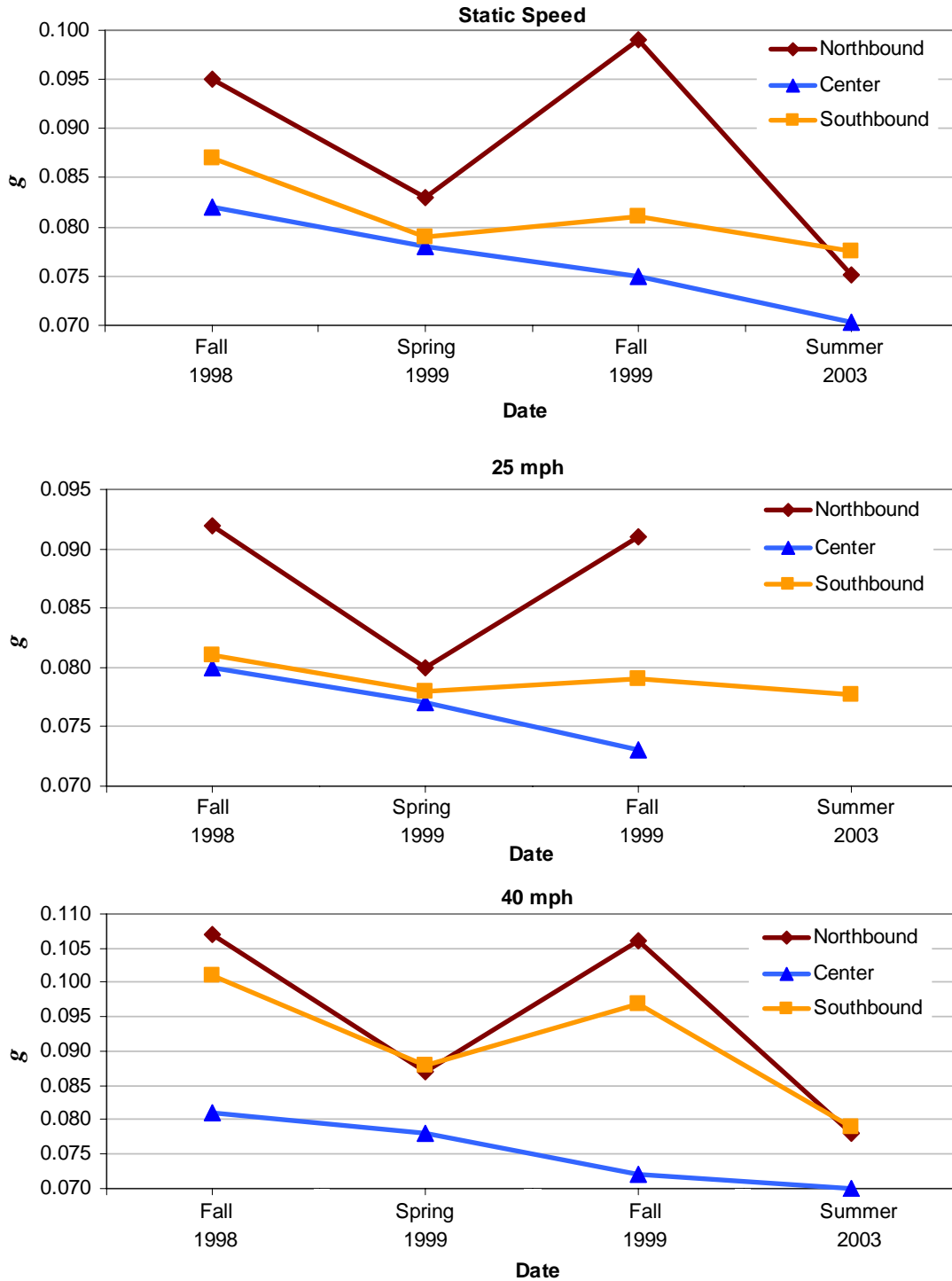


**Figure 4-5.** Average wheel load distributions for the Toms Creek Bridge over time, based on deflection measurements at three different speeds.

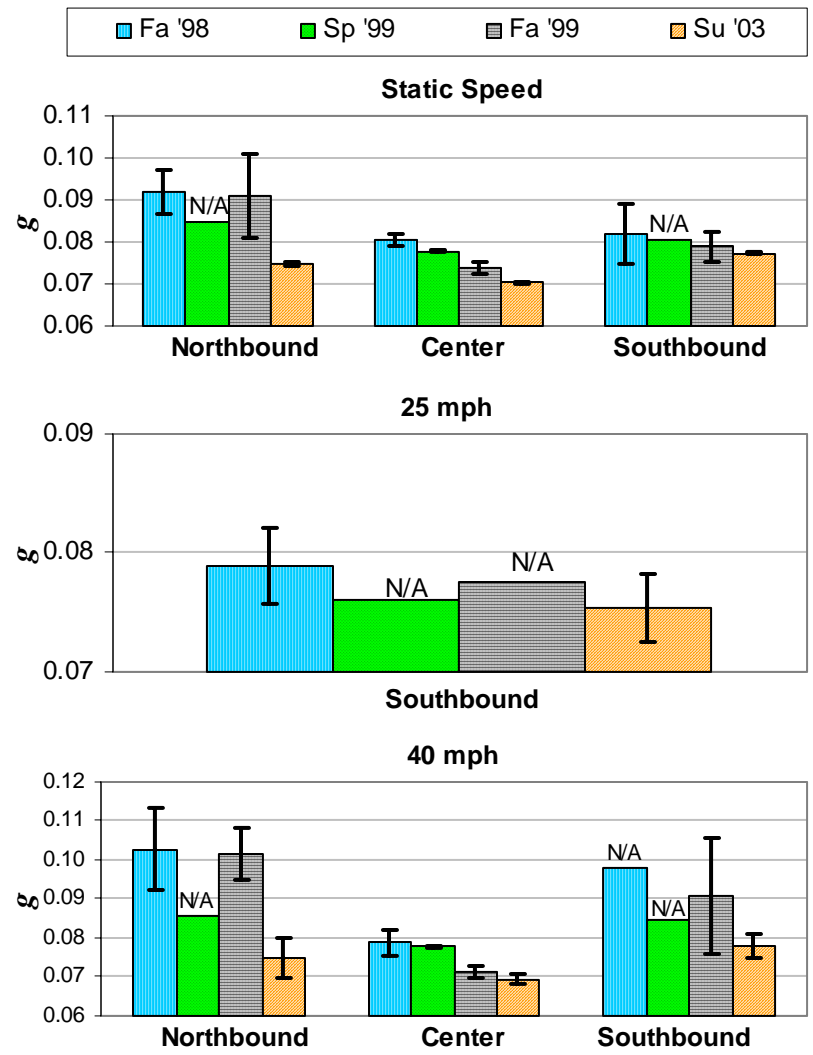
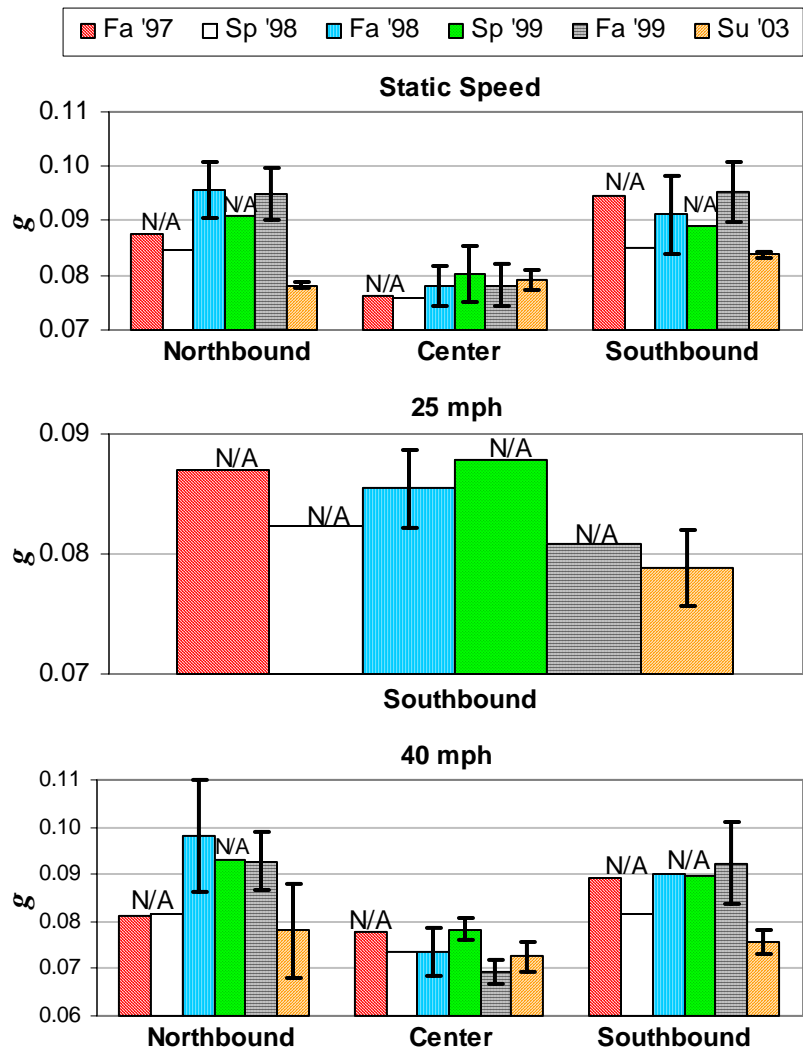


**Figure 4-6.** Error bars for average wheel load distributions in the Toms Creek Bridge, based on (a) strain and (b) deflection measurements. Data points marked “N/A” do not have enough tests to produce a statistically reliable set of bars; data points without error bars have errors that are too small to appear on the graph.

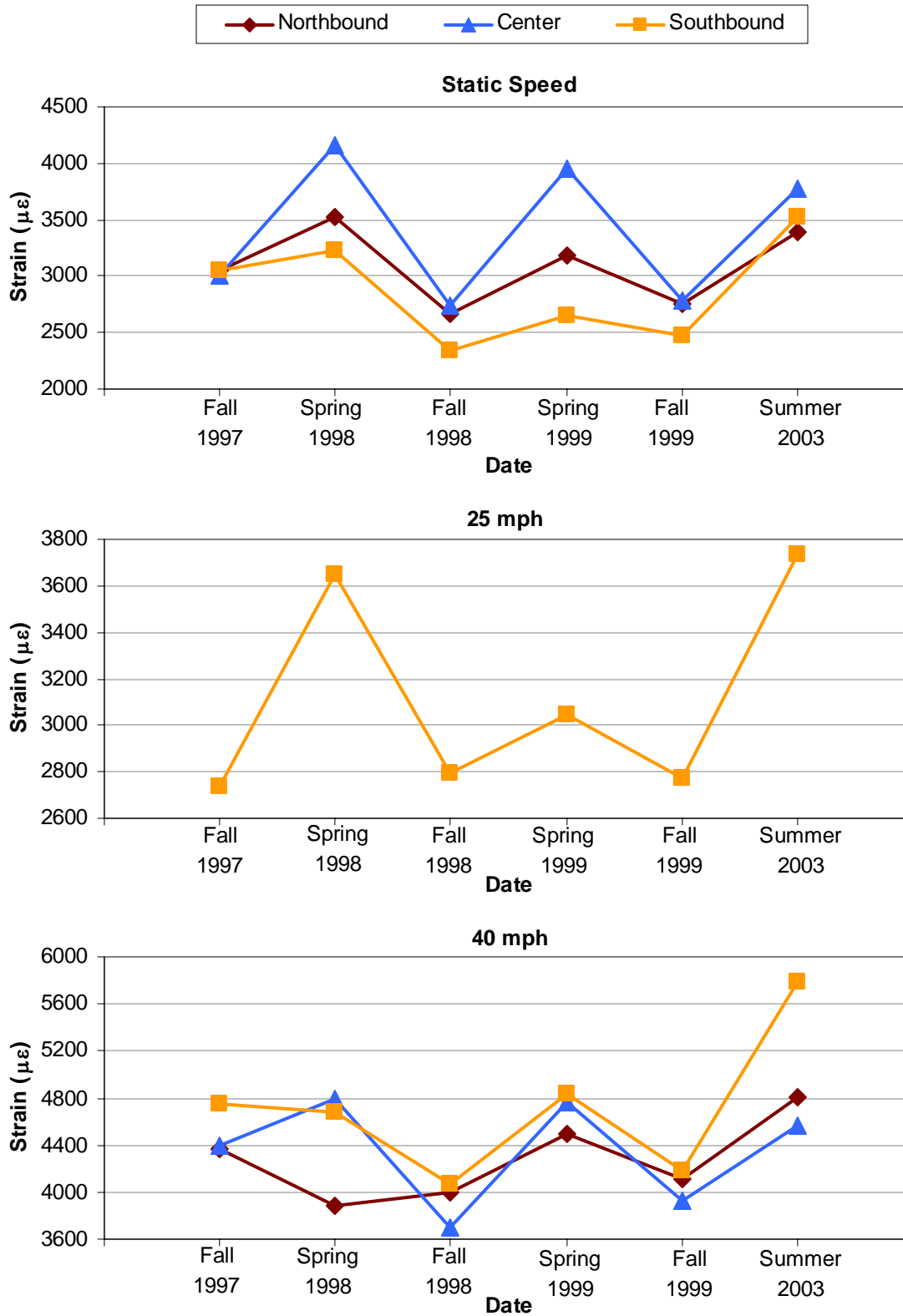


**Figure 4-7.** Average total peak strain in all of the girders for the different truck orientations and travel speeds in the Toms Creek Bridge.

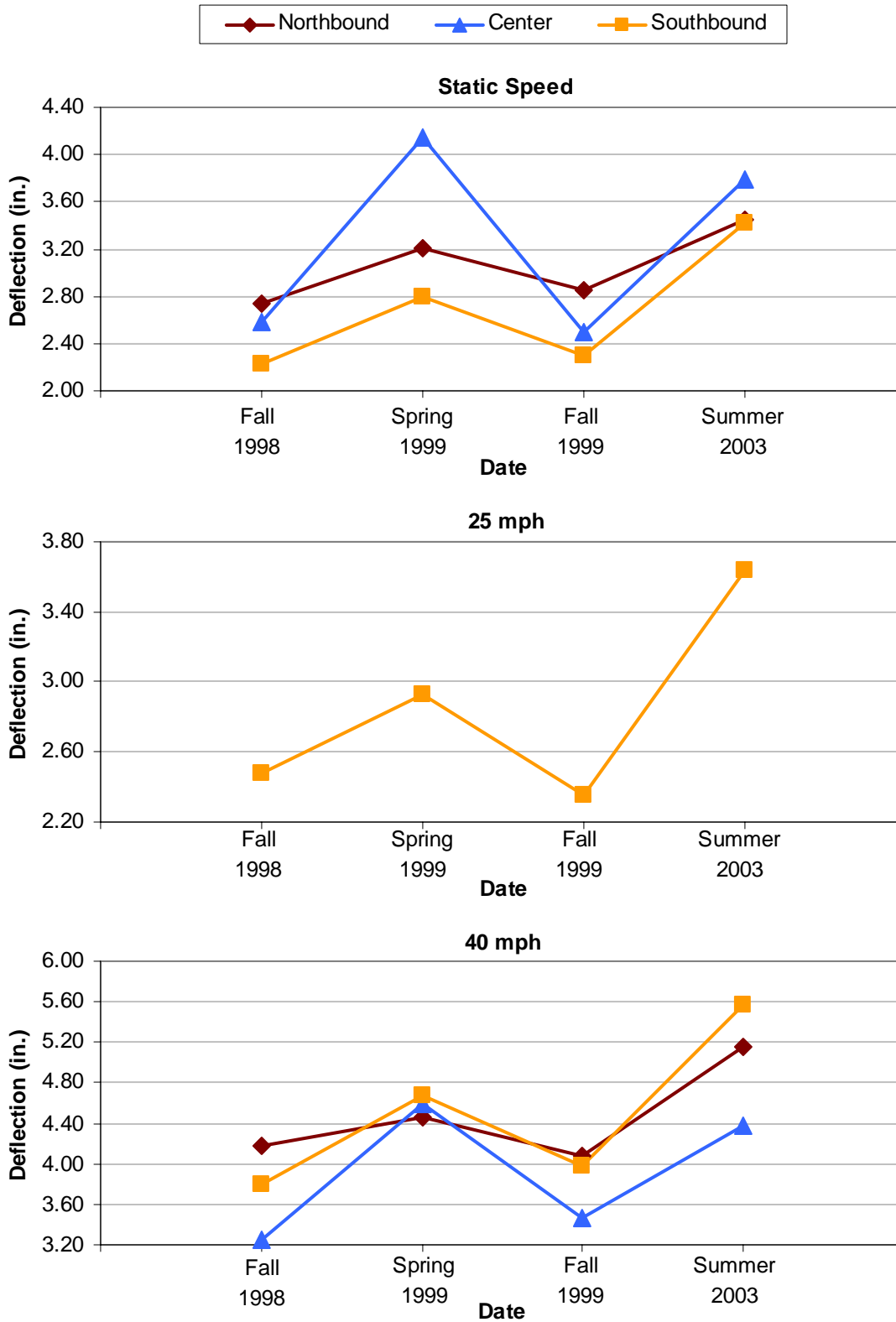
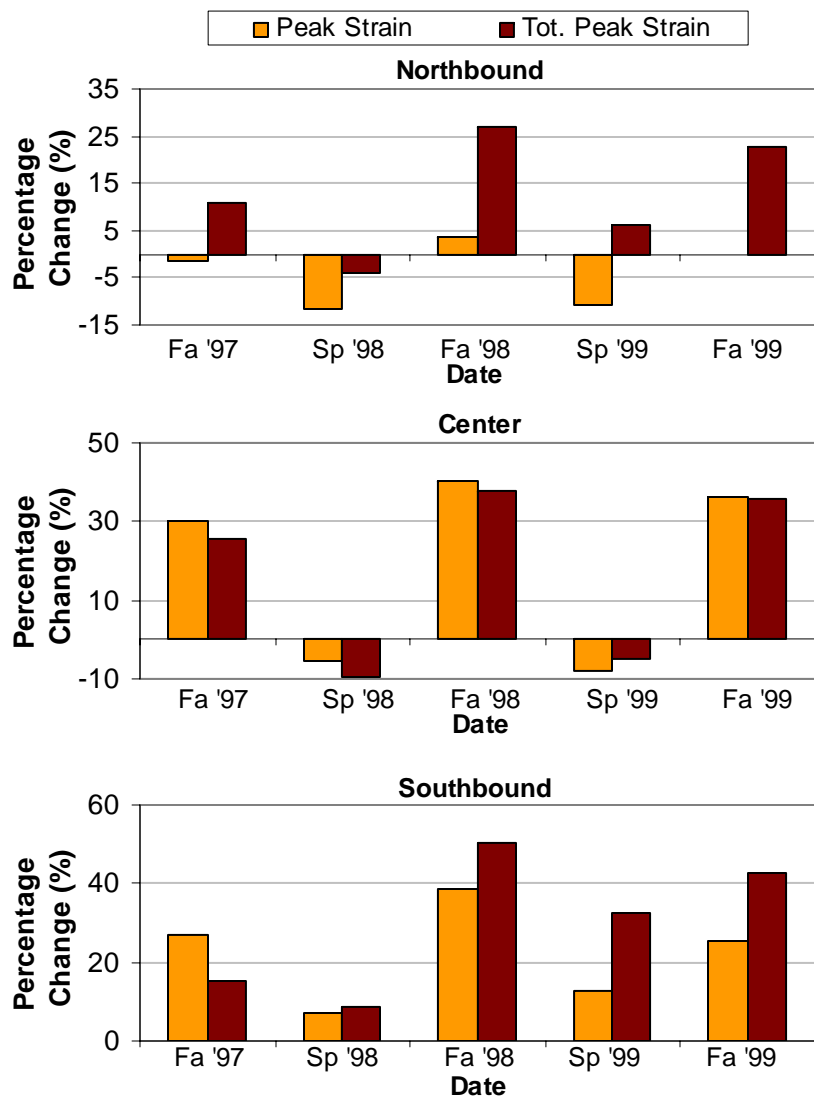
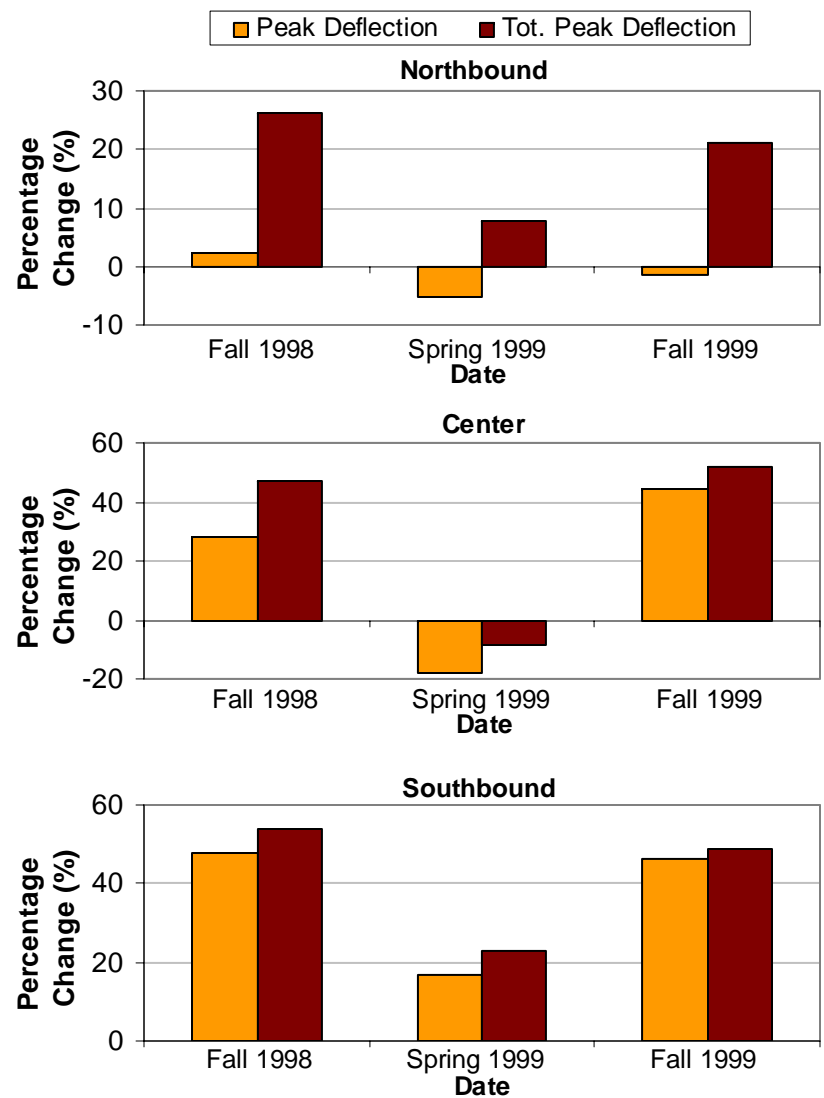


**Figure 4-8.** Average total peak deflection in all of the girders for the different truck orientations and travel speeds in the Toms Creek Bridge.

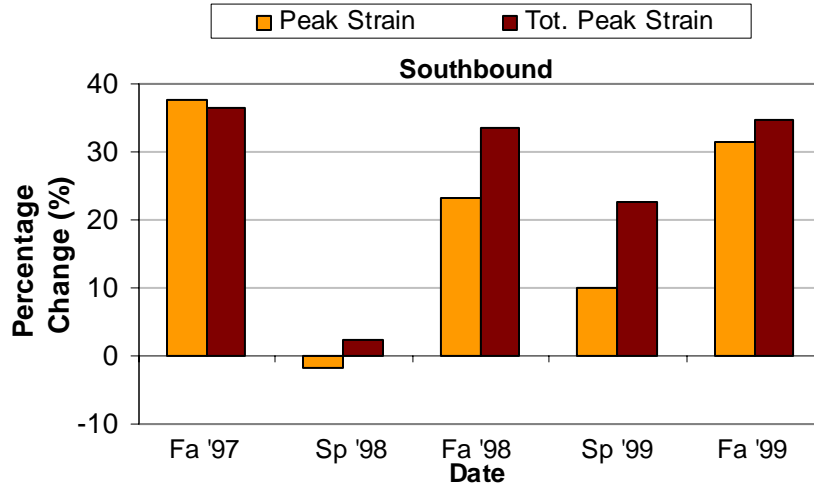


(a)

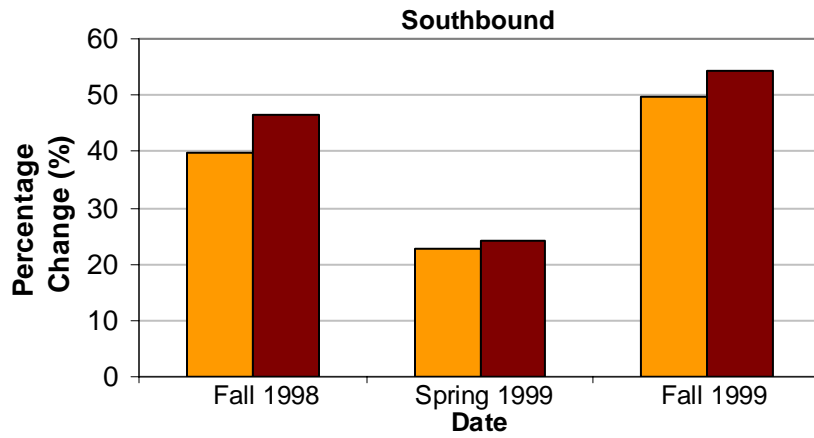


(b)

**Figure 4-9.** Percentage change of (a) peak strain versus total peak strain and (b) peak deflection versus total peak deflection from the given test date to the Summer 2003 test for the Toms Creek Bridge in the various truck orientations at static speed.



(a)



(b)

**Figure 4-10.** Percentage change of (a) peak strain versus total peak strain and (b) peak deflection versus total peak deflection from the given test date to the Summer 2003 test for the Toms Creek Bridge in the various truck orientations at 25 mph (40 kph).

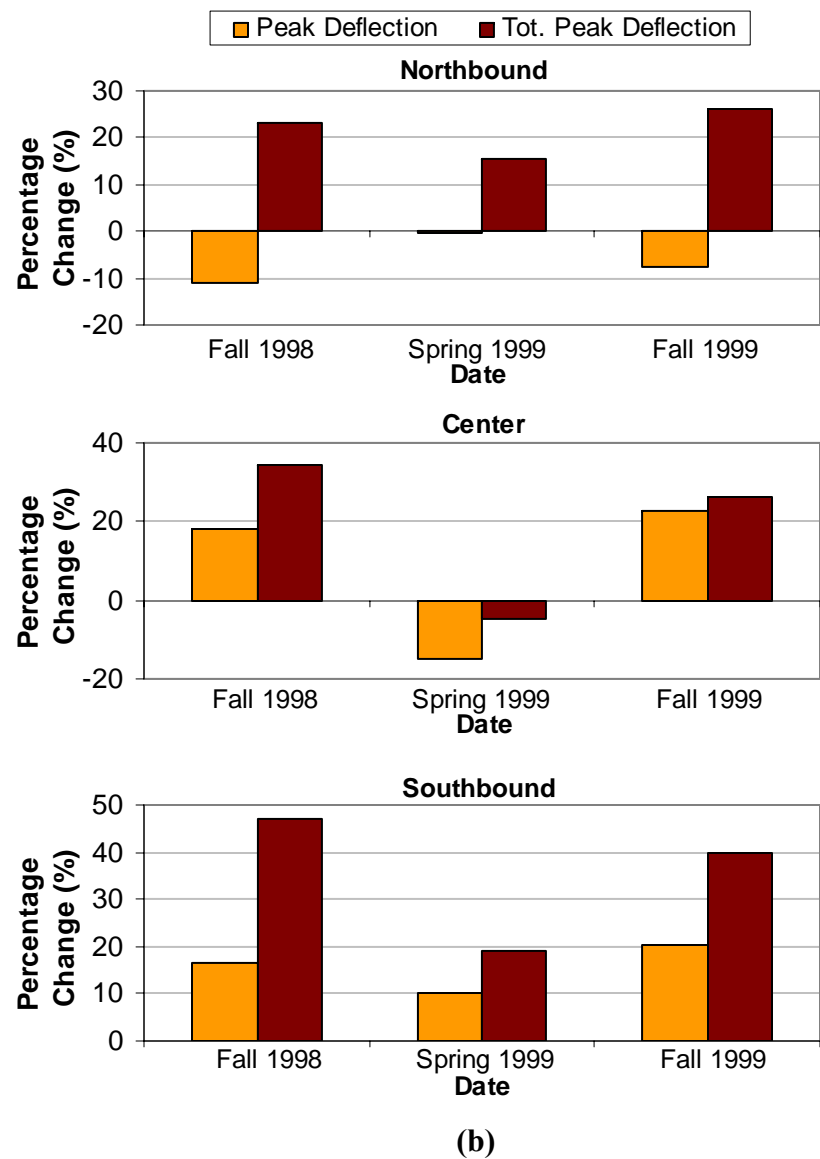
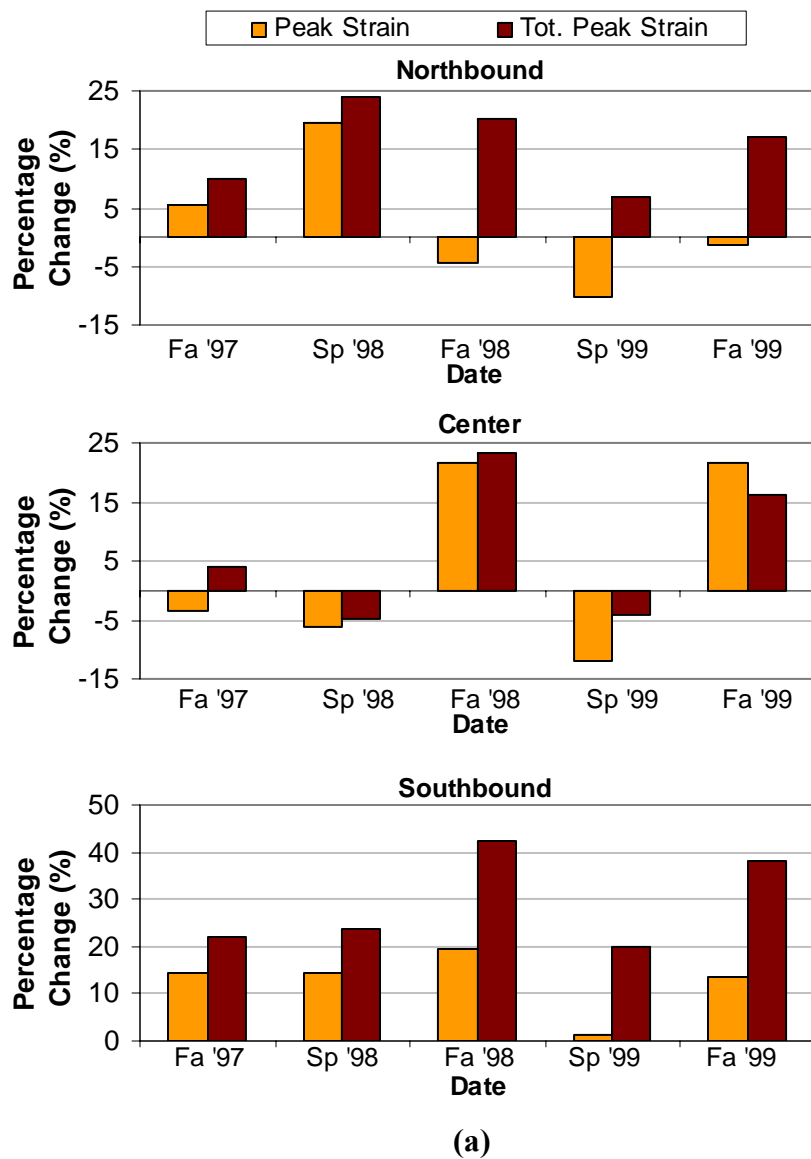
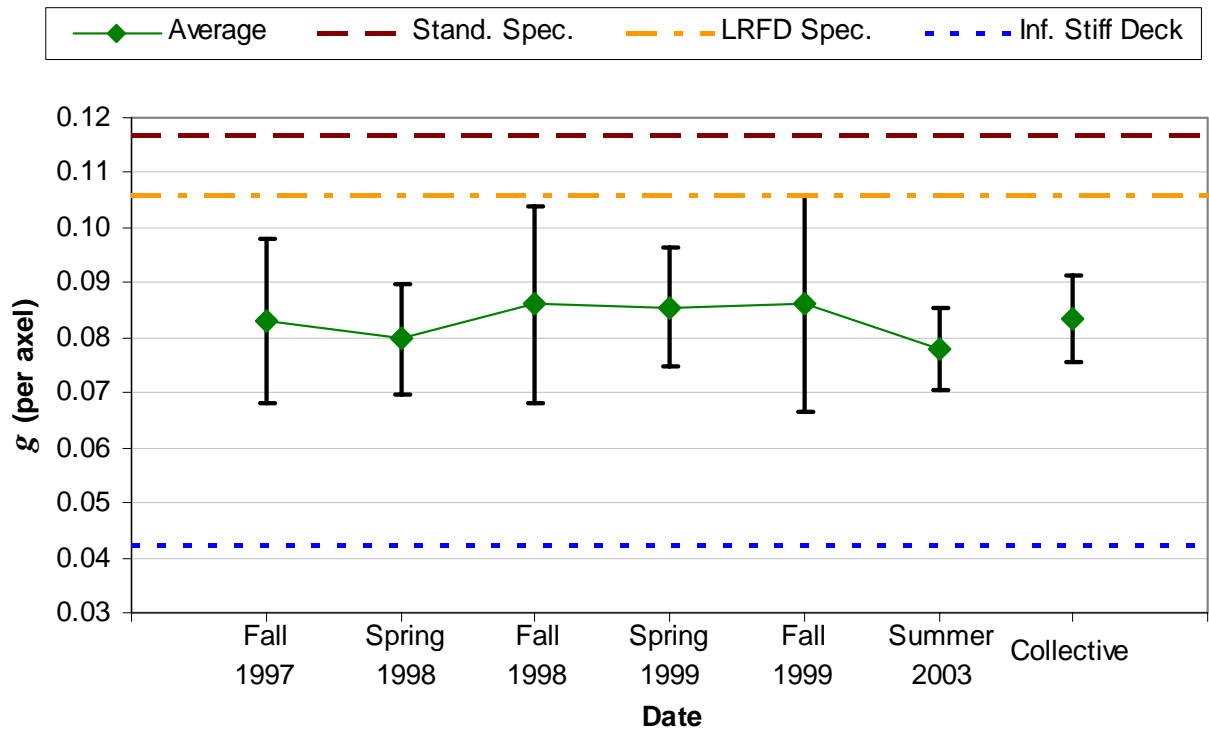
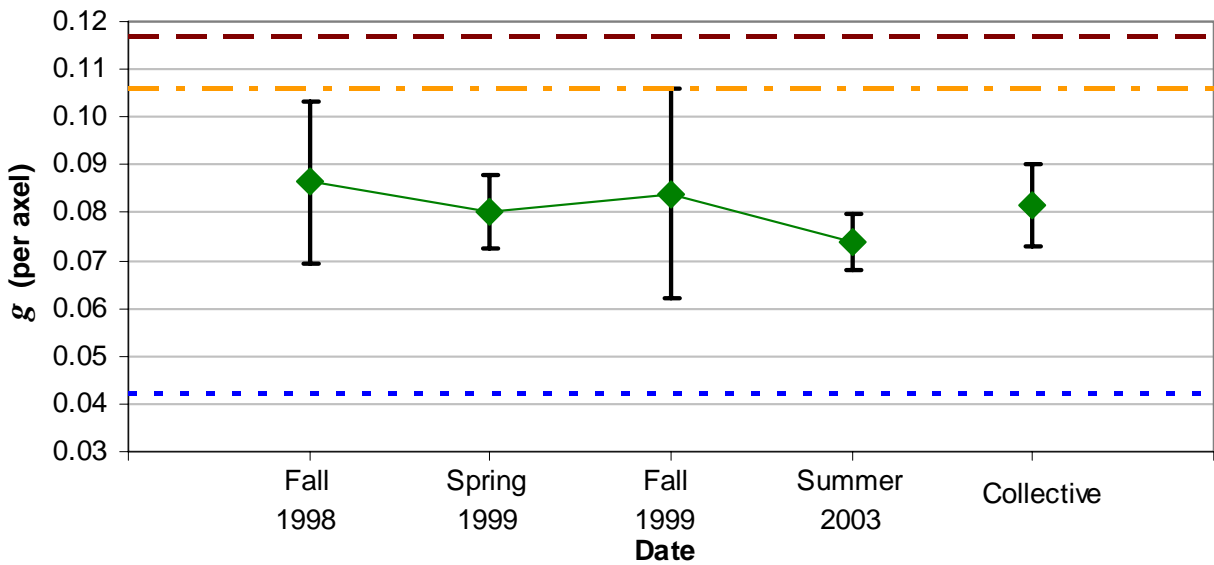


**Figure 4-11.** Percentage change of (a) peak strain versus total peak strain and (b) peak deflection versus total peak deflection from the given test date to the Summer 2003 test for the Toms Creek Bridge in the various truck orientations at 40 mph (64 kph).



(a)



(b)

**Figure 4-12.** Comparison of AASHTO *Standard Specifications* and *LRFD Specifications* with the overall results for wheel load distributions in the Toms Creek Bridge, based on (a) strain and (b) deflection. The averages shown here combine the results for all truck orientations and are calculated “per axle.” Error bars are equivalent to  $\pm 2\sigma$ .

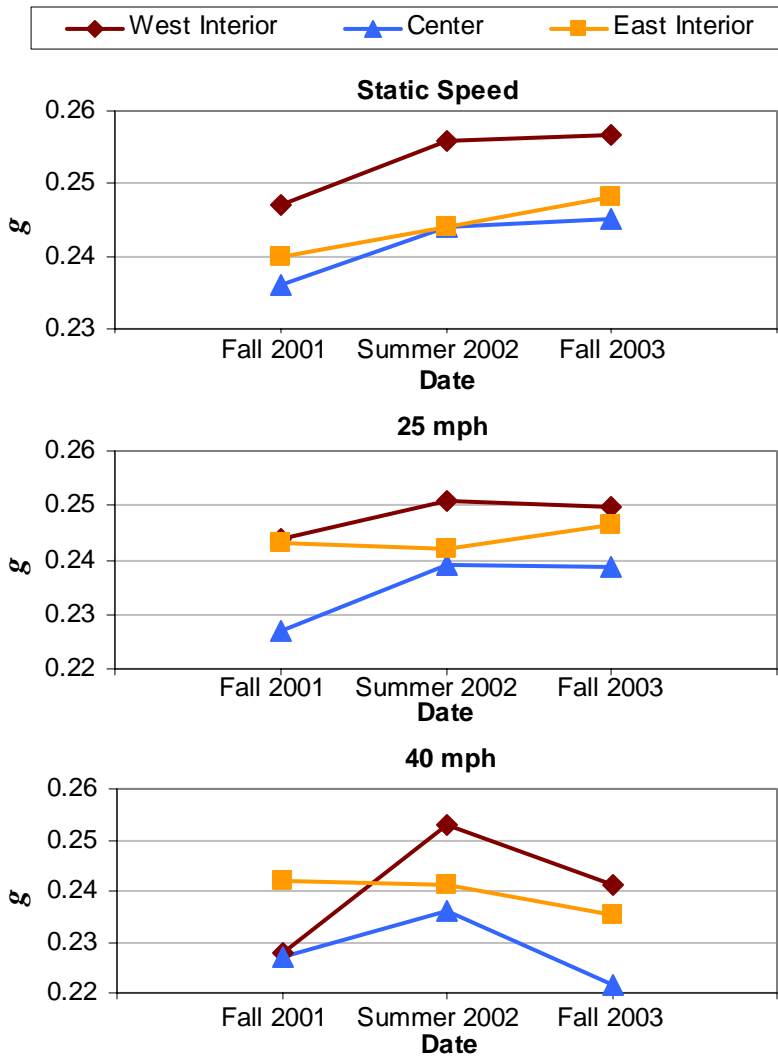


**Figure 4-13.** Average wheel load distributions for the Route 601 Bridge over time for three speeds, based on strain.

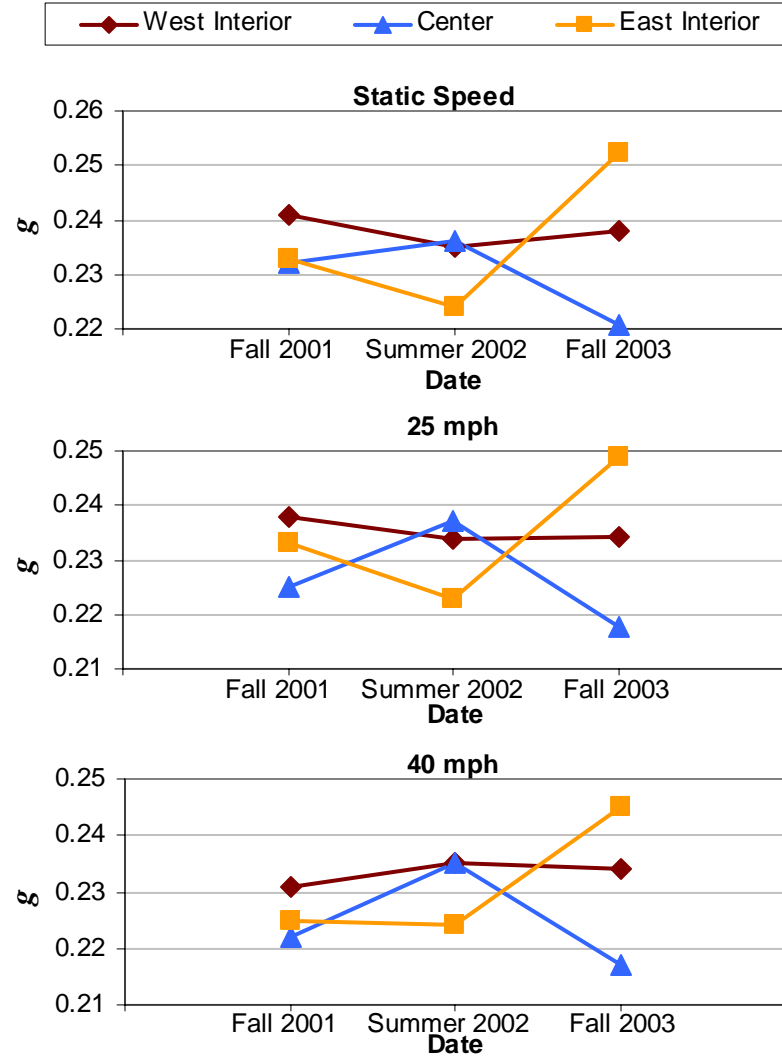


**Figure 4-14.** Average wheel load distributions for the Route 601 Bridge over time for three speeds, based on deflection.

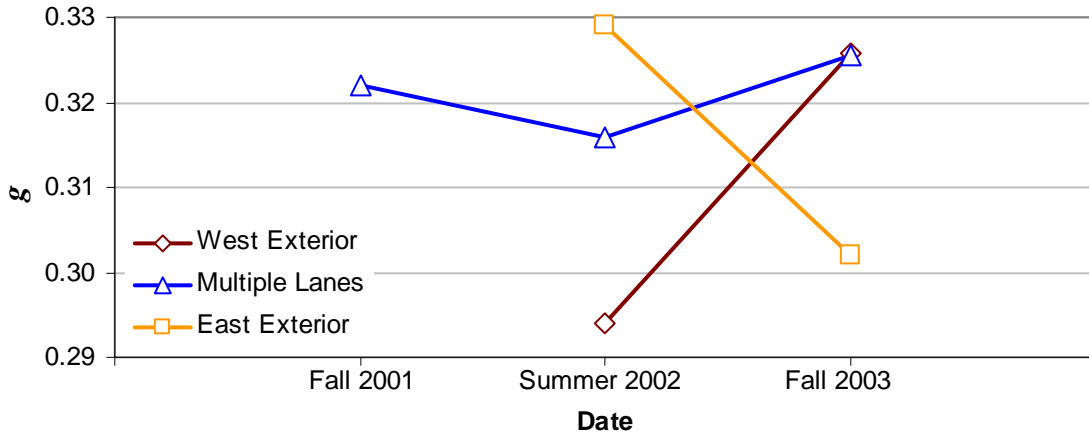


**Figure 4-15.** Average wheel load distributions calculated from strain data for the exterior orientations in the Route 601 Bridge. Note that these tests were only conducted at static speed.

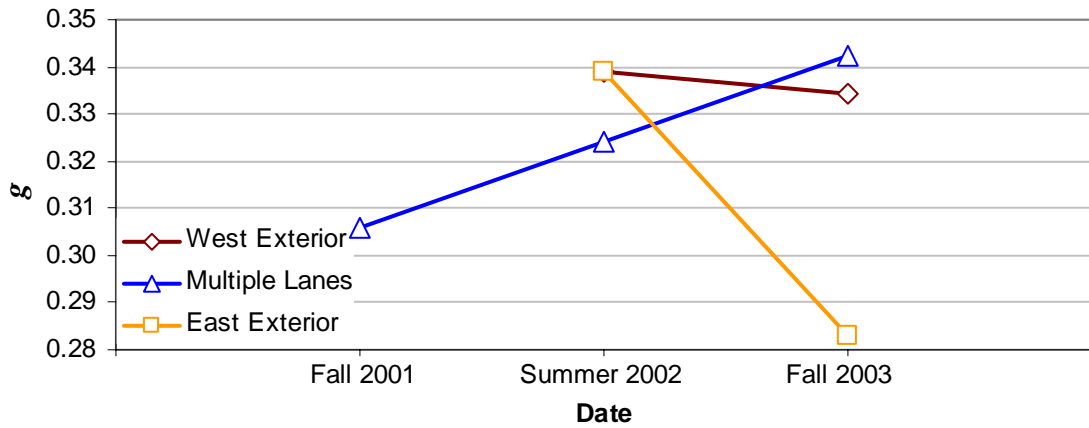


**Figure 4-16.** Average wheel load distributions calculated from strain data for the exterior orientations in the Route 601 Bridge. Note that these tests were only conducted at static speed.

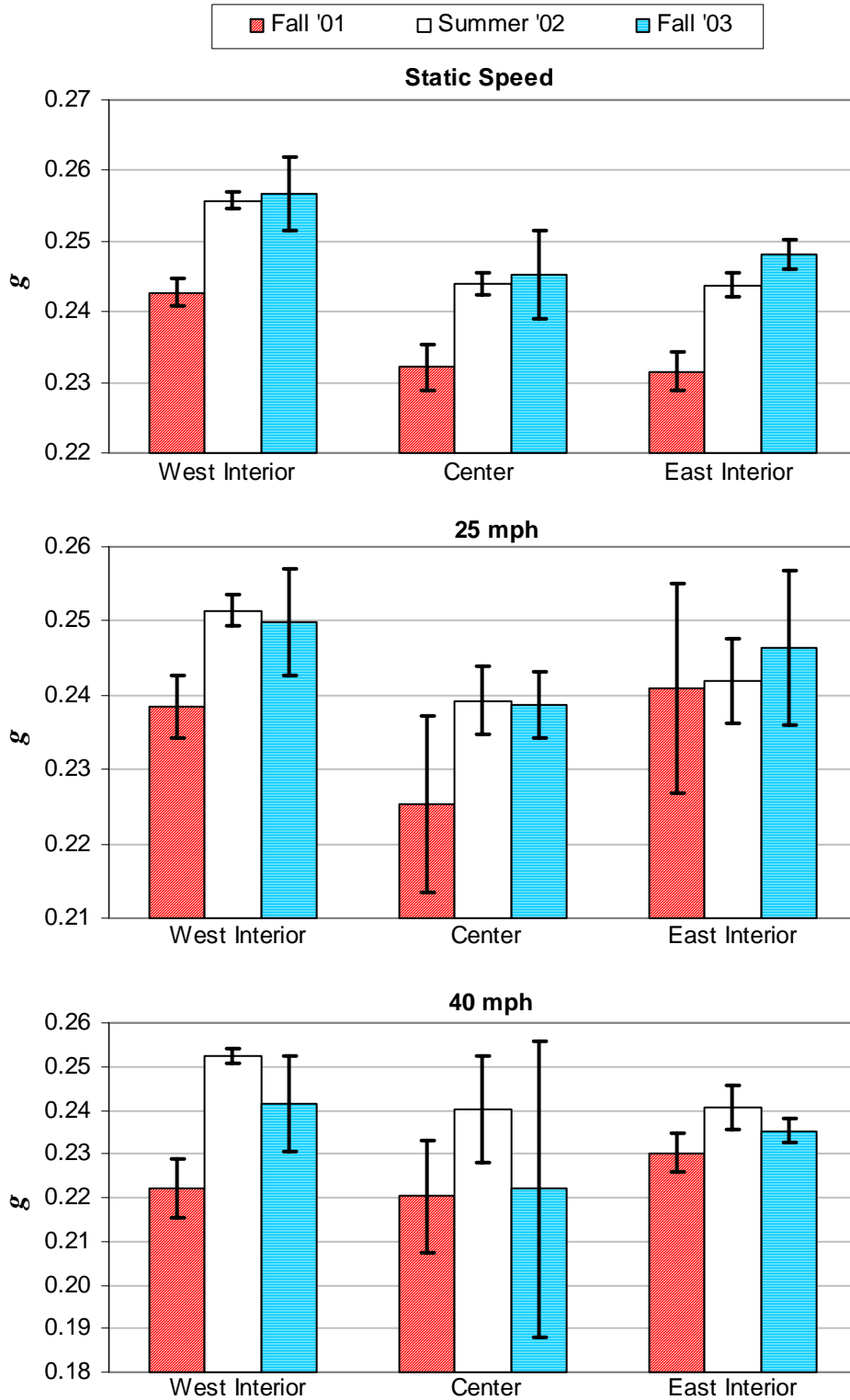


**Figure 4-17.** Error bars for average maximum wheel load distributions at three different speeds of the interior orientations in the Route 601 Bridge, based on strain measurements.

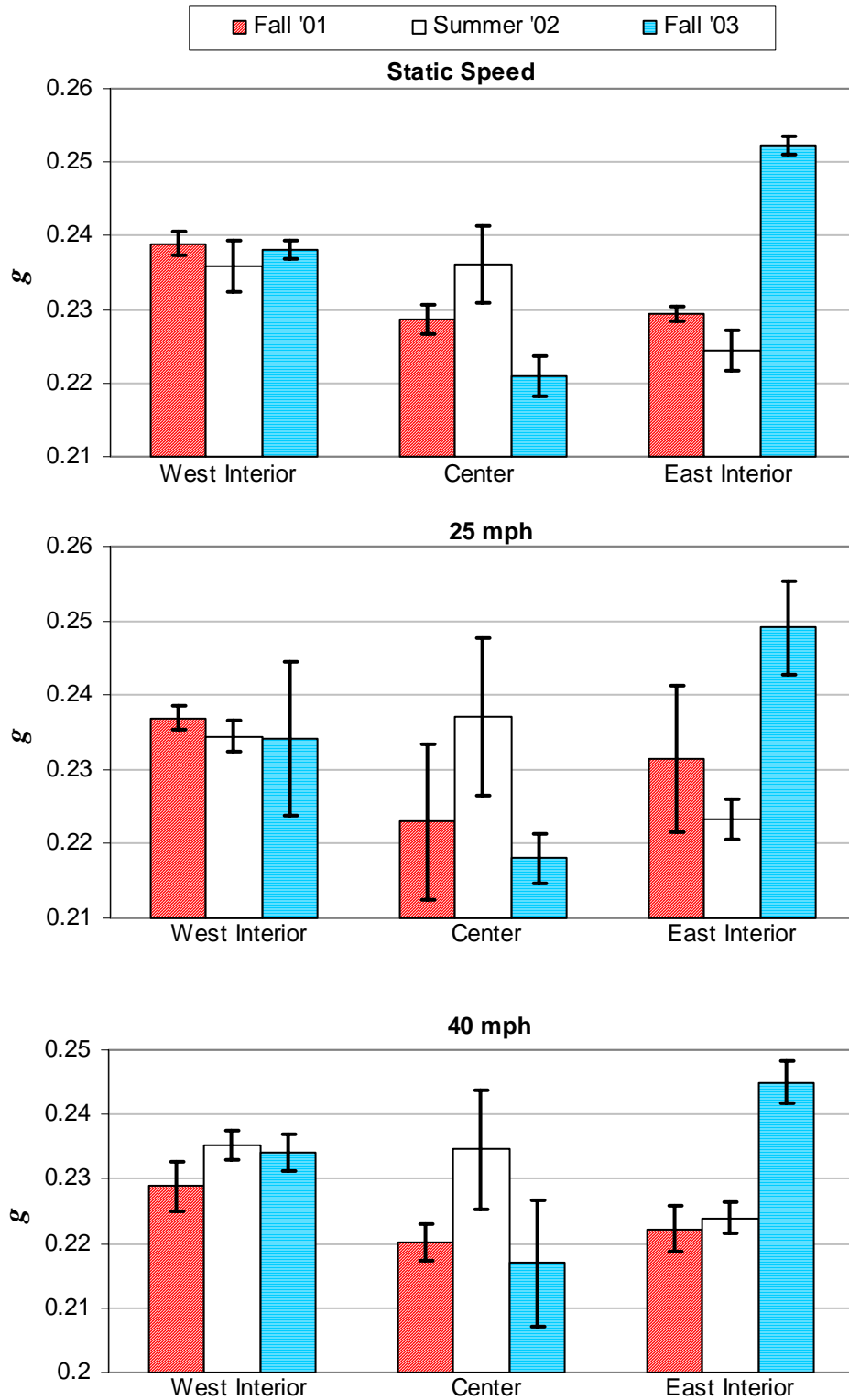
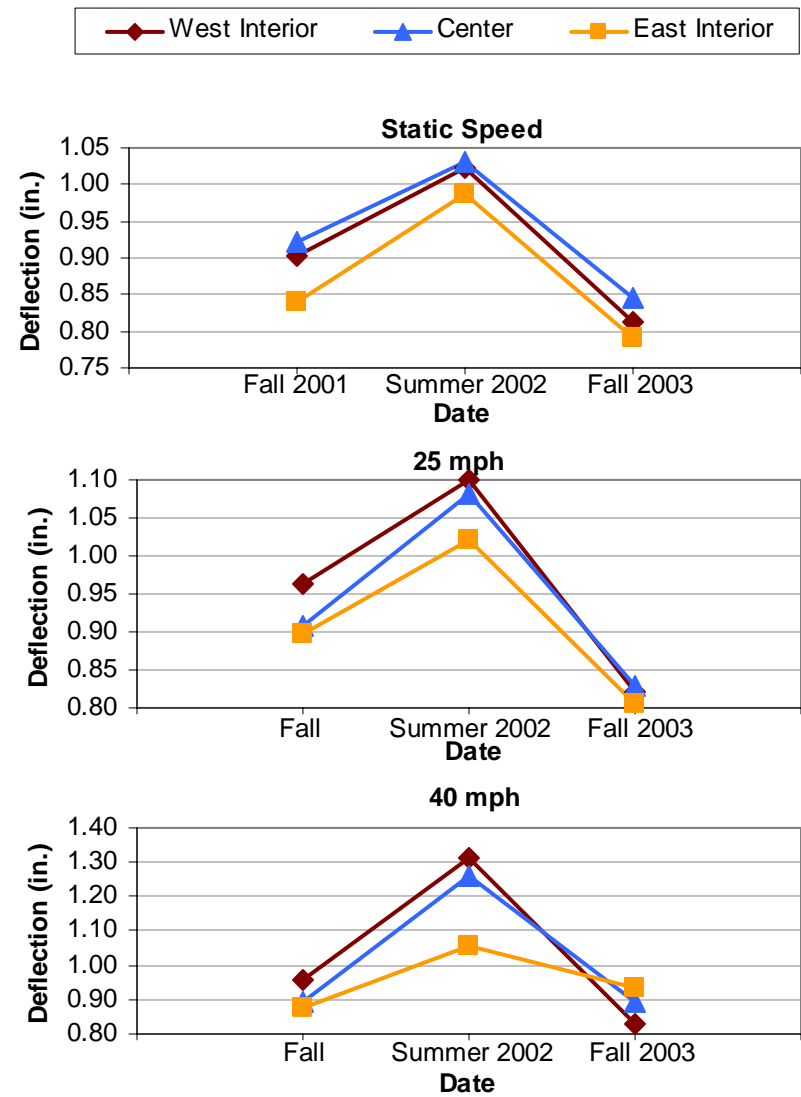
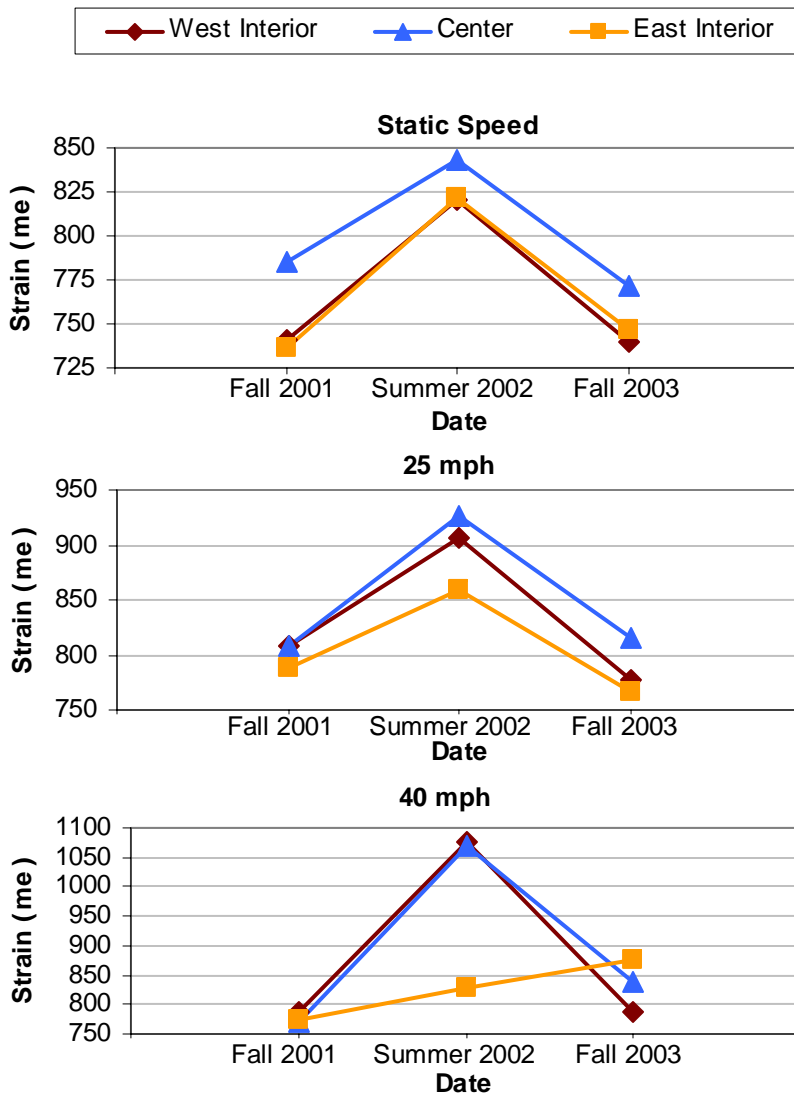
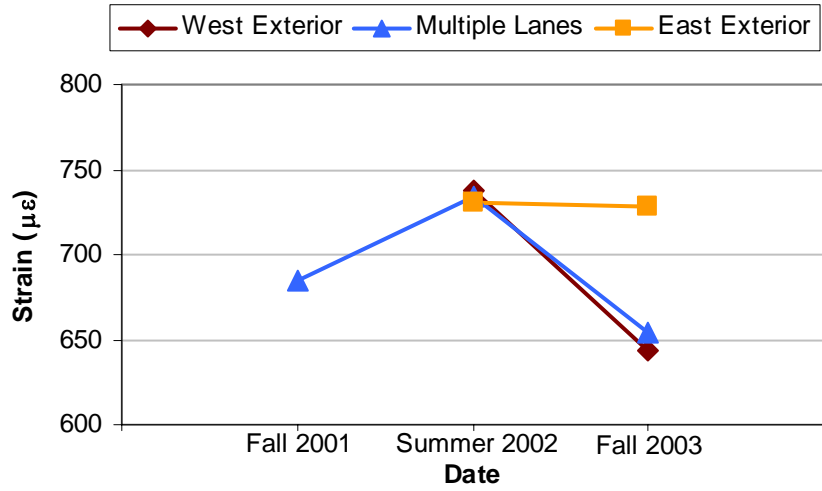


**Figure 4-18.** Error bars for average maximum wheel load distributions at three different speeds of the interior orientations in the Route 601 Bridge, based on deflection measurements.

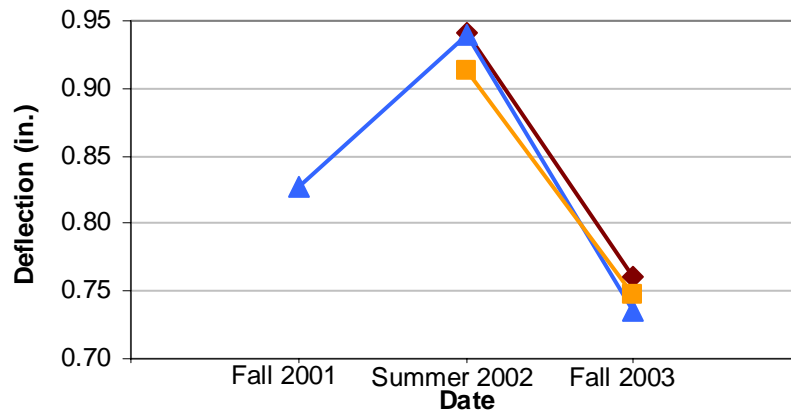


(a) (b)

**Figure 4-19.** Average total peak (a) strain and (b) deflection in all of the girders for the Interior truck orientations at the various speeds in the Route 601 Bridge.



(a)



(b)

**Figure 4-20.** Average total peak (a) strain and (b) deflection in all of the girders for the Exterior truck orientations at static speed in the Route 601 Bridge.

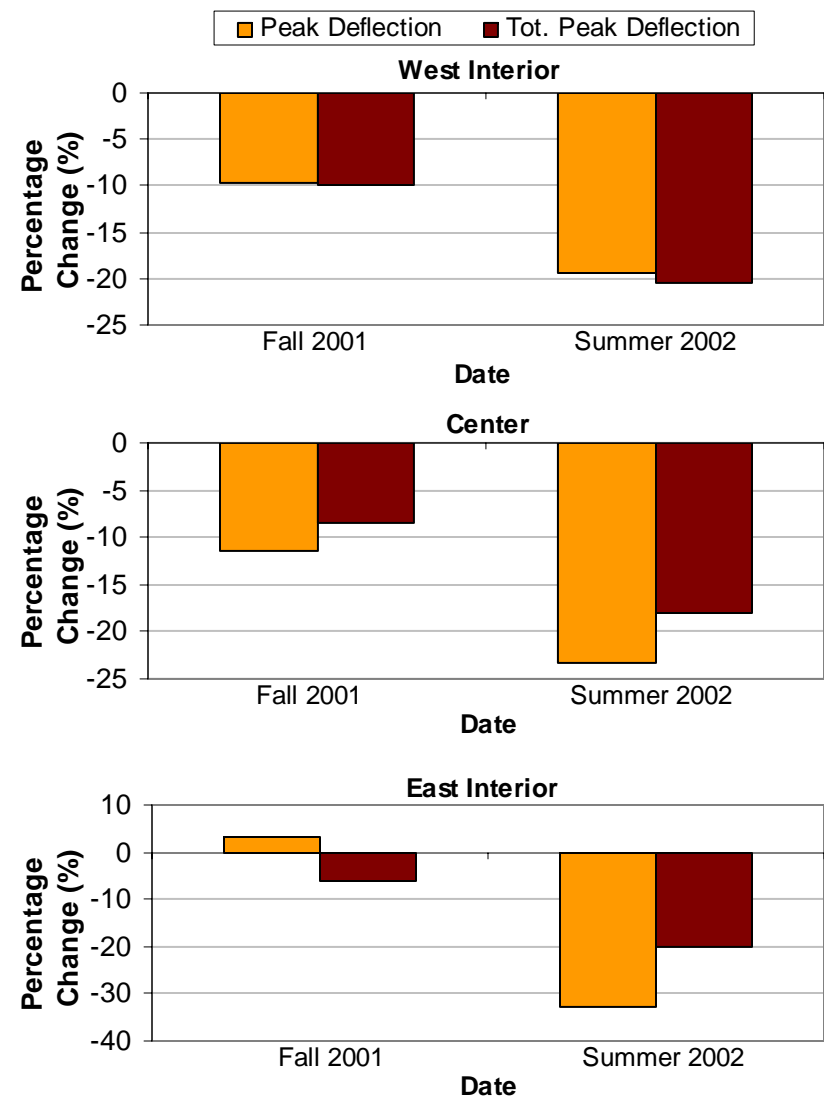
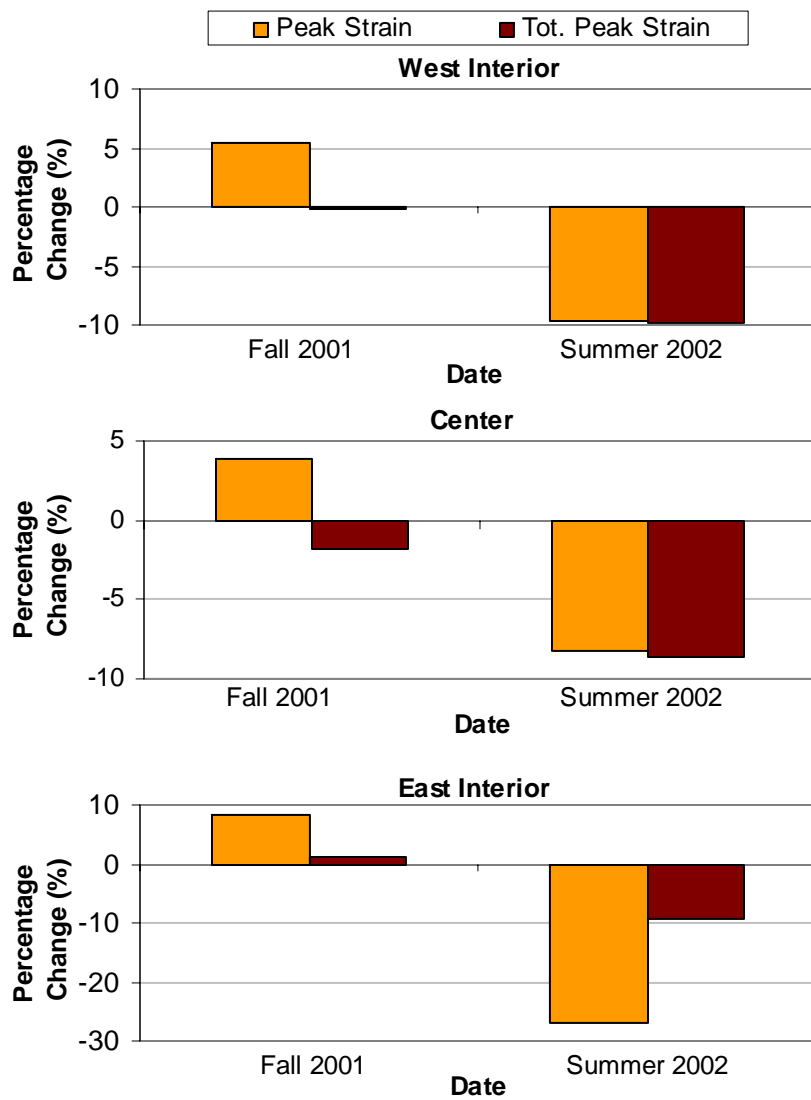
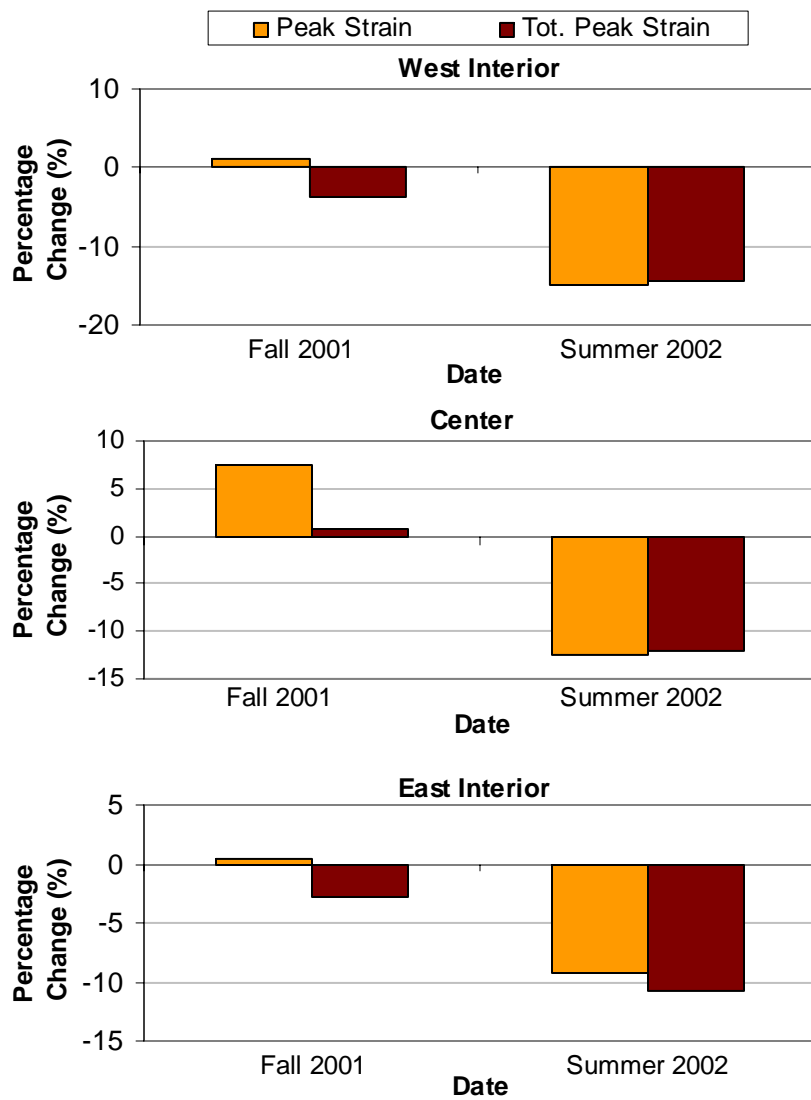
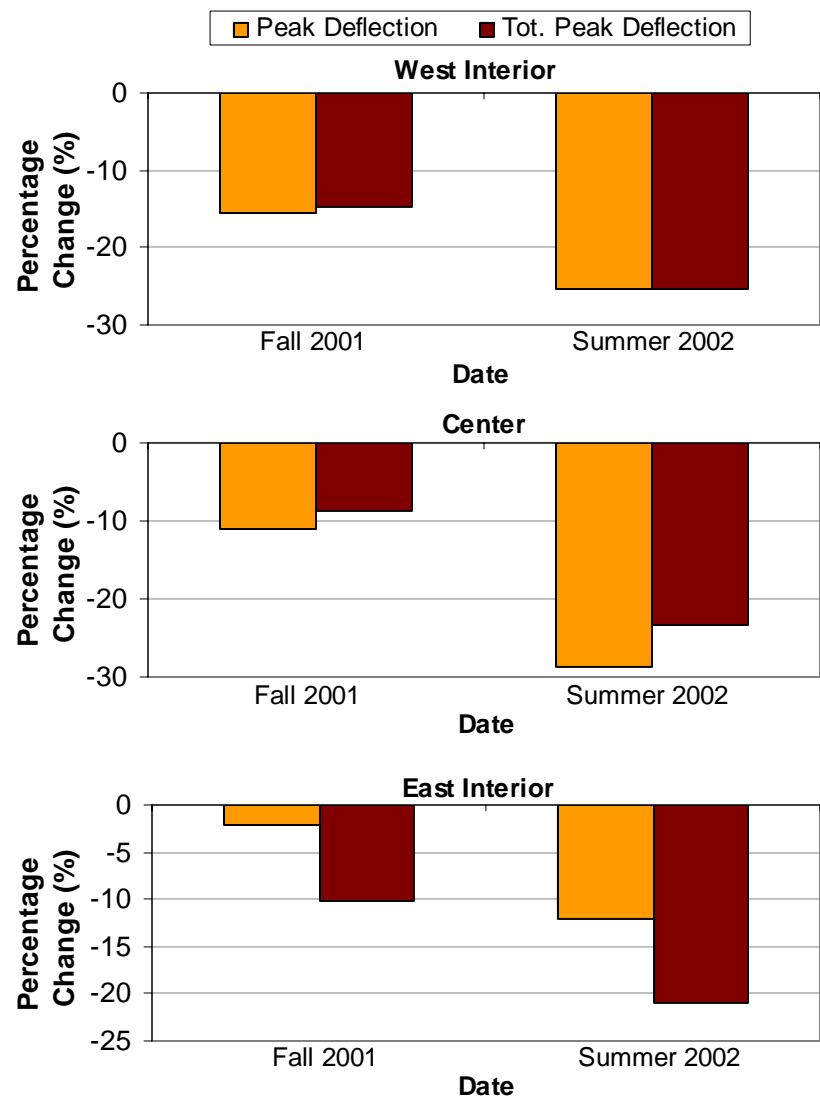


**Figure 4-21.** Percentage change of (a) peak strain versus total peak strain and (b) peak deflection versus total peak deflection from the given test date to the Fall 2003 test for the various interior truck orientations in the Route 601 Bridge at static speed.

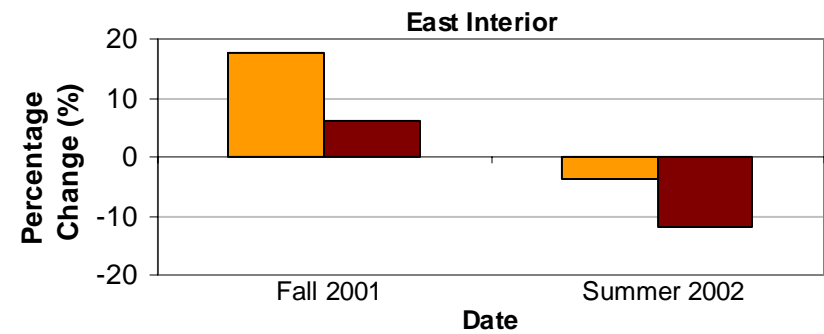
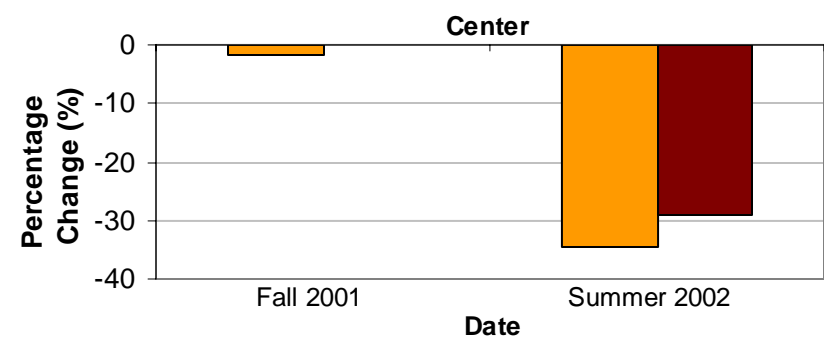
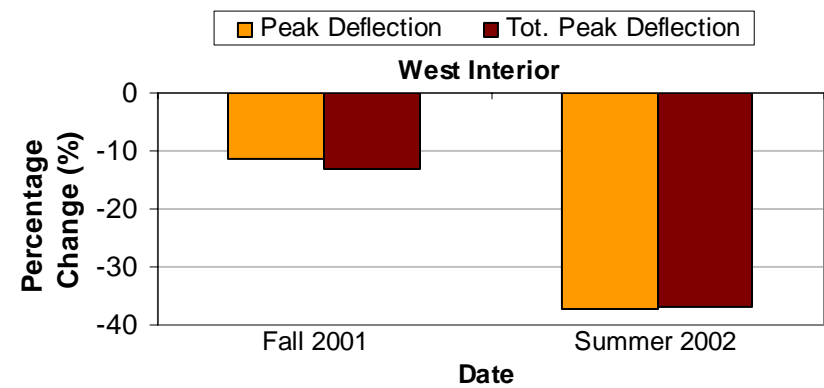
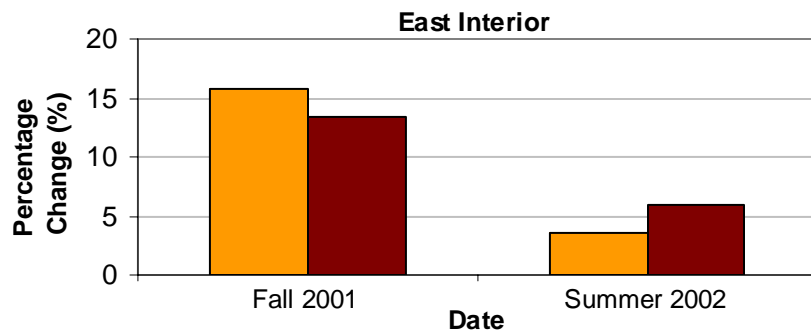
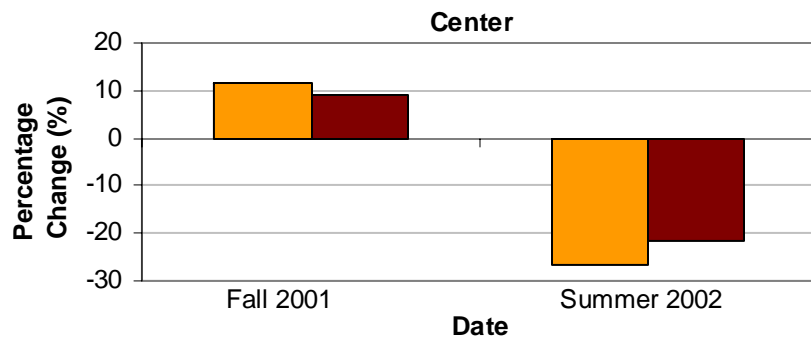
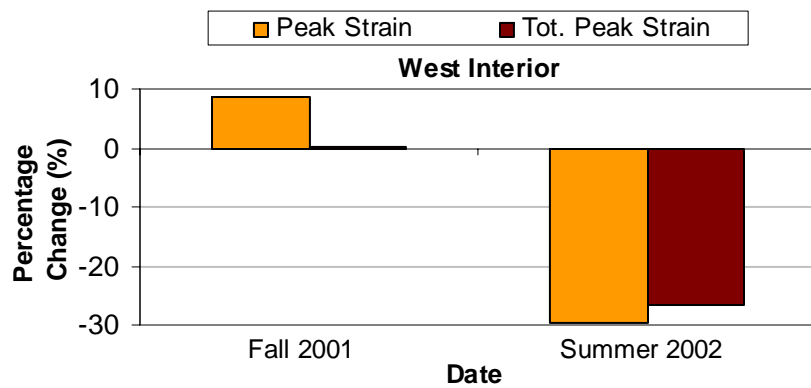


(a)



(b)

**Figure 4-22.** Percentage change of (a) peak strain versus total peak strain and (b) peak deflection versus total peak deflection from the given test date to the Fall 2003 test for the various interior truck orientations in the Route 601 Bridge at 25 mph (40 kph).



(a)

(b)

**Figure 4-23.** Percentage change of (a) peak strain versus total peak strain and (b) peak deflection versus total peak deflection from the given test date to the Fall 2003 test for the various interior truck orientations in the Route 601 Bridge at 40 mph (64 kph).

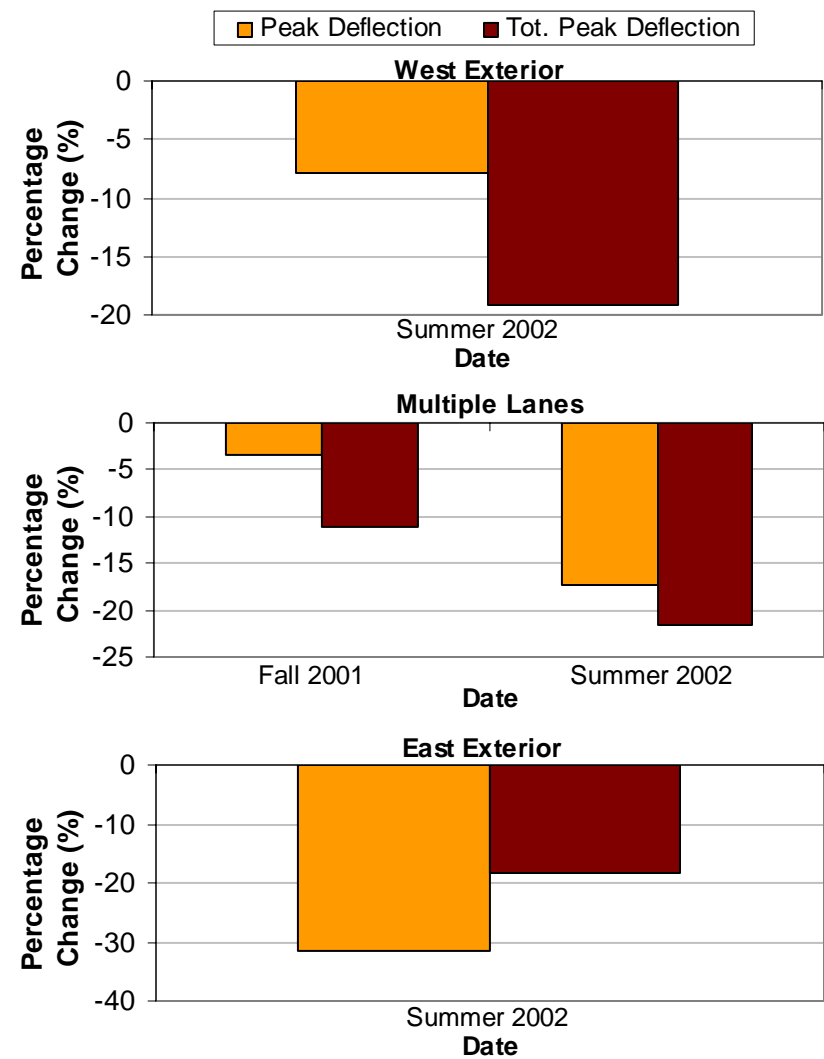
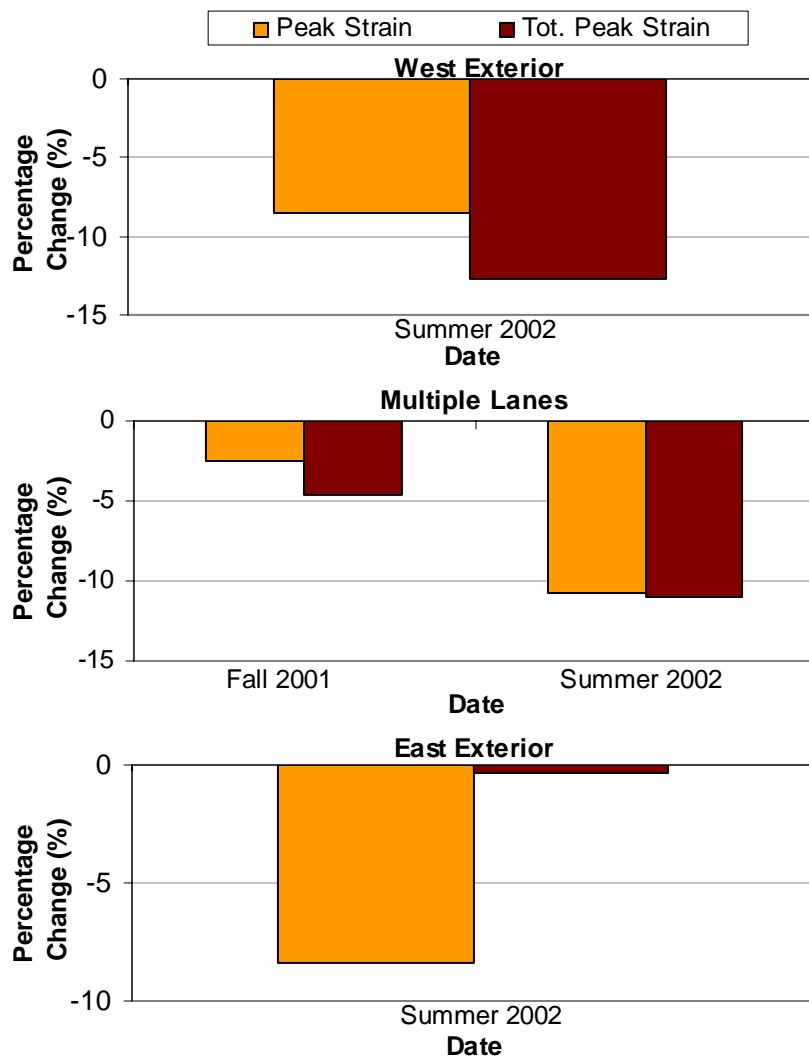
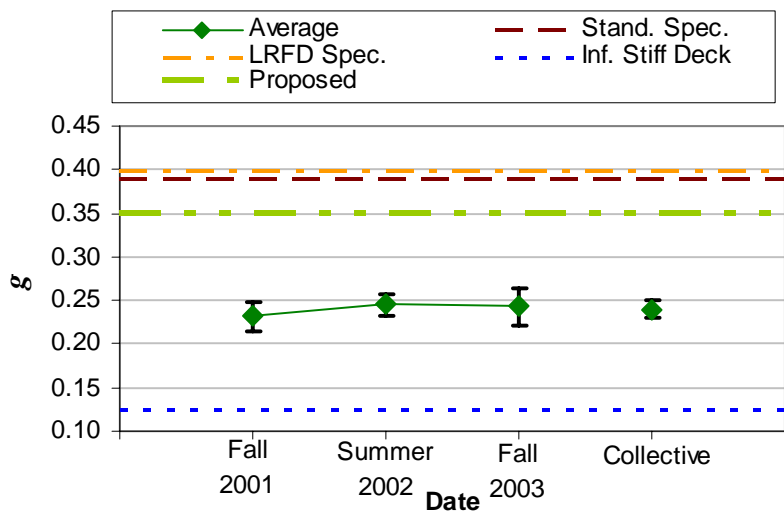
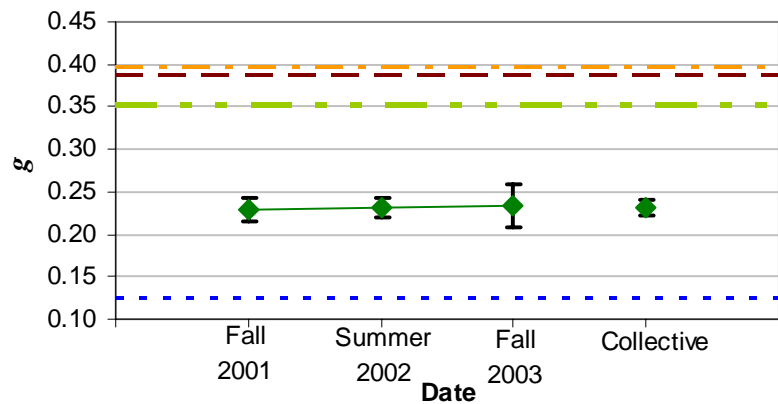


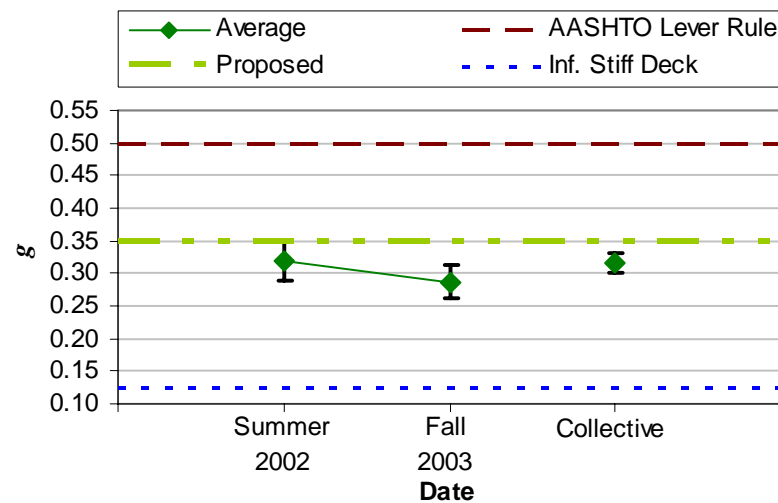
**Figure 4-24.** Percentage change of (a) peak strain versus total peak strain and (b) peak deflection versus total peak deflection from the given test date to the Fall 2003 test for the exterior truck orientations in the Route 601 Bridge at static speed. Note that the East and West Exterior orientations were not tested in the Fall of 2001.



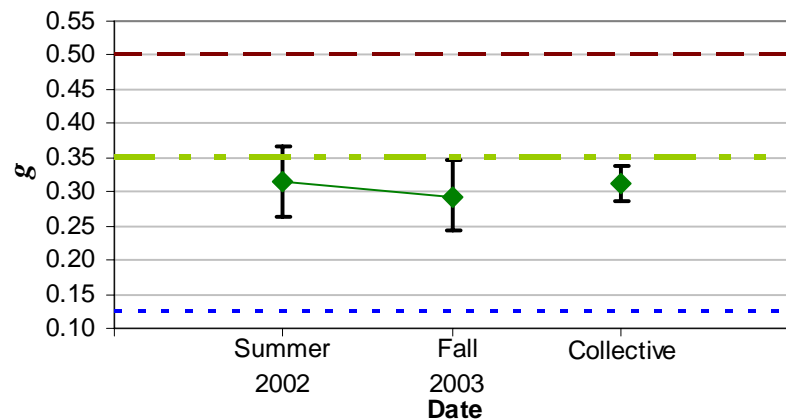
(1a)



(1b)

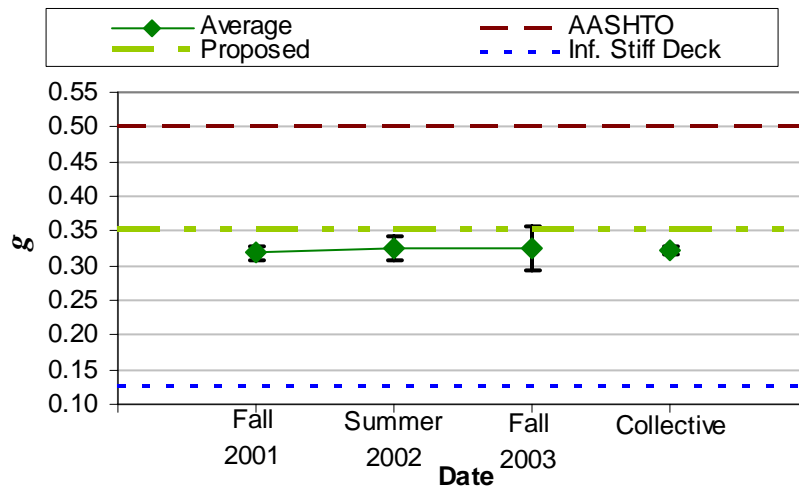


(2a)

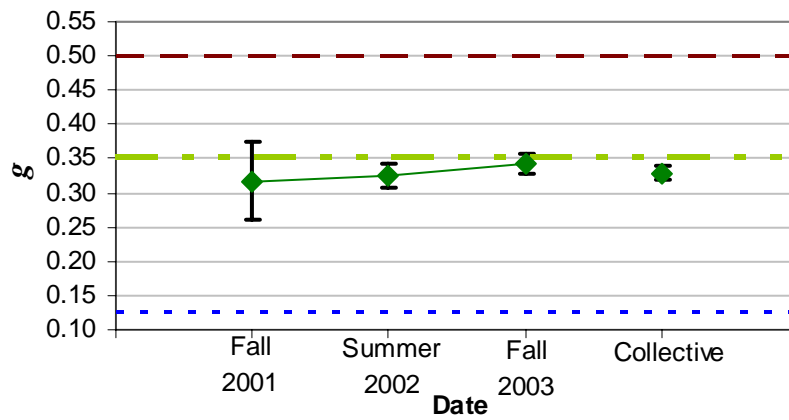


(2b)

**Figure 4-25.** Comparison of AASHTO *Standard Specifications* and *LRFD Specifications* with the overall average wheel load distribution in the Route 601 Bridge for a (1) single interior lane loaded and (2) single exterior lane loaded, based on (a) strain and (b) deflection. The averages shown here are calculated “per axle.” Error bars are equivalent to  $\pm 2\sigma$ .



(a)



(b)

**Figure 4-26.** Comparison of AASHTO specifications with the average wheel load distribution in the Route 601 Bridge for multiple exterior lanes loaded, based on (a) strain and (b) deflection. The averages shown here are calculated for a single truck axle. Error bars are equivalent to  $\pm 2\sigma$ .

## Chapter 5: Results for Dynamic Load Allowances, *IM*

The dynamic load allowance, *IM*, for both the Toms Creek Bridge and the Route 601 Bridge have been calculated using two different sets of data, first with the midspan flexural strain data, and then with the midspan deflections. Figure 5-1 shows a typical dynamic response based on strain measurements in the Toms Creek Bridge for both the 25 mph (40 kph) and 40 mph (64 kph) speeds in the southbound orientation. Although the 25 mph (40 kph) speed was only tested for the southbound orientation, the other two orientations exhibit similar responses for the 40 mph (60 kph) speed. Figure 5-2 shows the dynamic response based on deflection measurements in the Route 601 Bridge for the same aforementioned speeds in the east interior orientation. As explained later, Figure 5-2 is not typical for all of the dynamic tests in the Route 601 Bridge, but is shown here for the purposes of demonstrating the procedure for calculating *IM* for the bridge.

### 5.1 Procedure for Calculating the Dynamic Load Allowance

The procedure listed for calculating the dynamic load allowance is the same procedure that both Neely and Restrepo used in their research. This procedure follows the same steps regardless of whether the calculations use midspan flexural strain or midspan deflection data in the analysis. The first step is to arrange the data according to the truck orientation. For each individual truck orientation, the average peak static response is obtained from the results in Chapter 3. Then, for each dynamic load test, i.e., any test where the truck speed is 25 mph (40 kph) or 40 mph (64 kph), an *IM* factor is calculated using Eq. (1-9), discussed in Section 1.2.5.3. For each of the two dynamic speeds, an average dynamic load allowance is determined from the *IM* factors calculated for the five repetitions for the given speed. This procedure is repeated for the remaining truck orientations used in the Toms Creek Bridge and Route 601 Bridge.

### 5.2 Dynamic Allowance Results for the Toms Creek Bridge

#### 5.2.1 Dynamic Load Allowance from Current Study of Toms Creek Bridge

Table 5-1 and Table 5-2 show both the maximum and average dynamic load allowances results for the Summer 2003 tests, calculated from the strain and deflection data, respectively. The two measurement methods yield similar results for *IM*, although the dynamic load allowances based on deflection are consistently greater than those based on strain. The

difference between the strain and deflection results are generally between 0.03 and 0.06; however, the dynamic load allowance at 40 mph (64 khp) in the southbound orientation is 30% greater when calculated with the deflection data versus that which is calculated with the strain measurements (0.64 versus 0.49).

Whether considering strain or deflection, the *IM* for the Toms Creek Bridge varies greatly amongst the three truck orientations. Looking at the deflection data for the 40 mph (60 kph) speed, the southbound orientation has the largest average impact factor, 0.64, while the center orientation registers the lowest *IM* at 0.14. In addition to the truck's orientation, the speed at which the truck traveled across the bridge also plays an important role in the dynamic load allowance. While the 40 mph (60 kph) speed had the largest dynamic factor in the southbound orientation, the same orientation tested at 25 mph (40 kph) shows *IM* to be a much lower 0.04. Thus, a 60% increase in the truck speed results in a sixteen-fold increase in the dynamic load allowance, showing that the behavior of the FRP beams in the Toms Creek Bridge is highly influenced by the speed of the vehicle.

Such an increase in response can be a concern for state transportation departments, especially if design using FRP beams tends to be deflection controlled. Excessive deflection can lead to serviceability issues such as cracking in the surface treatment, which results in the superstructure elements being more susceptible to the effects of water. What's more, drivers feel unsafe using the bridge due to perception of large deflections in the bridge when traveling at elevated speeds. For this reason, AASHTO has set guidelines for dynamic load allowances. For example, AASHTO *Standard Specifications* recommend an *IM* of 0.30 for a glulam deck – steel girder bridge. AASHTO *LRFD Specifications* recommend an *IM* of 0.33 for the same type of bridge. The maximum average dynamic load allowance in the Summer 2003 test for the Toms Creek Bridge exceeds both of those recommendations by a factor of two.

One factor that can influence the dynamic load allowance is the condition of the approaches to the bridge. Optimally, bridges will have a smooth transition from the roadway just prior to the bridge, thus helping to minimize the dynamic effects of the vehicle traveling across the bridge. One way to ensure a smooth transition is to construct an approach slab underneath the roadway at the abutment; this slab helps to evenly distribute the vehicle's weight across the soil behind the abutment. However, in more rural settings with a lower traffic count, the lighter

traffic load does not justify the cost of constructing an approach slab. Therefore, construction crews typically highly compact the soil to provide a firm surface for the approach roadway.

In the case of the Toms Creek Bridge, the approach on the north abutment may have settled more than the approach at the south abutment, or might have been more uneven to begin with. When Neely tested the bridge, he conducted the tests for the dynamic effects for the center orientation in both the northbound and southbound direction. However, Neely realized that he had to differentiate between these two travel directions within the center orientation because the travel direction seemed to influence the resulting *IM* factor for that orientation. That is to say, the southbound direction gave a much larger dynamic load allowance than the northbound direction for the center orientation, which may be indicative of the roadway being lower than the bridge at the north abutment. This observation may explain why the *IM* based on deflection for the southbound orientation was much larger than the result for the northbound orientation (0.64 versus 0.48.).

### **5.2.2 Comparison of IM Results with Previous Toms Creek Bridge Tests**

In addition to the Summer 2003 tests, Table 5-1 and Table 5-2 also display the maximum and average dynamic load allowance results from the tests that Neely carried out between 1997 and 1999. Recall that there is no deflection information for Fall 1997 and Spring 1998 because there were an insufficient number of deflectometers available for those tests. The Summer 2003 test results are similar to the previous research in that the center orientation has a much lower value for *IM* than the other two orientations, and the dynamic load allowance at 40 mph (64 kph) is dramatically higher than at 25 mph (40 kph). These comparisons are true whether considering the dynamic effects calculated from strain measurements or deflection measurements. As with the Summer 2003 tests, the 1997 to 1999 tests resulted in deflection-based *IM* values that are generally greater than those calculated using the strain data.

Figure 5-3 and Figure 5-4 graphically represent the information presented in the two aforementioned tables. Looking at the 40 mph (60 kph) results based on the deflection data in Figure 5-4, the dynamic load allowances in the Summer 2003 tests are about the same or slightly higher than those results from the Spring 1999 tests, where the maximum difference is a 0.10 increase in the northbound orientation. However, when comparing the Summer 2003 test with Fall 1998 and Fall 1999, the *IM* factors drop considerably. For example, in the southbound orientation, the dynamic load allowance is 0.44 and 0.35 lower than the results for the respective

Fall tests (0.64 versus 1.08 and 0.99). The other two orientations in Summer 2003 have *IM* values that are 0.10 to 0.23 lower than the dynamic load allowances from the two Fall test dates. One possible reason for the large change in the southbound orientation could be because the Summer 2003 test used fewer deflectometers than the previous tests for the southbound orientation. Therefore, the larger differences between the Summer 2003 and the previous tests for this orientation may be due to greater error when trying to interpolate the deflection in the beams that were not instrumented with deflectometers in the Summer 2003 tests.

Like the results from the deflection data, similar analysis using the strain data for calculating the dynamic effects at 40 mph (64 kph) also show that the *IM* values in the Summer 2003 tests are generally lower than all of the previous tests, regardless of the season in which the tests were performed. Again, this decrease tends to be more pronounced in the Fall tests. The only anomaly in the strain results is between the Summer 2003 and Spring 1998 dates for the northbound orientation, where the *IM* is actually 0.37 greater in Summer 2003 than in Spring 1998. Generally speaking, however, the differences within the strain-based results are less than the differences found in the deflection data comparisons. The one interesting thing to note in Figure 5-3 is that the variation in *IM* appears to stabilize over time with the 40 mph (60 kph) tests.

While there is a large change over time with the dynamic load allowances for the 40 mph (64 kph) speeds, the variability within the 25 mph (40 kph) tests is much less (in between -0.12 and +0.11 for both the strain and deflection-based calculations). Note that the Summer 2003 test only included experiments for 25 mph (40 kph) in the southbound orientation. However, based on this single orientation, there does not appear to be a relationship between the season when a given test occurred and the resulting *IM* factor for the 25 mph (40 kph) speed.

As with the wheel load distribution results, the question is whether or not there is any statistical significance in the variation of the dynamic load allowances amongst the different test dates. Consider the error bars in Figure 5-5, which are superimposed over the average *IM* values for the different orientation-speed combinations. Data points demarked “N/A” do not have a sufficient number of load tests for calculating a reliable standard deviation. With the exception of the deflection-based dynamic load allowance for the southbound orientation at 40 mph (64 kph), the error bars in this figure show that there tends to be little distinction between the different results for the different test dates, using a  $2\sigma$  confidence interval. Yet, like the

additional statistical analyses done for service strains, service deflections, and wheel load distribution, the Anderson-Darling test showed that in fact the changes in *IM* are statistically significant.

The reason behind these significant variations may be temperature-related. Consider Figure 5-6, which superimposes the average temperature at the Toms Creek Bridge on top of the dynamic load allowances for all three truck orientations tested at 40 mph (64 kph). This figure suggests that there is an inverse relationship between temperature and the dynamic load allowance, particularly for the first four load tests (Fall 1997 through Spring 1999).

Additionally, a similar change in temperature seems to result in a comparable change in *IM*.

At the conclusion of his work, Neely proposed that the design *IM* for the Toms Creek Bridge should be 0.90, which is dramatically larger than the 0.30 and 0.33 limits for impact factors in the respective AASHTO *Standard Specifications* and *LRFD Specifications*. Figure 5-7 shows this proposed dynamic load allowance along with AASHTO's specifications.

Additionally, this figure presents the average dynamic load allowances calculated at 25 mph (40 kph) and 40 mph (64 kph) and the corresponding error bars for the different test dates. The dynamic load allowances shown in Figure 5-7 are determined from the deflection data, which generally give higher impact factors than the strain data. Neely suggested that the "design *IM*" should exclude the center orientation when averaging the dynamic load allowance results, because the center orientation tends to give a much lower impact factor. However, Figure 5-7 includes all of the truck orientations in the respective averages, taking the variability in the data into account through the use of the error bars, which are equal to  $\pm 2\sigma$ . The term  $\sigma$  is simply the standard deviation in the data, assuming a normal distribution.

With this method of averaging in mind, the dynamic load allowances at 25 mph (40 kph) are below AASHTO's guidelines for *IM*, even taking the variability into account. On the other hand, the average results for the 40 mph (60 kph) tests far exceed AASHTO's recommended guidelines, particularly the tests that took place in the Fall seasons. Furthermore, the superimposed error bars show that the statistical uncertainty places the dynamic load allowance above Neely's proposed value of 0.90 in all test dates except for the Summer 2003 tests. Given these results and their level of confidence, a new recommendation for *IM* in the Toms Creek Bridge is 1.35.

Although exceedingly high and potentially cost prohibitive, an impact value of this magnitude may be necessary to provide a level of serviceability beyond the impact demand determined through actual load tests in the Toms Creek Bridge. Naturally, a greater number of repetitions in a given orientation-speed combination, or testing a greater number of bridges similar to the Toms Creek Bridge may help to reduce the uncertainty in the dynamic load allowance, thus bringing the results more in line with Neely's proposed value for *IM*. If 1.35 holds for the design impact factor, then the estimated largest strain in the Toms Creek Bridge would be about 760  $\mu\epsilon$ , where the maximum measured peak strain at static speed is 324  $\mu\epsilon$ , in the center lane orientation during the Spring 1999 tests. The impact-enhanced static strain value would still only be about 13% of the ultimate strain for the 8-in. DWB.

### **5.3 Dynamic Allowance Results for the Route 601 Bridge**

#### **5.3.1 Dynamic Allowance Results from Current Study of Route 601 Bridge**

Table 5-3 shows both the maximum and average dynamic load allowances results for the Summer 2003 tests, calculated from the strain and deflection data. Recall that these dynamic experiments included only the east interior, center, and west interior orientations. When comparing the two measurement methods, the results are mixed. The dynamic load allowance at 25 mph (40 kph) calculated from the strain measurements are slightly greater than those determined using the deflection data. On the other hand, the 40 mph (64 kph) results show that the strain-based dynamic load allowances are somewhat *less than* those calculated with the deflection data. The fact that one measurement method gives a larger *IM* in one speed, but not the other, is surprising, particularly given the consistency in the results for the Toms Creek Bridge and the discussion in Section 4.2.1.

Looking at the strain-based results separately from the deflection results, there appears to be a minor amount of dynamic influence in the Route 601 Bridge when the load truck travels across the bridge at 25 mph (40 kph). At that speed, all three interior orientations have dynamic load allowances ranging from about 0.02 to 0.03. On the other hand, the 40 mph (64 kph) tests present a different picture. The most notable difference is the dynamic load allowance for the east interior orientation, where *IM* is 0.113. The other two orientations tested at this speed had impact factors of about -0.02 and zero. The negative *IM* value seems to indicate an "uplift" effect that occurs with elevated travel speed and is something that Restrepo observed in his

research, as discussed in Section 2.4.2. However, as mentioned in that section, VDOT crews attempted to ameliorate the conditions at the approaches with asphalt fill just prior to the Fall 2003 tests. Therefore, this ramping effect cannot be the cause for the negative *IM* values.

As further justification that the ramping effect should be discounted, the deflection results in Table 5-3 (b) show an even greater amount of “uplift” at the slower 25 mph (40 kph) speed. In the case of the center orientation, *IM* is -0.031 at 25 mph (40 kph) versus +0.039 at 40 mph (60 kph). If truck ramping were the culprit behind the negative dynamic factors, then the higher truck speed might lead to a more negative *IM* value. This possibility does not match the deflection results described above. Similar to the strain-based results, the deflection-based dynamic load for the east interior orientation at 40 mph (60 kph) is 0.144. This impact factor is the largest factor for all of the Fall 2003 test results. Otherwise, all of the other truck orientations show that *IM* is relatively small (0 to 0.04).

### **5.3.2 Comparison of *IM* with Previous Route 601 Bridge Tests**

In addition to the Fall 2003 tests, Table 5-3 also displays the maximum and average dynamic load allowance results from the tests that Restrepo carried out in 2001 and 2002. Figure 5-8 and Figure 5-9 provide a graphical representation of the data in Table 5-3 for the 25 mph (40 kph) and 40 mph (64 kph) truck speeds, respectively. The strain and deflection data follow the same general pattern over time, with the deflection results being consistently lower in the 25 mph (40 kph) tests.

Looking at the two truck speeds separately, the results for the 25 mph (40 kph) tests show that the dynamic load allowance is lower in Fall 2003 than in the previous two tests for the west and east interior orientations (0.03 to 0.09 lower), with a steady decline for the east interior orientation. On the other hand, the center orientation shows that Fall 2003 dynamic load allowance is only marginally higher than the Fall 2001 results, but is considerably *lower* than the Summer 2002 results (0.05 to 0.08 lower).

Tests at 40 mph (64 kph) show *IM* values that follow a pattern similar to the 25 mph (40 kph) tests for the center orientation over time. The case for the west interior orientation is somewhat similar to the center orientation at 40 mph (60 kph), where the dynamic load allowance is about the same when comparing Fall 2003 to Fall 2001 (i.e., 0.003 vs. -0.026, respectively, from the strain data), but is much lower than the *IM* calculated in Summer 2002 (0.294). On the other hand, the east interior orientation has a greater dynamic load allowance in

Fall 2003 than both of the previous tests. The deflection data shows the most dramatic change for this orientation, rising steadily from 0.006 in Fall 2001 to 0.144 in Fall 2003.

As with the calculations for wheel load distribution, the question is whether or not there is any statistical significance in the data presented for dynamic load allowance. Taking a look at Figure 5-10 and Figure 5-11 for a comparison between the individual test dates and their respective error bars, this type of analysis hints that there isn't much of a significant difference in *IM* when testing from year to year. However, the Anderson-Darling test concludes that data amongst the different test dates do come from different populations, and therefore the variation in the dynamic load allowance for the Route 601 Bridge is statistically significant.

However, these changes over time cannot be easily explained as easily as the case for the Toms Creek Bridge, since the dynamic load allowances in the Route 601 Bridge do not appear to have a clear inverse relationship with the ambient air temperature, as shown in Figure 5-12. Although *IM* at 40 mph (64 kph) for the east interior orientation changes in the opposite direction as the change temperature, the dynamic load allowances for the west interior and center orientations rise and fall in synch with the change in temperature when the load truck travels across the bridge at both 25 mph (40 kph) and 40 mph (64 kph). Because of these inconsistencies amongst the three interior truck orientations, temperature's effect on the *IM* factors for the Route 601 Bridge can not be definitively described. Furthermore, the results from the dynamic tests may be skewed by the changing approach conditions over the course of three load tests, as discussed in Section 2.4.2.

Regardless of what may be the source of the change in the dynamic load allowances for the Route 601 Bridge, the results need to be compared with specifications set forth by AASHTO. At the conclusion of his work, Restrepo suggested that the dynamic load allowance for the Route 601 Bridge be 0.30, which is what AASHTO dictates in its *Standard Specifications*. Restrepo's conclusion was based on the maximum average *IM* for any given speed-orientation combination, which, in the case of the Route 601 Bridge, is 0.294, based on the strain results for the west interior orientation tested at 40 mph (60 kph) in Summer 2002. Figure 5-13 shows the overall calculated *IM* values for 25 mph (40 kph) and 40 mph (64 kph); however, the averages in this figure combine all of the different truck orientations within each respective test date, with the variation in the different load tests presented in the form of error bars. These error bars are  $\pm 2\sigma$ , where  $\sigma$  is the standard deviation of the data. The results presented in this figure are based on

the strain data because the strain data consistently yields greater dynamic load allowances than the deflection data (which is opposite of the Toms Creek Bridge results).

Looking at Figure 5-13, the results for the 25 mph (40 kph) tests fall well below both the *Standard Specifications* and *LRFD Specifications* that AASHTO established. On the other hand, while averages for the 40 mph (64 kph) fall below the specifications, statistical analysis shows that there is some probability that the dynamic load allowance may exceed those specifications, particularly during the warmer seasons.

Based on the above results, the revised recommended dynamic load allowance for the Route 601 Bridge is 0.50. However, the important point to note is that there is a wide dispersion in the data which is probably partially due to the approach conditions for this bridge. Better design using approach slabs or better construction practices in compacting the soil at the abutments may help to reduce the scatter amongst the different truck orientations. Additionally, a larger number of individual load tests may also help to reduce the uncertainty in the results. Regardless of how many tests occur, bridge design using FRP may need to take the upper end of the temperature scale in a given climate into account in order to ensure adequate dynamic performance. If 0.50 holds for the design impact factor, then the estimated largest strain in the Route 601 Bridge would be about  $370 \mu\epsilon$ , where the maximum measured peak strain at static speed is  $247 \mu\epsilon$ , in the east exterior orientation during the Summer 2002 tests. This impact-enhanced strain would be less than 12% of the ultimate strain for the 36-in. DWB.

## 5.4 Tables and Figures

Table 5-1. Dynamic load allowances for the Toms Creek Bridge, based on strain data.

Researcher	Test Date	Truck Orientation	Speed			
			25 mph		40 mph	
			Max. IM	Avg. IM	Max. IM	Avg. IM
Neely	Fall 1997	Northbound	-0.09	-0.05	0.34	0.33
		Center	-0.09	-0.06	0.63	0.50
		Southbound	-0.13	-0.08	0.81	0.65
	Spring 1998	Northbound	-0.04	0.00	0.23	0.05
		Center	-0.13	-0.06	0.27	0.12
		Southbound	0.13	0.09	0.71	0.39
	Fall 1998	Northbound	0.11	0.05	0.68	0.54
		Center	-0.15	-0.04	0.45	0.29
		Southbound	0.16	0.12	0.75	0.72
	Spring 1999	Northbound	-0.10	-0.05	0.49	0.39
		Center	-0.16	-0.10	0.33	0.16
		Southbound	-0.04	-0.03	0.61	0.56
	Fall 1999	Northbound	-0.16	-0.13	0.54	0.44
		Center	-0.10	-0.09	0.41	0.22
		Southbound	-0.08	-0.05	0.69	0.64
Kassner	Summer 2003	Northbound	—	—	0.54	0.42
		Center	—	—	0.22	0.11
		Southbound	0.08	0.00	0.71	0.49

Table 5-2. Dynamic load allowances for the Toms Creek Bridge, based on deflection data.

Researcher	Test Date	Truck Orientation	Speed			
			25 mph		40 mph	
			Max. IM	Avg. IM	Max. IM	Avg. IM
Neely	Fall 1998	Northbound	0.21	0.07	0.85	0.71
		Center	-0.14	-0.07	0.39	0.24
		Southbound	0.13	0.09	1.13	1.08
	Spring 1999	Northbound	-0.10	-0.05	0.48	0.38
		Center	-0.26	-0.20	0.29	0.11
		Southbound	-0.09	-0.07	0.72	0.64
	Fall 1999	Northbound	-0.19	-0.11	0.70	0.58
		Center	-0.12	-0.07	0.56	0.31
		Southbound	0.06	0.01	1.09	0.99
Kassner	Summer 2003	Northbound	—	—	0.57	0.48
		Center	—	—	0.25	<b>0.14</b>
		Southbound	0.08	<b>0.04</b>	0.80	<b>0.64</b>

**Table 5-3.** Dynamic load allowances for the Route 601 Bridge, based on (a) strain and (b) deflection.

(a)

Researcher	Test Date	Truck Orientation	Speed			
			25 mph		40 mph	
			<i>Max. IM</i>	<i>Avg. IM</i>	<i>Max. IM</i>	<i>Avg. IM</i>
Restrepo	Fall 2001	West Interior	0.135	0.072	0.018	-0.026
		Center	0.117	-0.005	-0.034	-0.076
		East Interior	0.138	0.101	0.067	0.043
	Summer 2002	West Interior	0.097	0.087	0.316	<b>0.294</b>
		Center	0.080	0.077	0.357	0.230
		East Interior	0.041	0.038	0.071	-0.006
Kassner	Fall 2003	West Interior	0.100	0.022	0.038	0.003
		Center	0.065	0.028	0.016	-0.019
		East Interior	0.069	0.019	0.161	<b>0.113</b>

(b)

Researcher	Test Date	Truck Orientation	Speed			
			25 mph		40 mph	
			<i>Max. IM</i>	<i>Avg. IM</i>	<i>Max. IM</i>	<i>Avg. IM</i>
Restrepo	Fall 2001	West Interior	0.093	0.060	0.038	0.015
		Center	0.003	-0.040	-0.038	-0.066
		East Interior	0.089	0.065	0.044	0.006
	Summer 2002	West Interior	0.082	0.074	0.304	0.284
		Center	0.071	0.054	0.271	0.216
		East Interior	0.032	0.026	0.128	0.057
Kassner	Fall 2003	West Interior	0.062	-0.002	0.033	0.005
		Center	-0.008	<b>-0.031</b>	0.094	<b>0.039</b>
		East Interior	0.033	0.006	0.191	<b>0.144</b>

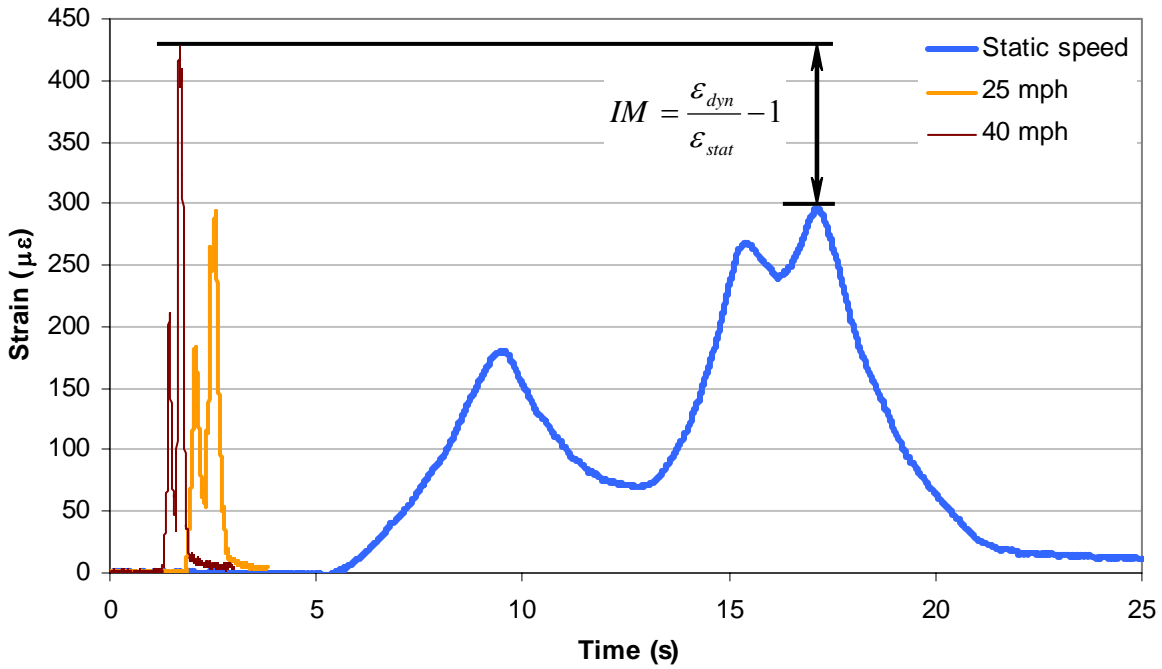


**Figure 5-1.** Typical comparison of peak dynamic loading versus static loading for the Toms Creek Bridge, with the *IM* factor based on strain measurements.

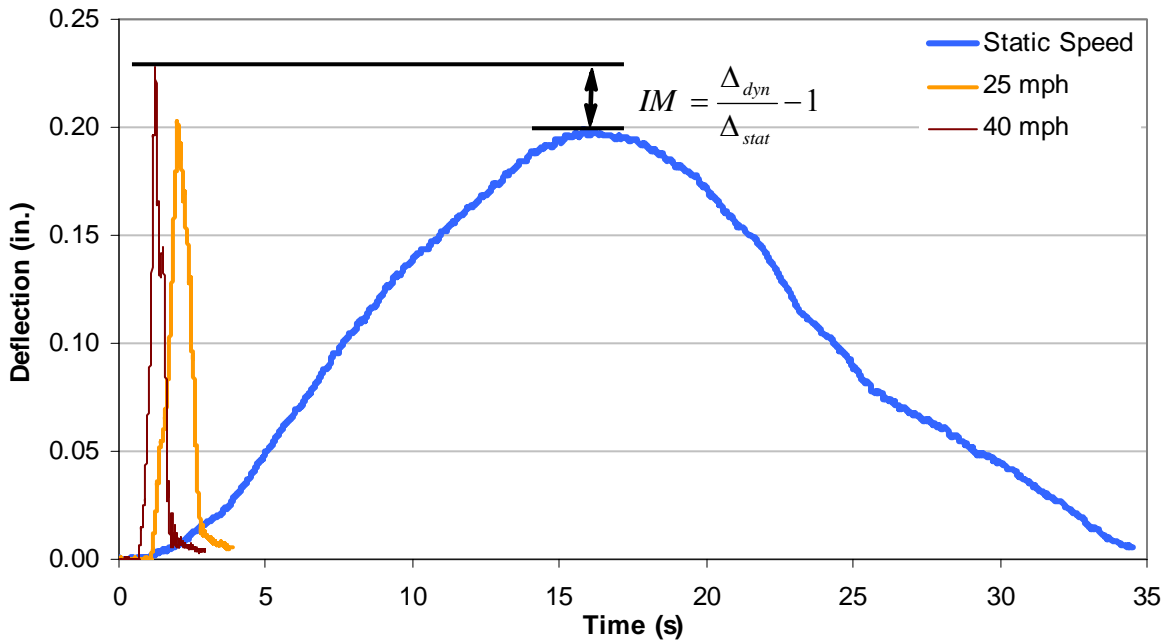


**Figure 5-2.** Comparison of peak dynamic loading versus static loading for the Route 601 Bridge, with the *IM* factor based on deflection measurements.

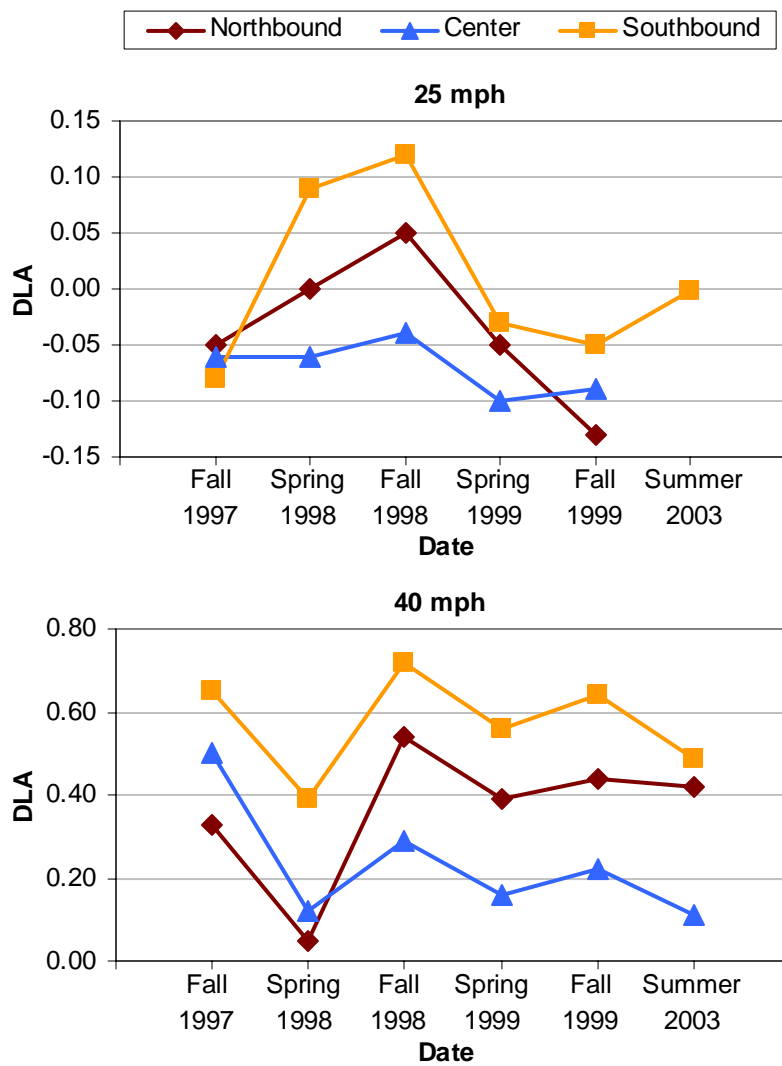


**Figure 5-3.** Average dynamic load allowance over time for the Toms Creek Bridge for two different speeds, based on strain data.

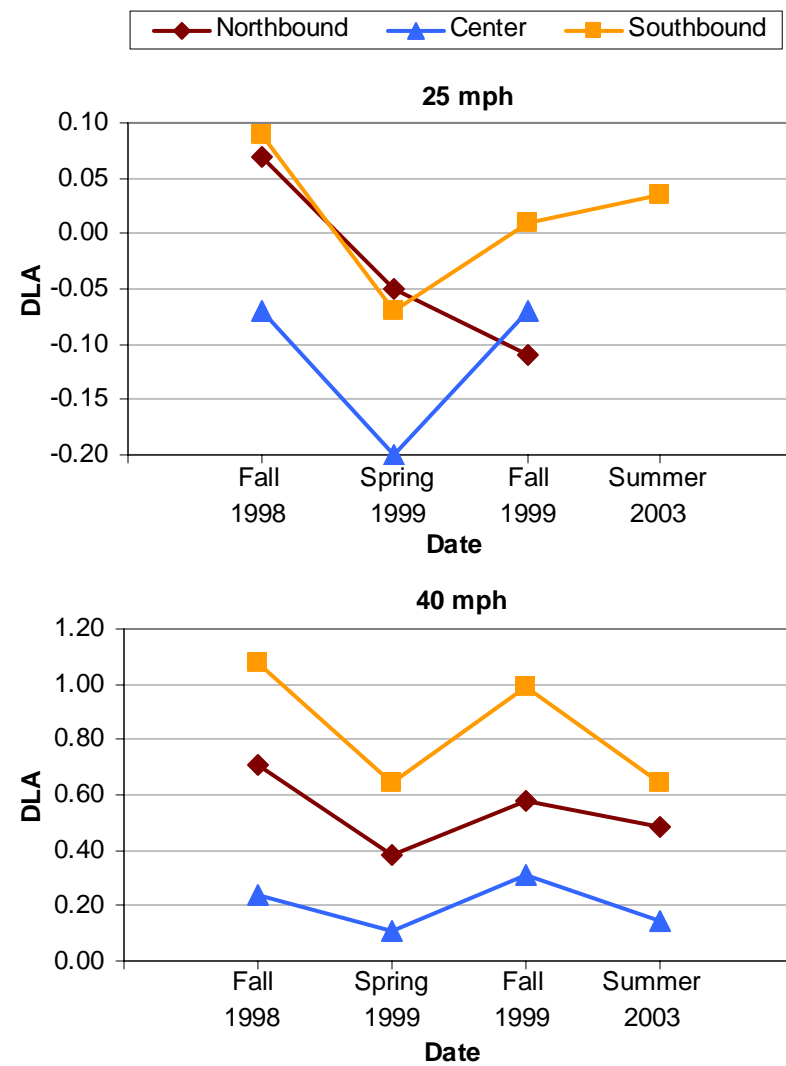
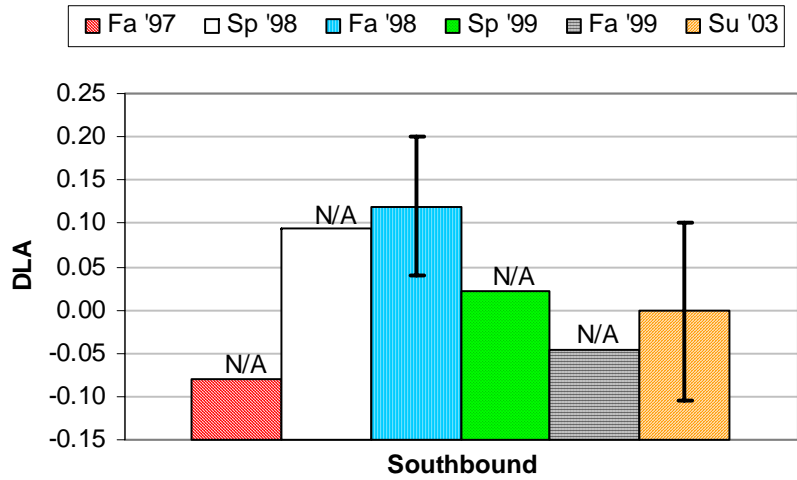
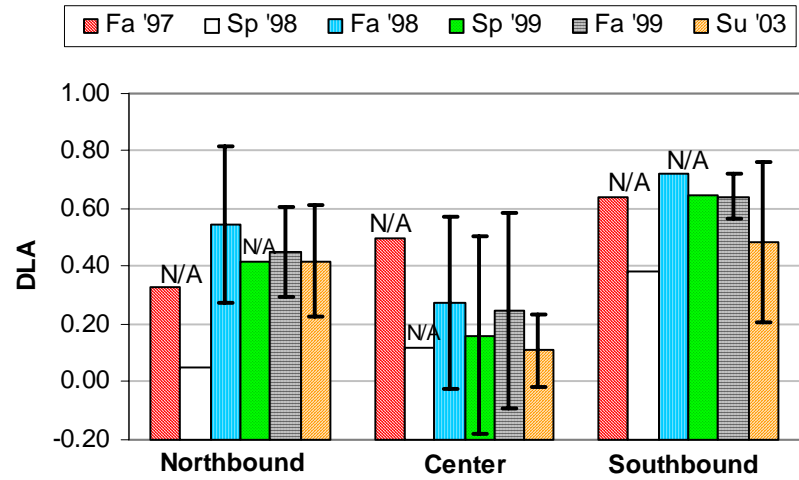


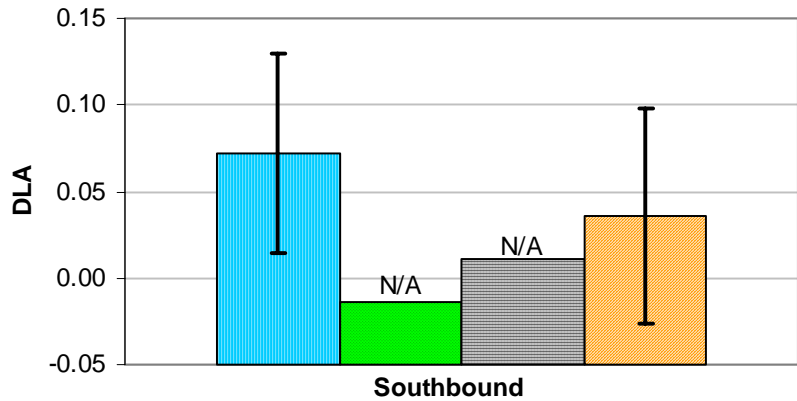
**Figure 5-4.** Average dynamic load allowance over time for the Toms Creek Bridge for two different speeds, based on deflection data.



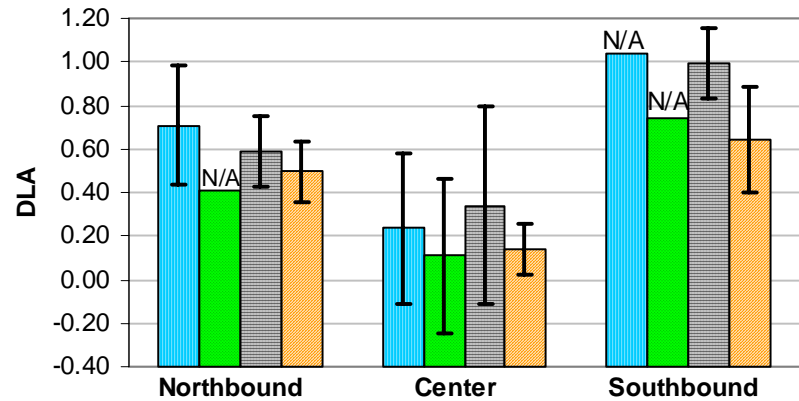
(1a)



(2a)

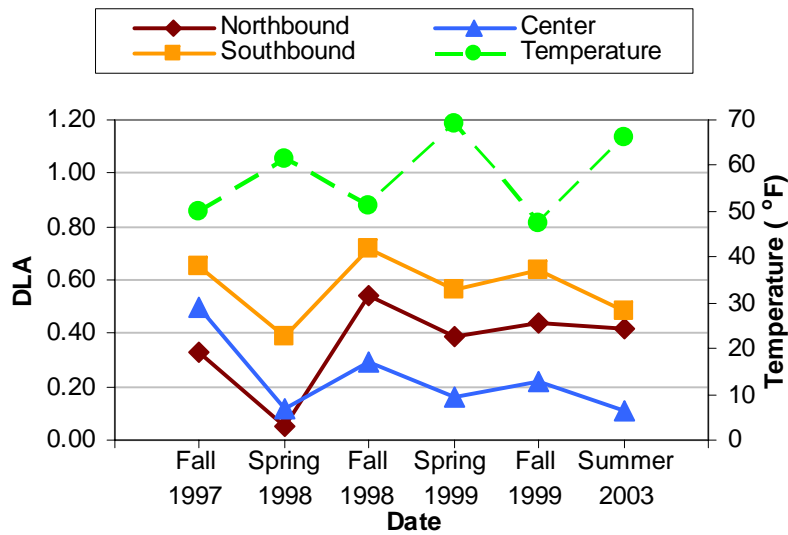


(1b)

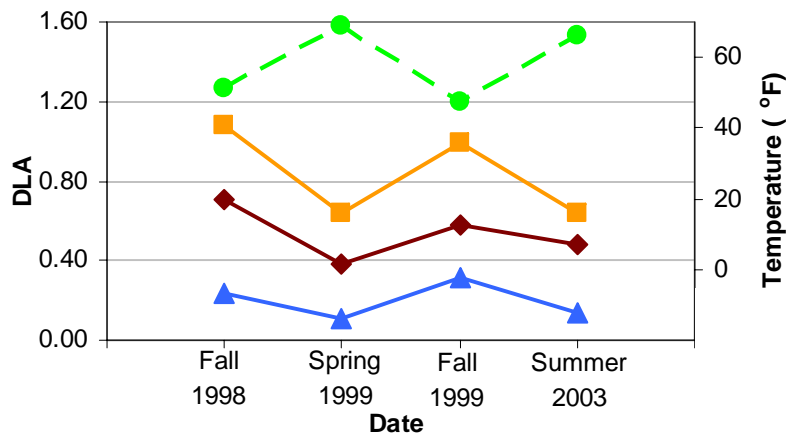


(2b)

**Figure 5-5.** Error bars for average dynamic load allowances for the (1) 25 mph and (2) 40 mph travel speeds across the Toms Creek Bridge. Dynamic load allowances based on (a) strain and (b) deflection measurements. Data points marked “N/A” do not have enough tests to produce a statistically reliable set of bars.

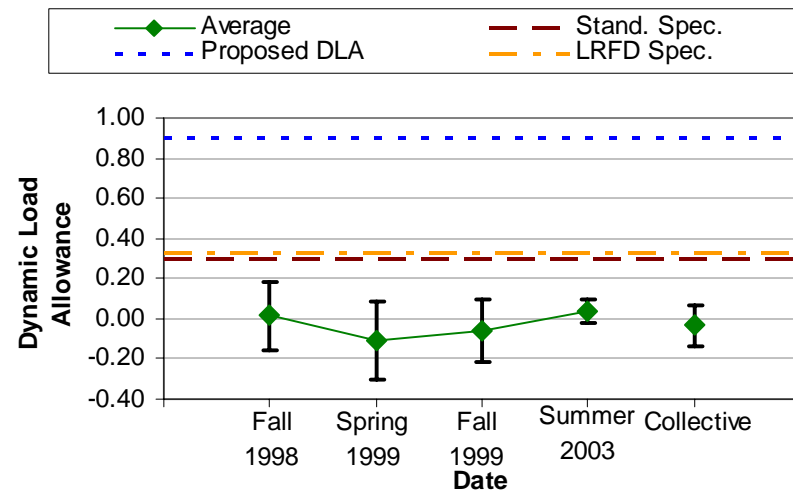


(a)

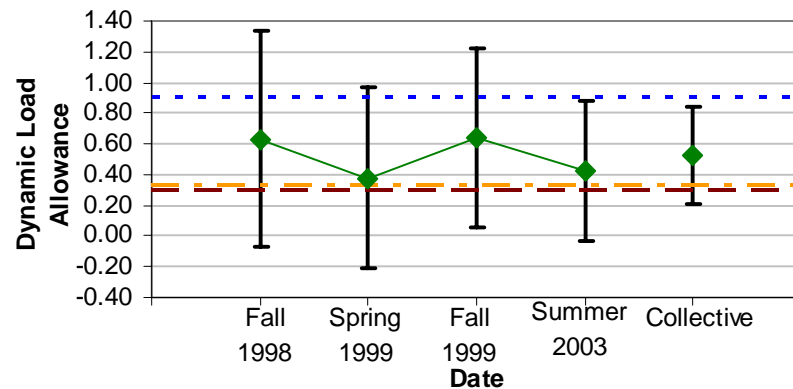


(b)

**Figure 5-6.** Comparison of temperature over time with dynamic load allowance at 40 mph in the Toms Creek Bridge. Based on (a) strain and (b) deflection.

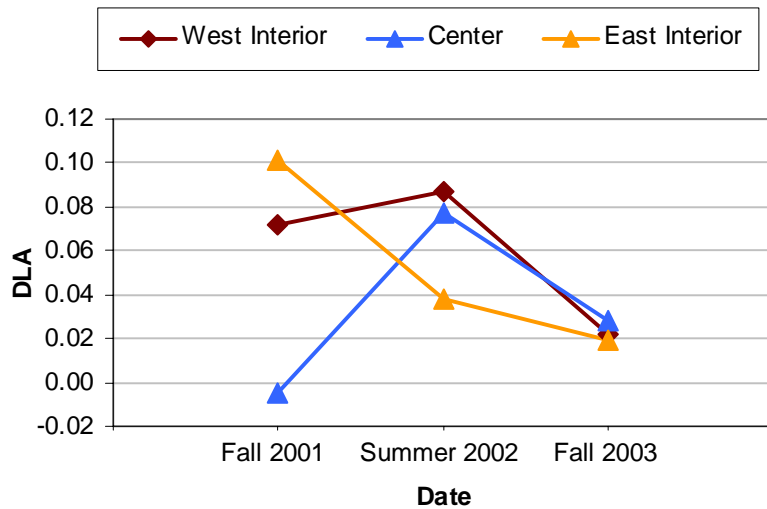


(a)

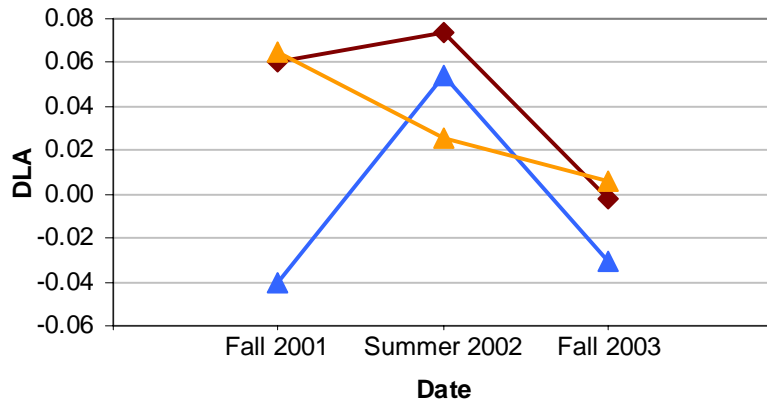


(b)

**Figure 5-7.** Overall dynamic load allowances calculated at (a) 25 mph and (b) 40 mph, averaged for all of the truck orientations on a given test date, shown with error bars, both AASHTO Specifications recommendations, and Neely's proposed IM. Averages shown here are based on deflection measurements, which tend to give the worst-case results.

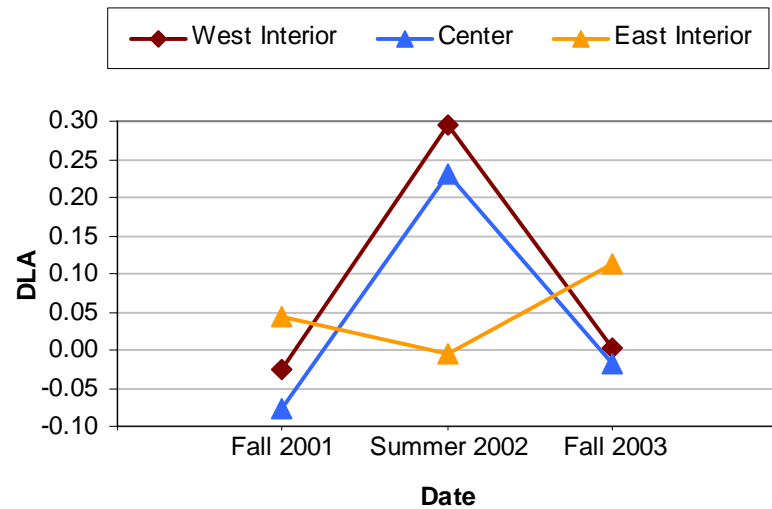


(a)

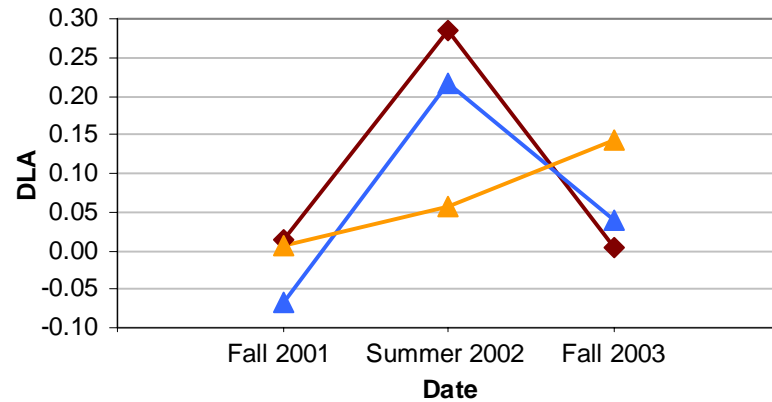


(b)

**Figure 5-8.** Average dynamic load allowances at 25 mph (40 kph) for the different interior orientations in the Route 601 Bridge, based on (a) strain and (b) deflection.

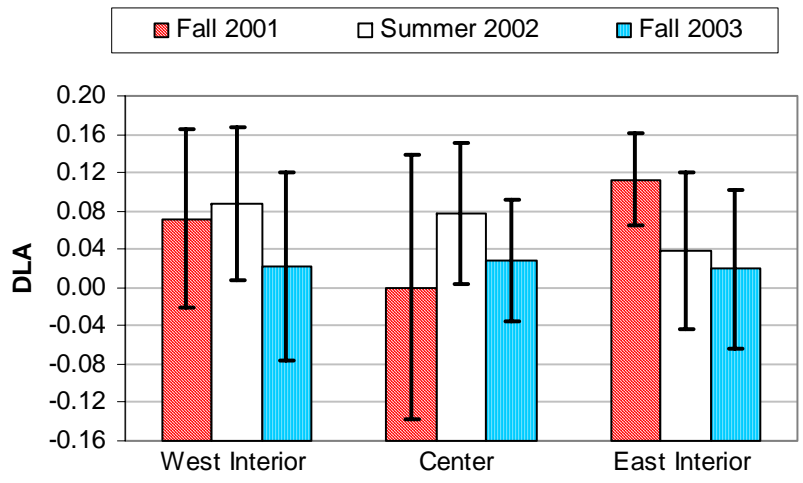


(a)

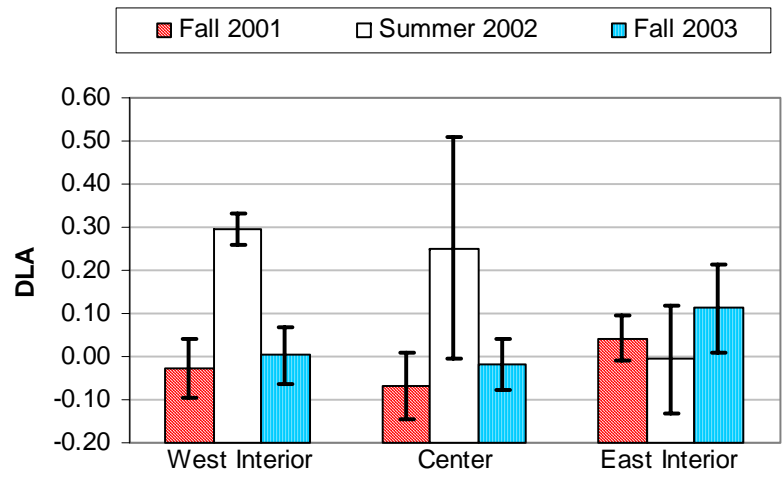


(b)

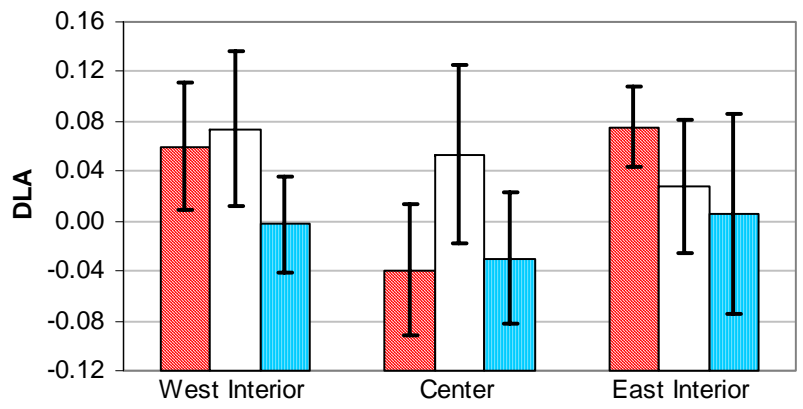
**Figure 5-9.** Average dynamic load allowances at 40 mph (64 kph) for the different interior orientations in the Route 601 Bridge, based on (a) strain and (b) deflection.



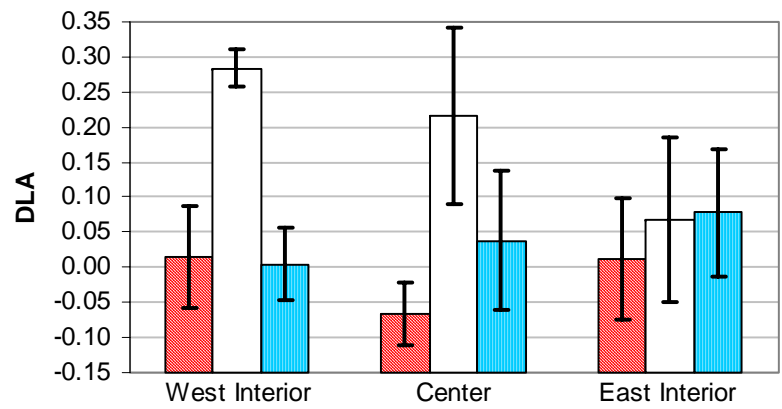
(a)



(a)



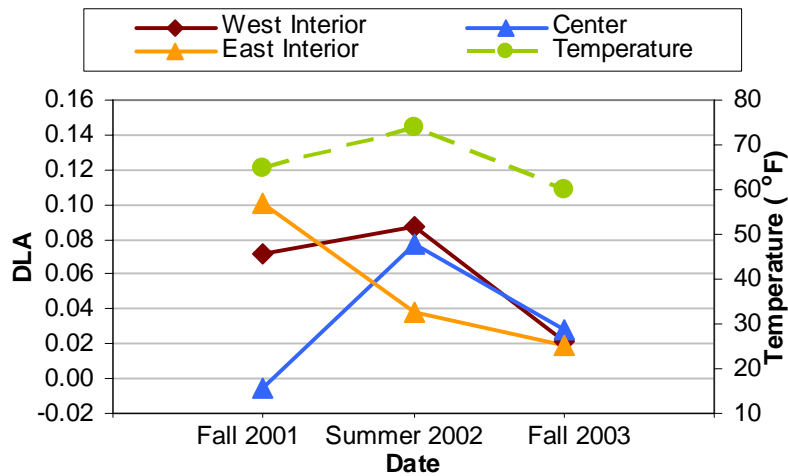
(b)



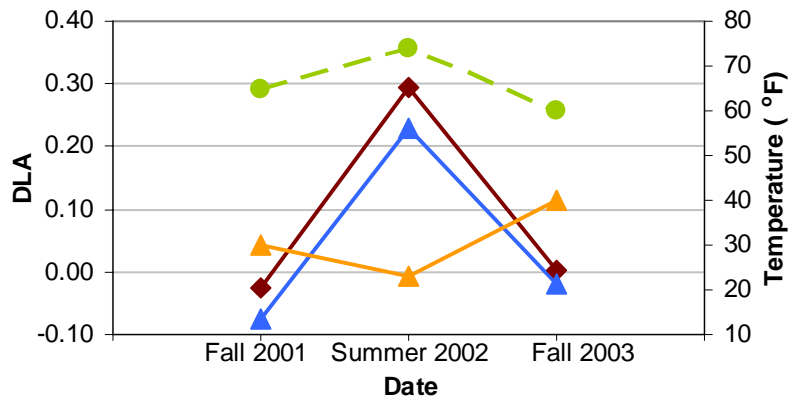
(b)

**Figure 5-10.** Average dynamic load allowances at 25 mph (40 kph) shown with error bars, based on (a) strain and (b) deflection.

**Figure 5-11.** Average dynamic load allowances at 40 mph (64 kph) shown with error bars, based on (a) strain and (b) deflection.

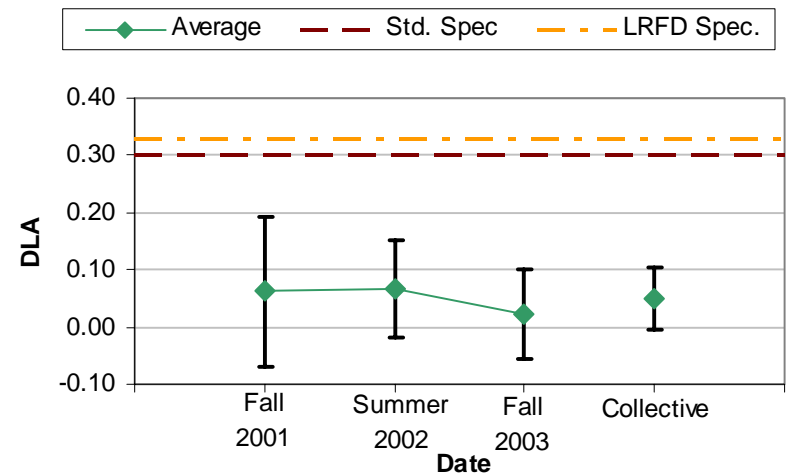


(a)

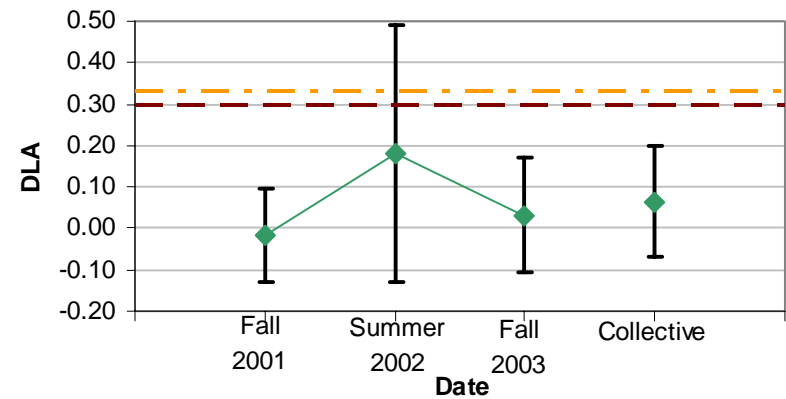


(b)

**Figure 5-12.** Average dynamic load allowance shown with temperature for the Route 601 Bridge at (a) 25 mph and (b) 40 mph, based on strain data.



(a)



(b)

**Figure 5-13.** Comparison of AASHTO Specifications with overall dynamic load allowances at (a) 25 mph and (b) 40 mph for the Route 601 Bridge, based on strain measurements.

## Chapter 6: Bridge Inspections

During testing for the Route 601 Bridge in the Fall of 2003, researchers noticed a number of “splinters” located on the bottom corners of the bottom flanges of several beams. Upon further examination, the two exterior girders exhibited “blisters” near the edges of the bottom of the bottom flange. Therefore, the researchers deemed that a detailed inspection was necessary at that time, as well as a follow-up inspection during the following Summer of 2004 in order to monitor any changes in the status of the bridge. A similar inspection took place at the Toms Creek Bridge in the Summer of 2004 as well. This portion of the study details the findings from these inspections.

### 6.1 Beams

Since the primary focus for this research is on FRP girders, most of the effort in inspecting the Route 601 Bridge focused on the beams. Figure 6-1 and Figure 6-2 diagram the deterioration or damage for Girder 1 and Girders 5 through 8; these two figures include the findings from both the Fall 2003 and Summer 2004 inspections. There were no noticeable problems for Girders 2 through 4. Generally speaking, the splinters discovered during the Fall 2003 inspection did not exhibit any change during the Summer 2004 survey. Likewise, the size of the individual blisters did not grow over the course of the two seasons. However, the extent of these blisters has grown, i.e., new blisters were located at a longer distance along the beams.

With regards to the “splinters,” they ranged in length from 1.5 in. to 12 in. (38 mm to 305 mm) long, with Girder 5 exhibiting the most extensive amount of this type of deterioration or damage. Typically, these splinters were about  $\frac{1}{8}$  in. to  $\frac{1}{4}$  in. (3 mm to 6 mm) wide, and in some cases, the splinters were still attached to the beam (see Figure 6-3). These splinters appear to consist only of the resin matrix material. However, in some cases, the carbon fibers were exposed. About two-thirds of the splinters occur within 4 ft (1.2 m) of midspan; the others range from 5 ft to 9 ft (1.5 m to 2.7 m) away from the ends of the beams. Apart from the ten splinters found during the Fall 2003 inspection, five additional splinters were discovered in the Spring of 2004. One splinter is along the downstream side of Girder 1, a second has been found near midspan on the upstream side of Girder 5, another is on the upstream side of Girder 6, and the

remaining two are along the downstream side of Girder 7. There is the possibility that these additional splinters were present but not noticed during the prior inspection.

While there does appear to be a couple of locations where damage occurred in Girders 1 and 5, the number of splinters in all of the beams is evenly split between being located on the upstream side of a girder versus the downstream side. Therefore, there is no conclusive evidence that this splintering effect is strictly due to damage from debris floating downstream during a high-water event. Furthermore, there was very little debris on top of the abutment or in between the girders, which again suggests that local flooding did not reach the girders.

Since a third of the splinters occur closer to the ends of the girders, there is only a small likelihood that the splintering was due to moment stresses at midspan. Besides, the failure mode that Waldron (2001) observed while loading a beam to failure was one of delamination between the carbon fiber and glass fiber interface in the *top* flange, not in the bottom flange, which is where most of the splintering has occurred in the Route 601 Bridge.

Ruling out the two aforementioned reasons behind the splinters leaves open the third possibility of construction damage that might have occurred while setting the beams in place. The splinter on the bottom of the top flange 6 ft (1.8 m) away from the west end of Girder 7 supports this theory. Representatives from Strongwell Corporation have also suggested that these splinters may actually be flaws due to production errors, where the fibers may have been set too close to the edge of the flange. If this theory were in fact true, then there would be an alarming rate of production flaws considering that four of the eight beams used in the Route 601 Bridge had splinters in them. Regardless of the reason, the splintering issue is one that needs continued monitoring to see if the splinters grow or any additional splinters appear. As noted before, the splinters discovered during the Fall 2003 inspection did not appear to increase in length.

The other previously mentioned problem is the “blisters” on the bottom flanges of the two exterior girders, i.e., Girders 1 and 8. Figure 6-4 represents a typical blister found on the girders. These blisters measured 1 in. to 3 in. (25 mm to 75 mm) in length, and appeared close to both the upstream and downstream edges of the bottom surface of the bottom flange. During the Fall 2003 inspection, these blisters were only noted on the western half of the two beams. However, the Spring 2004 inspection revealed a 1 in. (25 mm) blister located 4 ft (1.2 m) east of midspan in Girder 1 and a set of blisters extending 26 in. (660 mm) east of midspan in Girder 8.

Additional blisters were discovered about 3 ft (910 mm) away from the west end of Girder 8, as well as 20 in. (510 mm) beyond the extent of the original set of blisters in Girder 1 during the Fall 2003 survey.

The blisters were “hard” and could not be pressed inward with any degree of thumb pressure. Soundings taken by bouncing a quarter on the top of the bottom flange above the blistered area appeared normal versus unaffected FRP material. The same was true when tapping directly on the blisters. These soundings suggest that little if any delamination has occurred in these areas. Because the blistering occurred only on the two exterior girders, the primary suspect for the blistering is water intrusion. The fact that more blisters occurred on the exterior portion of the girder than the interior half helps to support this hypothesis, since the exterior half of the beam has greater exposure to water and moisture, thus is more prone to water intrusion. As previously mentioned, the blisters that were originally discovered during the Fall 2003 survey did not appear to have grown in size in the subsequent examination. Nevertheless, these blisters need continued monitoring in assessing the long-term viability of FRP in service conditions.

One problem that was not noticed during the Fall 2003 inspections is the presence of several longitudinal “cuts” in the surface of the bottom flange in several girders. These cuts appeared to be just that or like a deep scratch, rather than a crack; they had a constant thickness and remained straight along the length of the beam. Both Girders 5 and 6 exhibited a single cut along the full length of the beams. Girder 6 had an additional cut that was about 5 ft (1.5 m) long starting at the east end of the beam. Likewise, Girder 7 had a cut that was 25 in. (635 mm) long at the east end of the beam. While the cuts did not appear to be the result of deterioration, future surveys should measure their length and thickness in order to ensure that the cuts are not growing beyond the initial damage.

## **6.2 Abutments**

During the Fall 2003 survey, the east abutment showed two fairly severe cracks down the center of the abutment, which may be indicative of the large amount of settlement that has occurred since the bridge opened to traffic (see Figure 6-5). Note that the “east” abutment is on the right when looking downstream. Although no measurements were taken at that time, the crack may have become worse over the course of two seasons. As of the Spring 2004 inspection,

the larger of the two cracks extended for the full height of the abutment and was 0.2 in. (5 mm) wide just below the timber deck. Starting at the abutment seat, the second crack was 29 in. (735 mm) long and measured 0.075 in. (2 mm) at its widest point.

Similarly, the west abutment had two cracks near the center of the abutment, although these cracks were not as severe as those in the east abutment. One crack extended for the full height of the abutment and had a maximum width of 0.05 in. (1 mm), while the other was a hairline crack that was 17 in. (430 mm) long, measured from the abutment seat.

### **6.3 Beam Clearance**

In between the two inspection dates, a large amount of river stone collected underneath the eastern half of the bridge. Again, no measurements were taken during the Fall 2003 survey. However, during set up for testing, researchers had to extend their arms all the way upward to reach the bottom of Girder 1. Therefore, the distance from the ground to the bottom of Girder 1 at midspan was just under 8 ft (2.4 m) in the Fall of 2003. During the Spring 2004 inspection, however, that distance decreased to less than 5 ft (1.5 m).

Another measure of the pile-up of river stone is the comparison with the top of the abutment footing. During the Fall 2003 inspection, the level of the river stone was approximately 2 ft (600 mm) below the top of the abutment footing. However, the subsequent Spring 2004 survey showed that the rock pile was approximately 7 in. (180 mm) *above* the abutment footing.

If this type of sedimentation continues over time, the implication is that channel flow could become restricted, thus causing the river to flood the bridge and make the FRP beams more prone to damage from debris. Therefore, the clearance between the girders and the ground level should be closely monitored.

### **6.4 Road Surface**

As noted in Section 2.4.2, VDOT crews had repaired the slight dips at the approaches to the Route 601 Bridge in October 2003. These repairs appeared to remain in good condition during the Spring 2004 survey. On the other hand, the asphalt wearing surface over the timber deck had begun to show signs of cracking. Near midspan of the westbound lane, there was a 9-in. (230-mm) and a 6-in. (150-mm) longitudinal crack located 7.5 ft (2.3 m) from the edge of the

timber deck. There was also a 19-in. (480-mm) longitudinal crack near the centerline of the bridge. Along the east abutment, a transverse crack stretched across the westbound lane, measuring 10 ft (3.0 m) long. Likewise, a 3-ft (910-mm) transverse crack appeared along the west abutment in the eastbound lane. One other transverse crack was in the westbound lane at about midspan of the bridge, measuring 3 ft (910 mm) long. Unfortunately, the Fall 2003 inspection did not detail the cracks on the wearing surface; therefore, there can be no comparison between the two inspection dates.

## **6.5 Toms Creek Bridge Inspection**

Similar to the Route 601 Bridge, researchers inspected the Toms Creek Bridge in the Spring of 2004. There is very little to report for this bridge. All 24 beams appeared to be in good condition with no signs of splinters or blisters. The connections holding the FRP beams to the abutment as well as those connecting the timber deck to the beams appeared to be in satisfactory shape. The clearance between the beams and the stream did not appear to have changed over the course of a year. The only point of concern is the condition of the asphalt wearing surface. This surface showed a number of transverse cracks as well as a longitudinal crack. Such cracking is indicative of the relatively large degree of deflection in the beams, which can lead to cracking in non-structural elements and damage due to moisture, as discussed in Section 1.2.5.1.

## 6.6 Figures

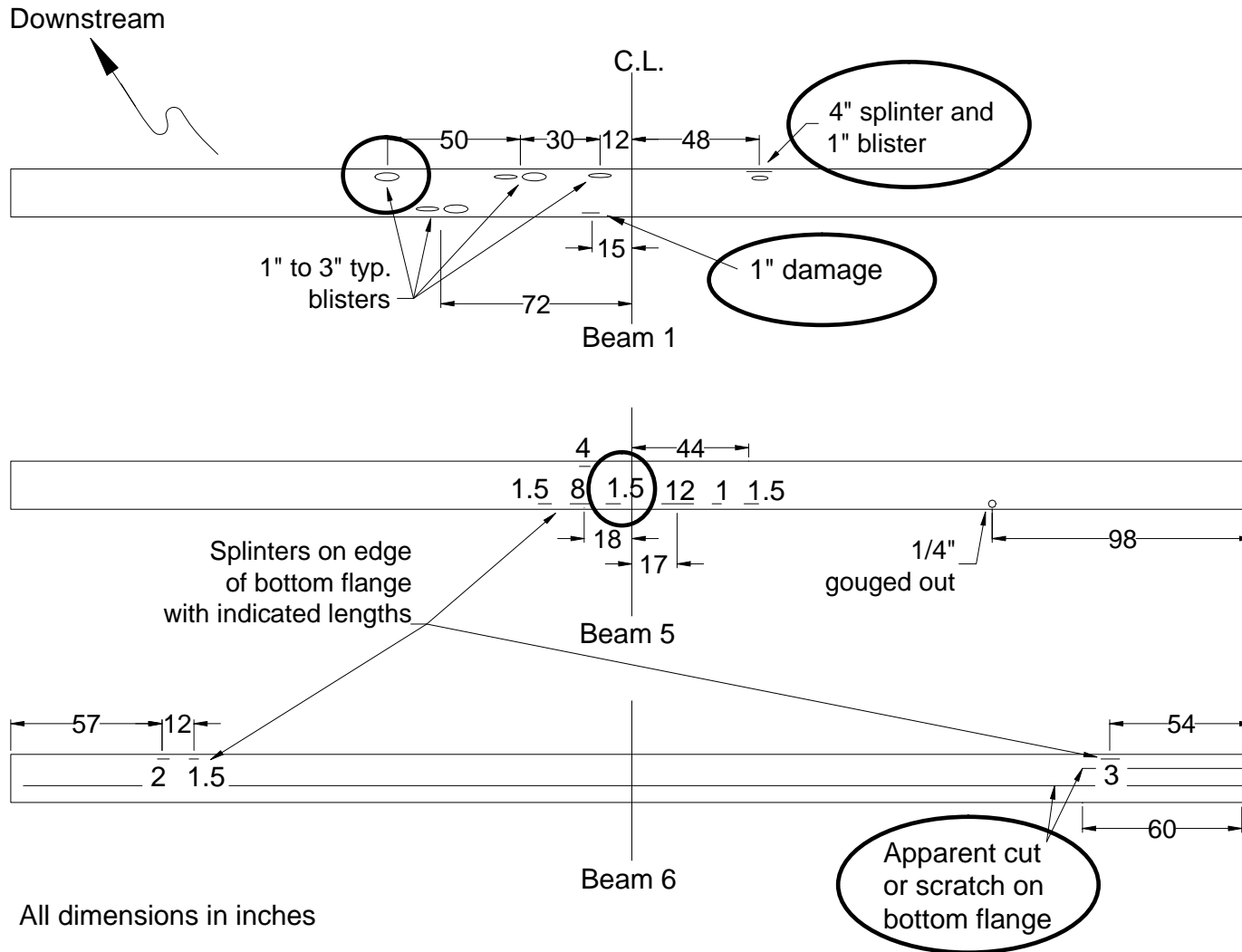


**Figure 6-1.** Detail of locations for damage or deterioration in Beams 1, 5, and 6 in the Route 601 Bridge. Circled items were discovered during the Spring 2004 inspection; all other items were noted during the Fall 2003 inspection.

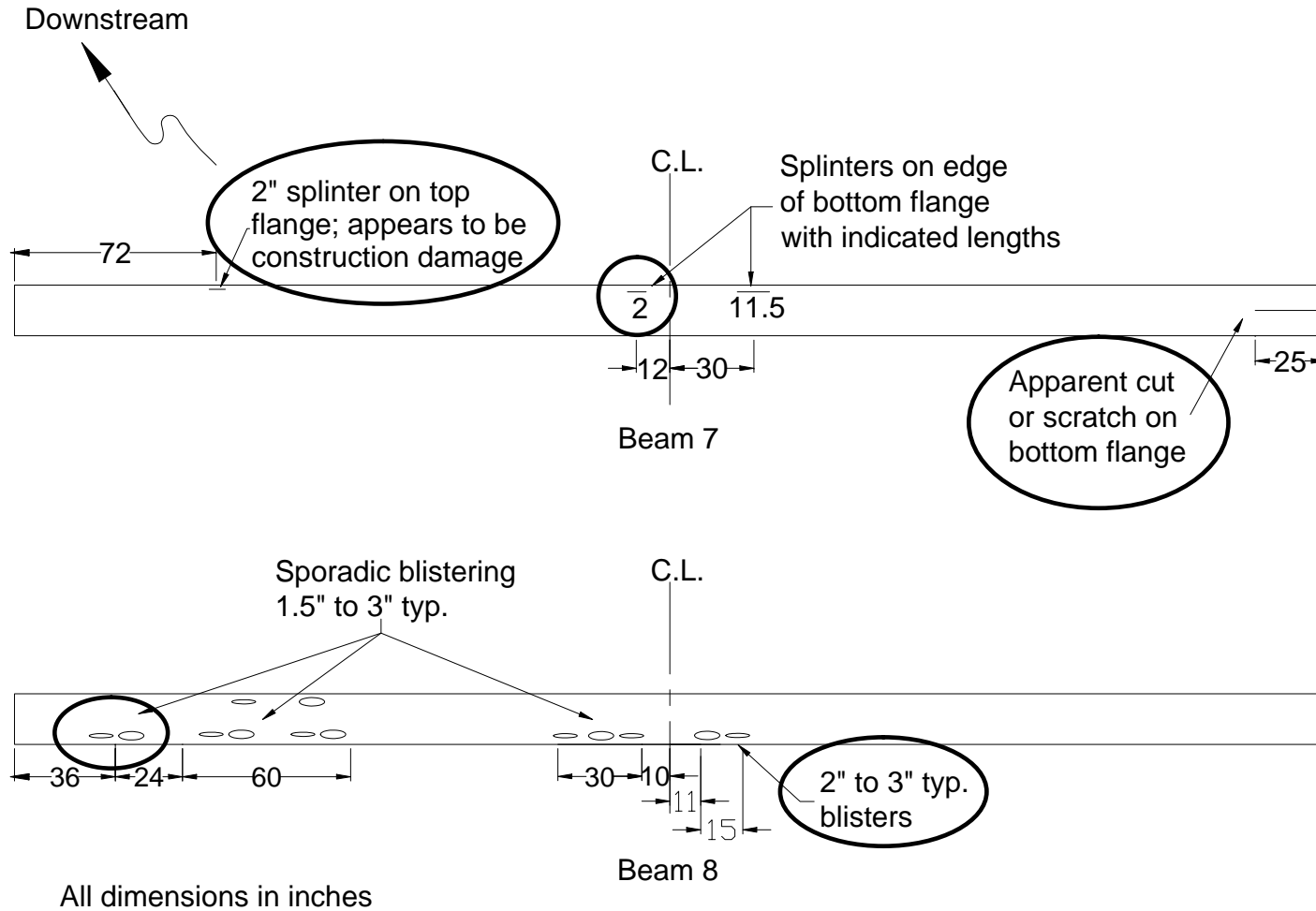


**Figure 6-2.** Detail of locations for damage or deterioration in Beams 7 and 8 in the Route 601 Bridge. Circled items were discovered during the Spring 2004 inspection; all other items were noted during the Fall 2003 inspection.



**Figure 6-3.** Matrix resin material splintering off from Girder 5 of the Route 601 Bridge (courtesy of Strongwell Corp).



**Figure 6-4.** Typical blister on the surface of the bottom flange in an exterior girder for the Route 601 Bridge.

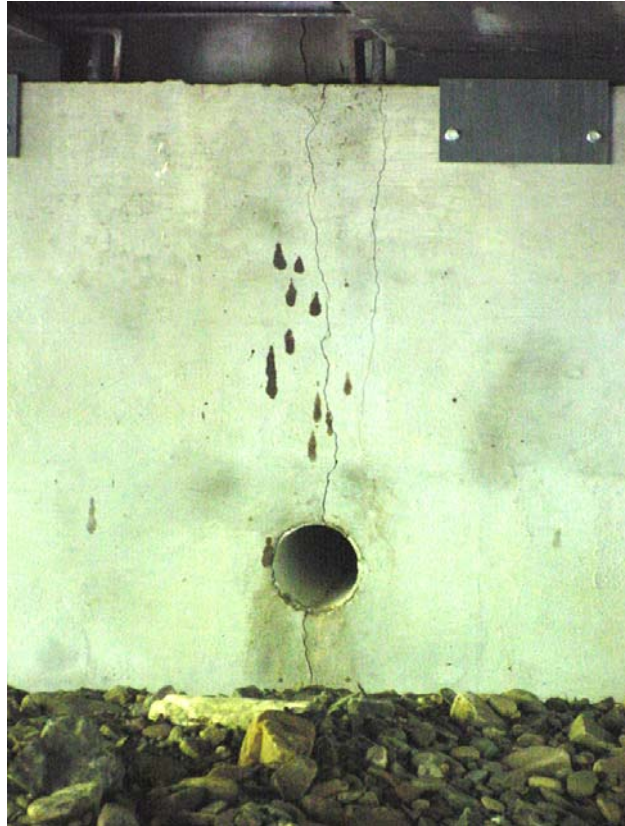


**Figure 6-5.** Crack down center of east abutment of the Route 601 Bridge.



**Figure 6-6.** Extent of river stone pile-up at east abutment during Fall 2003 inspection of the Route 601 Bridge.



**Figure 6-7.** Extent of river stone pile-up at east abutment during Spring 2004 inspection of the Route 601 Bridge.

## Chapter 7: Conclusions and Recommendations

The research presented in this work has helped in making the following conclusions and recommendations:

### 7.1 Conclusions

#### 7.1.1 Toms Creek Bridge

- A summary of conclusions of the three design parameters (deflection, wheel load distribution, and dynamic load allowance) is in Table 7-1, along with comparisons with AASHTO specifications.
- The largest average peak deflection during the Summer 2003 test is 0.434 in. (11 mm), which occurs at the 40 mph (60 kph) travel speeds. This deflection translates to a ratio of  $L/484$ , which exceeds the  $L/500$  limit in the AASHTO *Standard Specifications* for timber bridges, but is within the  $L/425$  guidelines set forth by the AASHTO *LRFD Specifications*. The severity of the cracking in the asphalt wearing surface is indicative of the amount of deflection.
- The largest average peak strain during the Summer 2003 tests for the Toms Creek Bridge is  $438 \mu\epsilon$ , which is 7% of the failure strain in the beams. Over the course of over 6 years of in-situ loading, there does appear to be a statistically significant change in both the average peak deflection and strain. This conclusion matches the observations that Neely made during the first five load tests for this bridge. This increase may be related to the variation in temperature from one test to the next, although the reason for the temperature effect is unclear. Taking temperature out of the equation by comparing tests that took place in similar temperature ranges appears to show that the bridge stiffness has remained about the same during 6 years of service.
- Although moisture does affect the mechanical characteristics of timber, past research tends to indicate that the potential changes in moisture content of the timber deck and

edge rails do not justify the relatively large variations in deflections of either the Toms Creek Bridge or the Route 601 Bridge.

- Despite the high degree of deflection, the largest peak strain recorded for all six series of tests is only 7% of the ultimate strain, which was determined during laboratory testing in 1997. This low level of strain is evidence of the large factor of safety against failure in the Toms Creek Bridge.
- The maximum average load distribution for the Summer 2003 test is 0.084, which translates to an  $S/D$  ratio of  $S/11.1$ . This value is lower than both the *AASHTO Standard* and *LRFD Specifications* (0.117 [ $S/8.0$ ] and 0.106 [ $S/8.8$ ], respectively). The strain-based values for  $g$  were only marginally higher than the  $g$ -values calculated using the recorded deflections. The wheel load distributions calculated at static speed were essentially equal to those calculated at dynamic speeds, which concurs with previous conclusions that speed does not play a role in load distribution.
- Generally speaking, the wheel load distributions for the Summer 2003 tests are either less than or equal to those calculated from the previous five tests. While there does appear to be a statistically significant variation in  $g$  over the course of the six tests, this change is may be due to the variations in temperature. Furthermore, the decrease in the wheel load distribution may be due to larger relative change in the total deflection in all of the beams compared to the change in the peak deflection of the most heavily-loaded beam.
- The suggested design wheel load distribution for the Toms Creek Bridge is 0.11, or  $S/8.5$ , on a per-axle basis. This value is nearly the same as the *AASHTO Standard Specifications* for steel stringers supporting a 4-in. (100-mm) timber deck. While the design  $g$  is substantially higher than the average distributions calculated in all of the field tests, the elevated  $g$  accounts for the variability in the test data.
- The largest dynamic load allowance calculated from the Summer 2003 test for the Toms Creek Bridge is 0.64. Generally speaking, the calculations from the strain and deflection measurements give similar results. However, the impact factor varies widely depending on the truck orientation as well as the travel speed. The southbound orientation yields a

larger *IM* than the other two truck orientations, and the 40 mph (60 kph) travel speed gives a much higher result than 25 mph (40 kph). At the time of testing, there were no noticeable problems with the approach conditions coming from either direction of the bridge.

- In looking at the strain data, the dynamic load allowance appears to have stabilized over time; however, temperature may affect this factor. Regardless, there seems to be no statistically significant change in *IM* over time.
- The revised recommended *IM* for the Toms Creek Bridge is 1.35, which is a large increase over the 0.90 value that Neely (2000) suggested in his research. The reason for the increase is the statistical uncertainty in the data from all six load tests. Note that the dynamic load allowances at 25 mph (40 kph) are well below both the 0.30 and 0.33 limits established by the AASHTO *Standard Specifications* and the AASHTO *LRFD Specifications*, respectively. However, the average values at 40 mph (60 kph) are above the stated guidelines, and the uncertainties in the overall results only exacerbate the problem. Nevertheless, the larger dynamic load allowance would still keep the strain in the beams below 13% of the ultimate strain. Thus the Toms Creek Bridge is more than adequate in terms for the traveling public.
- An inspection of the Toms Creek Bridge in the Summer of 2004 revealed no structural problems in the bridge. The only point of concern is the excessive cracking in the asphalt wearing surface on top of the timber deck.

### **7.1.2 Route 601 Bridge**

- A summary of the three design parameters (deflection, wheel load distribution, and dynamic load allowance) is in Table 7-2, along with comparisons with AASHTO specifications.
- The largest average peak deflection during the Fall 2003 test is 0.254 in. (6 mm), which occurred at static speed in the west exterior orientation. Even with factoring in a conservative dynamic load allowance of 0.50, this deflection is approximately equivalent

to  $L/1230$ , which is well below the AASHTO-recommended limit of  $L/800$  for steel, prestressed concrete, or reinforced concrete bridges without pedestrian traffic.

- The largest average peak strain during the Fall 2003 tests for the Route 601 Bridge is  $220 \mu\epsilon$ , which is 7% of the failure strain in the beams. Additionally, the largest peak strain recorded for all three series of tests,  $240 \mu\epsilon$ , is only 9% of the ultimate strain, which was determined during laboratory testing in 2001. Similar to the Toms Creek Bridge, this small fraction of the failure strain shows that there is a large factor of safety against failure in the Route 601 Bridge.
- As with the Toms Creek Bridge, temperature does appear to have an effect on the peak strain and deflection in the Route 601 Bridge, where the Summer 2002 tests occurred at the highest temperatures and yielded the largest strain and deflection. Taking this temperature effect into account, there is not enough evidence to conclusively say that the peak strains and deflections have increased during the two year service life of the bridge.
- The largest average value for wheel load distribution in the Fall 2003 test is 0.343, or  $S/10.2$ , per axle, based on deflection measurements for the multiple-lane loaded orientation. This distribution factor is below the 0.50 limit set in both the AASHTO *Standard* and *LRFD Specifications*. Unlike the Toms Creek Bridge or the guidance set forth by AASHTO, speed may have a small effect on  $g$  in the Route 601 Bridge. However, the conditions at the approaches to the bridge may have been a factor in this case.
- Although statistical analysis showed that there is a statistically significant difference in the results for wheel load distributions, there is no consistent conclusion that  $g$  in the Route 601 Bridge has increased over time. However, the potential for  $g$  to increase over time certainly does exist. Unlike the Toms Creek Bridge, temperature does not have a clear-cut effect on the Route 601 Bridge's performance in terms of wheel load distribution.
- The recommended distribution factor for the Route 601 Bridge remains at 0.35 or  $S/10$  on a per axle basis, which is what Waldron (2001) and Restrepo (2002) suggested in their

research. Note that this value is the recommended wheel load distribution regardless of truck position or the number of lanes loaded, and falls below the guidelines set forth by the AASHTO *Standard Specifications* (for a 4-in. [100-mm] timber deck supported by steel stringers) and the AASHTO *LRFD Specifications* (for a timber deck of any thickness supported by steel stringers). However, the wheel load distribution in the Route 601 Bridge could potentially exceed the suggested 0.35 design value, given the statistical uncertainty in the data. Presumably, additional test data for this and other similar bridges may help to reduce that uncertainty.

- The largest dynamic load allowance calculated from the Fall 2003 test for the Route 601 Bridge is 0.14, based on deflection measurements at 40 mph (60 kph). The dynamic effects at 25 mph (40 kph) are generally smaller than those at 40 mph (60 kph). Neither measurement method gives a consistently higher or lower *IM* factor for all of the combinations of truck orientation and travel speed. Like the Toms Creek Bridge, the *IM* for this bridge seems to depend on the truck orientation, and in some cases, actually yields a *negative* dynamic influence. That is to say that the peak strain or deflection at a dynamic speed is *less* than that for the static test. Restrepo (2001) experienced similar results in his research. Although Restrepo suggested that the approach conditions during his tests could have caused an “uplift” effect, that reason is not entirely clear for these latest tests.
- The revised recommended design *IM* for the Route 601 Bridge is 0.50, which marks an increase from the 0.30 value that Restrepo suggested. Again, the reason for this increase is the dispersion in the data for all of the different test dates. However, given the overall uncertainty in the dynamic load allowance results due to the amount of test data and the changing conditions for the approaches to the Route 601 Bridge, there is no definitive conclusion that the *IM* has changed over the two years for which this bridge has been in service. Even with the increased dynamic load allowance, the average peak strain in the bridge would be less than 12% of the failure strain. Thus the bridge is extremely safe for public use.

- There are a number of locations on the girders for the Route 601 Bridge that indicate some form of damage or deterioration. However, there is no certainty as to what caused these problem areas to occur. Regardless, the “splinters” that were discovered during the Fall 2003 inspection do not appear to have grown worse over the course of two seasons. Note that some splinters have left the outermost reinforcing fibers exposed. Other splinters were discovered during the Summer 2004 survey, but they may have already been present during the first inspection. On the other hand, the extent of the “blisters” that occur on both exterior girders seems to have increased. While the individual blisters have not increased in size, the number and distance along the beams have. Despite the observations made above, there were no areas in the beams that sounded as though delamination had occurred.

## **7.2 Recommendations**

- Continue inspecting the Route 601 Bridge on a semi-annual basis. Inspections should closely detail the girder conditions to be sure that there is no premature deterioration. Also, the clearance underneath the bridge, particularly for the eastern half, should be checked to ensure that there is enough area to allow water to flow during a flood event. Doing so will help lessen any probability of the beams being damaged due to debris floating downstream. In the meantime, standard maintenance should include repairing the cracks in both abutments.
- Conduct an additional load test on the Toms Creek Bridge. After six years of service, the Toms Creek Bridge seems fairly consistent in performance. A final load test should take place prior to any planned roadway expansion and bridge reconstruction. After dismantling the bridge, researchers should conduct additional stiffness, fatigue, and ultimate strength tests on individual beams to assess their performance after an extended in-situ test period.
- Conduct material tests on the Toms Creek Bridge beams. In addition to the mechanical tests mentioned above, researchers should perform material tests such as the moisture content and matrix volume of the FRP material. These results for FRP subjected to actual environmental conditions can give some guidance on the accuracy of laboratory tests,

which tend to subject materials to extreme conditions over relatively short periods of time.

- Conduct additional load tests on the Route 601 Bridge. Again, the behavior in this bridge seems fairly consistent. However, the bridge should be tested again within the next two years and then possibly five years after that. Each test interval should consist of a Summer and Fall test so as to obtain better data regarding temperature effects, as well as provide a comparable basis for the three tests that have been completed to date. The second set of tests for the 5-year interval merely serves as a way to monitor the bridge's performance over time.
- Continue studying the effects that temperature has on bridge performance. This research accompanied by previous results show that temperature plays an important role, particularly with regards to peak deflection and strain, as well as wheel load distribution factors. However, since the reason behind this effect is not yet clear, future testing may want to consider additional instrumentation on the bearing pads for both the Toms Creek Bridge and the Route 601 Bridge. The pads do provide some amount of rotational stiffness and may offer insight to the issue. Any future design codes may need to be developed with temperature effects in mind.
- Give further study to the effects that moisture has on bridge performance. Although the results for this study are small regarding moisture, this effect must be considered, especially if the stiffness of the timber deck or edge barriers is taken into account when designing for the stiffness of the entire bridge.
- Develop a system for composite action between the deck and girder. Neither the Toms Creek Bridge nor the Route 601 Bridge seems to display any composite action between the timber deck and FRP girders. Having such a system should dramatically increase the bridge's overall stiffness, thus making FRP a more competitive material in bridge design. Increasing the stiffness is critical since designing with FRP tends to be deflection-controlled.

- Determine how critical deflection is to non-structural elements. As mentioned above, deflection is a major criterion in designing with FRP. Yet, there is some debate as to what extent deflection is a factor in determining the overall lifespan of a bridge. Resolving this debate may help improve FRP's applicability in bridge design if the conclusion is that deflection in girders is not a determining factor in serviceability for non-structural elements.
- Study deflection and the dynamic effects perceived by motorists and pedestrians crossing the bridge. As with the above recommendation, determining whether or not the amount of deflection is important in controlling the dynamic effects can greatly enhance FRP's attractiveness as a material for civil infrastructure applications.

## Tables

**Table 7-1.** Summary of results for the key design parameters in the Toms Creek Bridge.

Design Parameter	2003 Test Results	AASHTO Limits		Proposed
		<i>Standard</i>	<i>LRFD</i>	
Deflection	<i>L/484</i>	<i>L/500</i>	<i>L/425</i>	<i>L/425</i>
Wheel Load Distribution, <i>g</i> (per axle)	<i>S/11.1</i>	<i>S/8.0</i>	<i>S/8.8</i>	<i>S/8.5</i>
Dynamic Load Allowance, <i>IM</i>	0.64	0.33	0.30	1.35

**Table 7-2.** Summary of results for the key design parameters in the Toms Creek Bridge.

Design Parameter	2003 Test Results	AASHTO Limits		Proposed
		<i>Standard</i>	<i>LRFD</i>	
Deflection	<i>L/1230</i>	<i>L/800</i>	<i>L/800</i>	<i>L/1017</i>
Wheel Load Distribution, <i>g</i> (per axle)				
Single Interior Girder	<i>S/13.8</i>	<i>S/9.0</i>	<i>S/8.8</i>	<i>S/10.0</i>
Exterior Girder	<i>S/10.2</i>	<i>S/7.0</i>	<i>S/7.0</i>	<i>S/10.0</i>
Dynamic Load Allowance, <i>IM</i>	0.14	0.33	0.30	0.50

## References

- American Association of State Highway and Transportation Officials (AASHTO) [1996]. Standard Specifications for Highway Bridges: Sixteenth Edition. Washington, D.C.
- American Association of State Highway and Transportation Officials (AASHTO) [1998]. LRFD Bridge Design Specifications: Second Edition. Washington, D.C.
- Bakis, C. E., Bank, L. C., Brown, V. L., Cosenza, E., Davalos, J. F., Lesko, J. J., Machida, A., Rizkalla, S. H., and Triantafillou, T. C. (2002). "Fiber-Reinforced Polymer Composites for Construction – State-of-the-Art Review." *Journal of Composites for Construction*, Vol. 6, No. 2, 73-87.
- Balázs, G. and Borosnyó, A. (2001). "Long-term Behavior of FRP." *Composites in Construction, A Reality: Proceedings of the International Workshop*, July 20-21, 2001, Capri, Italy, 84-91.
- Bank, L. C. (1987). "Shear Coefficients for Thin-walled Composite Beams," *Composite Structures*, Elsevier Applied Science, Vol. 8, 47-61.
- Barker, R. M., and Puckett, J. A. (1997). *Design of Highway Bridges*, John Wiley & Sons, Inc., New York, New York, pp. 96-100, 155-161, 276-290.
- Barr, P. J., Eberhard, M. O., and Stanton, J. F. (2001). "Live-Load Distribution Factors in Prestressed Concrete Girder Bridges." *Journal of Bridge Engineering*, Vol. 6, No. 5, 298-306.
- Choi, Y. and Yuan, R. L. (2003). "Time-Dependent Deformation of Pultruded Fiber Reinforced Polymer Composite Columns." *Journal of Composites for Construction*, Vol. 7, No. 4, 356-362.
- Foster, D. C., Richards, D., and Bogner, B. R. (2000). "Design and Installation of Fiber-Reinforced Polymer Composite Bridge." *Journal of Composites for Construction*, Vol. 4, No. 1, 33-37.
- Gillespie Jr., J. W., Eckell II, D. A., Edberg, W. M., Sabol, S. A., Mertz, D. R., Chajes, M. J., Shenton III, H. W., Hu, C., Chaudhri, M., Faqiri, A., and Soneji, J. (2000). "Bridge 1-351 Over Muddy Run." *Transportation Research Record*, No. 1696, Vol. 2.
- Green, D. W., Evans, J. W., Logan, J. D., Nelson, W. J. (1999). "Adjusting Modulus of Elasticity of Lumber for changes in Temperature." *Forest Products Journal*, Vol. 49, No. 10, 82-94.
- Green, D. W., and Kretschmann, D. E. (1994). "Moisture Content and the Properties of Clear Southern Pine." U.S. Department of Agriculture, Forest Service, Forest Products Laboratory, Res. Pap. FPL-RP-531, Madison, WI.

- Hayes, M. D. (1998). "Characterization and Modeling of a Fiber-Reinforced Polymeric Composite Structural Beam and Bridge Structure for Use in the Tom's Creek Bridge Rehabilitation Project." Master's Thesis, Virginia Polytechnic Institute and State University, Blacksburg, VA.
- Hollaway, L., and Head, P. R. (2001). *Advanced Polymer Composites and Polymers in the Civil Infrastructure*. Elsevier Science, Amsterdam, The Netherlands.
- Karbhari, V. M. and Seible, F., (2000). "Fiber Reinforced Composites – Advanced Materials for the Renewal of Civil Infrastructure." *Applied Composite Materials*, Vol. 7, Nos. 2-3, 94-124.
- Karbhari, V. M., Seible, F., Burgueño, R., Davol, A., Wernli, M., and Zhao, L. (2000). "Structural Characterization of Fiber-Reinforced Composite Short- and Medium-Span Bridge Systems." *Applied Composite Materials*, Vol. 7, No. 2-3, 155-182.
- Karbhari, V. M., Chin, J. W., Hunston, D., Benmokrane, B., Juska, T., Morgan, R., Lesko, J. J., Sorathia, U., and Reynaud, D. (2003). "Durability Gap Analysis for Fiber-Reinforced Polymer Composites in Civil Infrastructure." *Journal of Composites for Construction*, Vol. 7, No. 3, 238-247.
- Kim, S., and Nowak, A. S. (1997). "Load Distribution and Impact Factors for I-Girder Bridges." *Journal of Bridge Engineering*, Vol. 2, No. 3, 97-104.
- Kitane, Y., Aref, A. J., and Lee, G. C. (2004). "Static and Fatigue Testing of Hybrid Fiber-Reinforced Polymer-Concrete Bridge Superstructure." *Journal of Composites for Construction*, Vol. 8, No. 2, 182-190.
- Kretschmann, D. E., Green, D. W. (1996). "Modeling Moisture Content-Mechanical Property Relationships for Clear Southern Pine." *Wood and Fiber Science*, Vol. 28, No. 3, 320-337.
- Laman, J. A., Pechar, J. S., Boothby, T. E. (1997). "Dynamic Load Allowance for Through-Truss Bridges." *Journal of Bridge Engineering*, Vol. 4, No. 4, 231-241.
- Lesko, J. J., Hayes, M. D., Schniepp, T. J., and Case, S. W. (2001). "Characterization and Durability of FRP Structural Shapes and Materials." *Composites in Construction, A Reality: Proceedings of the International Workshop*, July 20-21, 2001, Capri, Italy, 110-120.
- Meier, U. (2000). "Composite Materials in Bridge Repair." *Applied Composite Materials*, Vol. 7, No. 2-3, 75-94.
- Mirmiran, A., Bank, L. C., Neale, K. W., Mottram, J. T., Ueda, T., and Davalos, J. F. (2003). "World Survey of Civil Engineering Programs on Fiber Reinforced Polymer Composites for Construction." *Journal of Professional Issues in Engineering Education and Practice*, ASCE, Vol. 129, No. 3, 155-160.

*Motor Carrier Service Operations* (October 2001). Virginia Department of Motor Vehicles, Richmond, VA.

Nagaraj, V. and Gangarao, V. S. (1998). "Fatigue Behavior and Connection Efficiency of Pultruded GFRP Beams." *Journal of Composites for Construction*, Vol. 2, No. 1, 57-65.

Neely, D. (2000). "Evaluation of the In-Service Performance of the Tom's Creek Bridge." Master's Thesis, Virginia Polytechnic Institute and State University, Blacksburg, VA.

Nishizaki, I. and Meiarashi, S. (2002). "Long-Term Deterioration of GFRP in Water and Moist Environment." *Journal of Composites for Construction*, Vol. 6, No. 1, 21-27.

Restrepo, E. (2002). "Determination of AASHTO Bridge Design Parameters through Field Evaluation of the Rt. 601 Bridge: A Bridge Utilizing Strongwell 36 in. Fiber-Reinforced Polymer Double Web Beams as the Main Load Carrying Members." Master's Thesis, Virginia Polytechnic Institute and State University, Blacksburg, VA.

Seible, F. (2003). "Fiber Reinforced Polymers in Bridge Design and Construction." *High Performance Materials in Bridges: Proceedings of the International Conference on High Performance Materials in Bridges*, Kona, HI, July 29-August 3, 2001, 227-237.

Siimes, F. E. (1967). "The Effect of Specific Gravity, Moisture Content, Temperature and Heating Time On the Tension and Compression Strength and Elasticity Properties Perpendicular to the Grain of Finnish Pine Spruce and Birch Wood and the Significance of These Factors on the Checking of Timber at Kiln Drying." The State Institute for Technical Research, Publication 84, Helsinki, Finland.

Taly, N., (1998). *Design of Modern Highway Bridges*, McGraw-Hill, New York, NY, pp. 194-203.

Ueda, T. (2002). "Codes and Standards for FRP as Structural Material in Japan." *Proc., The International Workshop*, July 20-21, 2001, Capri, Italy

Waldron, C. J. (2001). "Determination of the Design Parameters for the Route 601 Bridge: A Bridge Containing the Strongwell 37 in. Hybrid Composite Double Web Beam." Master's Thesis, Virginia Polytechnic Institute and State University, Blacksburg, VA.

Wallace, C. (1999). "Design of Falls Creek Trail Bridge." *Transportation Research Record*, No. 1652, Vol. 1, 133-142.

Watkins, S. E., Unser, J. F., Nanni, A., Chandrashekhara, K., and Belarbi, A. (2001). "Instrumentation and manufacture of a smart composite bridges for short-span applications." *Smart Structures and Materials 2001: Proceedings of SPIE*, Newport Beach, CA, March 5-7, 2001, 147-158.

The Weather Underground, Inc., "Weather Underground: History," [Online document], 2004, [cited 2004 April 19], Available HTTP:  
<http://www.wunderground.com/history/airport/KBCB/2003/7/30/DailyHistory.html>

Yazdani, N., Kadner, J., Kainz, J. A. and Ritter, M. A. (1999). "Field Performance of Three Stress-Laminated Southern Pine Timber Bridges," *Journal of Bridge Engineering*, ASCE, Vol. 4, No. 4, 279-286.

Zokaie, T., Osterkamp, T. A., and Imbsen, R. A. (1991). *Distribution of Wheel Loads on Highway Bridges*, Final Report Project 12-26, National Cooperative Highway Research Program, Transportation Research Board, National Research Council, Washington, D.C.

## Appendix A: Sample Calculation for Effect of Moisture Content on Deflection

### Toms Creek Bridge

Given:

$$I_{beam} = 129 \text{ in}^4 \text{ (Hayes, 1998)}$$

$$E_{beam} = 6700 \text{ ksi (average of the twelve beams in consideration [Hayes, 1990])}$$

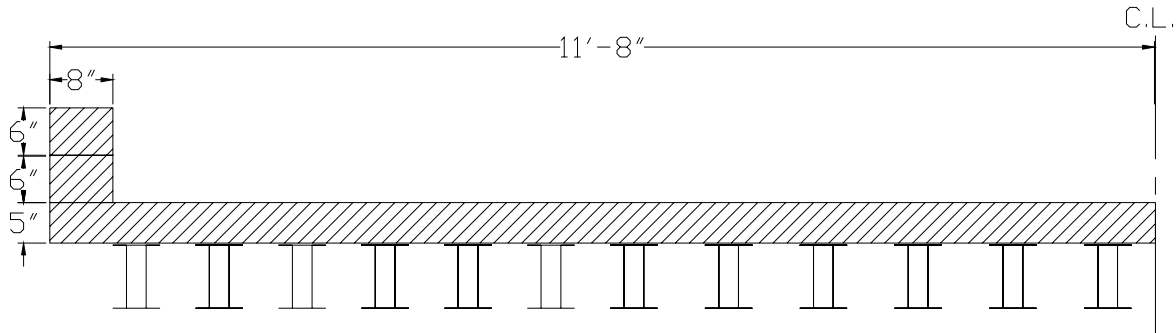


**Figure A-1.** Cross-section used for calculating the effects of moisture content on the deflection of the Toms Creek Bridge.

### Assumptions:

Perform a two-dimensional analysis, assuming the beams are simply supported and do not have composite action with the deck.

Use one-half of bridge, i.e., twelve beams, in calculations, since the northbound orientation generally had largest deflections, with Beam 8 or 9 registering the peak deflections.

Moisture content in the timber at the Toms Creek Bridge ranges from 12% to 16%.

At 12% moisture content,  $E_{timber} = 1850 \text{ ksi}$

At 16% moisture content,  $E_{timber} = 1680 \text{ ksi}$

Have a point load at midspan causing maximum deflection (not necessarily true for a load test, but will be sufficient for comparison purposes).

### Calculations:

$$I_{deck} = \frac{1}{12}bh^3 = \frac{1}{12}(140 \text{ in.})(5.125 \text{ in.})^3 = 1570 \text{ in}^4$$

$$I_{curb} = \frac{1}{12}bh^3 = \frac{1}{12}(8 \text{ in.})(12 \text{ in.})^3 = 1152 \text{ in}^4$$

Deflection assuming 12% moisture content:

$$\Delta_{12\%M.C.} = \frac{PL^3}{48EI} = \frac{PL^3}{48} \left[ \frac{1}{E_{beam}I_{beam} + E_{timber}(I_{deck} + I_{curb})} \right]$$

$$\Delta_{12\%M.C.} = \frac{PL^3}{48} \left[ \frac{1}{(6700\text{ksi})(129\text{in}^4)(12\text{beams}) + (1850\text{ksi})(1570\text{in}^4 + 1152\text{in}^4)} \right]$$

$$\Delta_{12\%M.C.} = \frac{PL^3}{48} (6.49 \times 10^{-8} k - \text{in}^2)$$

Deflection assuming 16% moisture content:

$$\Delta_{16\%M.C.} = \frac{PL^3}{48EI} = \frac{PL^3}{48} \left[ \frac{1}{E_{beam} I_{beam} + E_{timber} (I_{deck} + I_{curb})} \right]$$

$$\Delta_{16\%M.C.} = \frac{PL^3}{48} \left[ \frac{1}{(6700ksi)(129in^4)(12beams) + (1680ksi)(1570in^4 + 1152in^4)} \right]$$

$$\Delta_{16\%M.C.} = \frac{PL^3}{48} (6.69 \times 10^{-8} k - in^2)$$

**$\Delta_{16\%M.C.}$  is approximately 3% greater than  $\Delta_{12\%M.C.}$**

### Route 601 Bridge

Given:

$$I_{girder} = 15,291 \text{ in}^4 \text{ (Waldron, 2000)}$$

$E_{girder, eff} = 5330 \text{ ksi}$  (average effective modulus of the four girders in the westbound lane [Waldron, 2000]).

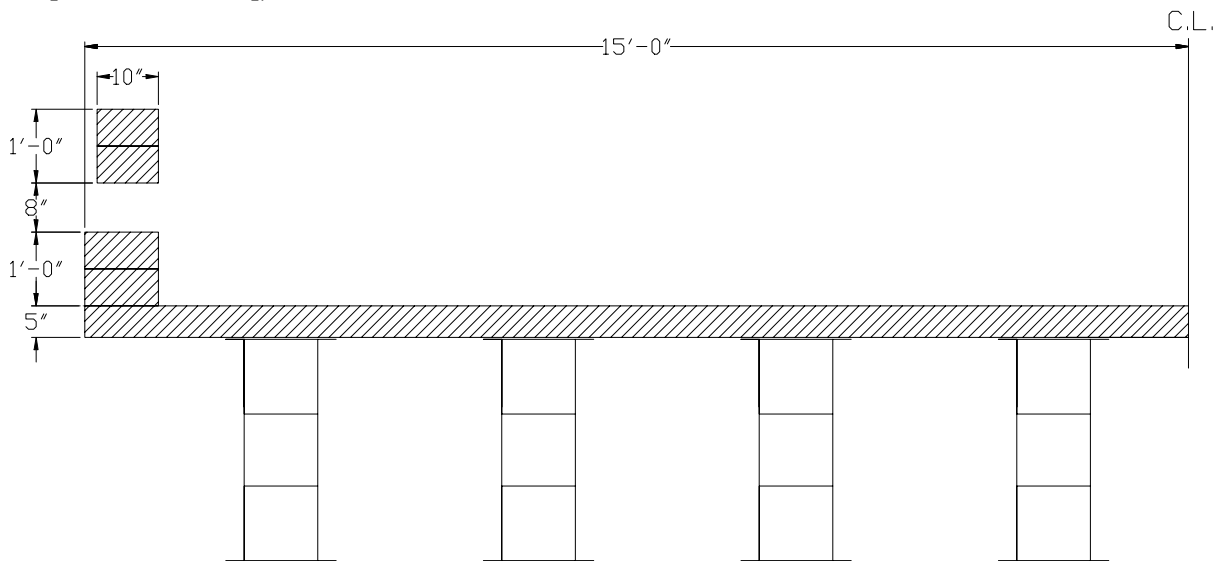


**Figure A-2.** Cross-section used for calculating the effects of moisture content on the deflection of the Toms Creek Bridge.

### Assumptions:

Perform a two-dimensional analysis, assuming the beams are simply supported and do not have composite action with the deck.

Use one-half of the bridge, i.e., four girders, in calculations, since the westbound exterior orientation generally had largest deflections, with the four girders carrying a large majority of the load.

Use the average effective modulus of the four girders, where the effective modulus accounts for shear deformations that are not accounted for in Bernoulli/Euler beam theory (Waldron, 2000).

Moisture content in the timber at the Route 601 Bridge ranges from 12% to 16%.

At 12% moisture content,  $E_{\text{timber}} = 1850 \text{ ksi}$

At 16% moisture content,  $E_{\text{timber}} = 1680 \text{ ksi}$

Have a point load at midspan causing maximum deflection (not necessarily true for a load test, but will be sufficient for comparison purposes).

Calculations:

$$I_{\text{deck}} = \frac{1}{12}bh^3 = \frac{1}{12}(180 \text{ in.})(5.125 \text{ in.})^3 = 2019 \text{ in}^4$$

$$I_{\text{curb}} = \frac{1}{12}bh^3 = \frac{1}{12}(12 \text{ in.})(12 \text{ in.})^3 = 1728 \text{ in}^4$$

$$I_{\text{rail}} = \frac{1}{12}bh^3 = \frac{1}{12}(10 \text{ in.})(12 \text{ in.})^3 = 1440 \text{ in}^4$$

Deflection assuming 12% moisture content:

$$\Delta_{12\%M.C.} = \frac{PL^3}{48EI} = \frac{PL^3}{48} \left[ \frac{1}{E_{\text{beam}} I_{\text{beam}} + E_{\text{timber}} (I_{\text{deck}} + I_{\text{curb}} + I_{\text{rail}})} \right]$$

$$\Delta_{12\%M.C.} = \frac{PL^3}{48} \left[ \frac{1}{(5330 \text{ ksi})(15291 \text{ in}^4)(4 \text{ beams}) + (1850 \text{ ksi})(2019 \text{ in}^4 + 1728 \text{ in}^4 + 1440 \text{ in}^4)} \right]$$

$$\underline{\underline{\Delta_{12\%M.C.} = \frac{PL^3}{48} (2.98 \times 10^{-9} \text{ k} - \text{in}^2)}}$$

Deflection assuming 16% moisture content:

$$\Delta_{16\%M.C.} = \frac{PL^3}{48EI} = \frac{PL^3}{48} \left[ \frac{1}{E_{\text{beam}} I_{\text{beam}} + E_{\text{timber}} (I_{\text{deck}} + I_{\text{curb}} + I_{\text{rail}})} \right]$$

$$\Delta_{16\%M.C.} = \frac{PL^3}{48} \left[ \frac{1}{(5330 \text{ ksi})(15291 \text{ in}^4)(4 \text{ beams}) + (1680 \text{ ksi})(2019 \text{ in}^4 + 1728 \text{ in}^4 + 1440 \text{ in}^4)} \right]$$

$$\underline{\underline{\Delta_{16\%M.C.} = \frac{PL^3}{48} (2.99 \times 10^{-9} \text{ k} - \text{in}^2)}}$$

**$\Delta_{16\%M.C.}$  is essentially the same as  $\Delta_{12\%M.C.}$**

**Appendix B: Test Data**

**Maximum Recorded Values for Toms Creek Bridge for All Tests Based on Strain**

Speed (mph)	Orientation	Fall 1997			Spring 1998			Fall 1998		
		Strain	Load Distr.	DLA	Strain	Load Distr.	DLA	Strain	Load Distr.	DLA
Static	North	264	0.086	—	287	0.082	—	248	0.094	—
		271	0.089	—	294	0.084	—	259	0.099	—
		—	—	—	294	0.084	—	253	0.095	—
		—	—	—	323	0.089	—	256	0.092	—
		—	—	—	—	—	—	258	0.098	—
	Center	230	0.076	—	313	0.075	—	204	0.077	—
		227	0.077	—	321	0.078	—	205	0.076	—
		—	—	—	310	0.073	—	222	0.081	—
		—	—	—	318	0.077	—	214	0.077	—
		—	—	—	—	—	—	222	0.079	—
	South	253	0.093	—	265	0.085	—	207	0.089	—
		264	0.096	—	270	0.083	—	213	0.090	—
		—	—	—	274	0.084	—	210	0.094	—
		—	—	—	290	0.087	—	212	0.090	—
		—	—	—	—	—	—	218	0.087	—
25	North	243	0.077	-0.090	297	0.081	-0.008	265	0.099	0.041
		266	0.083	-0.005	318	0.077	0.063	247	0.095	-0.030
		—	—	—	288	0.079	-0.038	277	0.091	0.087
		—	—	—	—	—	—	284	0.084	0.116
	Center	209	0.072	-0.084	273	0.074	-0.133	204	0.074	-0.042
		214	0.080	-0.063	310	0.078	-0.018	182	0.074	-0.147
		219	0.079	-0.041	294	0.072	-0.068	211	0.078	-0.010
		—	—	—	317	0.077	0.004	215	0.076	0.008
		—	—	—	—	—	—	223	0.078	0.045
	South	255	0.086	-0.015	293	0.078	0.066	245	0.087	0.148
		221	0.088	-0.145	298	0.083	0.085	242	0.085	0.133
		—	—	—	310	0.086	0.128	227	0.086	0.065
		—	—	—	—	—	—	248	0.086	0.162
		—	—	—	—	—	—	233	0.083	0.092

**Maximum Recorded Values for Toms Creek Bridge for All Tests Based on Strain**

Speed (mph)	Orientation	Spring 1999			Fall 1999			Summer 2003		
		Strain	Load Distr.	DLA	Strain	Load Distr.	DLA	Strain	Load Distr.	DLA
Static	North	298	0.088	—	243	0.092	—	263	0.078	—
		303	0.089	—	246	0.093	—	264	0.078	—
		292	0.093	—	248	0.094	—	263	0.078	—
		293	0.091	—	285	0.097	—	266	0.078	—
		296	0.091	—	275	0.098	—	267	0.079	—
		297	0.093	—	279	0.096	—	—	—	—
	Center	104	0.075	—	206	0.077	—	291	0.078	—
		318	0.081	—	208	0.077	—	298	0.079	—
		326	0.081	—	211	0.079	—	300	0.080	—
		316	0.081	—	210	0.078	—	302	0.080	—
		326	0.082	—	253	0.081	—	302	0.079	—
		324	0.082	—	—	—	—	—	—	—
	South	274	0.090	—	226	0.097	—	290	0.083	—
		280	0.089	—	226	0.097	—	296	0.084	—
		254	0.087	—	224	0.098	—	296	0.084	—
		262	0.090	—	246	0.094	—	296	0.084	—
		262	0.089	—	242	0.090	—	296	0.084	—
		240	0.090	—	246	0.096	—	—	—	—
25	North	283	0.083	-0.046	223	0.082	-0.153	—	—	—
		299	0.083	0.008	245	0.081	-0.066	—	—	—
		272	0.090	-0.081	226	0.093	-0.140	—	—	—
		—	—	—	—	—	—	—	—	—
	Center	273	0.080	-0.152	198	0.072	-0.090	—	—	—
		286	0.080	-0.112	192	0.073	-0.118	—	—	—
		280	0.080	-0.130	202	0.073	-0.072	—	—	—
		286	0.081	-0.112	—	—	—	—	—	—
		309	0.081	-0.040	—	—	—	—	—	—
		304	0.081	-0.056	—	—	—	—	—	—
	South	265	0.087	0.011	216	0.079	-0.081	319	0.081	0.083
		274	0.088	0.045	226	0.083	-0.036	278	0.080	-0.056
		265	0.089	0.011	230	0.081	-0.020	294	0.078	-0.003
		—	—	—	—	—	—	290	0.078	-0.018
		—	—	—	—	—	—	292	0.078	-0.011
		—	—	—	—	—	—	—	—	—

**Maximum Recorded Values for Toms Creek Bridge for All Tests Based on Strain**

Speed (mph)	Orientation	Fall 1997			Spring 1998			Fall 1998		
		Strain	Load Distr.	DLA	Strain	Load Distr.	DLA	Strain	Load Distr.	DLA
40	North	353	0.079	0.320	342	0.078	0.143	340	0.089	0.335
		358	0.084	0.338	275	0.093	-0.083	381	0.097	0.496
		—	—	—	270	0.077	-0.098	413	0.102	0.621
		—	—	—	369	0.079	0.233	428	0.104	0.680
		—	—	—	—	—	—	405	0.100	0.592
		—	—	—	—	—	—	—	—	—
	Center	374	0.077	0.638	300	0.072	-0.047	223	0.074	0.043
		311	0.079	0.359	390	0.075	0.236	277	0.071	0.297
		—	—	—	314	0.071	-0.003	311	0.078	0.456
		—	—	—	407	0.076	0.292	278	0.072	0.301
		—	—	—	—	—	—	272	0.073	0.274
		—	—	—	—	—	—	—	—	—
	South	369	0.078	0.428	307	0.081	0.117	355	0.087	0.667
		479	0.101	0.853	454	0.079	0.652	367	0.090	0.723
		—	—	—	470	0.081	0.711	373	0.093	0.750
		—	—	—	287	0.085	0.045	372	0.091	0.745
		—	—	—	—	—	—	—	—	—
		—	—	—	—	—	—	—	—	—

**Maximum Recorded Values for Toms Creek Bridge for All Tests Based on Strain**

Speed (mph)	Orientation	Spring 1999			Fall 1999			Summer 2003		
		Strain	Load Distr.	DLA	Strain	Load Distr.	DLA	Strain	Load Distr.	DLA
40	North	406	0.093	0.369	384	0.088	0.463	358	0.074	0.353
		447	0.095	0.508	409	0.095	0.559	350	0.074	0.321
		375	0.090	0.265	352	0.091	0.338	364	0.075	0.377
		449	0.094	0.515	371	0.092	0.411	399	0.082	0.509
		—	—	—	375	0.093	0.428	406	0.085	0.536
		—	—	—	395	0.097	0.505	—	—	—
	Center	313	0.077	-0.028	233	0.070	0.071	322	0.070	0.077
		322	0.078	0.000	245	0.070	0.128	364	0.071	0.221
		338	0.079	0.050	259	0.068	0.188	324	0.073	0.087
		425	0.078	0.320	304	0.071	0.398	317	0.074	0.064
		412	0.079	0.280	317	0.068	0.458	327	0.074	0.097
		432	0.080	0.342	—	—	—	—	—	—
	South	412	0.088	0.572	383	0.093	0.630	395	0.074	0.338
		447	0.090	0.706	393	0.093	0.675	440	0.076	0.492
		447	0.091	0.706	374	0.098	0.594	428	0.076	0.450
		424	0.089	0.618	381	0.086	0.622	423	0.075	0.433
		—	—	—	396	0.092	0.688	505	0.077	0.713
		—	—	—	—	—	—	—	—	—

**Maximum Recorded Values for Toms Creek Bridge for All Tests Based on Deflection**

Speed (mph)	Orientation	Fall 1998			Spring 1999			Fall 1999			Summer 2003		
		Deflection	Load Distr.	DLA	Deflection	Load Distr.	DLA	Deflection	Load Distr.	DLA	Deflection	Load Distr.	DLA
Static	North	0.232	0.088	—	0.275	0.082	—	0.221	0.087	—	0.257	0.075	—
		0.260	0.095	—	0.280	0.083	—	0.225	0.089	—	0.258	0.075	—
		0.249	0.091	—	0.271	0.088	—	0.236	0.091	—	0.257	0.075	—
		0.261	0.094	—	0.259	0.082	—	0.322	0.099	—	0.259	0.075	—
		0.256	0.092	—	0.273	0.085	—	0.290	0.094	—	0.260	0.075	—
		—	—	—	0.274	0.088	—	0.270	0.086	—	—	—	—
	Center	0.201	0.081	—	0.322	0.078	—	0.172	0.073	—	0.264	0.070	—
		0.203	0.080	—	0.319	0.078	—	0.173	0.074	—	0.265	0.070	—
		0.209	0.081	—	0.327	0.078	—	0.173	0.073	—	0.266	0.070	—
		0.210	0.080	—	0.317	0.078	—	0.175	0.074	—	0.268	0.070	—
		0.211	0.081	—	0.323	0.078	—	0.229	0.075	—	0.269	0.070	—
		0.213	0.080	—	0.325	0.078	—	—	—	—	—	—	—
	South	0.165	0.076	—	0.241	0.079	—	0.164	0.080	—	0.262	0.077	—
		0.188	0.087	—	0.239	0.077	—	0.164	0.080	—	0.263	0.077	—
		0.187	0.083	—	0.219	0.080	—	0.166	0.081	—	0.265	0.077	—
		0.190	0.083	—	0.227	0.082	—	0.198	0.078	—	0.266	0.077	—
		0.183	0.081	—	0.228	0.082	—	0.194	0.076	—	0.267	0.077	—
		0.182	0.082	—	0.201	0.084	—	0.200	0.078	—	—	—	—

**Maximum Recorded Values for Toms Creek Bridge for All Tests Based on Deflection**

Speed (mph)	Orientation	Fall 1998			Spring 1999			Fall 1999			Summer 2003		
		<i>Deflection</i>	<i>Load Distr.</i>	<i>DLA</i>									
25	North	0.251	0.092	-0.002	0.249	0.077	-0.085	0.212	0.081	-0.187	—	—	—
		0.253	0.089	0.006	0.277	0.080	0.018	0.262	0.101	0.007	—	—	—
		0.275	0.092	0.093	0.267	0.079	-0.018	0.224	0.086	-0.140	—	—	—
		0.304	0.092	0.208	—	—	—	—	—	—	—	—	—
	Center	0.199	0.080	-0.043	0.239	0.076	-0.258	0.173	0.073	-0.063	—	—	—
		0.179	0.081	-0.139	0.258	0.077	-0.199	0.164	0.072	-0.110	—	—	—
		0.195	0.082	-0.062	0.253	0.077	-0.215	0.169	0.073	-0.081	—	—	—
		0.196	0.080	-0.057	0.255	0.075	-0.208	—	—	—	—	—	—
		0.206	0.081	-0.009	0.276	0.076	-0.143	—	—	—	—	—	—
		0.193	0.081	-0.071	0.273	0.076	-0.153	—	—	—	—	—	—
	South	0.194	0.081	-0.067	—	—	—	—	—	—	—	—	—
		0.191	0.078	0.047	0.227	0.078	0.006	0.175	0.076	-0.032	0.286	0.076	0.081
		0.197	0.077	0.079	0.222	0.075	-0.016	0.182	0.079	0.008	0.264	0.078	0.000
		0.190	0.080	0.041	0.219	0.076	-0.030	0.191	0.078	0.056	0.278	0.075	0.049
		0.203	0.081	0.112	—	—	—	—	—	—	0.270	0.075	0.020
	0.197	0.078	0.079	—	—	—	—	—	—	0.272	0.074	0.027	

**Maximum Recorded Values for Toms Creek Bridge for All Tests Based on Deflection**

Speed (mph)	Orientation	Fall 1998			Spring 1999			Fall 1999			Summer 2003			
		<i>Deflection</i>	<i>Load Distr.</i>	<i>DLA</i>										
40	North	0.376	0.094	0.494	0.361	0.086	0.327	0.418	0.098	0.604	0.366	0.073	0.417	
		0.419	0.103	0.665	0.405	0.087	0.489	0.446	0.106	0.711	0.370	0.073	0.435	
		0.448	0.105	0.781	0.358	0.083	0.316	0.385	0.099	0.480	0.388	0.073	0.503	
		0.465	0.107	0.848	0.410	0.087	0.507	0.402	0.100	0.545	0.404	0.077	0.565	
		0.441	0.105	0.753	—	—	—	0.409	0.101	0.570	0.403	0.078	0.560	
		—	—	—	—	—	—	0.428	0.105	0.643	—	—	—	
	Center	0.196	0.078	-0.057	0.298	0.077	-0.075	0.201	0.072	0.093	0.301	0.070	0.130	
		0.279	0.078	0.342	0.296	0.077	-0.081	0.221	0.072	0.201	0.331	0.069	0.245	
		0.288	0.081	0.386	0.322	0.078	-0.001	0.231	0.071	0.256	0.295	0.069	0.108	
		0.260	0.078	0.251	0.411	0.078	0.276	0.280	0.072	0.522	0.292	0.070	0.098	
		0.260	0.079	0.251	0.401	0.078	0.245	0.300	0.071	0.629	0.299	0.070	0.122	
		—	—	—	0.415	0.078	0.288	—	—	—	—	—	—	—
	South	0.364	0.094	0.995	0.382	0.083	0.692	0.371	0.097	1.055	0.387	0.074	0.462	
		0.372	0.098	1.038	0.398	0.084	0.763	0.352	0.083	0.946	0.447	0.076	0.690	
		0.369	0.101	1.022	0.413	0.088	0.830	0.355	0.097	0.962	0.433	0.076	0.637	
		0.381	0.100	1.088	0.383	0.082	0.697	0.343	0.082	0.898	0.428	0.075	0.620	
		—	—	—	—	—	—	—	—	—	—	—	—	—
		—	—	—	—	—	—	—	0.378	0.095	1.091	0.475	0.077	0.797

**Maximum Recorded Values for the Route 601 Bridge for All Tests Based on Strain**

Speed (mph)	Orientation	October 2001			June 2002			October 2003		
		Strain	Load Distr.	DLA	Strain	Load Distr.	DLA	Strain	Load Distr.	DLA
Static	West Ext.	—	—	—	236	0.318	—	213	0.334	—
		—	—	—	221	0.299	—	211	0.325	—
		—	—	—	235	0.319	—	212	0.330	—
		—	—	—	227	0.309	—	206	0.318	—
		—	—	—	227	0.308	—	206	0.321	—
	West Int.	180	0.242	—	211	0.256	—	190	0.260	—
		179	0.242	—	209	0.255	—	189	0.255	—
		181	0.244	—	210	0.256	—	191	0.259	—
		179	0.242	—	208	0.256	—	188	0.254	—
		180	0.243	—	211	0.256	—	191	0.255	—
	Center	180	0.231	—	206	0.245	—	188	0.242	—
		182	0.231	—	205	0.244	—	189	0.244	—
		182	0.232	—	206	0.243	—	190	0.251	—
		185	0.235	—	205	0.243	—	189	0.245	—
		182	0.232	—	206	0.244	—	189	0.244	—
	Multiple	218	0.157	—	233	0.158	—	215	0.170	—
		219	0.160	—	233	0.159	—	211	0.163	—
		212	0.155	—	245	0.167	—	213	0.171	—
		220	0.160	—	240	0.164	—	209	0.152	—
		221	0.162	—	—	—	—	216	0.159	—
	East Int.	171	0.233	—	201	0.244	—	185	0.247	—
		168	0.232	—	200	0.244	—	184	0.250	—
		172	0.232	—	201	0.245	—	186	0.248	—
		169	0.229	—	200	0.242	—	184	0.248	—
		173	0.231	—	200	0.244	—	187	0.249	—
	East Ext.	—	—	—	226	0.304	—	221	0.304	—
		—	—	—	247	0.343	—	222	0.306	—
		—	—	—	241	0.328	—	219	0.300	—
		—	—	—	247	0.343	—	219	0.300	—
		—	—	—	242	0.328	—	219	0.299	—

**Maximum Recorded Values for the Route 601 Bridge for All Tests Based on Strain**

Speed (mph)	Orientation	October 2001			June 2002			October 2003		
		Strain	Load Distr.	DLA	Strain	Load Distr.	DLA	Strain	Load Distr.	DLA
25	West Int.	197	0.240	0.093	227	0.251	0.074	185	0.245	-0.028
		196	0.240	0.097	220	0.253	0.052	188	0.254	-0.007
		204	0.240	0.125	226	0.250	0.078	200	0.248	0.052
		183	0.235	0.025	241	0.253	0.158	186	0.247	-0.022
		183	0.237	0.019	227	0.251	0.074	209	0.252	0.100
	—	—	—	—	—	—	197	0.252	0.036	
	Center	176	0.222	-0.034	214	0.238	0.042	188	0.241	-0.008
		185	0.229	0.016	215	0.237	0.044	194	0.240	0.025
		172	0.222	-0.056	231	0.240	0.121	190	0.235	0.003
		204	0.234	0.117	219	0.239	0.066	200	0.240	0.057
		174	0.219	-0.043	229	0.243	0.113	201	0.238	0.065
	East Int.	194	0.253	0.138	219	0.244	0.091	188	0.240	-0.023
		189	0.237	0.108	196	0.238	-0.021	194	0.245	-0.019
		194	0.241	0.138	209	0.245	0.041	190	0.254	0.014
		185	0.234	0.085	204	0.240	0.021	200	0.246	0.069
187		0.239	0.097	212	0.243	0.058	201	0.247	0.056	
40	West Int.	166	0.225	-0.075	271	0.252	0.290	181	0.235	-0.047
		178	0.223	-0.011	276	0.251	0.316	194	0.237	0.020
		177	0.225	-0.017	271	0.253	0.290	193	0.243	0.015
		172	0.217	-0.042	266	0.252	0.267	197	0.244	0.038
		183	0.220	0.018	274	0.253	0.308	187	0.249	-0.014
	Center	172	0.227	-0.057	270	0.245	0.314	184	0.208	-0.025
		159	0.213	-0.126	214	0.231	0.040	185	0.242	-0.021
		175	0.225	-0.037	275	0.244	0.336	177	0.208	-0.065
		165	0.213	-0.094	249	0.237	0.212	189	0.239	0.001
		176	0.223	-0.034	279	0.244	0.357	192	0.212	0.016
	East Int.	173	0.227	0.014	214	0.243	0.071	191	0.234	0.029
		173	0.229	0.015	211	0.243	0.056	206	0.236	0.114
		182	0.230	0.067	190	0.241	-0.050	213	0.235	0.150
		181	0.233	0.060	189	0.239	-0.058	206	0.235	0.112
		181	0.232	0.059	191	0.237	-0.048	215	0.237	0.161

**Maximum Recorded Values for the Route 601 Bridge for All Tests Based on Deflection**

Speed (mph)	Orientation	October 2001			June 2002			October 2003		
		Deflection	Load Distr.	DLA	Deflection	Load Distr.	DLA	Deflection	Load Distr.	DLA
Static	West Ext.	—	—	—	0.293	0.309	—	0.256	0.339	—
		—	—	—	0.265	0.281	—	0.251	0.331	—
		—	—	—	0.282	0.300	—	0.253	0.333	—
		—	—	—	0.269	0.289	—	0.256	0.334	—
		—	—	—	0.272	0.288	—	0.255	0.335	—
	West Int.	0.217	0.239	—	0.242	0.235	—	0.195	0.237	—
		0.218	0.240	—	0.240	0.235	—	0.193	0.238	—
		0.213	0.238	—	0.240	0.234	—	0.192	0.238	—
		0.217	0.239	—	0.242	0.239	—	0.193	0.238	—
		0.211	0.239	—	0.242	0.235	—	0.194	0.239	—
	Center	0.209	0.229	—	0.249	0.241	—	0.187	0.223	—
		0.214	0.230	—	0.240	0.234	—	0.186	0.220	—
		0.209	0.228	—	0.244	0.236	—	0.186	0.220	—
		0.213	0.228	—	0.242	0.236	—	0.186	0.221	—
		0.210	0.228	—	0.243	0.235	—	0.187	0.220	—
	Multiple	0.266	0.154	—	0.297	0.158	—	0.249	0.172	—
		0.261	0.184	—	0.300	0.159	—	0.252	0.172	—
		0.252	0.148	—	0.315	0.167	—	0.248	0.177	—
		0.261	0.153	—	0.308	0.164	—	0.255	0.167	—
		0.266	0.155	—	—	—	—	0.256	0.168	—
	East Int.	0.193	0.230	—	0.225	0.227	—	0.200	0.253	—
		0.194	0.230	—	0.221	0.225	—	0.199	0.253	—
		0.192	0.228	—	0.221	0.223	—	0.199	0.252	—
		0.195	0.229	—	0.220	0.224	—	0.199	0.252	—
		0.191	0.230	—	0.221	0.223	—	0.200	0.252	—
	East Ext.	—	—	—	0.299	0.322	—	0.215	0.283	—
		—	—	—	0.315	0.347	—	0.214	0.283	—
		—	—	—	0.306	0.337	—	0.214	0.282	—
—		—	—	0.316	0.349	—	0.218	0.284	—	
—		—	—	0.309	0.338	—	0.216	0.282	—	

**Maximum Recorded Values for the Route 601 Bridge for All Tests Based on Deflection**

Speed (mph)	Orientation	October 2001			June 2002			October 2003		
		Deflection	Load Distr.	DLA	Deflection	Load Distr.	DLA	Deflection	Load Distr.	DLA
25	West Int.	0.226	0.237	0.047	0.257	0.234	0.071	0.181	0.231	-0.061
		0.232	0.238	0.077	0.250	0.235	0.042	0.188	0.230	-0.027
		0.236	0.237	0.093	0.255	0.233	0.061	0.193	0.232	-0.003
		0.221	0.236	0.027	0.271	0.236	0.128	0.194	0.244	0.006
		0.228	0.237	0.056	0.257	0.234	0.071	0.205	0.235	0.062
	—	—	—	—	—	—	0.195	0.233	0.009	
	Center	0.202	0.228	-0.042	0.255	0.242	0.046	0.176	0.221	-0.056
		0.196	0.217	-0.071	0.248	0.235	0.018	0.179	0.217	-0.038
		0.201	0.228	-0.048	0.269	0.241	0.103	0.180	0.218	-0.035
		0.212	0.218	0.003	0.249	0.229	0.022	0.184	0.216	-0.012
		0.203	0.224	-0.040	0.263	0.239	0.079	0.185	0.218	-0.008
	East Int.	0.211	0.240	0.095	0.236	0.224	0.064	0.199	0.244	-0.001
		0.207	0.229	0.072	0.222	0.222	-0.001	0.192	0.248	-0.037
		0.210	0.231	0.089	0.228	0.224	0.027	0.203	0.251	0.016
		0.206	0.228	0.069	0.223	0.222	0.003	0.203	0.252	0.019
0.203		0.228	0.054	0.232	0.224	0.044	0.206	0.250	0.033	
40	West Int.	0.205	0.230	-0.050	0.306	0.235	0.274	0.186	0.232	-0.037
		0.222	0.229	0.032	0.310	0.233	0.291	0.197	0.233	0.018
		0.223	0.231	0.034	0.308	0.236	0.283	0.196	0.236	0.013
		0.224	0.229	0.038	0.305	0.235	0.269	0.200	0.235	0.033
		0.220	0.226	0.020	0.314	0.236	0.304	0.193	0.234	-0.003
	Center	0.191	0.221	-0.094	0.298	0.232	0.222	0.204	0.216	0.094
		0.194	0.219	-0.080	0.269	0.238	0.106	0.183	0.222	-0.017
		0.197	0.219	-0.067	0.303	0.230	0.246	0.194	0.213	0.038
		0.203	0.220	-0.038	0.300	0.241	0.234	0.185	0.223	-0.008
		0.200	0.222	-0.051	0.309	0.232	0.271	0.202	0.211	0.085
	East Int.	0.185	0.221	-0.041	0.250	0.224	0.128	0.213	0.243	0.004
		0.187	0.220	-0.030	0.252	0.224	0.136	0.229	0.245	0.080
		0.204	0.223	0.056	0.228	0.226	0.028	0.235	0.244	0.109
		0.202	0.225	0.045	0.225	0.223	0.015	0.228	0.245	0.075
		0.198	0.222	0.026	0.228	0.224	0.027	0.238	0.248	0.122

## **Vita**

Bernard Leonard Kassner was born to Dennis and Jo Anne Kassner on June 12, 1973. Growing up in Laurel, Maryland, he graduated from Eleanor Roosevelt High School. Although he had dreams of becoming an architect ever since visiting Thomas Jefferson's Monticello in the fifth grade, he transitioned into the Civil Engineering program at Virginia Tech, focusing on structural design. After achieving his Bachelor's Degree summa cum laude, Bernard decided to remain at the home of the Hokies to earn his Masters Degree, concentrating on bridge design. After completing his graduate degree, he will continue investigating bridge design and construction methods by working for the Virginia Transportation Research Council, the research arm of the Virginia Department of Transportation.